Nonlinear and nonautonomous dynamical properties of the cardiovascular response to a range of ambient temperatures

Sultan Salem ALATAWI

A thesis submitted for the degree of

Doctor of Philosophy

DEPARTMENT OF PHYSICS
LANCASTER UNIVERSITY
LANCASTER, UK

March, 2024

Declaration

This thesis is my original work and has not been submitted, in whole or in part, for a degree at this or any other university. Nor does it contain, to the best of my knowledge and belief, any material published or written by another person, except as acknowledged in the text.

Abstract

There is a significant relationship between temperature and human health. The cardiovascular system undergoes a process of coordinated changes when the external temperature or the amount of heat generated changes. To maintain the internal temperature of the body at a constant level, a variety of physiological and behavioural processes must be controlled. These responses in the cardiovascular system have been shown to manifest themselves in significant changes in cardiac output and regional blood flow. An increase or decrease in blood flow in the skin is the basic response of the circulatory system to changes in skin surface temperature.

In this work, we used the optical technique of laser Doppler flowmetry (LDF) to study the dynamics of blood flow at three different ambient temperatures (20°C, 26°C, and 32°C). We investigated the changes that may be caused by ambient temperature in healthy young subjects on blood flow and cardiovascular dynamics, e.g., heart rate, stroke volume, cardiac output, and blood pressure. Optical methods were used along with a variety of other sensors to assess these changes. In addition, the instantaneous frequencies of heartbeat and respiration were extracted from the measured ECG, blood pressure, and respiration time series. Two additional time series were created from blood pressure, instantaneous systolic and instantaneous diastolic blood pressure.

The resulting time series were then analysed using algorithms developed for irregular periodic signals. The wavelet power spectrum was applied to evaluate the contribution of the oscillatory components within the frequency range from 0.0027 to 2 Hz. The physiological characteristics of the six oscillatory components in this range and their changes with temperature are evaluated and discussed. Phase coherence analysis was used to study the interaction between the oscillatory components, and the effects of temperature are evaluated and discussed. We show that while average values are highest at lower temperatures, the coherence is highest at higher temperatures.

Publications

Parts of the work presented in this thesis have been published in the following conference:

- Bjerkan, J., Alatawi, S., Ugland, N., Elstad, M., & Stefanovska, A. (2022, October). Cardio-respiratory wavelet phase coherence at three ambient temperatures. In 2022 12th Conference of the European Study Group on Cardiovascular Oscillations (ESGCO) (pp. 1-2). IEEE.
  Oral & poster presentation.

The following manuscripts are currently in preparation:

- Nora Ugland, Aihua Lin, Sultan Alatawi, Juliane Bjerkan, Tone Kristin Bergersen, Ilias Zilakos, Aneta Stefanovska, Maja Elstad (order to be decided). Static cardiovascular response to ambient temperatures within human thermoneutral zone.

- Sultan Alatawi, Juliane Bjerkan, Nora Ugland, Aihua Lin, Tone Kristin Bergersen, Ilias Zilakos, Aneta Stefanovska, Maja Elstad Oscillatory (or dynamic) cardiovascular response to ambient temperatures within human thermoneutral zone.

Acknowledgements

First and foremost, I would like to express my appreciation to my supervisor Professor Aneta Stefanovska, for two reasons: the first is that she provided me with the chance to work in such an interesting field and exposed my eyes to knowledge that I would hardly learn/ find somewhere else, and the second is that she has provided me with support and guidance over the course of the past five years, which has enabled me to develop not only as a researcher but also as a person. It has been a wonderful and tough experience for me to be able to work so closely with her in an area that is so fascinating. Life experience comprehension, personal fortitude, and supervisory encouragement made this effort possible.

Many thanks to Dr. Maja Elstad and her research group (University of Oslo. Norway) for providing me the data. I am especially thankful to Juliane Bjerkan who introduced me to the methods I used for analysing time series using MATLAB. I owe her an enormous amount of thankfulness for the helpful responses she provided to my analytical questions at the time of analysis. Many thanks go out to Dr. Miroslav Barabash, who was quite helpful in responding to my programming and analysis questions, particularly in the early stages of my research. I am truly indebted and thankful to Professor Peter McClintock for his final corrections. Although I did not directly collaborate with the majority of my Nonlinear Biomedical Physics Group colleagues, I am indebted to two of them, Samuel Barnes and Mansour Alanazi, for making my time at work enjoyable. A tremendous amount of thanks is due to the Saudi government (represented by Tabuk University) for enabling me to pursue my education abroad and providing me with financial support.

Finally, my sincerest gratitude goes to my nearest and dearest, my wife (whom I adore) and my five wonderful children (Murad, Ghada, Ghaida, Amjad, and Sama) for their unending love, support, patience, and understanding.

Contents

List of Figures

List of Tables

Glossary & Abbreviations

BP Blood pressure; the force (pressure) exerted by the blood against the walls of the blood vessels.

sBP sytolic blood pressure; maximum blood pressure during ventricular contraction.

dBP diastolic blood pressure; minimum pressure measured between contractions.

LDF Laser Doppler flowmetry.

LDFAL Laser Doppler flux forearm left.

LDindR Laser Doppler flux right index finger.

LDindL Laser Doppler flux left index finger.

AU Arbitrary unit used in laser Doppler flowmetry.

Rhythms In the context of the human body, a biological rhythm is a naturally occurring or changing process in the body that follows a periodic pattern.

ECG Electrocardiogram; A non-invasive recording of the heart's electrical activity taken from the body's surface.

HR Heart rate; number of times that heart beats per minute.

SV Stroke volume; refers to the volume of blood that is pumped out of the left ventricle of the heart during a single contraction.

CO Cardiac output; it represents the amount of blood that is pumped out of the heart in one minute.

HRV Heart rate variability; variability in heart rate as a function of time.

IHR Instantaneous heart rate.

IRR Instantaneous respiration rate.

RSA Respiratory sinus arrhythmia. it refers to the modulation of heart rate by the frequency of respiratory activity.

NO Nitric oxide; It acts as a vasodilator, which means that it causes the muscles in the blood vessels to relax, which in turn extends the blood vessels and improves circulation.

ACh Acetylcholine; vasodilator that works by relaxing the smooth muscle cells in the body indirectly through the endothelial cells.

in vitro Studies employing organisms, cells, or biological molecules that have been removed from their natural biological environment are called in vitro.

In vivo research conducted on organisms or individual cells.

SBF Skin blood flow; refers to the flow of blood within the skin's vascular system.

TBF Tissue blood flow; refers to the circulation of blood within the different tissues of the body, such as the muscles, organs, and other structures.

IAAFT Iterative amplitude adjusted Fourier transform; A technique for creating surrogate of a signal.

Phase it describes where in time a signal occurs in relation to its overall duration, or phase of a signal is its position or timing relative to the period of that signal.

Phase coherence In the context of signal processing, it refers to the degree of correlation or synchronisation between two signals of different frequencies.

Phase difference or phase shift it refers to the angular difference between the phases of two signals at the same frequency at a given time. It is determined by subtracting the phases of the first and second signals.

Thermoregulation is the process by which mammals keep their internal temperatures stable regardless of the ambient temperature.

1. Introduction

Temperature has a vital role in the growth and survival of every living being [5]. Environmental temperature fluctuations trigger thermoregulatory mechanisms to protect homeothermy, such as heat-conserving and heat-producing responses, and heat-dissipating processes, respectively. Hyperthermia and hypothermia, can be life-threatening conditions that result when external temperatures are too high or too low, respectively, for the body's regular thermoregulatory mechanisms to handle, or when the normal functioning of the thermoregulatory system is disrupted [6]. Changes in external temperature or in heat generation cause the cardiovascular system to go through a series of coordinated adjustments [7]. In order to maintain a stable body temperature, a wide variety of physiological and behavioural processes must be tightly controlled [5]. These responses in the cardiovascular system are manifested in substantial shifts in cardiac output and regional blood flow. The primary circulatory response to changes in skin temperature is a rise or fall in blood flow to the skin [7].

The impact of temperature on human health and disease is significant. Maintenance of thermal homeostasis is crucial for normal cellular activity and, by extension, the survival of the human. The temperature of internal organs is the most important factor to consider when discussing the physiology's relationship to temperature in medicine. This temperature of the organs within the body is referred to as the body core temperature [8]. In this research, body temperature and body core temperature will not be used. Instead, we will refer to temperature in terms of ambient

temperature, which is defined as the temperature of the surrounding environment [9]. However, in this study, and for the purpose research, ambient temperature was controlled to study the effect of increasing ambient temperature on human cardiovascular system. Additionally, temperature propagation is closely related to metabolic demand energy usage, and as we have three different temperatures, we will be able to reason about energy expenditure.

1.1 Measuring the variability of human skin temperature

Evaluation of microcirculatory variations and assessment of blood microcirculation (blood flow in capillaries and surrounding micro vessels) are important in the modern clinical assessment and diagnosis of many diseases [10, 11]. It is crucial to catch such diseases early, when treatment is still an option. These conditions first show up in the microcirculatory bed, which is part of the vascular system [12]. The determining the connections between the micro- and macro-level blood supply systems and the accompanying metabolic, thermoregulatory, and other processes are still open questions in fundamental medicine [13].

In relation to the preceding, there is a significant interest in the development and improvement of tools that are capable of accurate and non-invasive monitoring of blood flow in various parts of the body under various conditions [14] as well as in systems that are able to record all vascular components of the blood stream, specifically arterial, capillary, and venous components [12]. The existing techniques for recording blood microcirculation can be categorised according to the physical principles that are used for measurement. These techniques include optical techniques such as laser Doppler flowmetry (LDF). A key property of microcirculation is its continuous variability, which is shown to exist in the form of spontaneous variations

in the blood flow through tissue. A subjective measure of the vital activity in tissues is provided by the variable microcirculation that exists within those tissues. Changes and rhythmic oscillations in blood flow can reveal the precise links between the systems that set the stage for microcirculation. The microcirculation system is characterised by relatively complex oscillatory processes due to the nature of their oscillatory activities. It is widely accepted that vasomotions is responsible for the majority of the spontaneous variation in blood flow that occurs within tissues. However, this does not mean that vasomotions is the only factor. Surface body temperatures fluctuate throughout a broad spectrum of amplitudes and frequencies as a result of the physiological activities. Heartbeat pulsations are linked to this behaviour, and they are characterised by a tiny amplitude and a maximal frequency of temperature oscillations. Microcirculation is of tremendous interest to research and consequently medicine, hence data on temperature oscillations in all frequency ranges is needed [12].

1.2 Outline of thesis

The main goal of this thesis is to use oscillations in microvascular blood flow and cardiovascular dynamics to investigate the effect of increasing ambient temperature on the human cardiovascular system. More specifically, the aim is to test the hypothesis that blood flow dynamics and other cardiovascular variables are altered by different ambient temperatures, and to investigate how the metabolic rate responds to these changes. In addition to this, the data and analysis methods are utilised to determine whether or not the local or central mechanism regulatory processes are altered as a result of whole body heating, and to glean as much information as possible regarding the regulation of human cardiovascular activity at both systemic and peripheral levels. The oscillations are also studied in terms of their relationship to a variety of ambient

temperature ranges.

Chapter 2 provides an introduction to the physiology of the cardiovascular system and oscillations in cardiovascular flow under the effect of whole body heating. It also provides a literature review on the effect of increasing ambient temperature on cardiovascular variables. The techniques of measurement that were applied in the process of data collection are outlined and discussed in chapter 3. In addition to that, this chapter discusses dynamical systems, highlights the necessity of viewing biological systems as thermodynamically open and nonautonomous, and explains the nonlinear time series analysis techniques that were utilised in order to obtain the results. An analysis of data recorded on subjects during a rise in ambient temperature is presented in chapter 4. This provides an opportunity to assess physiological parameters during whole-body heating. The aim of this chapter is to investigate the dynamics of blood flow and the variability of heart rate, respiration rate, blood pressure, and cardiac output under the effect of heating.

Finally, chapter 5 discusses the results and summarises their physiological significance.

2. Physiological and thermoregulation background

In the human body, relatively few processes can be said to be in a state of constant motion. The vast majority shift and change over time as they interact with one another and with their surroundings. The existence of life depends on these differences. Studying the dynamics of complete systems like the circulatory and respiratory systems requires thinking at every level of organisation, from the whole organ down to the single cell to the organelles. Understanding life requires taking into account not only one but all possible scales, and hence all possible oscillators. Continuous perturbations, either deterministic or stochastic, can affect living systems at all scales. These can originate in adjacent dynamical systems or be the result of random fluctuations [15]. However, before attempting to research the interactions that occur between physiological processes, it is crucial to first understand their fundamental physiology as well as the methods that are employed to observe these processes.

2.1 The blood vessels: physiological background

The blood vessels provide the primary connections that exist between the heart and the tissues. The intima, also known as the inner layer, the tunica media, often known

as the middle layer, and the tunica externa, also known as the outer layer, make up the vascular wall [16]. The blood vessels are separated into arteries, capillaries, and veins according to their respective functions, locations, and sizes (see figure 2.1).

The distribution of blood to the organs is the primary role that the arteries play in the body. Because of the high pulse pressure in the arteries, their wall thickness is greater than that of the other vessels. Depending on where they are located in the arterial tree, arteries can be categorised as either conducting arteries, conduit arteries, or resistance arteries. Conducting arteries are the largest arteries in the body and have a substantial amount of elastic tissue. This allows the vessel to expand and recoil to smooth out the oscillatory fluctuations in blood pressure that are caused by cyclical ventricular contractions. The aorta, the pulmonary artery, and the carotid artery are all examples of conducting arteries in the body [17]. Conduit arteries, such as the brachial, radial, and femoral arteries, are branches of conducting arteries; they carry blood to specific parts of the body [18]. The microcirculation is made up of the resistance arteries that branch off from the conduit arteries and are responsible for supplying enough blood to the organ tissue. Arterioles are small blood vessels that dilate and close in response to sympathetic (de)activation. They are made up primarily of smooth muscle cells and are densely innervated by sympathetic nerves [19]. Shear stress, which is defined as the dragging frictional force that is applied on the arterial wall by laminar blood flow, is an additional stimulus that might trigger arteriole dilatation [20].

Capillaries, along with arterioles, are a part of the microcirculation and are where tissue perfusion actually takes place [19]. The primary role that capillaries play in the body is to facilitate the movement of gases, metabolites, and nutrients from the blood into the surrounding tissue. This is made possible by the capillary walls, which are made up of a single layer of endothelial cells.

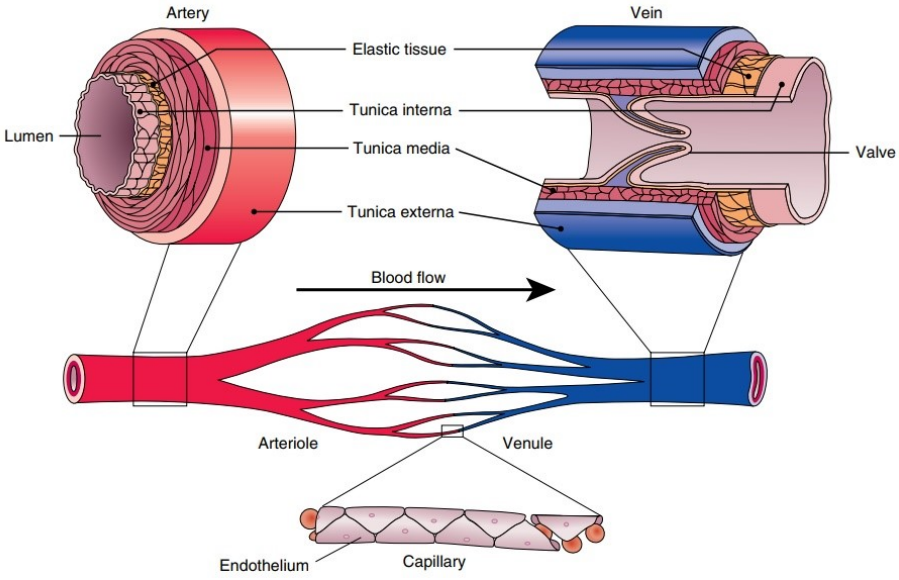

Figure 2.1: Structure of blood vessels (artery, vein, and capillary). Arteries and veins are connected to each other through capillaries [1].

As a result, the channel for diffusion between the blood and the tissue fluid is made significantly shorter. The slow blood flow serves to increase the time that is available for diffusion, which helps to further raise the efficiency of the diffusion process [21]. After this process of gaseous exchange, the blood with its metabolites enters the venules, where additional gaseous exchange may take place.

Superior and inferior vena cavae, which are attached to the heart, receive blood from the peripheral veins. The closer a vein is to the heart, the larger its diameter will be. Vein walls are thinner and more flexible than artery walls because of the lower blood pressure in the venous system. As a result, veins can store a lot of blood at relatively low pressure. Veins have valves to prevent blood from flowing backwards, and the presence of smooth muscle cells in the vascular wall causes veins to constrict, elevating blood pressure and so facilitating greater venous return [22].

The veins carry blood back to the heart from the rest of the body. There are normally two groups of veins in fingers, which are referred to as the superficial veins

and the deep veins. The superficial veins are very important for the body's cooling system. According to research carried out by Hirata et al. [23], when the body is subjected to high temperatures, the blood from the periphery travels back to the heart mostly via the superficial veins. This helps to ensure that the body does not overheat.

2.1.1 Blood flow of arteriovenous anastomoses

Arterio-venous anastomoses, also known as AVAs, are connections that are found between small artery and venous plexuses (Figure 2.2). These AVAs are found in abundance in distal extremities, such as the fingertips and toes [24]. According to Bergersen et al. [25], one of the potential causes of cold-induced vasodilation (CIVD) is an abrupt expansion of the AVAs. When the ambient temperature is higher, the AVAs will open, allowing blood to flow back directly through small veins from the small arteries that are found in AVA branches. This results in dramatically increased blood flow and, as a consequence, greater heat loss. As the ambient temperature drops, the AVAs will close, which will result in a decrease in the amount of blood that flows through the skin [3]. This will help the body retain its heat.

In response to exposure to low temperatures, blood from the body's periphery travels back to the heart via the deep veins in order to minimise the amount of heat that is lost. This, in turn, causes the blood in the nearby arteries to become cooler by means of a mechanism that facilitates countercurrent heat exchange. As a direct consequence of this, the blood in the arteries is pre-chilled before it flows into the capillaries, whereas the blood in the veins is pre-heated before it flows into the larger veins. This mechanism ultimately limits the body's heat dissipation in cold settings, which helps to keep the core temperature within a particular range, while also creating lower hand skin temperatures [26, 27, 2].

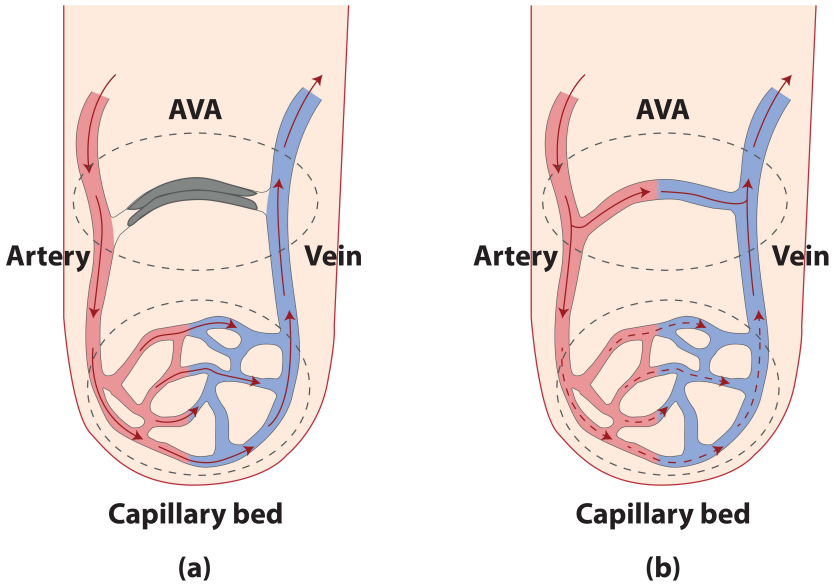

Figure 2.2: Illustration of an arteriovenous anastomosis (AVA) in the fingers. AVA Closed in (a) and Open in (b [2].

2.2 Oscillations in skin Doppler perfusion and the physiological roots of these oscillations

Only four years after Maiman [28] had successfully demonstrated the first working laser, Cummins et al. [29] proposed a method by which the velocity of particles in solution could be estimated by interpretation of the Doppler frequency shift in light in back-scattered light. After a few years had passed, Riva et al. [30] utilised this method to measure the velocities of red blood cells while they were flowing through a glass tube model. However, Stern [31] was the first person to employ the laser-Doppler technique in order to quantify blood perfusion in a microcirculation that had not been disturbed. Watkins and Holloway [32] and Nilsson et al. [33] were the first

to develop the corresponding instruments for measuring blood perfusion, and they were pioneers in this field. The findings of Fischer et al. [34] showed that there is a strong association between the readings obtained from the devices and microvascular blood flow. Despite the fact that clinical trials conducted in a variety of settings had positive outcomes, applications of the method have not been particularly prevalent. Clinicians typically cite, as the primary reason, the fact that the absence of absolute units makes it difficult to compare data from multiple subjects. On the other hand, there is no comparable method that we are aware of for the noninvasive continuous recording of peripheral blood flow.

According to data, blood flow is shown to oscillate in a regular pattern around a stable value [35, 36, 37]. The lack of absolute units does not affect the detection of oscillatory variations in the flow, and we can calibrate the system by use of a reference value. Oscillation periods are continually varied (aperiodic) as a result of physiological perturbations brought on by the open nature of the biological system. Consequently, a time-frequency analysis of the signal is required. However, issues with time and frequency resolution arise when oscillations exist on drastically different time scales. Calculating the Fourier transform of a physical signal (e.g, blood flow) allows one to evaluate the dynamic qualities of the signal. Within this transform, the original signal is windowed either to reduce leakage or to achieve time localization (in this case, the short time Fourier transform is obtained). Both of these goals can be accomplished by windowing the signal. Throughout the entirety of the investigation, the decision of window length remains an extremely important factor. Stefanovska et al. [38] however, presented a method to eliminate the explicit choosing of a window length by using the wavelet transform on blood flow signals. The time and frequency of the fluctuations can be observed at the same time.

Stefanovska et al. [38] used the wavelet transform to study the oscillations in the peripheral blood flow signal. The frequency region that ranged from 0.005 to 2Hz

was investigated. As there is no known physiological rhythm with a frequency that is higher than that of the heart beat, the highest frequency limit was set at 2Hz. The spectrum analysis of cardiovascular functions revealed that frequencies over 2Hz contain only higher harmonic components.

The selection of a lower frequency limit was determined in relation to a number of physiological oscillations that were seen across a continuous time variation [39]. In order to explore the lower frequencies and capture the sluggish oscillations, we needed to make the recordings for a longer period of time. The amount of blood that is pumped out of the heart (when it is at rest) in one minute is roughly equivalent to the total amount of blood that is found in the body [38]. When analysing the dynamics of blood distribution, it is sufficient to set a low frequency limit of 0.005 Hz as a limit on the frequency range. This line of thinking prompted a large number of studies in which researchers explored the dynamics of microvascular blood flow at frequency intervals ranging from 0.005 to 2 Hz.

Six distinct frequency intervals were identified by using the wavelet transform of the blood flow signals averaged over a period of time [4, 38, 40]. This was done in conjunction with prior physiological knowledge. These frequency intervals make their presence known in the dynamics of blood flow, which in turn reflects a variety of physiological processes taking place affecting the microvascular system.

These similar frequency intervals have been used in the analysis of heart rate variability as well as blood pressure signals [41]. Table 2.1 provides a summary of the physiological contributions made by oscillatory processes within these intervals, and we will now analyse these contributions in further detail:

Band	Frequency range (Hz)	Physiological origin
I	0.6 – 2 Hz	Cardiac activity
II	0.145 – 0.6 Hz	Respiration
III	0.052 – 0.145 Hz	Myogenic activity
IV	0.021 – 0.052 Hz	Neurogenic activity
V	0.0095 – 0.021 Hz	NO-dependent endothelium activity
VI	0.005 – 0.0095 Hz	NO-independent endothelium activity

Table 2.1: Oscillations in blood flow dynamics and their physiological causes in various frequency intervals [4].

2.2.1 Frequency interval I: Cardiac

The heart is the most obvious cause of physiological oscillations. Its self-sustained oscillations allow it to perform its fundamental task of pumping blood through the circulatory system, although these oscillations are not completely autonomous from other activities in the body. The heartbeat's frequency and strength are strongly controlled by a demand/supply mechanism [42], which maintains the system's stability and coordination through inter-oscillatory interactions. Heart activity in healthy subject can be detected in a signal recorded on the skin using laser-Doppler flowmetry (LDF), indicating that the heart's pumping action has spread to the peripheral capillary level [43].

It is commonly recognised the heart of a healthy, resting human beats at a rate of roughly 1Hz, while this rate can drop to as low as 0.6Hz in athletes and rise to as high as 1.6Hz in those with compromised cardiovascular systems. In the same way that cardiac activity may be detected all over the body, including in the microvascular skin perfusion signal, it is also reflected in all arterial blood vessels [44, 45]. As a result of pressure differences generated by the heart and lungs, blood flows through the body's

peripheral arteries.

2.2.2 Frequency interval II: Respiration

The expansions and contractions of the lungs during respiration cause an oscillatory pressure to be generated in the network of vessels [46]: the mechanism of its propagation in the blood flow is more nuanced than that of cardiac oscillations, and the shape of a respiratory peak in the power spectra of LDF signals is more sensitive to the subject and location. In addition, the respiratory activity modulates over the heart, causing the heart's rhythm to quicken and slow down with each breath that is taken thanks to a coupling that is known as respiratory sinus arrhythmia (RSA) [43, 47].

In 1993, Bolinger et al.[48, 49] discovered that changes in respiration were responsible for inducing high-frequency (HF) waves, which corresponded to oscillations at a frequency of approximately 0.3 Hz [49]. In contrast to the oscillation of the heart, the blood flow signal from the microvascular system does not substantially display the activity of the respiratory system [48].

2.2.3 Frequency interval III: Myogenic

It is believed that the vascular myogenic process is responsible for the establishment of spontaneous vascular tone as well as the narrowing of blood vessels in response to an increase in intravascular pressure and their widening when the pressure is reduced. Theoretically, the myogenic response is physiologically significant for producing a background vasomotor tone against which vasodilators can function, and for regulating blood flow and capillary pressure [50]. At a frequency of roughly 0.1 Hz, which is typical of myogenic activity. The cardiovascular and respiratory systems work together to pump blood via the circulatory system. Myogenic autoregulation is

a process by which the latter can aid in regulating blood flow. Increased intravascular pressure causes the vascular smooth muscles to contract, while decreased pressure causes them to relax [51, 52]. The amplitude of myogenic oscillations has been shown to rise as a result of exercise [53, 54] and to decrease as a result of local cooling [55] by the use of wavelet analysis.

2.2.4 Frequency interval IV: Neurogenic

The peripheral circulation is controlled in such a way that it distributes cardiac output to the body's many organs and tissues according to their specific metabolic or functional requirements. This occurs while the arterial blood pressure is maintained within a relatively narrow range. The innate capacity of vessels to react to a wide variety of mechanical factors (for example, wall tension and shear stress) in addition to chemical stimuli allows for the effective regulation of regional blood flows at the local level (e.g., tissue metabolites and O_2). On top of this local control system is another level of regulation that is governed by changes in central brain activity.

This level of regulation adjusts the function of the cardiovascular system so that it can meet the requirements of the body as a whole. This type of remote control is an important means to effect rapid changes in blood pressure, in the amount and distribution of cardiac output, and in the distribution of blood volume. These changes are essential to maintain vital perfusion of the heart and brain in the face of physiological and environmental challenges. Thus, these changes to cardiovascular function need coordinated activity of central cerebral outflow to the heart and blood vessels, and cannot be accomplished exclusively by local vascular control systems [56].

The heart, lungs, and all blood vessels, with the exception of capillaries, are all innervated by the autonomic nervous system. Its constant activity works to maintain the baseline level of vascular constriction in the body. The nerves are responsible for the release of substances that have an effect on the actions of smooth muscles, which

in turn leads to changes in the radii and resistance of the vessels. Because of this, the nervous system is involved in the process of vasoconstriction [57]. Blood pressure, blood flow, and HRV signals have all been seen to exhibit a peak at approximately 0.03 Hz. It was postulated that it could have arisen either from metabolic [58] or neurogenic activity [59].

2.2.4.1 Control of skin blood flow

There are cutaneous circulatory processes that control the amount of blood being pumped through the skin. This function is directly related to the regulation of the body's temperature. Both thermoregulatory reflexes (reflexes that are driven by the skin's temperature and by the body's core temperature) [60] and non-thermoregulatory reflexes can affect the blood flow to the skin (e.g, baroreflex). Such reflex control, in nonglabourus skin, is produced by two arms of the sympathetic nervous system: an adrenergic vasoconstrictor system like that found innervating practically all the blood vessels and a distinct, nonandrogenic vasodilator system. Moreover, the cutaneous blood vessels respond to direct cooling or warming of the tissues with decreases or increases in blood flow, respectively, depending on the direction of the response [61].

All areas of nonglabrous skin are innervated by sympathetic vasoconstrictor and vasodilator nerves, whereas glabrous skin (palms, soles, lips) is innervated only by sympathetic vasoconstrictor nerves. Norepinephrine is released by sympathetic vasoconstrictor nerves, and it binds to postsynaptic α_1- and α_2-receptors on cutaneous arterioles and AVA, where it causes these receptors to contract. In addition, noradrenergic vasoconstrictor neurons are responsible for the release of one or more cotransmitters, which are also responsible for vasoconstriction. In thermoneutral environments, the vasoconstrictor system that is present in human skin remains tonically active [62]. The vasoconstrictor system is also responsible for the reductions

in cutaneous blood flow that occur when an individual is exposed to cold temperatures. During hyperthermia, the activity of these nerves is inhibited, which leads to a 10% to 20% increase in the cutaneous vasodilation [62].

In humans, hyperthermia can cause the blood flow to the skin to increase to between 6 and 8 L/min, which is equivalent to around 60% of the cardiac output [63]. The activation of sympathetic vasodilator nerves in the skin is responsible for the majority (80–90%) of the substantial increases in skin blood flow that occur as a result of the stimulation [60, 64]. In humans, the sympathetic active vasodilator system is not tonically active when the body is at its normal temperature of normothermia; rather, it is only activated when there is an increase in the body's internal temperature, such as that which takes place during exercise or when the body is exposed to heat exposure [60, 65, 66].

2.2.4.2 Control of heart rate

The dynamics of the heartbeat as well as its own spontaneous fluctuations are directly controlled by the outflow of the autonomic nervous system (ANS) to the heart [67]. Parasympathetic (vagal) and sympathetic (adrenal) ANS branches interact in complex manners, illustrating the multipath feedback system for brain control of the heart [68]. The time-varying, spontaneous variability of HR is regulated via three key physiological controls: blood pressure management, temperature regulation, and respiration. Sympathetic and parasympathetic activity interact to affect sinus node activity and cause this variability. Indeed, the purpose of the cardiovascular homeostatic regulation is to keep the arterial blood pressure at a constant level in accordance with the amount of blood that is being demanded from the peripheral circulation [69].

2.2.4.3 Control of blood pressure

The arterial baroreflex functions to achieve and sustain a constant blood pressure. This reflex system adjusts heart rate, peripheral vascular tone, and other autonomic cardiovascular factors to restore blood pressure to a normal range. Baroreceptors, also known as stretch receptors, are mostly found on the arterial walls of the carotid arteries and the aorta. These walls are where information about blood pressure is detected. These receptors are able to detect a shift in the dilation of artery walls whenever there is a change in blood pressure. This shift in dilation is then communicated via afferent neural fibres to the control centres that are situated in the brain stem. In order to ensure correct control over blood pressure, these centres receive the inputs from baroreceptors and adjust autonomic outflow, causing changes in cardiovascular variables (primarily heart rate, cardiac contractility, and vasoconstriction) [70].

Vasoconstriction and vasodilation work together to maintain a constant blood pressure throughout the body. (i.e., by adjustment of vascular resistance). The change in the resistance of the vessel is related to the length (L) of the vessel and the viscosity (η) of the blood. Inversely proportional to the radius of the vessel raised to the fourth power (r^4). This relationship makes it clearly evident that the sympathetic nervous system, which is responsible for controlling vessel diameter, may exert a great influence over the regulation of blood pressure with relatively minor alterations in artery diameter [71].

$$R \propto \frac{\eta L}{r^4} \tag{2.1}$$

2.2.5 Frequency interval V: NO-dependent endothelial activity

The vascular endothelium is a single cell layer that forms the inner lining of blood vessels and performs various tasks that are important to the homeostasis and tone of the vascular system. Vascular tone is regulated locally by the endothelial, which releases both vasodilator molecules (such as endothelium-derived relaxing factor [EDRF] = nitric oxide, NO) and vasoconstrictor compounds (such as endothelin) [72].

The layer of endothelial cells that lines the inside of blood vessels not only acts as a barrier between the blood and the tissues of the vessels, but it also controls the contraction and relaxation of smooth muscle by releasing a variety of different compounds. It would appear that the activity of endothelial cells is what adjusts the amounts of various chemicals in order to mediate the metabolic regulation of blood flow. Nitric oxide, chemical formula NO, is considered to be one of the most vital vasoactive chemicals. It was observed that the interval V was controlled by the suppression of NO production of the endothelium [73], which suggests that this interval is related to NO produced by the endothelium. The dependence on NO of the oscillations in this frequency interval has been demonstrated by a study that was conducted on its own [74].

A frequency of around 0.01 Hz, corresponds to NO-related endothelial activity. While it travels through the network of vessels, the blood delivers nutrients to the cells and eliminates the waste products that are produced by their metabolism. Compounds that are involved in metabolism, such as oxygen or carbon dioxide, have an immediate influence on the degree to which the muscle of the blood vessels contracts. The term "metabolic regulation" refers to the process of controlling blood flow based on quantities of metabolites in the body. The oscillations around

0.01 Hz appear to originate from endothelial activity, as shown by Stefanovska and Kvernmo and their co-authors through the simultaneous iontophoretic application of acetylcholine (ACh, an endothelial-dependent vasodilator) and sodium nitroprusside (SNP, an endothelial independent vasodilator) [38, 73, 75, 76, 77].

2.2.6 Frequency interval VI: NO-independent endothelial activity

In contrast to frequency interval V, oscillations around 0.005-0.0095 Hz were found to be significantly higher in response to ACh compared with SNP. It is inferred that the genesis of these oscillations originated from endothelium-related mechanisms such as endothelium-derived hyperpolarizing factor (EDHF) [78, 77].

A frequency of around 0.007 Hz, appears to correspond to NO-independent (possibly prostaglandin-dependent) endothelial activity. This interval was not discovered in some of the earlier research, most likely due to the fact that 20 minute recordings did not give sufficient low frequency resolution, and these oscillations were filtered out during the data pre-processing stage. On the other hand, a significant peak was found to exist about 0.007 Hz later on [78, 55], and this peak can be seen quite plainly in the work that has been done. When ACh was introduced iontophoretically, it was discovered that the wavelet amplitude at the corresponding frequencies varies between healthy subjects and patients suffering from heart failure [77].

2.3 Temperature and cardiovascular response

2.3.1 Thermoregulation within thermoneutral zone

The thermoneutral zone has been studied since the 1940s and 1950s [79], when Scholander and his colleagues first proposed the idea. The temperature range in which

metabolic heat generation and evaporative heat loss may be controlled independently of one another, leaving temperature regulation solely to the control of sensible (dry) heat loss [80]. The regulation of sensible heat loss in this context refers to the processes of controlling heat loss via conduction, convection, or radiation [81]. This indicates that vasomotor control is the only method of thermoregulation that can take place in the thermoneutral zone [82, 83, 84, 85].

Figure 2.3 illustrates the thermoneutral zone (TNZ) idea. When the temperature drops below the TNZ's lower critical temperature (LCT), the body can maintain a steady internal temperature by increasing metabolic heat generation (via shivering and/or non-shivering thermogenesis). Once temperatures rise over the upper critical temperature (UCT), heat can be balanced by means of increased evaporation (sweating). Sweating and its accompanying vasodilation help humans keep their core temperatures stable by increasing the rate at which heat is transferred from the internal to the external environment [86]. Above the UCT, there is also an increase in heat production, which is caused by greater blood circulation, the activity of sweat glands, and an overall higher body temperature [87].

The relationship between the TNZ and the ambient temperature is defined differently by various research fields. For instance, in the built environment, operating temperature is utilised, which is a weighted mixture of air temperature and radiative temperature [88, 89, 90]. Others use the temperature of the air (dry bulb) or directly control the temperature of the skin via water immersion or a suit that is perfused with water. The thermoneutral zone in water is higher (33–35.5 °C) than in air (28.5–32 °C) due to the different thermal characteristics (mostly conduction) [85]. In this research, the TNZ refers to air temperature (i.e. dry bulb temperature).

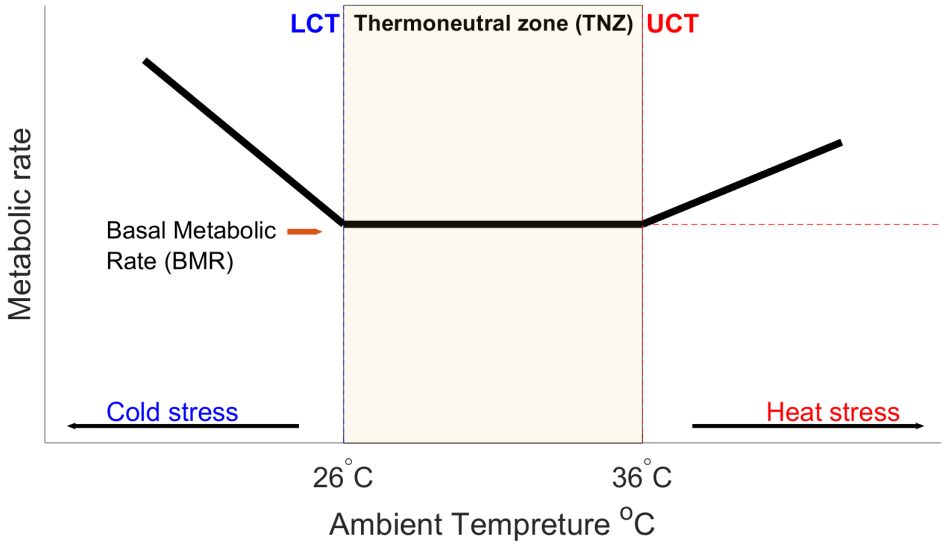

Figure 2.3: A diagram showing how the resting metabolic rate of an unclothed human varies with the temperature of the surrounding environment [3].

2.3.2 Impact on blood flow of raising the ambient temperature

Temperature is an essential factor that changes because of several factors in the body that affect the cardiovascular system's operations, such as blood flow. Fenton et al. [91] agree that ambient temperature in humans increases because of pathological situations like inflammation and fever, which impact the cardiovascular system. The study reveals that increased core temperature in extreme cases even to 42°C will contribute to cardiovascular dysfunction. So, the research offers insight into how high ambient temperature contributes to issues like increased heartbeat and high blood circulation rate. Gordon [92] reported that increased body or ambient temperature affects cardiovascular functions. The study focused on mice's response to changes in temperature and concepts of core temperature regulation and variability to understand how a shift in ambient temperature will affect the cardiovascular

system. The research outcomes showed that control of skin blood flow, insulation, and conductance of heat from the body to the surroundings are vitally connected thermos-regulatory factors directly influenced by ambient temperatures.

Savage and Brengelmann proved [83] that temperature change is influential in managing skin blood flow. The authors used four men and four women to investigate how temperature changes affect the control of skin blood flow. The study's outcomes reveal that increased body temperature significantly impacts blood flow because of the reflex response to skin temperature. Another study by Mitchell et al. [93] agreed that ambient temperature in endotherms including humans has a credible impact on peripheral blood flow. The focused on systematic reviews of various studies that offer ideas on the relationship between temperature and cardiovascular functions like blood flow. The outcomes depict how a shift in the body or ambient temperature is related effectively to an increase in blood flow rate in the body. For example, if the existing thermoregulatory drive focuses on protecting body heat, the peripheral flow is reduced, and the surface temperature reduction may tend towards ambient temperature. However, if the thermoregulatory purpose is to dispel body heat, the peripheral blood flow increases, causing a rise in body temperature and arterial blood temperature. Therefore, the study effectively explains how knowledge about thermoregulatory factors in the body or surroundings and ambient temperature gives insight into cardiovascular factors like blood flow.

Ogawa et al. [94] agreed that there is a close connection between ambient or room temperature and blood flow. The authors studied 16 healthy male volunteers, including eight elderly individuals aged 68-78 and 8 young people aged 20-25 years to test how people of different ages respond to changes in temperature. In the experiment, blood flow was considered a credible indicator in testing how the body or cardiovascular system responds to ambient temperature changes. The study outcomes revealed that blood flow is standard at warm temperatures, reduced at

cool temperatures, and increased at high temperature in young individuals compared to older adults. However, Natsume et al. [95] revealed that the change in blood flow with temperature arises because of factors like vasoconstriction and vasodilation. The analysis proves temperature change interferes with cardiovascular processes like blood flow.

2.3.3 Impact on respiration of raising the ambient temperature

Respiration is another activity of the cardiovascular system that is influenced by the changes in ambient temperature. Collaco et al. [96] agree that ambient temperature affects respiration. They considered the function of the lung in seeking insight into how ambient temperature affects respiration rates. Besides, the study describes temperature as a risk factor for several adverse outcomes in respiratory diseases. Collaco and the team considered a cohort study that included 14088 men and 14036 females to test the connection between ambient temperature and lung function. The study outcomes reveal that warm ambient temperature lowers lung functions, and an increase in ambient temperature will affect the respiration rate in human beings.

Jensen and Brabrand [97] agree that a heightening of respiratory rate always precedes an increase in body temperature. Their survey focused on the impact of factors like temperature on respiration and concluded that adjusting blood temperature contributes to elevated respiration rates. Cho et al. [98] showed experimentally that an ambient temperature causes increased respiration rates. The research revealed how respiration rate could be determined effectively by monitoring the temperature changes around the nostrils. Essentially, the use of a robust respiration tracking algorithm showed that the cyclical changes in temperature around the nostrils occurs because of the exhalation and inhalation breathing cycles. Also, in

high ambient temperature, the lungs and cardiovascular system respond by increasing the respiration rate to restore the temperature to the normal range.

2.3.4 Impact on blood pressure of raising the ambient temperature

Blood pressure is affected by changes in ambient temperature [99]. The researchers found that a low temperature causes blood vessels to narrow, elevating blood pressure. Increasing ambient temperature leads to the dilation of blood vessels, raising blood pressure. Besides, to understand how raising ambient temperature affects different measures of blood pressures, Inoue et al. [100], studied how temperature change shifts the diastolic and systolic blood pressures. Their research tested how the blood pressures of older and younger men respond to changes in temperature, through measurements on nine younger men and ten older men. It was found that, older men experienced a higher rise in both their systolic and diastolic blood pressures after being exposed to cold temperatures.

Contrary, the reduction in skin temperature results in lessened diastolic and systolic blood pressure in young men compared to older men. Besides, to prove this allegation, Lossius et al. [101] investigated how thermoregulatory fluctuations affect the mean blood pressure in humans because of its connection with heart rate and blood velocity. Their study used nine healthy volunteers, four males and five females, without a background of cardiovascular diseases to test the thermoregulatory response of their bodies. The researchers concluded that the vasoconstrictor impulse resulting from the increased temperature in the body lowers mean blood pressure. Jansen et al. [102] studied 20 adult normotensive volunteers to investigate how ambient temperature impacts systolic and diastolic temperature levels. They concluded that, raising ambient temperature contributes to reduced diastolic and systolic blood

pressures.

2.3.5 Impact on cardiac output (heart rate and stroke volume) of raising the ambient temperature

Heart rate and stroke volume can also be affected by changes in ambient temperature. The study by Lossius et al. [101] concluded that change in temperature, such as cooling or heating of the surroundings, contributes to fluctuations in heart rate. They used nine healthy volunteers to define how a change in temperature affects heart heart rate and other cardiovascular system. The study showed that thermoregulatory fluctuations interfere with heart rates. For example, an increased skin temperature makes the heart beat faster. Shin [103] used pulse rate variability to prove the assertions that ambient temperature affects heart rate. Pulse rate variability acted like an alternative to heart rate variability that can be determined using wearable equipment. The researchers enrolled twenty-eight healthy young participants in a temperature-controlled room with an electrocardiogram to measure heart rate variability in different ambient temperatures. It was found that increased ambient temperature raises the heart rate. Madaniyazi et al. [104] focus on improving the understanding of the link between ambient temperature and heart rate. They analysed data from 47591 residents, alternating ambient temperature from 22°C to 28°C while observing blood pressure and heart rate. The results revealed that increased temperature will always contribute to an elevated heart rate.

Similarly, the rise in ambient temperature interferes with stroke volume in the cardiovascular system. Wilson and Crandall [105] agree that hot and cold ambient temperatures impact the control mechanism of stroke volumes like diastolic function, afterload, preload, and systolic inotropy or function. For example, hot ambient temperature conditions raise cardiac output, which can also slightly elevate the

stroke volume. The study focuses on systematic reviews that understand ambient temperate's impact on cardiac output, including stroke volume. A survey by Lafrenz et al. [106] describes how ambient temperatures affect cardiovascular drift, contributing to a rise in heart rate and a reduction in stroke volume. The research centered on male subjects to emphasise the consequences of the connection between ambient temperatures and stroke volume, Lian et al. [107] demonstrated that an increase in temperature elevates stroke risks. Essentially, the study outcomes revealed that exposure to ambient temperature by 1°C increased the risk by 1.13 % (0.58–1.68), while a decrease in 1°C increased the risk by 1.2 % (0.84–1.57).

3. Physiological measurements and methods of analysis

Significant advancement in measurement techniques based on a variety of fundamental principles, from light to electricity, have made it possible to observe and record spontaneous dynamics in living systems. Methods of data acquisition are described in this chapter. Methodologies for monitoring and analysing the physiological signals covered in Chapter 3 are presented in this chapter.

3.1 Participants

The research was conducted on a total of twenty-nine young and healthy human subjects, fifteen of whom are females and the rest (14) are males. However, due to lack of data, one subject was excluded from analysis and later on when coherence analysis was performed another subject was removed due to lack of respiration signals. Therefore, most of the analysis was performed on 28 subjects (power and coherence analysis), but when coherence analysis was performed between respiration or instantaneous respiration rate (IRR) with other physiological variables, 27 subjects were included. The participants' ages ranged from 22 to 27 years old, their height was between 176 and 181 cm, and their weight ranged from 61 to 75 kg. The participants are non-smokers, and with the exception of contraceptives, they did not use any

medications. They were instructed to not consume any beverages containing caffeine and not to engage in physical activity for at least twelve hours before the experiment. In addition to that, they consumed a dinner consisting primarily of lighter fare two hours before the beginning of the experiment. Every participants indicated that they were in good health, and none of them had any signs or symptoms of cardiovascular illness. A review of the protocol (Letter of exemption (IRB 00001870/XXX))was conducted by the regional ethics committee, and the procedure was subsequently accepted by NSD (ref. code 658935).

3.2 Experimental protocol

The experiments were carried out inside a climate chamber. The participants were wearing shorts and a singlet while lying supine on a bench and being subjected sequentially to three different ambient temperatures (see figure 3.1). Two protocols were used, and each participant was randomly assigned to one of them. As shown in figure figure 3.1, protocol 1 included a temperature rise from 20°C to 32°C, with three distinct plateaus at 20°C, 26°C, and 32°C. Protocol 2 resulted in a cooling effect with temperature plateaus at 32°C, 26°C, and 20°C, as shown in figure 3.1.

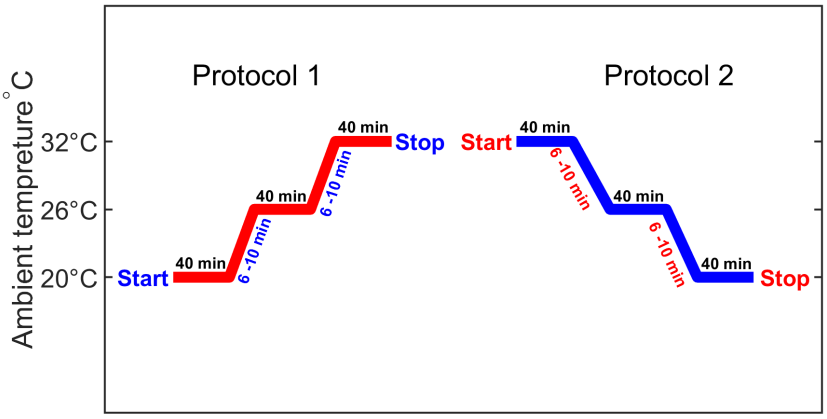

Figure 3.1: Two different experimental protocols were used for the study: Protocol 1 and Protocol 2. The temperature plateaus that last for forty minutes. The transitions between the plateaus take between 6 and 10 minutes.

The duration of each temperature plateau was 40 minutes. It took around 6 to 10 minutes for the temperature to go from one phase to the next. During each of the three temperature plateaus, the speed of the fan that was controlling the temperature adjustments was slowed down. A relative humidity of 20% was maintained throughout the chamber. All signals that are investigated in this thesis was obtained from Maja Elstad and her group, University of Oslo, Norway.

3.2.1 Measurement setup

Laser Doppler (DRT4, Moor Instruments, Devon, UK) was calibrated before each protocol and simultaneously captured the beat-by-beat blood flux from the pulp of both index fingers and the volar side of the left forearm. The laser-Doppler sensor had a wavelength of 820 nm, and the noise-limiting filter had a frequency setting of 21 kHz. A filter with a time constant of 0.1 sec was applied to the flux output signal (ref: Bergersen/Vangaard). The temperature of the skin (YSI-401, YSI Inc., OH, USA), as measured by EXACON, was taken from the pulp of the left third finger and from the

non-acral skin in the forehead using probes that were connected with surgical tape (3M Benderm, Micropore No). The heart rate (HR) was measured using a three-lead ECG (SD 100, Vingmed, Horten, Norway), as well as the room temperature (20°C, 26°C, and 32°C), end-tidal CO2 (CAP10), and respiration movement (Respiration and Body position Amplifier, Scan-Med a/s, Drammen, Norway). Continuous non-invasive recordings of arterial blood pressure were taken from the right middle finger using a Finometer manufactured by Finapres Medical System in the Netherlands. These readings provide an estimate of the beat-to-beat cardiac stroke volume (SV) as well as mean arterial pressure (MAP). At the beginning of each temperature plateau, the arterial pressure signal was calibrated in order to ensure accuracy. All of the measurements were recorded in a manner that was continuous and simultaneous, and they were sent online to the computer (program for real-time data acquisition, Morten Eriksen, Norway). The sample rate for arterial blood pressure, electrocardiogram, and respiration movements was set to 100 Hz. On the other hand, the heart rate, mean arterial pressure, systolic blood pressure, pulse rate, and laser Doppler flux data were averaged over one heart beat, leaving the sampling frequency beat-by-beat. The diagram below (Figure 3.2) illustrates the measuring setup and the output of the signal that were recorded.

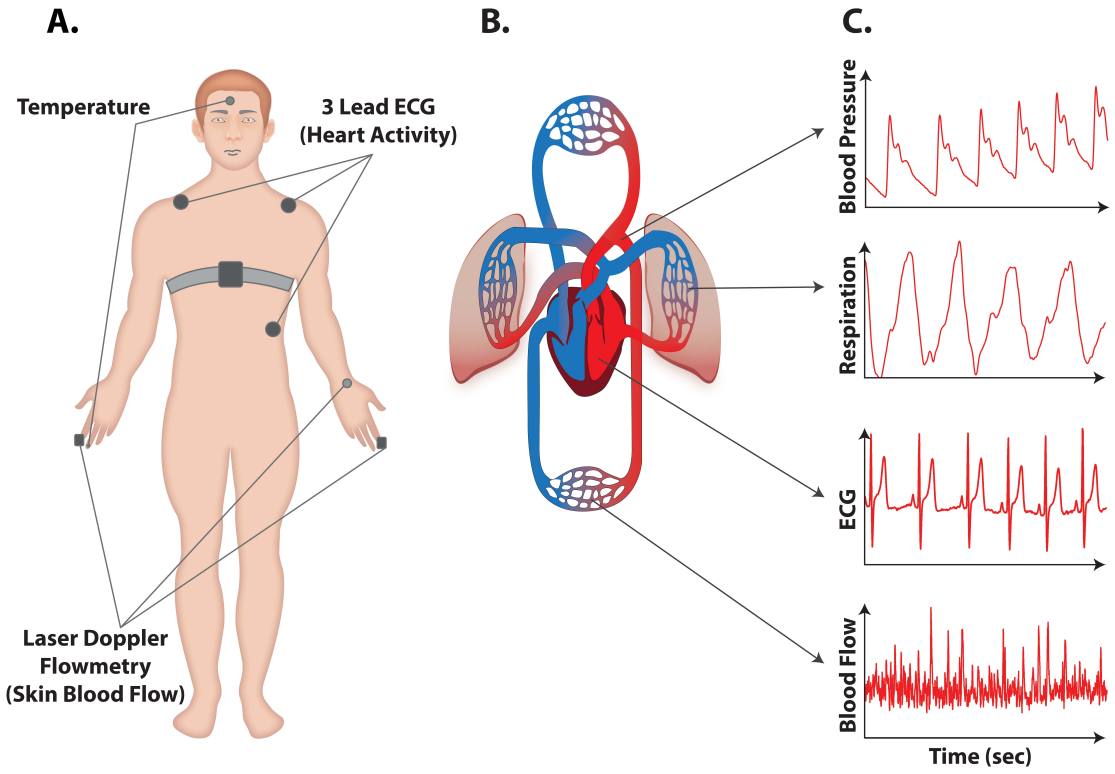

Figure 3.2: Illustration of measurement set-up and output of the recorded signals. A) Location and function of probes on human body during measurements. B) Cardiovascular system with sites of measurement. C) Examples of the recorded signals with arrows indicating their origins: blood pressure captured from artery; ECG measured the heart electrical activity; Respiration measured breathing under the effect of heating or cooling. Finally, blood flow was captured from capillary in the skin of the forearm.

3.3 Cardiovascular variability

The cardiovascular system is extremely important in complex living beings since it is responsible for the delivery of nutrients and oxygen to the major organs, as well as the removal of metabolic products and waste. There are many subsystems within the cardiovascular system that interact with one other and are influenced

by internal and external elements, such as central commands, reflex mechanisms and humoral factors [108]. All of these regulatory mechanisms exhibit a rhythmic mode of action, which results in continuous changes to the cardiovascular variables (e.g. heart rate, heart contractility, blood pressure, vascular tone, etc.) that are observable in recordings made from beat to beat. These fluctuations are referred to as "cardiovascular variability" and can occur across a wide frequency range, including very slow rhythms. The dynamic complexity of cardiovascular variables is caused by the presence of various regulatory mechanisms that are both active at the same time over different time scales and capable of altering the relationships between variables over time.

In order to reduce the dimensionality of the cardiovascular system, the presence of mechanisms favouring synchronisation among the activities of subsystems in accordance with n:m coupling ratios (i.e. n cycles of activity of one subsystem correspond to m cycles of activity of the other) is essential (i.e. on their degree of isolation) [109]. A growing body of research suggests that this variability, which may have both linear and nonlinear components, provides crucial biological information that can be used in the diagnosis and prognosis of cardiovascular dysfunctions. Signal processing techniques and mathematical models are crucial in identifying and extracting the important characteristics from cardiovascular variability [108].

3.3.1 Electrocardiogram

The human heart is considered to be one of the most essential oscillators in the body. Recording an electrocardiogram (ECG) constitutes a non-invasive method that allows for the monitoring of the electrical activity of the heart over time. ECG signals are graphical representations of the bioelectrical and biomechanical activity of the cardiac system, and they are used to diagnose heart disease. An ECG provides essential information regarding the functional features of the heart and circulatory

system [110].

In the heartbeat signal (Figure 3.3), the P wave, QRS complex, and T wave are three features that occur during each beat cycle. Each event has its own peak [111] and they relate to the various actions that take place in the heart during a single heart beat [112]. This is critical in the diagnosis of cardiac arrhythmias since it allows us to examine their shape, amplitude, and duration [111]. The QRS complex is the most recognisable wave set in an ECG signal, and it depicts the depolarization of the ventricles of the heart [110].

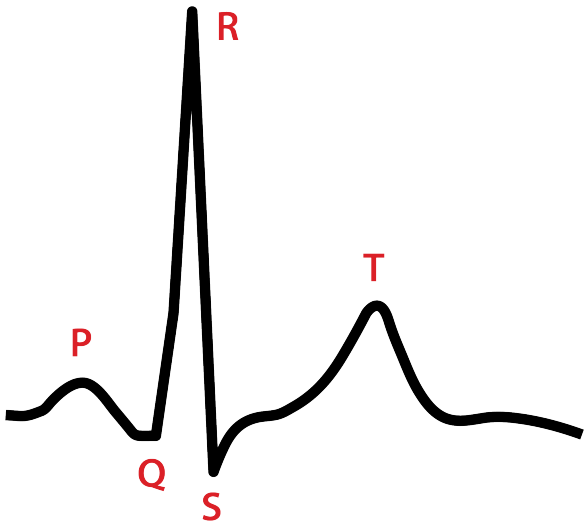

Figure 3.3: ECG waveform for a normal one-cycle recording.

The P wave is produced by the sinoatrial node, which is located high up in the wall of the right atrium. This node is responsible for initiating atrial depolarization. Following the P wave, the Q wave has a downward deflection and indicates septal depolarization. The R-wave is often the easiest wave to detect, and it is regarded to be useful for measuring the heart rate and heart rate variability. This is because the R wave indicates early ventricular polarisation and is also the wave that is most likely to be detected. The S wave indicates the late ventricular depolarization, whereas the T

wave represents the ventricular repolarization (the recovery of the ventricles), which is the last event of the cycle. Together, these waves make up the electrocardiogram (ECG) [113].

3.3.2 Heart rate variability (HRV)

The instantaneous heart rate (IHR) or heart rate variability (HRV) can be calculated from an ECG signal using a variety of different approaches. The time domain method is by far the most frequent and widely used method. In these methods, the positions of the R-peaks are marked, and each interval between subsequent RR peaks is taken as a whole period of oscillation with phase intervals ranging from 0 to 2π. The IHR can then be calculated by taking the reciprocal of the distance between each RR peak. The R-peaks are selected because they are the most conspicuous part of the heart beat and can be found in every cycle. The resolution of this method is affected by the period of the oscillation, which means that there is no instantaneous information accessible between events regarding the frequency or phase. This is one of the method's drawbacks. Since the sampling frequency of the HRV signal is anticipated to vary depending on the period of oscillation, this method necessitates signal linear interpolation. Nonlinear mode decomposition (NMD) [114] is one way to extract the instantaneous frequency from a wavelet transform of an ECG signal while maintaining the same resolution as the original time series. An investigation into HRV can be carried out by analysing the received signal with techniques that will characterise the temporal fluctuations, such as the continuous wavelet transform.

The pattern of the heart rate is determined by the spontaneous respiratory cycle, which causes the heart rate to fluctuate very slightly between inspiration and expiration. This pattern is determined by the rhythm of the heart rate. The term "respiratory sinus arrhythmia" (RSA) [115] is used to describe this alteration. The presence of RSA is a reliable indication that the heart is able to keep up with the

needs of the body on a continual basis. Heart rate is often used as an indicator of overall health. For instance, a high resting heart rate or tachycardia ($>$ 100 breaths per minute) is usually a sign of a heart complication, whereas a low resting heart rate is usually associated with exercise or sports. However, the heart rate variability is more informative because it is widely regarded as a quantitative marker of autonomic activity. Several studies have documented the impact of HRV in various pathological conditions; specifically, HRV is seen to be dramatically decreased in hypertension, atherosclerosis, and diabetic neuropathy.

3.3.3 Respiration Rate Variability (RRV)

Measuring respiration can be done mechanically, which involves taking a direct measurement of chest displacement, or analytically, which involves determining the amount of carbon dioxide that has been exhaled. Using the marked events method described earlier, one is able to determine their respiratory rate. It is feasible to explore cardiorespiratory coupling by employing respiration and heart rate signals [116].

3.3.4 Blood pressure time series

A pulsatile blood pressure is produced in the arteries as a result of blood being ejected from the left ventricle of the heart into the aorta. The greatest pulsatile pressure in the arteries is referred to as systolic blood pressure, and the minimum pulsatile pressure in the arteries is referred to as diastolic blood pressure. The diastolic pressure minimum occurs right before the subsequent ventricular contraction [117].

Several intermediate steps, including peak identification, interpolation, resampling, and spectrum analysis, are required to convert raw signals such as ECG, respiration and blood pressure into heart rate variability, respiration rate variability

and the systolic or diastolic blood pressure extracted from signals. Systolic peaks were identified in the blood pressure data, and values of the systolic blood pressure were obtained by linearly interpolating from the most recently accepted systolic value to the next one as shown in figure 3.4.

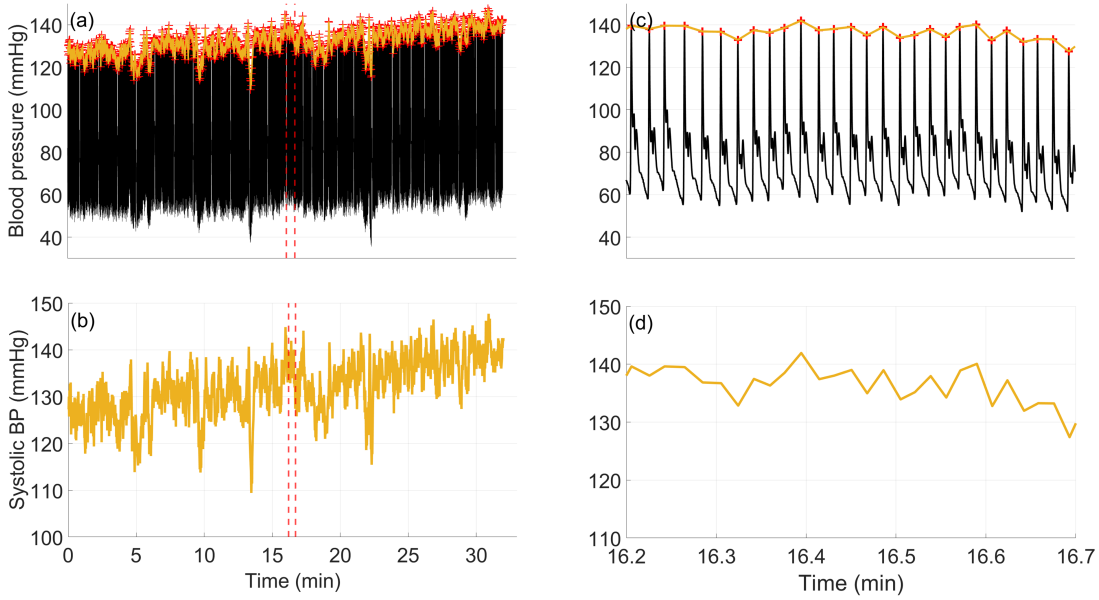

.

Figure 3.4: Example extraction of systolic BP from the BP time series. (a) whole BP time series with detected systolic blood pressure peaks by linear interpolation method. (b) sBP signal after being extracted in panel (a). (c) and (d) panels are 5 sec portion of the BP and systolic BP time series shown in (a) and (b), marked by vertical red dashed lines

Similar analysis steps to those used for systolic blood pressure were also applied to diastolic blood pressure peaks as shown in figure 3.5.

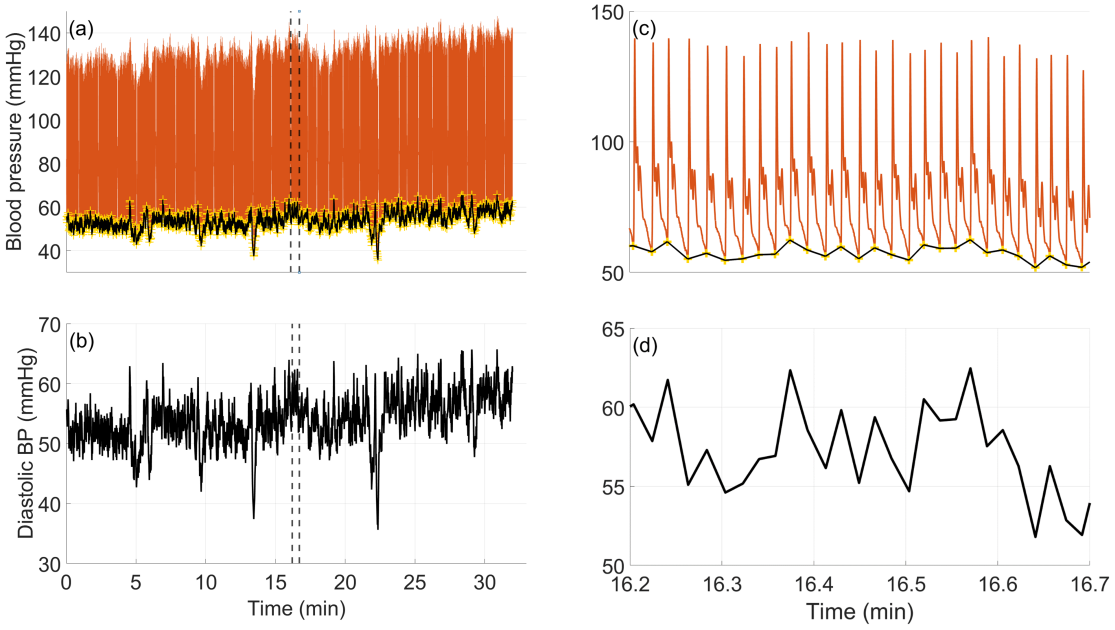

.

Figure 3.5: Example extraction of diastolic BP from the BP time series. (a) whole BP time series with detected diastolic blood pressure peaks by linear interpolation method. (b) dBP signal after being extracted in panel (a). (c) and (d) panels are 5 sec portion of the BP and systolic BP time series shown in (a) and (b), marked by vertical black dashed lines

3.4 Blood flow

3.4.1 Laser Doppler Flowmetry (LDF): A single point measurement

Laser Doppler flowmetry relies on the fact that a laser light beam impinging on tissue is dispersed by both stationary structures and moving red blood cells. The Doppler effect shifts the frequency of light scattered from moving red cells, while light scattered from stationary tissue remain unchanged [33].

When a small area of tissue is illuminated by a beam of laser light, the photons

of the light will be dispersed by both static and moving particles. Depending on the scattering angle, the wavelength, and the velocity vector of the scatterer, the moving red blood cells will impart a Doppler shift to the photon. This shift will depend on the direction of the velocity vector of the scatterer. When a wave with frequency ω is scattered by a moving particle with velocity υ, the Doppler shift can be expressed mathematically as follows:

$$\Delta\omega = \mid \vec{\upsilon} \mid\mid \vec{k_I} - \vec{k_S} \mid \cos\beta, \tag{3.1}$$

where k_I is the incident wave vector, k_S is the scattered wave vector, and β is the angle between the velocity vector and the scattering vector, which is defined as $(\vec{k_I} - \vec{k_S})$. By taking into account: the scattering angle α, and wavelength of light in the medium λ, the Doppler shift can be expressed mathematically as:

$$\Delta\omega = 2(\frac{2\pi}{\lambda}) \mid \vec{\upsilon} \mid \sin(\alpha/2)\cos\beta, \tag{3.2}$$

The photodetector generates a dynamic speckle pattern due to the interference of Doppler shifted light and non-Doppler shifted light. The detector's current signal will fluctuate as a result of these patterns. Homodyne signals in laser Doppler terminology are those that are created solely by the photodetector using Doppler-shifted light. Heterodyne occurs when Doppler-shifted light interferes with non-Doppler shifted light, which is the case when the scattering is from a tissue matrix with a sufficiently tiny volume of blood (dynamic scatterers) [118]. When multiple scattering is neglected, the first-order photocurrent spectral moments are proportional to the product of the mean concentration and speed of moving blood cells (MBCs), and this is consequently known as the flux of blood perfusion and can be found in practically every commercial LDF device [119].

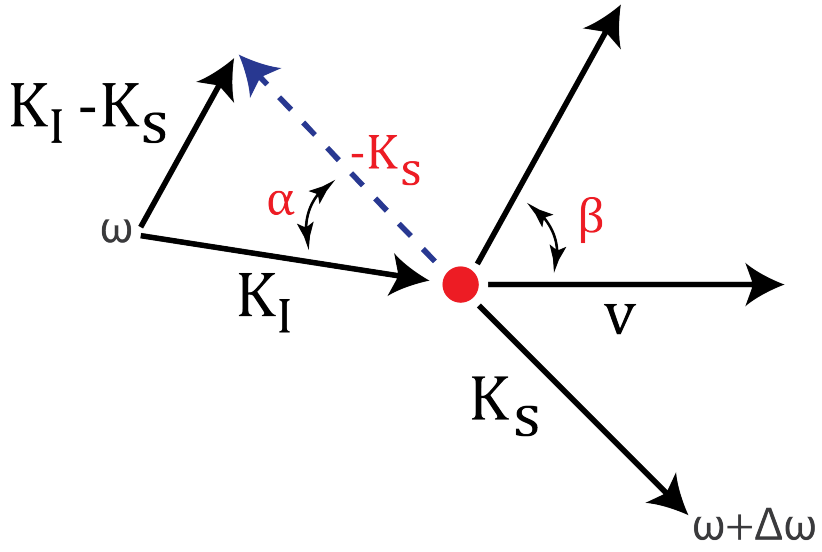

Figure 3.6: Interactions between photons and red blood cells from a physical optics perspective. A photon with the propagation vector k_I being scattered by a red blood cell travelling at the velocity v. After being scattered, the photon now has the propagation vector k_S.

Laser Doppler flowmetry (LDF) can be used to measure variations in human cutaneous blood flow. Oscillations are found in the frequency range (0.0095–2.0Hz) in the frequency spectrum of LDF signals [78].

3.5 Dynamical systems and analysis methods

3.5.1 Introduction

Understanding the fundamental dynamics of living systems calls for a methodology distinct from that used to investigate mechanical systems. Analysis of recorded signals from living systems can be used to derive statistical aspects of the data or to probe possible oscillatory characteristics by quantifying oscillation amplitude, power, and phase. Particular attention will be paid to the characterization of time-varying

oscillatory features, and the resolution of the dynamics will be achieved through optimal temporal localization and frequency resolution.

A dynamical system is referred to as the mechanism that causes a state to change over the course of time. The simplest form can be represented by:

$$\frac{dx}{dt} = f(x), \tag{3.3}$$

where the infinitesimal change of the state x in time t has some dependence on the previous state. This differential equation characterises the dynamical behaviour of the system over an infinite period of time. Although iterated maps can be useful in discrete time [120], this thesis focuses exclusively on continuous time and, consequently, differential equations. Nonautonomous refers to a dynamical system that is explicitly dependent on time, which is also the case in the majority of biological systems. The simplest form of this type of system is:

$$\frac{dx}{dt} = f(x, t), \tag{3.4}$$

It is possible to find an exact solution to a linear dynamical system, or one with a linear output. Most biological systems are nonlinear [121], which makes study more challenging but also more interesting. In contrast to linear systems, nonlinear dynamical systems have the potential to display self-sustained oscillations, which, when they do occur, will lead to the formation of a stable limit cycle in the phase space of the system. A limit cycle is an isolated closed trajectory, and depending on the stability of the limit cycle, the surrounding trajectories will either spiral towards it or away from it [120].

As time approaches infinity, most dynamical systems in nature exhibit a bounded nature of their states; this bounded region is called an attractor, and it is one of the most important features of these systems. Without this property, a system

subjected to persistent disturbances will always deviate from its initial condition beyond recovery.

3.5.2 The connection between living systems and dynamical systems theory

Nonlinearity

If one is provided with all of the details about a linear system at one point in time, it is simple to determine the state of the system at any other point in time, which makes it easy to develop analytical solutions to the problem. This signifies, in essence, that it is possible to understand all of the attributes of the system in the context of a linear model without observing the dynamics of the system. On the other hand, nonlinear systems such as living systems are not capable of being examined in this manner. Even if some of their properties may still be determined analytically, it is not feasible to know what trajectory a nonlinear system will follow without the assistance of computer simulations or by studying the dynamics of real systems. It is also important to note that this is not a question of the complexity of the system; a linear system can be extremely complicated, while a nonlinear system can be rather straightforward, but these fundamental rules still apply to the analysis of both of these types of systems.

Nonlinearity tends to have significant impacts. Mathematical complications aside, it leads to interesting phenomena like hysteresis. This effect represents the situation in which the trajectory that a system follows from one state to another is different from the trajectory that it takes in the opposite direction between the same two states. Because of this, it is vital to consider the arrow of time when performing an analysis of nonlinear systems. The analysis of nonlinear oscillations using techniques developed for linear systems allows for the detection of harmonics, which are modes

caused by nonlinearity [122].

Openness

The openness and ability to interchange energy and matter with the environment are two sides of the same coin that can be used to explain the aforementioned attributes of living systems in the previous section. Dynamical theory often operates under the assumption that the system is closed. The primary theories of dynamical systems often begin with the assumption that the system in question is closed, which indicates that it is independent and can be entirely characterised by its state in space. Living systems, on the other hand, are non-autonomous and open, which implies that their states need to be characterised in terms of both space and time. Therefore, it is very important to incorporate time-dependent factors into the analysis of living systems. It is important to remember that the dynamics of closed systems can nonetheless change over time, making the system statistically nonstationary. Chaotic behaviour is commonly used to describe the complex nonstationary dynamics of closed systems, in which minor disturbances in the trajectory accumulate exponentially with time [123]. Instead of using a chaotic method, stochastic systems are commonly used to represent complex dynamics where the nonstationarity results from the influence of external random variables. Both of these methods are applicable to autonomous systems because they exclude time-dependent variables from the analysis. However, neither of them can reliably be utilised here, because biological systems are not only nonstationary but also non-autonomous [124].

3.5.3 Discerning dynamical systems: Inverse approach

When a living system is considered nonautonomous, a wide range of features can be described. Despite this, the difficulties in their analysis have led to many fruitless attempts to adapt approaches more appropriate to autonomous systems. Analyzing a

phase space attractor is a common first step for deterministic systems. This method works well for autonomous systems, but it ignores the possibility of time-dependent attractors. Despite the fact that this strategy is workable for autonomous systems, all that it does is take into consideration time-dependent attractor patterns [125]. The problem is that incorporating time dependence into the system would in turn lead to extra dimensions in the phase space, which would introduce additional complexity into the system.

Problems involving dynamical systems can be approached in two ways: by modelling the system using a set of equations or by directly measuring the system. For time series analysis, the first instance provides the ideal condition, in which the exact state of the system at any one time is known and all of the parameters may be changed directly. In the latter approach, just a one-dimensional description of the system trajectory is often obtained, making it far more difficult to characterise the phase and inner workings of the system. Both approaches are equally beneficial for the inverse problem. The only difference is that when modelling the uncertainties is added by the constraints of the model rather than by data [124]. In this thesis, all time series were measured directly from the system.

3.5.4 General characteristics of time series

Time series are defined as continuous sequences of data points generated experimentally or numerically. Time series analysis allows one to obtain information about a system's dynamical behaviour. In this thesis, time series were extracted experimentally. It is common practise to take multiple measurements of a system in order to obtain data/information from an experiment. Information can be obtained by two methods; the first is to control the conditions of the system and then assess the response after a time delay. The second method is to start with an arbitrary set of beginning conditions and make N successive measurements over a time step Δt to

create a time series revealing the system's dynamics (time-dependent attributes).

Both procedures are valid, as they eventually yield the same information when sufficient measurements are taken. For complex systems, the simplest method to understand them is to observe the dynamics in a time series. Additionally, time series are more closely tied to real-world situations, because the initial conditions of a system are rarely known [124].

3.5.5 Frequency interval

Generally, to recored a time series experimentally, two fundamental characteristics should be taken into account; the interval $L = N\Delta t$ during which it is recorded (the recording length) and the sampling rate $f_s = 1/\Delta t$ at which samples are taken (the sampling frequency). These characteristics limit the timescales on which the dynamics can be obtained. According to the Nyquist–Shannon sampling theorem, the highest detectable frequency in the frequency domain equals half the sampling frequency, or Nyquist frequency, $f_s/2$. Additionally, $1/L$ denotes the lowest detectable frequency. To achieve a continuous frequency distribution that covers the range 0 to ∞, both L and f_s must be indefinitely large, which cannot be achieved using discrete and finite time series derived from simulations and real-world measurements [124].

3.6 Time series analysis in time domain

Preprocessing

Preprocessing a signal is necessary for effective analysis, but data manipulation should be kept to a minimum. Time series, particularly those obtained experimentally by measuring living systems, may contain artefacts. The causes of these artefacts could be movements or noises made by the equipment utilized in the experiment. These

artefacts affect the statistical parameters of the recorded time series over the whole investigation interval, causing a trend. The process of removal a trend from a time series is called detrending. Detecting, defining, and eliminating trends from time series are essential for data analysis in nearly every field. For statistical approaches like computing correlations and spectral analysis, preprocessing has become a necessary step [126]. Filtering is another consideration in pre-processing. Data should be detrended if mean values are computed or frequency analysis is applied to remove trends. This is because the impacts of frequencies lower than the frequencies of interest in this research may have an influence on the outcome results. The removal of a trend can be achieved by a variety of methods. It could be either statistically or mathematically, and is most often performed in the time domain.

Detrending is best applied by use of a smoothing technique called moving average. This is defined by calculating the statistical mean of the data contained within the window and using that value as the centre point of the window. After that, the window is moved by a single data point. The new mean is then computed, and so on. The effect of this method on the time series can be noticed in the amplitudes. Time series with high frequency components (rapidly changing fluctuations in amplitude) are averaged over and minimized, while slow trends represented in low-frequency components (amplitudes of long-term trends) stay mostly unchanged. It is important to note that, the window length, l, is the crusial parameter that determines how much smoother the output time series appears. In addition to the high-frequency components that are eliminated for smaller windows (i.e. more smoothing), the lower-frequency components are removed if the window is made larger [124]. Additionally, for frequency or time-frequency analysis, it is essential to average the signal and subtract it from the original one.

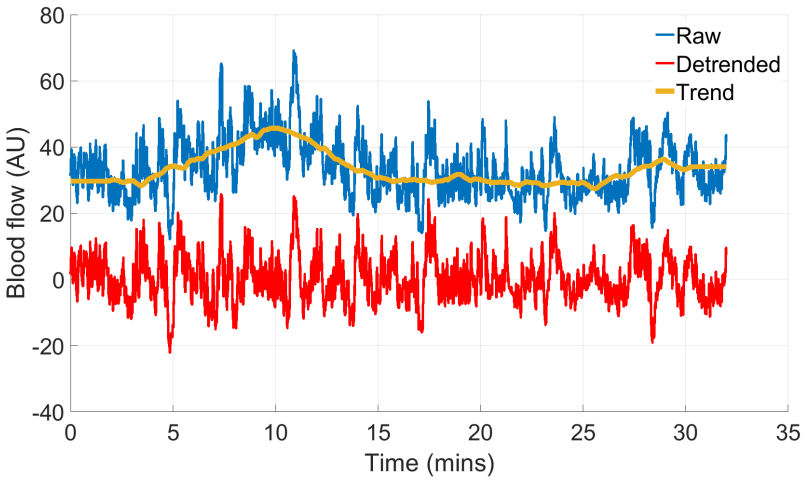

Figure 3.7: A blood flow signal (blue) with the detrended version of the signal (red). In a moving average, a 200s window was utilised to construct the trend (yellow). Low frequencies below the interest were removed and the mean is also subtracted from the total.

However, it is necessary to distinguish between smoothing and filtering. In the frequency domain, filtering contains a direct manipulation or removal of information. In contrast, the effect caused by time domain methods can be described as smoothing. Using time domain smoothing instead of filtering has the advantage of retaining information at each step. However, Fourier components over a specific frequency range can be removed using simple frequency domain filtering and does not preserve information and works poorly when the time series contains non-sinusoidal components (i.e. the harmonics are not affected). Smoothing can be used on nonstationary time series since it operates in the time domain and maintains all time-dependent information in the time series [124].

3.7 Instantaneous phase

Time series of a biological system are subjected to noises of many origins, which are typically unstable in nature. To better understand the individual behaviour of elements of biological systems as well as the characteristics of their interactions, it is required to develop and employ specialised techniques. When it comes to the analysis of complex signals, there is one significant, although quite rare, subject to consider: that of the study of instantaneous phases of oscillations [127]. The separation of 'amplitude' dynamics from 'phase' dynamics is critical to much of the study. The notion of phase used in this context is a generalisation of the 1-dimensional phase that is used in simple harmonic oscillators [124].

$$x(t) = A\cos(2\pi ft + \phi_0), \tag{3.5}$$

The term "rotational frequency" which is univalently related to linear frequency according to the formula: $\omega = 2\pi f$, is usually used for convenience. It is the instantaneous phase of the system that is represented by the *cos* function in equation (1), and it has the meaning of the number of oscillations the system performs in time t since it began taking measurements as an argument of this function, equation (2).

$$\phi(t) = 2\pi ft + \phi_0 = \omega t + \phi_0, \tag{3.6}$$

According to the definition and equation (3.6), the instantaneous phase can never decrease in time, but it can generally grow at a variable rate. Radians or degrees are used to quantify the instantaneous phase (which are univalently related). The phase changes by 360 degrees throughout a whole oscillation cycle, which is 2π radians. In equation (3.6), ϕ_0 is the initial phase of oscillations. Oscillations with basic waveforms may not require instantaneous phase analysis, but complex signals can benefit greatly

from the addition of this information, which can be used to describe their features.

The introduction of instantaneous phase, on the other hand, is a difficult challenge to solve during the study of nonperiodic oscillations, because the fundamental notions of period and frequency cannot be introduced rigidly. Typically, the terms instantaneous period and instantaneous frequency are used in this context, together with their averaged values, which are referred to as characteristic period and characteristic frequency. For the most part, when dealing with instantaneous phase, it is impossible to define it precisely; hence, approximate formulas and numerical approaches are employed [127].

3.8 Instantaneous frequency (IF)

It is common in real-world applications for the spectral characteristics of signals (e.g. frequencies) to change with time. If one is dealing with time-varying signals, it is impossible to define the notion of frequency directly; instead, one must employ a parameter that takes into account this time-varying nature. The concept of instantaneous frequency (IF) arose as a result of this requirement. The concept of an instantaneous value for the frequency must first be justified before we can explore any ways of computing the IF. In the study of any oscillatory motion, frequency is a critical variable to consider and calculate [128]. Frequency (f) is defined simply in terms of elementary physics as the inverse of the length of time (T), that is;

$$f = \frac{1}{T}, \tag{3.7}$$

Following the equation above, the most straightforward method of determining frequency should be the measurement of time intervals between consecutive zero-crossings. This is very obvious for a simple sinusoidal wave with a well-defined period.

When dealing with real data, measuring the period is no longer straightforward because there may be multiple extremes between two consecutive zero crossings. The frequency definitions provided above are only applicable to signals operating in extremely narrow bands. In practice, data are treated as a real variable. Because there are likely to be many extrema between consecutive zero-crossings of the variable. At any given point in time, there will be no frequency value. Instead, we should seek for the frequency content of a data collection, which is generally characterised using Fourier transform. In this case, the frequency of the data is considered constant over the whole time span T of the time series $x(t)$ that we are considering. This definition requires that, the data set contain multiple frequency values at any given time, and that those frequency values remain constant during the whole period covered by the integration. The Fourier definition of frequency shows that the frequency content is physically relevant only if the data are stationary, and the process is linear throughout the integrating span, as demonstrated by Fourier analysis [129].

An important reason for using the IF concept is that signal analysts often have to deal with signals whose spectral features (in particular, the frequency of spectral peaks) change with time. The term "nonstationary" is often used to describe these kinds of signals. For these signals, the IF is critical; it is a time-varying parameter that determines where the signal's spectral peak will be at any given point in time. It can be thought of as the sine wave frequency that best fits the signal being analysed at a given location. In terms of physics, it only applies to signals with a single frequency or a small range of frequencies that change in relation to time. If a signal has more than one component, the concept of a single-valued IF is invalid, and a breakdown into its components is required [130].

As an extension of the classical Fourier transform, the data can be divided by the number of discrete time spans. In this case, the frequency is supposed to be constant or at changing at a slow rate, which matches with the integral span of time.

The uncertainty principle limits the Fourier frequency as a result of this integrating procedure. A theoretical basis for Fourier transform theory states that this time interval cannot be too small in relation to the oscillation's period. In any case, a single period cannot resolve frequency fluctuation. Fourier spectral analysis can only be applied to linear and stationary processes because of this seemingly minor restriction. Frequency changes are frequent, if not dominating in both real-world and theoretical investigations [129].

There are many different mathematical approaches for performing a time-frequency transform, and we must explore beyond Fourier analysis in order to discover a solution to the problem. Indeed, the need for the frequency to be a function of time, as well as the need that it should have an instantaneous value, can be justified on both mathematical and physical grounds [131].

In this literature, the definition of IF is derived by assuming the signal is a sinusoidal oscillation with a phase defined in equation (3.8). After defining the phase for each cycle, the instantaneous angular frequency can be calculated by taking the time derivative of the phase value for each cycle [124].

$$\omega = \frac{d\phi}{dt}, \tag{3.8}$$

In biomedical applications, instantaneous frequency is a useful description of a number of different physical phenomena. Instantaneous frequency was reported to be an excellent technique for analysing blood flow data. Studying blood flow in an area with unexpected flow patterns due to complicated geometry requires measuring the instantaneous frequency [129].

3.9 Methods for extracting phase from experimental data

In the study of the ECG signal, one of the most critical steps is the detection of the R-peak. A more extensive evaluation of the ECG signal including the heart rate, can be undertaken once the R peak has been detected. The detection of R peaks in the ECG signal on the other hand, is a difficult process. This refers to time-varying physiological fluctuations of the patients as well as noise. Consequently, in the analysis of ECG data, the development of an efficient feature extraction algorithm is critical [132]. Generally, the oscillations that exist in biological system (e.g, heart rate) can be characterized by the variables: phase, amplitude, and frequency. Phase is utilized to evaluate the relative progress of a particular oscillatory cycle at a given period. Phase analysis can also be used to investigate the relationship between two correlated signals, which can assist in understanding the integrated activity of the components in a given system. There are a variety of ways to interpret the phase of an *in vivo* signal, and these interpretations are dependent on context [133]. In this thesis, defining instantaneous phase was done in one of two ways: marked events and wavelet ridge extraction.

Marked events

The number of events per unit time is used in the method of marked events to determine the frequency of an oscillation. An "event" can occur at any point in the phase of a single cycle of the continuous oscillations observed in a time series [124]. An illustration of the marked events method as applied to an ECG signal is discussed in figure 3.8 (a), which exhibits the R peaks sampled from an ECG signal. The marked event can be thought of as the R peak, and the times of succeeding R-peaks can be represented as t_k and t_{k+1}. Therefore, the average instantaneous heart

frequency (heart rate) can be defined as the reciprocal of the time interval between successive-R peaks, which is calculated as

$$f_i(t_{k,k+1}) = \frac{1}{(t_{k+1} - t_k)}, \tag{3.9}$$

It is simple to obtain the phase of such a process. Indeed, the time interval between two R-peaks is equal to the time period between two complete cardio-cycles. As a result, the phase increases throughout this time interval inversely is 2π.

$$\phi(t) = 2\pi \frac{t - t_k}{t_{k+1} - t_k} + 2\pi k, \tag{3.10}$$

The marked events method has significant limitations: the sampling frequency of the generated time series may vary during individual cycles of the oscillation, requiring that interpolation be performed before analysis.

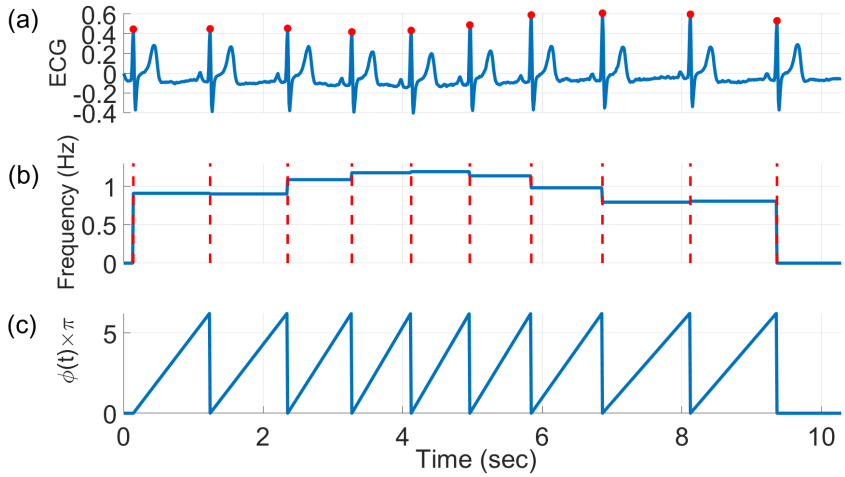

Figure 3.8: The process of determining the heart rate and phase by marked events method. (a) Raw ECG signal where the red circles indicate that the marked R-peaks. (b) Heart rate/instantaneous heart rate defined by calculating the inverse of times at the R-peaks were detected. (c) Instantaneous phase. Both instantaneous heart rate and phase were calculated by using definitions in equations (3.9) and (3.10).

Due to the fact that the frequency and phase of events cannot be determined between the marked events, this method is always an estimation. Another drawback of this method is that, the time resolution cannot be less than the period of the oscillation [4].

3.10 Time series analysis in frequency domain

Frequency domain

Biological signals are often comprised of waveforms that appear to be complex. We may desire to break down those waveforms into their component frequencies because we believe that a specific frequency of activity has biological and/or psychological "meaning" associated with it. For example, there is an oscillation in the cardiac period that is synchronised with the breathing frequency (approximately 0.12-0.4 Hz in adult humans). This oscillation in heart period (or heart rate) is caused by respiratory oscillators in the central nervous system and feedback from the lungs, and under certain conditions, this oscillation will have a perceptible impact on the heart period that corresponds to the frequency of breathing [134]. Plotting the frequency spectrum of a time series is a typical approach to see how it changes over time. This view displays the frequency distribution of oscillations and fluctuations in a given time series [124]. Considering Fourier series first helps to better understand the Fourier transform. With the use of sine and cosine functions, Fourier attempted to represent a periodic function $f(t)$ mathematically as:

$$f(t) = a_0 + \sum_{\omega=1}^{\infty} [a_\omega \cos(\omega t) + b_\omega \sin(\omega t)] \ , \tag{3.11}$$

where ω is the angular frequency and a_0, a_ω and b_ω are Fourier coefficients. Based on the structure of the function, these coefficients will take on specific values, with the

largest values corresponding to components of the time series that have stationary frequencies (also referred to as modes). However, data obtained from biological systems are based on discrete sampling and as a consequence, the discrete Fourier transform (DFT) is used. The DFT of time series $f(n)$ is defined as:

$$F(\omega) = \sum_{n=0}^{N-1} f(n) e^{\frac{-2\pi i \omega n}{N}}, \tag{3.12}$$

This equation can be used to convert a time series from the time domain to the frequency domain, or to convert a time series with a dependence on t to one with a dependence on ω. This means that periodic terms in the time series will appear as peaks in the Fourier transform at the frequency corresponding to the periodic terms in the time series.

When a time series contains frequencies that are outside the observable range (i.e. $1/5L$ as used in practice), problems arise with the Fourier transform. Low-frequency components ($< 1/L$) no longer appear to be periodic, but instead resemble a trend at these frequencies. The Fourier series of a non-periodic function is an infinite sum of infinite sines and cosines. It follows from this that most oscillation amplitudes at lower frequencies are shown at $\omega = 0$, whereas those that occur at higher frequencies are spread out across the spectrum. As a result, before performing a Fourier transform, it is critical to eliminate any trends from a time series in order to ensure that the components that may be detected in the detectable frequency range have accurate amplitudes.

Even at frequencies that are within the observable range, the Fourier transform presents challenges when used as a frequency domain representation. Figure 3.9 illustrates how amplitudes of periodic components of various shapes can be separated into modes distributed over the frequency domain by the transform's focus on sinusoidal components. Therefore, it is possible that the higher frequency modes

of components with high amplitudes may be wrongly classified as independent components in the time series. In the same way, comparing the height of the major 1 Hz component in (d) and (f) in figure 3.5 shows that determining the amplitude of an oscillation using the Fourier transform is not straightforward, as can be shown. Because the nonlinear factors in nonlinear dynamical systems tend to result in non-sinusoidal oscillations, this issue is particularly difficult to address.

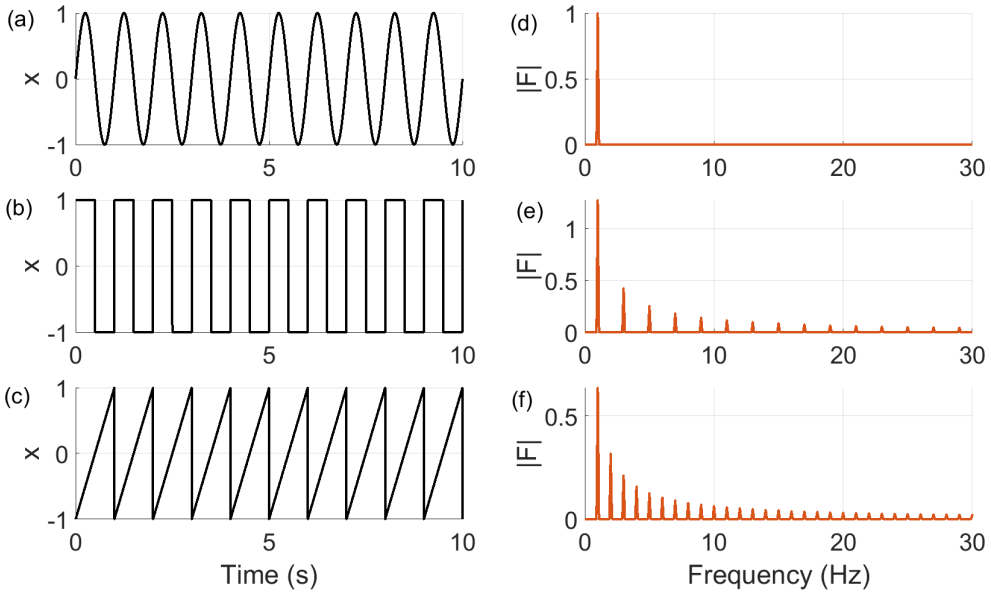

Figure 3.9: Time series of three different periodic functions: (a) A sine wave, (b) square wave and (c) sawtooth shape, as well as their one-sided Fourier transform amplitudes, are shown in panels (d), (e), and (f). The sampling frequency was 1000Hz.

Nonstationarity of time series is another issue that arises when using Fourier transform. The amplitudes and frequencies of the sines and cosines that serve as the foundation of the transform remain constant across time. The Fourier transform can only be easily understood when applied to time series in which the qualities of interest do not change over time as a result of this. An example of a chirp signal is shown in figure 3.10, which is a sine wave with a frequency that increases linearly with time.

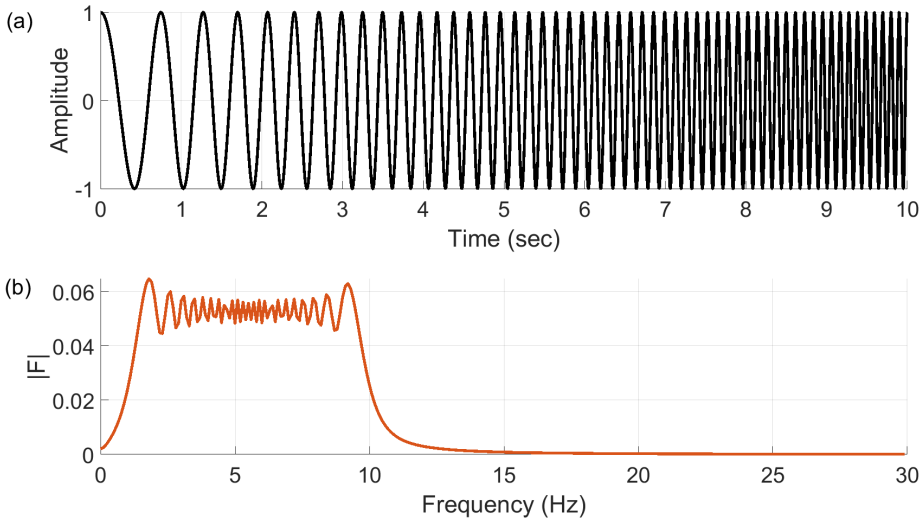

Figure 3.10: A chirp signal with a frequency range of 1–10 Hz created over 10 s with a sampling frequency of 1000 Hz, as seen in the time domain (a), and its representation in the one-sided Fourier transform (b).

As can be observed, this is represented by a broad range of much smaller peaks across the frequency interval of the chirp, which, when combined together, would yield the right amplitude of the chirp when the chirp is played again. Although they are clearly visible in the time domain, these non-stationary oscillations become extremely difficult to detect as soon as other components are introduced into a time series.

3.11 Time-frequency Representation (TFR)

Time or frequency domains can be used to represent a physical signal [135]. Although the methods for time domain decomposition have some benefits that the Fourier transform does not, it would still be great to have spectral approaches that could be applied successfully to the time series of complicated systems. Although a Fourier transform can reveal much information about a time series in the frequency domain, it is only applicable to series with periodic and stationary components. As non-

stationary dynamics is simply represented by discrete stationary components, it cannot provide clear information on how the components evolve over time. As a result, a method for tracking the phase and frequency of various components over time is required [124]. It is common for real-world and physiological signals to be irregular in some aspects [136]. Numerous time-varying amplitudes and/or frequencies are seen in these oscillatory components. It is difficult to study these fluctuations in the time domain or using Fourier transforms, but the heartbeat is a good example. Although cardiac frequency is often centred around 1 Hz, it fluctuates continuously around this average. Since time and frequency are two dimensions, it is typically more beneficial to analyse a signal's properties in both time and frequency at the same time. This can be done by looking at specific projections of the signal onto a (two-dimensional) time-frequency plane to create what is known as a time-frequency representation (TFR).

Tracking the frequency content over time is particularly useful for multicomponent and nonstationary time-series with time-varying spectral features, which can be analysed using this method. The ability to recover the signal's oscillatory components (some of which may have time-varying qualities) is a critical aspect of a TFR [137]. With aid of the ridge extraction method, the amplitude and frequency-modulated components (AM/FM components) of a given signal can be separated, and the instantaneous features (e.g. frequency, amplitude, and phase) of its spectral content can be traced in time [130]. This method works well with cardiovascular signals that have a wide range of time and frequency components, with the high-frequency components often having a shorter duration than the low-frequency components. Moreover, physiological perturbations cause the characteristic frequencies of cardiovascular signals to change over time. Consequently, time-frequency approaches are best suited for capturing these changes [135]. In this research, we focus on real signals such as ECG, and blood flows, respiration, and blood pressure that are recorded from healthy subjects. As these signals are non-

stationary and non-linear, a time-frequency analysis based on wavelet transforms is highly appropriate for dealing with their complexity. For the purpose of identifying the characteristic rhythms of these diverse signals, as well as their temporal variability, a wavelet-based extraction method was used [138].

3.11.1 Short time Fourier transform (STFT)

As an alternative to the Fourier transform, Gabor (1946) developed a windowed Fourier decomposition to measure the time-frequency content of signals. Using STFT (also known as the windowed Fourier transform), the signal can be decomposed in a time–frequency plane whose partition is stratified by rectangular/Gaussian cells of the same dimension [139]. In living systems, the frequency content of the recorded signal can slowly change over time. This type of signal requires a window of short time interval as in short-time Fourier transform, in order to investigate it [140]. This method divides the signal into windows of finite duration, within which the frequency content is analysed [135]. Then, in order to achieve time localisation, the window is moved along the signal and its frequency content is analysed. In this method, not only are the characteristic frequencies in the signal evaluated, but also the time changes associated with those frequencies. The results are given in the form of a time–frequency representation. Using the assumption of weak stationarity, an average over all windows can be used to provide information on the frequency content of the signal [140]. The STFT is defined mathematically as:

$$G_s(\omega, t) = \int_{-L/2}^{L/2} g(u-t) f(u) e^{\frac{-2\pi i \omega u}{l}} du, \tag{3.13}$$

Wherer $f(u)$ is a signal of length l and $g(u)$ is a rectangular function of length l that is zero outside -$l/2 \leq u \leq l/2$. ω is a selected analyzing frequency, and t is an arbitrary time shift. The variable ω has a direct relationship with the frequency f_ω through

$f_\omega = \frac{\omega}{l\Delta t}$. The complex coefficients of the STFT provide information on the phase of the components in addition to the frequency spectrum (i.e. the position in the cycle with respect to time) [124]. It should be noted that if $g(u)$ is a Gaussian function, the transform is then known as the Gabor transform [141]. The Gaussian window function is defined as:

$$g(u) = \frac{1}{\sqrt{2\pi} f_0} e^{-u^2/2f_0^2} \tag{3.14}$$

If we consider the resolution parameter f_0, Gaussian window spread determines the trade-off between the time and frequency resolution of a WFT: The smaller f_0 resolution parameter is, the faster changes in time are reflected, but the more difficult it is to discriminate between two components that are very near in frequency [137].

3.11.1.1 Limitation of STFT

The duration of the window used to isolate a segment of the signal at a specific time is an important parameter of the time-frequency representation [142]. Time and frequency are fundamentally incompatible since frequency cannot be measured instantly. For a frequency to be detected, the signal must be observed for at least one period of this frequency. Consequently, it is impossible to tell precisely when the signal had this frequency. The time and frequency resolutions are dictated by the window length. Wide windows are required for good frequency resolution and identification of low-frequency components, whereas narrow windows provide good time localization [135]. Since all frequencies have the same frequency resolution, the time–frequency localization of this strategy can be inefficient. Localization in time (with higher frequencies) requires a high level of time resolution. Low-frequency structures, on the other hand, may be resolved with a lower time resolution [139]. This is a consequence of the time-frequency to uncertainly principle. Time-frequency analysis relies on the uncertainty principle as a foundational result. It restricts the

ability of a signal to simultaneously be localised in time and frequency [143].

3.11.2 Wavelet transform

The fundamental concept behind wavelets is that they provide optimal time frequency localization, which means that they can accurately determine the frequency of a component within a time series at a particular time. A window function known as the mother wavelet is used as a starting point, and this function is stretched or compressed so that the frequency response matches the desired frequency range [124]. Within this transform, it becomes possible to obtain good temporal localisation for high frequencies and also achieve better frequency resolution for low frequencies in a single transform. The wavelet transform decomposes a signal into functions (wavelets) that are narrow when high frequency features are concentrated and large when low frequency structures are concentrated. This decomposition results in a favourable trade-off for the time-scale resolution, which is connected to the frequency resolution. This also allows for good localization in both time and frequency (see figure. 3.11), which is particularly useful for examinations of the temporal evolution of aperiodic and transient signals [139]. In the wavelet transform, the shape of the basic time-domain wavelet function changes with frequency to provide a better match to nonlinear, irregular biological data. The wavelet analysis enables the separation and sorting of different structures on various time scales at various moments, providing both scale and temporal information [144]. The wavelet transform is defined as

$$W_T(s,t) = \frac{1}{\sqrt{|s|}} \int_{-L/2}^{L/2} \Psi\Big(\frac{u-t}{s}\Big) f(u) du, \tag{3.15}$$

where $\Psi(\frac{u-t}{s})$ is the mother wavelet. All wavelets are defined by this single wavelet by its being scaled according to the scale s in order to adjust its frequency distribution and time-shifted according to the time t [122]. The $1/\sqrt{|s|}$ term ensures that the

energy of the scaled wavelet remains constant or equal in comparison to the energy of the original mother wavelet [122]. As s changes, the wavelet's shape is compressed or stretched to encompass a wider range of frequencies.

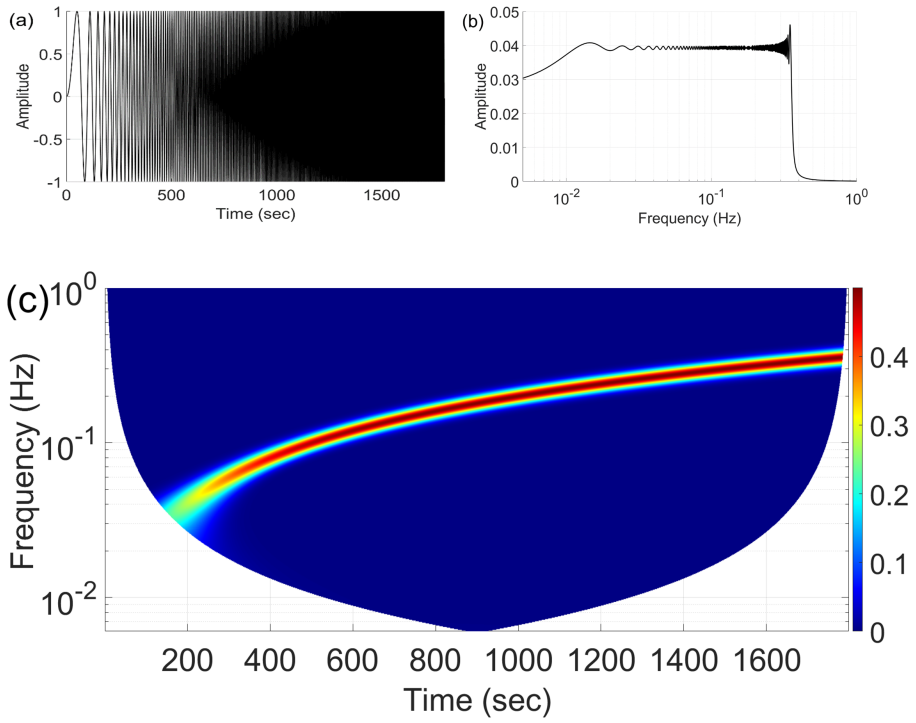

Figure 3.11: The frequency of the nonlinear chirp signal, $sin(2 \times 0.0001 \times time^2)$, grows as time increases. Since the signal in (a) varies with time, (b) cannot be accurately represented by the Fourier transform in the frequency domain. (c) represents the continuous wavelet transform.

The time localization centre can be moved around and wavelets can be translated through all of the data points. In this approach, the wavelet transform gives a time-frequency representation of a given signal. In contrast to the windowed Fourier transform, the wavelet transform is capable to "zoom in" and "zoom out" to/from structures at various scales [144]. In other words, instead of conducting a "stand-alone transform" for each time window, the wavelet transform conducts a separate calculation for each time window based on both time and frequency (or more

specifically, s).

3.11.2.1 Morlet wavelet

The wavelet window must have a Gaussian shape in order to achieve the highest possible time–frequency resolution up to the absolute limit defined by the uncertainty principle. This idea, along with the Fourier transform's sinusoidal base, results in the Morlet wavelet [124]. A mother wavelet can be either a real or a complex function, depending on the application. Although both options will provide the magnitude of the wavelet coefficient, implementing a complex wavelet will result in a complex wavelet coefficient. It is more appropriate to capture oscillatory behaviour with a complex wavelet function since it returns information on both amplitude and phase information. A real wavelet allows to one isolate peaks or discontinuities because it returns only one component [145]. The additional phase information (provided by complex wavelet) appears to be useful in the discussion of wavelet coherence measures since it allows for more accurate comparisons. The Morlet wavelet is given by

$$\psi(t) = \frac{1}{\pi^{1/4}} e^{i2\pi f_0 t} e^{-t^2/2}, \tag{3.16}$$

Here, f_0 ($\omega_0 = 2\pi f_0$) is the central frequency of the mother wavelet. The term $e^{-t^2/2}$ is the Gaussian envelope which has unit standard deviation and contains the complex sinusoidal waveform. Figure 3.12 represents the Morlet wavelet's real and imaginary components, as well as the constricting Gaussian envelope. Figure 3.12 (c) shows there is a quarter-period difference in phase between the actual and imaginary sinusoids. In order to ensure that the wavelet has the same amount of energy, the $(1/\pi^{1/4})$ term is used [146].

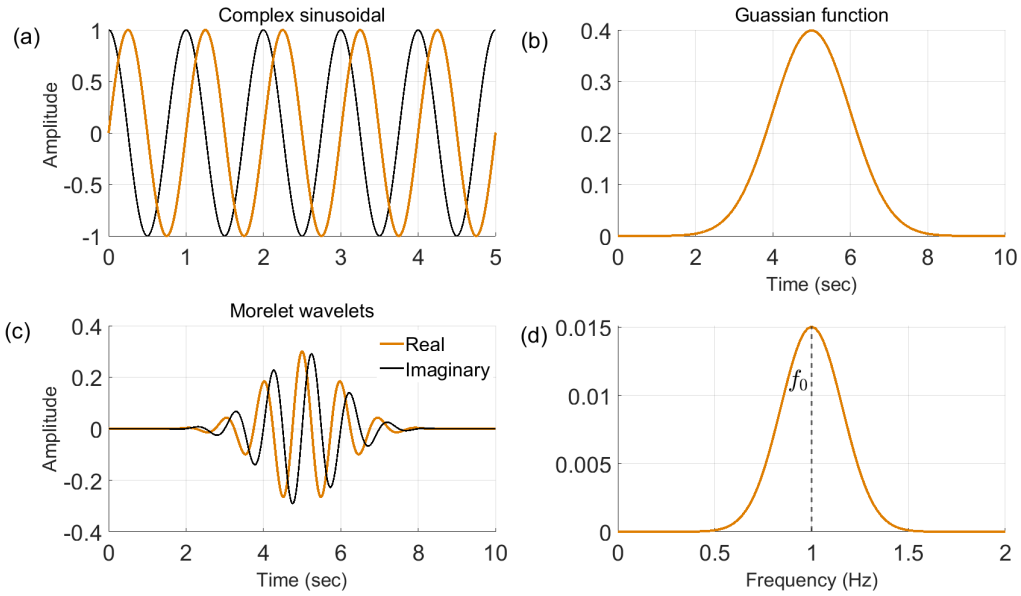

Figure 3.12: Construction of Morlet wavelet. The dot product of (a) complex sinusoid with (b) A Gaussian function will generate (c) a Morlet wavelet in both forms (real & imaginary). (d) is in the frequency domain

3.11.2.2 Central frequency of Morlet wavelet

The central frequency f_0 ($\omega_0 = 2\pi f_0$) is so named because it corresponds to the peak frequency of a Gaussian distribution of components over a range of frequencies in the Morlet wavelet, i.e., it is located in the middle of the Gaussian distribution of components [147]. The 'effective frequency' of the sine-cosine pair can be altered to match harmonic components in the signal via dilations or scaling of the spatially localised mother wavelet [148]. With the central frequency parameter, the user can select how many oscillations the wavelet has within its Gaussian envelope, and how large or small that envelope should be [149].

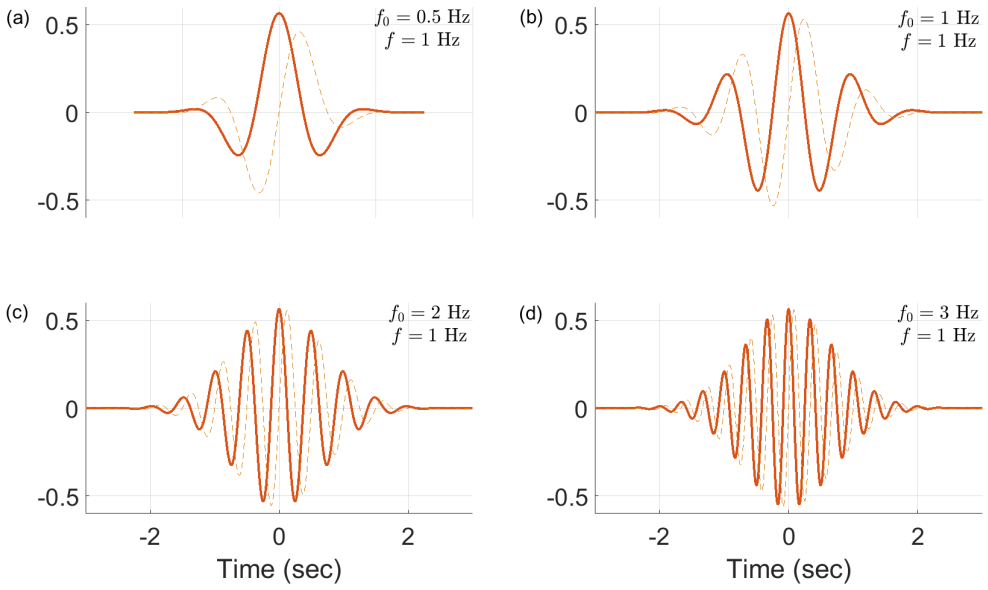

Figure 3.13: Commonly used Morlet wavelets showing the effect of increasing the central frequency. An increase in the central frequency leads to an increase in the number of oscillations that occurr within a particular window. This results in improved frequency resolution, which assists in the determination of the instantaneous frequency.

The number of oscillations or cycles of the Morlet wavelet can be determined by the value of f_0 as shown in figure 3.13. In general, greater values of f_0 lead to better spectral resolution but a lower temporal resolution. For the Morlet to be admissible as a wavelet, a minimum value of $f_0 = 6$, or $f_0 \sim 1$ Hz, is necessary. For a given f_0, increasing the Morlet wavelet's variance improves frequency resolution while decreasing temporal resolution, and vice versa [150].

3.11.2.3 Relation between scale and frequency

The most obvious difference between the wavelet and Fourier transforms is that wavelet basis functions are indexed by two parameters (s and t) whereas Fourier basis functions are indexed by the single parameter ω ($2\pi f$). This means that in

physical terms, wavelet transforms (or coefficients) are characteristics of the function's local behaviour, whereas Fourier transforms (or coefficients) are characteristics of the function's global behaviour. A time location is represented by the second parameter (t), while the first parameter (s) determines the 'width' of the wavelet (s). In the case of Fourier analysis, the parameter ω corresponds to the physical interpretation of frequency. In other words, the wavelet parameters and the Fourier frequency parameter have no direct physical connection. However, if the mother wavelet possesses "oscillatory" properties, we can infer a connection between the two parameters ω and s. If the mother wavelet (e.g, Morlet function) has "oscillatory" properties, which means that as s decreases, oscillations become compressed in the time domain, i.e. they exhibit high frequency' behaviour, whereas as an increases they become drawn out (i.e. they exhibit 'low frequency' behaviour) [151]. Consequently, each scale represents a frequency band rather than a single frequency. While large scales are related with low frequencies (equivalently, long periods), very small scales are connected with high frequencies [152]. The relationship between scale and frequency is inversely proportional $f = 1/s$. However, the exact scaling constants that characterise the proportionalities differ depending on which wavelet is used. With a scaling constant, the connection can be expressed as

$$f = \frac{f_c}{s}, \tag{3.17}$$

where f_c is a constant that specifies the characteristic frequency of the wavelet. The characteristic frequency f_c of the wavelet employed in the wavelet transform is reflective of the entire frequency makeup of the wavelet [147]. The spectral peak frequency (the frequency value with the greatest spectral density), the centre frequency of the passband, and the centre frequency of the wavelet itself are all possible options for the value of f_c [153]. Figure 3.14 shows how time-scale translations of

multi-scale wavelets is performed.

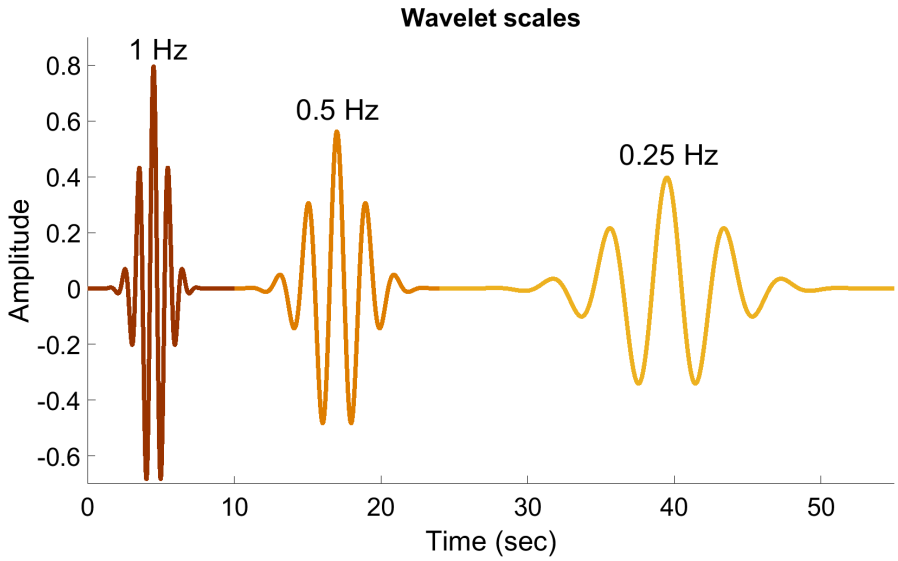

Figure 3.14: A demonstration of how wavelets of varying scales can be translated in time.

3.11.2.4 Cone of influence (COI)

The wavelet is a windowed transform. Therefore, at a given moment in time t_0 always contains information about nearby data points. The number of these points varies depending on the wavelet used and the scale considered. As a result, if the wavelet is centred near the beginning or end of the time series, edge effects will arise [152]. One option to solve this issue is to pad the time series with zeroes at the boundaries in order to increase the total length to the next-higher power of two. As a result, the edge effects are minimized and the Fourier transform straightforwardly applied. However, padding with zeroes produces discontinuities at the endpoints and, as one moves to higher scales, reduces the amplitude around the edges as more zeroes are introduced into the analysis [145].

The Cone of Influence (COI) is a line drawn on a scalogram that denotes the parts that are affected by edge effects. Data outside this range may appear distorted.

The COI is computed by the wavelet's e-folding time, which is the time at which the wavelet power has reduced to e^{-2} of the power at the edge of the signal, as a result of the discontinuities generated by padding the ends with zeros. In this case of the Morlet wavelet, the e-folding is $\tau = \sqrt{2s}$. The choice of wavelet and the wavelet parameters have an impact on the COI adjustment. The central frequency is a key factor in determining a wavelet's size (Morlet). Changing a parameter will have an impact on the time–frequency resolution of the system [153].

3.11.2.5 Lognormal wavelet: An extra choice

The Morlet wavelet, like many other wavelets, has a frequency scale that is linear. Due to the fact that WT has logarithmic frequency resolution, it appears that it would be more appropriate to design a wavelet with log as its argument. As a result, the lognormal wavelet would be a more accurate WT analogue for the Gaussian window than the Morlet. Compared to the Morlet, the wavelet has greater resolution properties among other advantages, making the lognormal wavelet the preferred option. Although it is "infinitely admissible" unlike the Morlet wavelet, this wavelet is "finite" which means that it can be used to reconstruct any order time-derivative from the component's WT. In the present research, the lognormal wavelet was used only in ridge extraction analysis. The lognormal formula is given by:

$$\hat{\psi}(x) = \begin{cases} e^{-\frac{(2\pi f_r \log x)^2}{2}} & x > 0 \\ 0 & x \leq 0 \end{cases} \tag{3.18}$$

3.11.3 Wavelet spectral power

The power spectrum of data can be examined for significant peaks to see if oscillatory activity is present. Due to the nonstationary nature of most physiological signals and the possibility of several time-varying frequency modes, it is advised that power

spectral computations be performed over time by using any of the computational methods [154]. For both linear and nonlinear signals, frequency peaks in the power spectrum indicate oscillatory behaviour [155]. In the frequency domain, the power spectrum of a time series is defined as the integral of the square of the amplitude. This is a straightforward operation for the Fourier transform because the frequency scale is linear, resulting in the square of Fourier transform being precisely proportional to the power spectrum. In the same way, the wavelet power spectrum can be calculated by:

$$P_W(\omega^{'}, t) = \int_{\omega^{'} - \frac{d\omega}{2}}^{\omega^{'} + \frac{d\omega}{2}} |W_T(\omega, t)|^2 d\omega, \tag{3.19}$$

However, the wavelet transforms uses a logarithmic frequency scale which means that higher frequencies correspond to larger frequency intervals. As the Morlet wavelet transform is continuous, obtaining the power spectrum is not as straightforward. That is why the integration of squared amplitude is always an approximation when dealing with finite data, even if it is equivalent to Fourier amplitudes (a continuous curve cannot be integrated discretely). Time series data can be analysed by taking the average of wavelet power over time. In this case, it is used to determine the primary oscillatory components' frequency range. Once this information is gathered, it will be possible to track the changes in power over time for each individual component [122].

The average power (ξ_{mean}) may be calculated over a period of time within any frequency band of interest. In this thesis, we focus primarily on the frequency interval $0.005 - 2$ Hz, which is manifested in the microvascular blood dynamics. In the time series $x(t)$, the power of each frequency band f_{i1} to f_{i2} connected with the time series is denoted by:

$$\xi_i(f_{i1}, f_{i2}) = \frac{1}{t} \int_0^t \int_{\omega_0/2\pi f_{i2}}^{\omega_0/2\pi f_{i1}} \frac{1}{s^2} |W_x(s, t)|^2 ds dt, \tag{3.20}$$

where the scale s is related to frequency f by $s = \omega_0/(2\pi f)$ and $W_x(s, t)$ refers to the wavelet transform of the signal $x(t)$ that being analyzed [135].

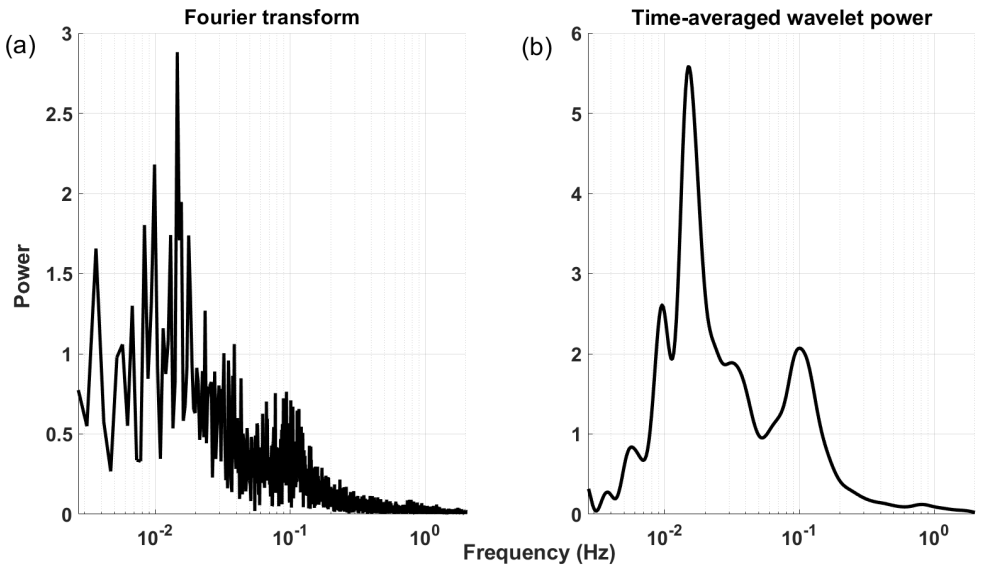

Figure 3.15: Time averaged wavelet transform vs. Fourier transform of blood flow time series. (a) Fourier representation, while (b) shows the wavelet representation of the same signal. The wavelet transform offers higher resolution at lower frequencies for time-varying oscillations, and this is true even when the data are averaged over time.

3.11.4 Wavelet ridge extraction

With aid of the ridge extraction method, the amplitude and frequency-modulated components (AM/FM components) of a given signal can be separated, and the instantaneous features (e.g. frequency, amplitude, and phase) of its spectral content can be traced in time. As seen in figure 4.1, the components that are present in the signal are depicted in its TFR as "curves" in reality, temporal sequences of close peaks. Ridge curves will be the term that will be used to describe these types of curves. In a general sense, the ridge curve of a component can be described as the sequence of TFR amplitude peaks onto which the majority of the energy of that component is projected at each time [130].

This method works well with cardiovascular signals that have a wide range of

time and frequency components, with the high-frequency components often having a shorter duration than the low-frequency components. Moreover, physiological perturbations cause the characteristic frequencies of cardiovascular signals to change over time. Consequently, time-frequency approaches are best suited for capturing these changes [135].

3.11.5 Wavelet phase coherence

Waves can be spatially coherent, and oscillations can be temporally coherent. Coherence in time is a general term to describe all qualities of correlation between physical quantities that occur during a single oscillation or multiple oscillations. Specific frequencies are defined for coherence like power and phase [122]. It is possible to employ phase information to study the correlations between the oscillations of different signals. An oscillation at the same frequency in two different noisy signals may not always indicate that they are connected. It is feasible to discover plausible correlations by comparing the instantaneous phases of two signals using wavelet phase coherence analysis [156]. Wavelet phase coherence uncovers consistent phase correlations between signals and can be used to infer causality between them. In contrast to cross-spectra, it is possible to detect strong phase coherence between signals even when their common powers are modest. This is particularly relevant for low-frequency components, which contribute significantly to total power while not necessarily making huge contributions to total power. We initially calculate the wavelet transform of the signals in order to assess their wavelet phase coherences. The use of the complex Morlet wavelet allows for the extraction of instantaneous phase variations at each point in time and on each scale in the image (inverse of frequency) [157].

$$W(s_k, t_n) = W_{k,n} = a_{k,n} + ib_{k,n}, \tag{3.21}$$

The instantaneous phase can be calculated from here using the angle variable:

$$\phi_{k,n} = \arctan\left(\frac{b_{k,n}}{a_{k,n}}\right), \tag{3.22}$$

Instantaneous phases are calculated for both signals: $\phi_{1k,n}$ and $\phi_{2k,n}$ at each time t_n and frequency f_k. The relative phase difference between them is therefore calculated as $\Delta\phi_{k,n} = \phi_{2k,n} - \phi_{1k,n}$. The sine and cosine components of the phase differences are calculated and averaged in time throughout the whole length of the signal, resulting in the final phase difference. Finally, the phase coherence function is denoted by the expression

$$C_\phi(f_k) = \sqrt{\left\langle \cos\Delta\phi_{2k,n}\right\rangle^2 + \left\langle \sin\Delta\phi_{1k,n}\right\rangle^2} \tag{3.23}$$

The phase coherence function $C_\phi(f_k)$ can take a value between 0 and 1. When the phase difference between the two signals at a specific frequency remains constant, the phase coherence value would be close to 1. In contrast, when they are unconnected, the phase difference between two oscillations varies continuously in time and as a result, their phase coherence is close to zero [55]. Values of phase coherence must, however, be treated with caution. In signals of finite length, low-frequency components have fewer periods than high-frequency components. As a result, there is less variance in phase difference at low frequencies, leading to an artificially exaggerated phase coherence. Phase coherence between two unrelated signals rises monotonically at decreasing frequencies. Surrogate analysis is used to find a frequency-dependent floor that accurately reflects the degree of coherence [156].

3.12 Surrogate test

Surrogates can be particularly valuable in the search for underlying dynamics in univariate time series, and they can also be critical when investigating interactions

between systems when two or more time series are presented. Surrogates can be used to test for phase synchronisation and coupling between oscillators by employing a variety of discriminating statistics, including phase coherence, the phase synchronisation index (PSI), dynamical Bayesian inference, and synchronisation likelihood, among many other techniques [158].

Complex nonstationary signals originating from biological systems frequently exhibit random fluctuations in frequency and phase. Even for uncoupled signals, frequency and phase coincidences can exist and be mistakenly recognised as sections of phase synchronisation. It is possible that such events will lower the estimated PSI and thus reduce the accuracy of outcomes. False detections are substantially more likely to occur in the scenario where the characteristic frequencies of the analysed signals are near to each other. As a result, when analysing experimental data, it is critical to consider the possibility that the PSI will take on a particular value as a result of random fluctuations in the signals rather than just a result of specific coupling dynamics between the studied systems [127].

It is important to keep in mind that the coherence that is computed (using equation 3.22), in the first instance, does not necessarily reflect a genuine phase relationship and needs to be carefully evaluated. Although, coherence values can vary anywhere from 0 to 1, the problem occurs due to the fact that some of the coherence values that are acquired can be negative. After that, the negative coherence values are deducted from the total. Following this approach, the very low frequency oscillations may appear to have a coherence values that are close to 1. This bias is caused by the use of recordings that are too short to encompass the content at low frequencies.

We used the surrogate method [159, 158] to check the significance of the computed coherence by setting as a null hypothesis that, for all frequencies, the phases in the signals are independent, thereby reducing the influence of random effects that can give rise to apparent (but spurious) coherence. We removed the bias associated with

the power spectrum of the more often used amplitude adjusted Fourier transform (AAFT) surrogates by using iterative amplitude-adjusted Fourier transform (IAAFT) surrogates to estimate the significance level of the apparent coherence. This allowed us to more accurately determine the level of apparent coherence. To begin, the IAAFT surrogates are constructed by first shuffling all of the characteristics of the signals under the examination, with the exception of the phases $\phi_{1k,n}$ and $\phi_{2k,n}$, which are left unshuffled. After that, this is performed in an iterative manner, simply by utilising the ideal value and re-scaling the distribution to substitute Fourier amplitudes. This enables us to obtain likeness between the distributions and power spectra of the surrogates and the original signals. Afterwards, this is accomplished in an iterative manner. At each frequency, we determined the coherence threshold to be the 95th percentile of the greatest value produced by 100 random realisations of IAAFT surrogates. This was done across all surrogate realisations. The computation of wavelet phase coherence between two different time series is illustrated in figure 3.22.

Inter-subject surrogate analysis can also be used to validate the results of significant coherence. These values are computed for n combinations of randomly selected inter-group subjects, as a substitute for the actual values of the coherence between the two signals, such as blood flow and respiration. The surrogate is built using, for example, blood flow from subject A and respiration from subject B, which makes the surrogate a composition of mutually independent signals. At each frequency, effective coherence was calculated by taking the original coherence and subtracting the significance threshold from that value [160].

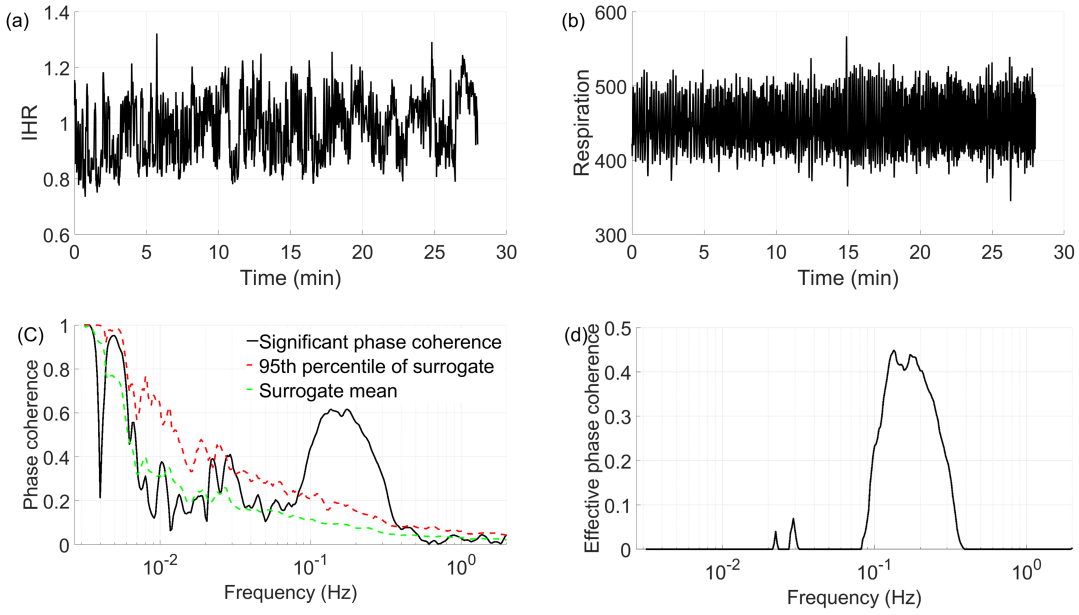

Figure 3.16: This is a typical example of the wavelet phase coherence between two different time series. (a) The time-series of IHR and (b) respiration exhibit wavelet phase coherence. Significant phase coherence is indicated in figure (c) when the coherence (black line) is greater than the 95th percentile of 100 pairs of IAAFT surrogates (red line). The effective significant phase coherence presented in panel (d) is produced by subtracting the 95th percentile of the surrogate.

3.13 Statistical analysis

Quantitative research employs statistical methods that can be classified as either parametric or nonparametric, depending on the nature of the data. The parameters of parametric tests are based on the assumption that the data adhere to a particular probability distribution, which is commonly the normal distribution. They also frequently make the assumption that the differences across groups are homogeneous. In situations where these presumptions are satisfied, parametric testing is recommended. Compared to parametric tests, nonparametric tests make fewer assumptions about the distribution of the population being tested. It is not necessary

for the data to adhere to a particular distribution. Tests that are nonparametric are more resistant to the violation of assumptions and thus are appropriate for situations in which the data do not satisfy the assumptions that parametric tests make [161, 162, 163]. Medical researchers frequently employ nonparametric statistics due to various factors:

- Accuracy of presumptions based on data: Data from the medical field frequently diverges from the assumptions that parametric statistics make, such as the assumption of normality or the assumption of homogeneity of variance. When it comes to the analysis of medical data, nonparametric methods are safer and more trustworthy because they do not rely on these assumptions.

- Limitation of small samples:

  Due to practical limits, medical investigations sometimes include the use of small sample numbers. Due to the fact that they do not rely on assumptions about the distribution of the population, nonparametric tests are ideally suited for the analysis of small samples.

- Comparing group differences [164]:

  In physiological investigations, it is common practice to compare physiological parameters between groups, such as healthy controls and patients with a specific disease or treatment. It is common practice to employ nonparametric tests such as the Kruskal-Wallis test (for more than two independent groups) in situations where parametric tests do not hold or where the data do not follow a normal distribution.

- Assessing relationships: Research in the field of physiology may have the objective of examining patterns of association or correlation between physiological variables.

- Comparing paired data: It is common practice in research to measure the same subjects twice under different circumstances. When the data fails to meet the criteria of parametric tests, such as normality of differences, nonparametric tests are employed to compare paired observations. One such test is the Wilcoxon signed-rank test.

  In general, nonparametric statistics are useful for analysing physiological data, especially when dealing with ranked or ordered data, data that does not follow a normal distribution, or when the assumptions of parametric tests are not met. They are flexible, reliable, and can be used to answer many different kinds of physiological research questions. All of the statistical tests used in this work are non-parametric, which means that they did not assume that the data followed any particular underlying distribution. Note that we illustrate the data using violin plots (introduced in detail in the section 3.13.3) which help visualize whether data are normally distributed. As can be seen from the violin plots provided in this chapter, data are mostly not normally distributed. Therefore, non-parametric test were used and they allowed for more reliable conclusions to be drawn.

3.13.1 Statistical tests

In order to detect significant powers, coherence, and variations with ambient temperature, we calculated medians and ranges. Initially, the Kruskal-Wallis (multi-comparison) test was performed to compare all of the groups. This test was used to determine if two or more independent samples are from the same distribution, and it does not assume a normal distribution. If significance was found, the Wilcoxon signed rank test (pairwise) for paired data was used to examine pairs of groups. The signed

rank test can be used to determine if two samples with matching counts are drawn from the same statistical distribution.

The term "paired data" refers to a situation in which the values of the two groups being compared are inextricably connected. This situation typically occurs when an individual is measured more than once. For instance, if subject A's symptoms were measured both before and after therapy, then the measurement taken before treatment would make sense to pair with the data taken after treatment. They most certainly cannot be regarded as being independent from one another due to the fact that attributes of subject A will influence both measurements. In this research project, significance tests were taken with variations in heating among the same group. As a result, the Wilcoxon-signed rank test was used. [165]. In all cases, a p-value of less than 0.05 was determined to be statistically significant.

3.13.2 Testing for normality of data

Analysing the distribution visually is one method that can be used to determine whether or not it is normal. Several visual representations can be employed to visually assess normalcy, such as the histogram, boxplot, stem-and-leaf plot, P-P plot, and Q-Q plot. Instead of plotting each individual score in the data, a Q-Q plot depicts the quantiles of the data set, which are numbers that divide a data set into equal sections. Additionally, when dealing with high sample numbers, the Q-Q plots are better suited for interpretation.[166, 167].

Visualising the data in relation to its frequency distribution, which shows the observed values as a bell curve, can help in judging the distribution's form and identifying data gaps or outlying numbers [168]. We found no consistent normal distributions of data among the groups compared using the Lilliefors test (Figure 3.17).

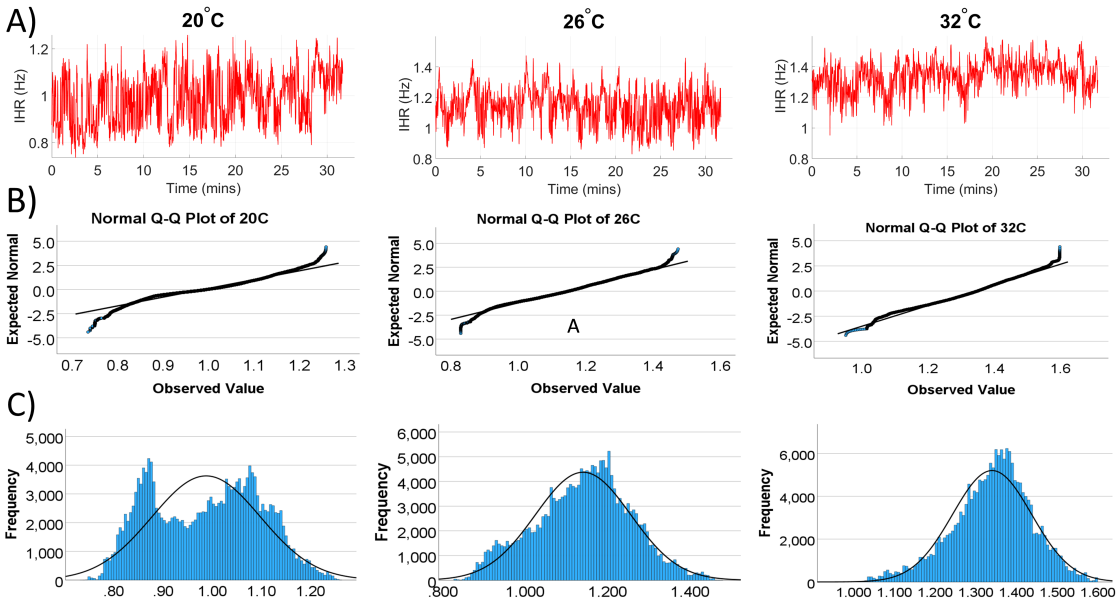

Figure 3.17: Visual inspection of the distribution of instantaneous heart rate (IHR). A) shows IHR signals. B) Q-Q plot. C) The frequency distribution (histogram) with bell curve.

3.13.3 Violin plots

The violin plots represent the distribution of data for particular groups, or particular parameters. In this work, they are used to compare the power spectra, phase coherence, and phase shift for entire frequency of interest (0.0095–2 Hz), and for each for each frequency interval of interest (see table 2.1). The Kruskal-Wallis test was used to compare data between several groups. If significance is found, a red asterisk is shown on the relevant figure. Otherwise, there is no significant difference. Similarly, a pair-wise (Wilcoxon signed rank test) was also carried out for each individual band, and where significance is found, it is shown on the same violin plots. Figure 3.18 shows the violin plot, which is a combination of the box plot and density traces. To the left and right of the (vertical) box plot, there is a symmetrical plot of the density

trace.

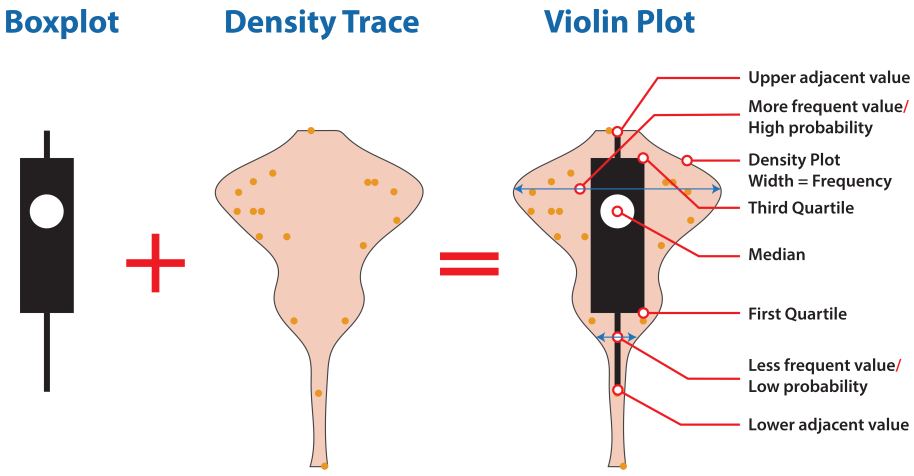

Figure 3.18: Common components of a violin plot. Combination of a box-plot and its distribution values (density trace) forms a violin plot as can be seen.

The only thing that differentiates these density traces from one another is the direction in which they extend. When two density traces are added together, a symmetric plot is produced, which means that the magnitude of the density may be seen more clearly. This combination of the density trace and the box plot makes it easy to compare many distributions quickly and effectively [169].

4. Results

4.1 Time series analysis

The amplitude, power, and phase characteristics of oscillations can be measured and analysed using recorded signals to extract statistical properties from the data. Time-varying oscillatory features are of particular interest in our study, where we attempt to resolve the dynamics in terms of time localization and frequency resolution.

Frequencies that are very prominent in the examined signal appear as peaks in power spectral. In order to track their evolution over time, the wavelet transform employs a time dimension. The time average of the wavelet transform is used to determine the spectral amplitudes. What we mean by "total spectral amplitude" refers to the average amplitude of the wavelet transform over time for the entire frequency range (0.002 Hz − 2.0 Hz). Wavelet phase coherence is a measure that discovers consistent phase correlations between signals and gives inferential evidence for causation resulting from links between the processes giving rise to the links between signals. Even when the power of the signals being compared are rather weak, it is still possible to detect significant phase coherence between them. This is particularly significant for low-frequency components, which contribute significant contributions to total power even though those contributions are not necessarily very substantial.

In order to quantify wavelet phase coherences between signals, we first estimated their wavelet transforms. The complex Morlet wavelet is used so that phase differences

at any given time and frequency can be extracted. Wavelet phase coherences are then determined from the relative phase differences and their temporal variations. with values ranging from 0 (no coherence) to 1 (perfect coherence). The phase difference can also be used to establish which of two coherent oscillators is leading, and is therefore more likely to be the source of the dynamics.

4.2 Time domain and power spectrum analysis

4.2.1 Heart rate and heart rate variability

Extraction of instantaneous frequency from ECG time series

The instantaneous heart rates (IHR) of each subject were determined by employing wavelet ridge extraction to isolate the cardiac oscillation included within the ECG signals that were obtained for that subject. Ridge extraction analysis was performed on the ECG signal in the frequency range of 0.6–2Hz, which allowed the IHR to be determined for each individual at each temperature. This resulted in a time series of the heart rate variability over time of the same duration as the original signal, one for each subject at each temperature range (i.e. 20°C, 26°C, etc.). For each subject, both the mean and the standard deviation of the IHR time series were computed. Figure 4.1 shows how the ECG data can be used to extract the time-varying heart rate.

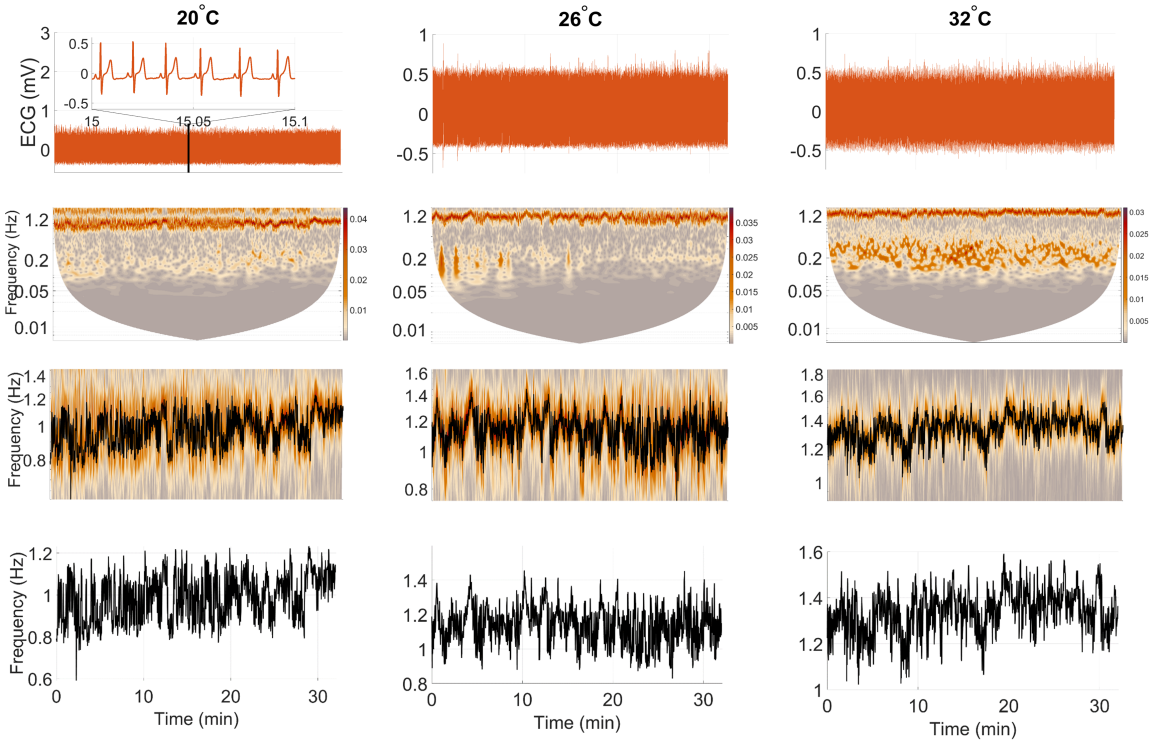

Figure 4.1: An example of extracting the instantaneous heart rate from the ECG signal from one subject for three different temperatures. The first row represents the entire ECG time series. In the second row, the ECG signal is subjected to a complete wavelet transformation. A noticeable oscillating pattern can be noticed around the predicted heart rate of 1 Hz as can be seen in third row. Instantaneous frequency time series derived from a wavelet transform via ridge extraction are shown in the fourth row.

Results obtained using either method were found to be nearly similar. Figure 4.2 (a) displays the heart rate, while (b) heart rate variability. Heart rate variability and respiration rate variability signals were computed by taking the standard deviation of heart and respiration rates that were calculated by wavelet transform and comparing them.

As can be seen in figure 4.2 (a,b) both heart rate variability (HRV) and instantaneous heart rate (IHR) increased significantly with increasing temperature. Significant differences in median heart rate were found between 32°C and 20°C (p

= 0.000) as well as between 32°C, and 26°C (p = 0.002). Pairwise test also showed significant changes for the pairs: 20°C and 32°C and (p =0.003); 26°C and 32°C (p = 0.000). The pair comparison of 20°C and 32°C exhibited significantly higher heart rates at 32°C.

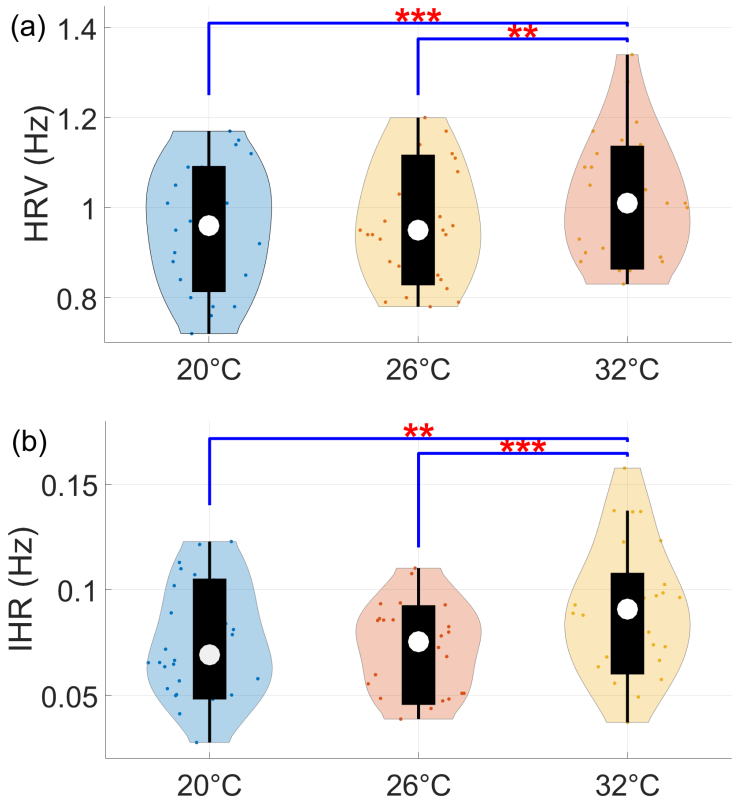

Figure 4.2: Violin plots of the average (a) Heart rate variability and (b) Instantaneous heart rate at three ambient temperatures. Statistical significance difference was observed in heart rate and HRV by Kruskal-Wallis (multi-comparison test) and Wilcoxon signed rank (pairwise test) for paired data. p -values for heart rate are recorded as follows: 20°C - 26°C (0.279), 20°C - 32°C (0.000), and 26°C - 32°C (0.002). While p -values for HRV were 20°C - 26°C (0.255), 20°C - 32°C (0.003), and 26°C - 32°C (0.000). In terms of group test, significant difference was observed in HRV (0.043), but not heart rate (0.312).

A single heart rate value for each individual was calculated by averaging the heart rate signal across all ambient temperatures. These individual figures were then used

to make comparisons between various ambient temperatures as can be seen in figure 4.3 (a). Similar steps were taken for the heart rate variability as shown in 4.3 (b).

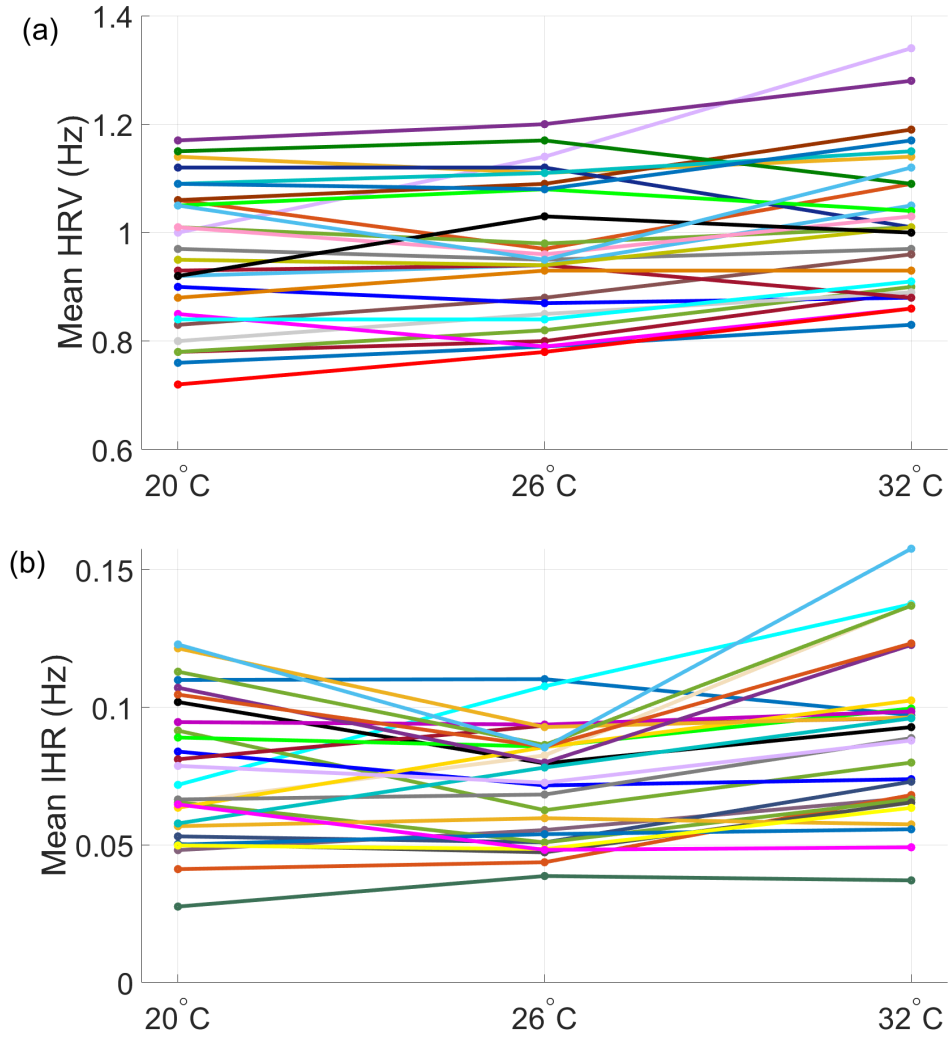

Figure 4.3: Mean values of (a) heart rate (calculated by marked events) and (b) HRV (STD of wavelet ridge frequency) at three ambient temperatures. The purpose of presenting the linear connections between points is simply to assist with visually identifying the changes that have occurred for specific subjects, with each subject being represented by a unique colour.

4.2.1.1 Spectral power of the instantaneous heart frequency/heart rate variability (IHR/HRV)

Figure 4.1 shows an example of the time-frequency representation for continuous wavelet transforms of ECG signals while they are being affected by heating. These transforms are performed on the data as they are being analysed. The oscillations that can be seen in the ECG signal when it is recorded under any circumstance are depicted quite clearly in the figure. Figure 4.4 displays the time-averaged group median spectral power of the oscillations found in IHR signals. The 25^{th} and 75^{th} percentiles respectively.

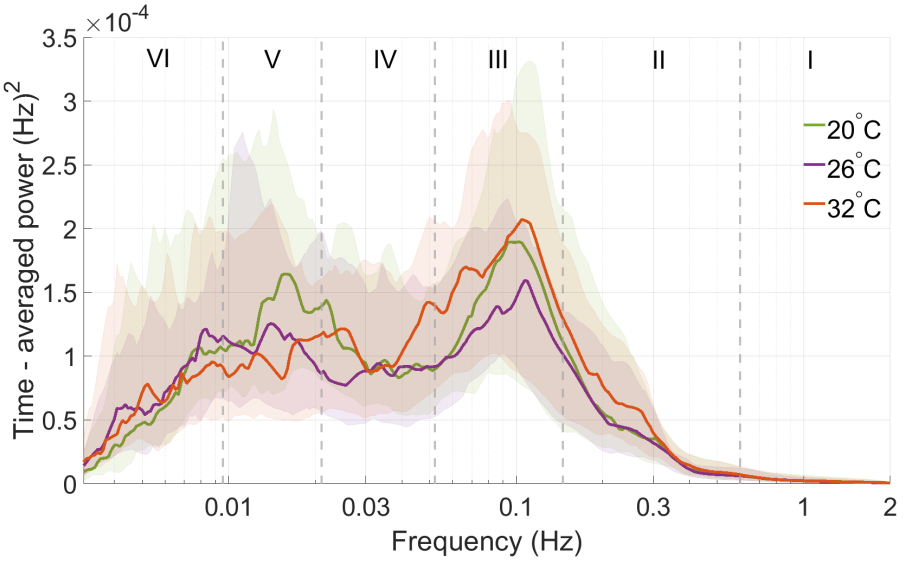

Figure 4.4: Time-averaged wavelet powers of heart rate variability. Group median time-averaged spectral power calculated from the wavelet transforms of heart rate variability for 32 minutes for each ambient temperature (20°C, 26°C, and 32°C). Dashed lines indicate the frequency intervals of oscillations observed in heart rate variability (HRV). No statistical significant difference was observed across all the frequency intervals.

HRV showed significant difference in the myogenic and respiratory spectral bands components of HRV as shown in figure 4.5. The power spectrum of HRV revealed

an increase for the low frequency band at low ambient temperature (although not significant) and an increased power in myogenic band at high ambient temperatures. These changes were not significant as shown by the Kruskal-Wallis test.

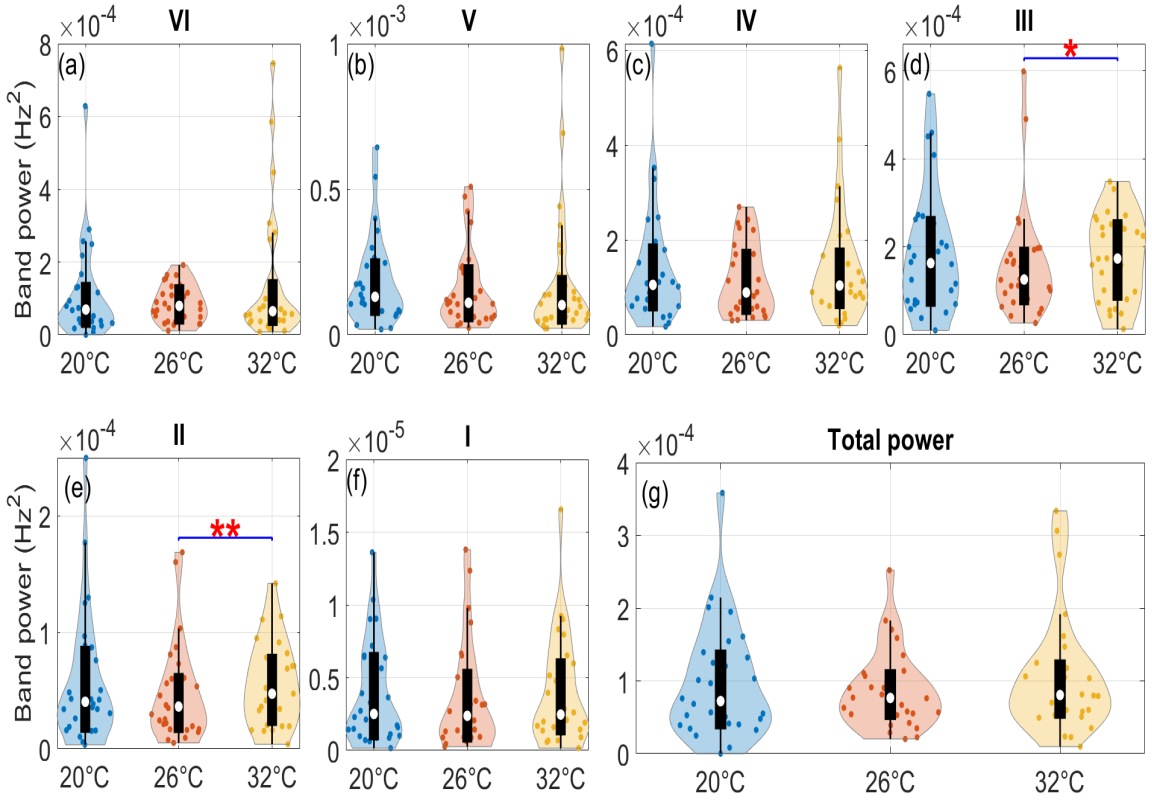

Figure 4.5: Violin plots compare the median power content within the bands investigated for the (a) Endothelial activity, (b) Endothelial metabolic activity, (c) Neurogenic activity, (d) Myogenic activity, (e) Respiration, (f) Cardiac activity oscillations, and finally the total power in the HRV signal. The central circle indicates the median. Wilcoxon signed rank test which was applied for comparisons in each frequency band between the three ambient temperatures and statistical significance was set at $p < 0.05$. Significance is considered as $^{*}p < 0.05$,$^{**}p < 0.01$, $^{***}p < 0.001$.

However, significant differences obtained by pairwise test were revealed by comparing median powers of 26°C with 32°C at myogenic and respiration bands ($p = 0.026$ and $p = 0.003$, respectively).

4.2.2 Stroke volume

Time domain analysis

Figure 4.6 displays the results of calculating the average for each subject across the three different environmental temperatures (a). While the results of standard deviation calculations performed on the same signals (b).

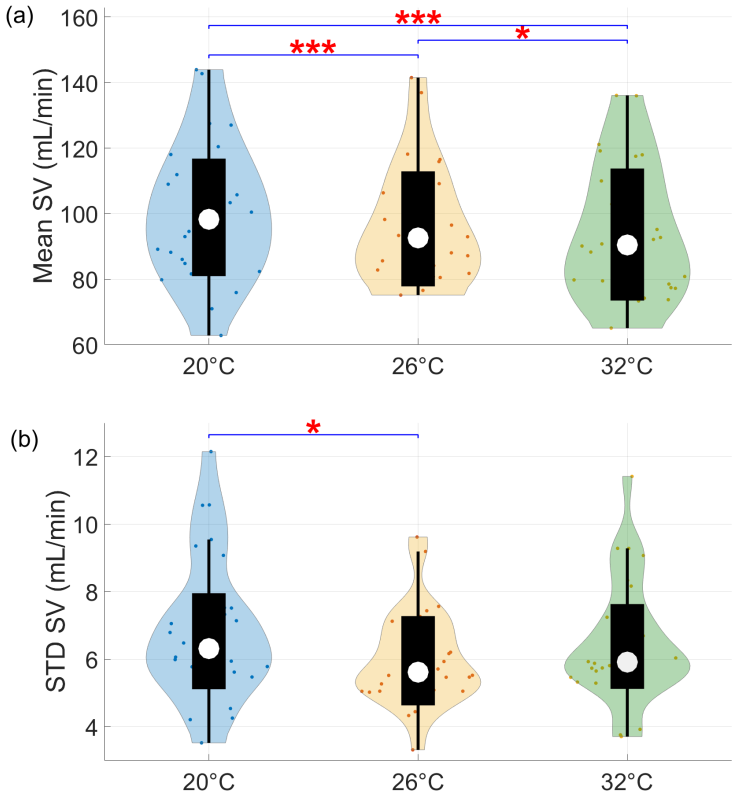

Figure 4.6: Violin plots of the average (a) and (b) standard deviation of stroke volume signals at three ambient temperatures. Statistical significance difference was observed in mean STD of SV and STD by Kruskal-Wallis (multi-comparison test) and Wilcoxon signed rank (pairwise test) for paired data. p -values for heart rate are recorded as follows: 20°C - 26°C (0.007), 20°C - 32°C (0.000), and 26°C - 32°C (0.043). While p -values for STD, 20°C - 26°C (0.072), 20°C - 32°C (0.943), and 26°C - 32°C (0.042). In terms of group test, no significant difference was observed in mean values (0.341), or STD values (0.375).

A single "stroke-volume" value for each individual was calculated by averaging the stroke volume signal across all ambient temperatures. These individual figures were then used to make comparisons between various ambient temperatures as can be seen in figure 4.7 (a). Similar steps were taken for the standard deviation of stroke volume as shown in (b).

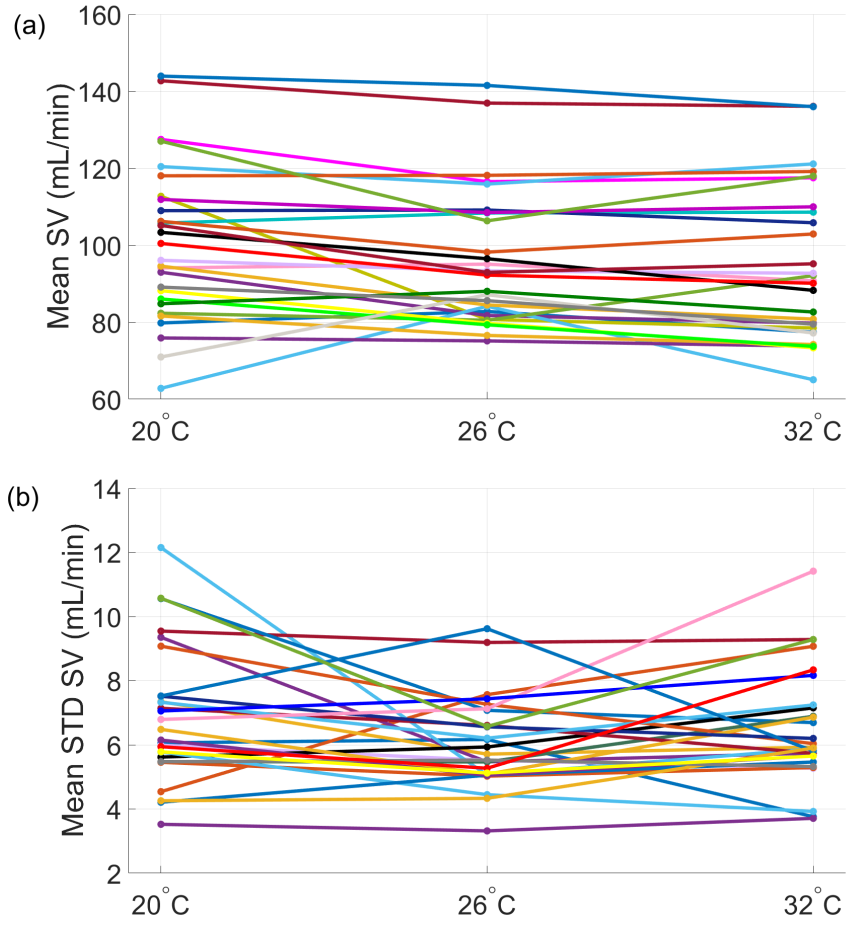

Figure 4.7: Mean values of (a) stroke volume and (b) STD of stroke volume at three ambient temperatures. The purpose of presenting the linear connections between points is simply to assist with visually identifying the changes that have occurred for specific subjects, with each subject being represented by a unique colour.

4.2.2.1 Spectral power of the stroke volume

Figure 4.8 depicts the effect of heat on the wavelet power spectra of stroke volume time series. Time-averaged wavelet powers were calculated for each subject throughout the three ambient temperature, and a median value was then calculated. In order to allow the function to calculate frequencies as low as feasible, the minimum frequency was left unspecified and the maximum frequency was set to 2 Hz. The central frequency is 1 Hz.

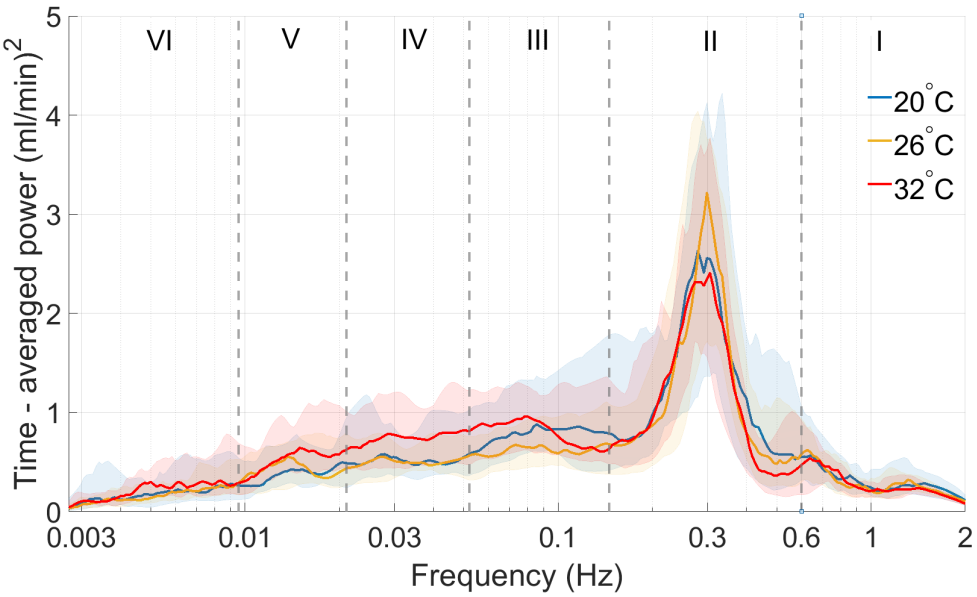

Figure 4.8: Time-averaged wavelet powers of the stroke-volume time-series. Group median time-averaged spectral power calculated from the wavelet transforms of stroke volume for 32 minutes for each ambient temperature (20°C, 26°C, and 32°C). No statistically significant difference in time averaged wavelet power was observed across all the frequency intervals.

The stroke volume power spectrum contained an intensity peak at the respiratory frequency ($\leq$ 0.3 Hz) in addition to the cardiac peak and both peaks were reduced by heating. Nevertheless, no significant differences were found either by multi-comparison

or pairwise tests for this particular band. Indeed, the changes in power were not significantly different as shown by multi-comparison test. However, significant differences determined by pairwise test were observed across all the frequency bands except the respiration band (where most of the power of the oscillations is concentrated).

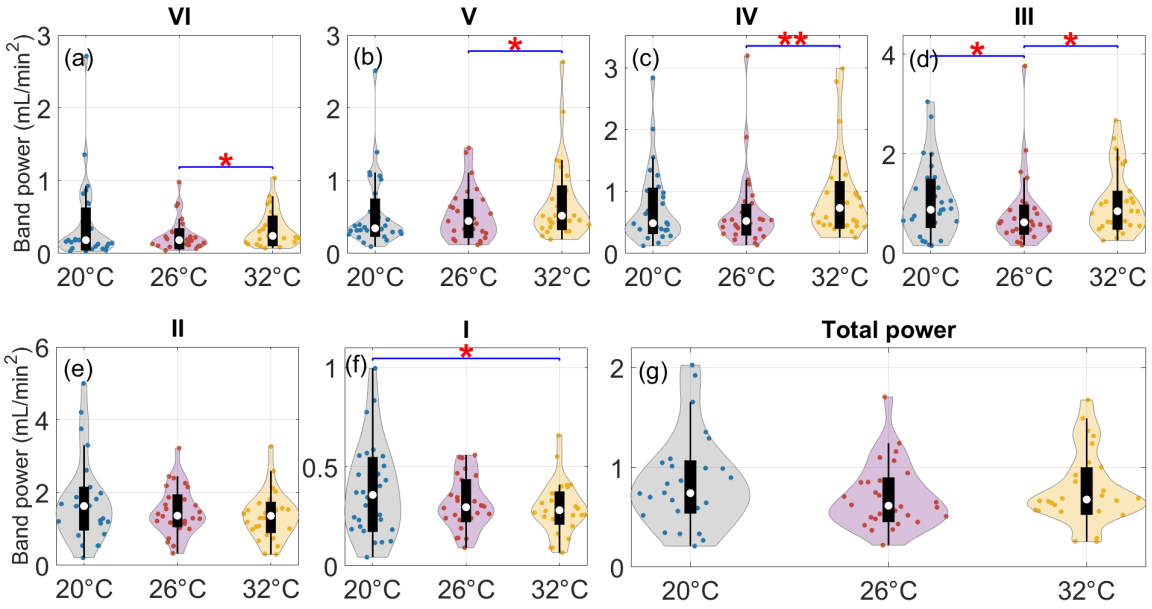

Figure 4.9: Spectral power of stroke-volume time-series within frequency bands. The spectral power of stroke volume investigated for each frequency band including the total power in the stroke volume power spectrum. The central circle indicates the median value and dots show the distribution of individual value. The Wilcoxon signed rank test was applied for comparisons in each frequency band between the three ambient temperatures and statistical significance was set at $p < 0.05$. Significance is considered as $^*p < 0.05$,$^{**}p < 0.01$, $^{***}p < 0.001$.

In the low frequency intervals (VI, V, and IV), significant differences were found between 26°C and 32°C only ($p = 0.031$, 0.017, and 0.003, respectively). The myogenic frequency interval shared the same significant difference with the previous band in addition to the pair of 20°C and 26°C ($p = 0.024$ and 0.010, respectively). In the cardiac band, significant differences were observed between the lowest and highest

ambient temperatures 20°C and 32°C ($p = 0.043$) as illustrated in figure 4.9.

4.2.3 Cardiac Output

Calculation of cardiac output time series

Cardiac output was calculated in the time domain for each subject and before any further analysis carried out. Cardiac output relies on heart rate and stroke volume and both of these were measured for each subject.

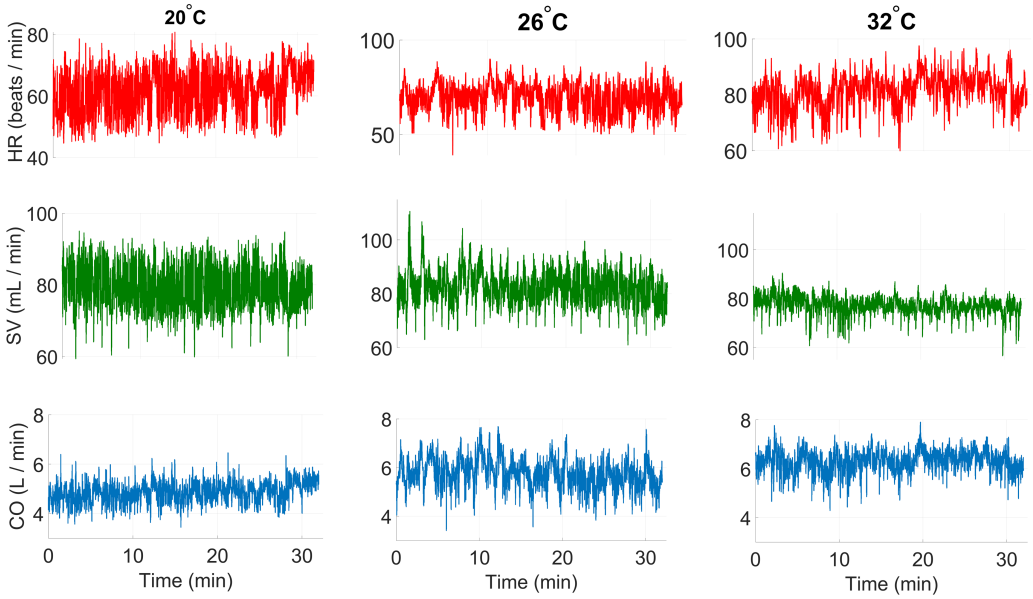

Figure 4.10: Example of calculating cardiac output. A typical heart rate time series is shown in the first row at three different temperatures. The second row shows the stroke volume. The third row shows the result of multiplying the first and second rows which yields the cardiac output for three different temperatures.

Consequently, cardiac output was calculated by multiplying the heart rate by the stroke volume. The impact of temperature on cardiac output time series is shown in figure 4.10. Mean values were calculated for all subjects for the three ambient temperatures to see the how the mean varies with varying temperature as

demonstrated in figure 4.11 (a). The standard deviation was calculated also for the same signals as demonstrated in figure 4.11 (b).

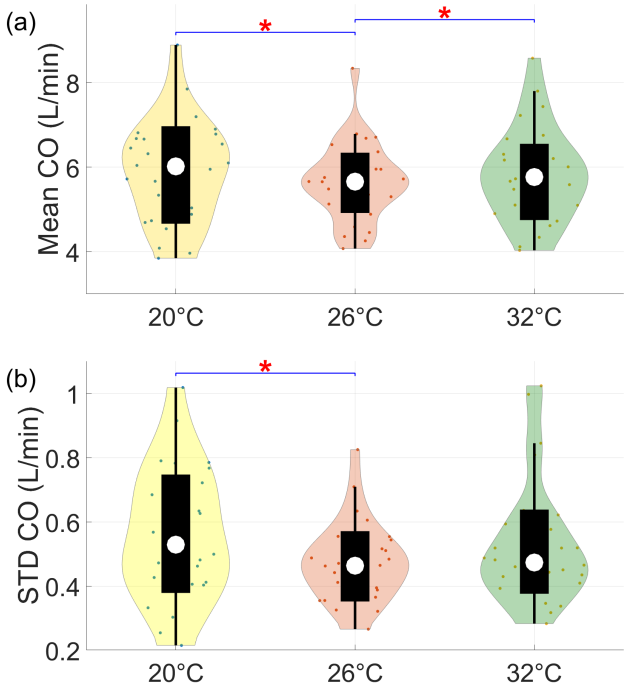

Figure 4.11: Violin plots of the average (a) and (b) standard deviation of cardiac output signals at three ambient temperatures. A statistically significant difference was observed in the means of SV and STD of SV by the Kruskal-Wallis (multi-comparison test) and the Wilcoxon signed rank (pairwise test) for paired data. p -values for heart rate are as follows: 20°C - 26°C (0.031), 20°C - 32°C (0.716), and 26°C - 32°C (0.045). The p -values for STD were: 20°C - 26°C (0.024), 20°C - 32°C (0.682), and 26°C - 32°C (0.133). In terms of group test, no significant difference was observed in mean values (0.616), or STD values (0.283).

A single cardiac output value for each individual was calculated by averaging the stroke volume signal across all ambient temperatures. These individual figures were then used to make comparisons between various ambient temperatures as can be seen in figure 4.12 (a). Similar steps were taken for the standard deviation of cardiac output as shown in figure 4.12 (b).

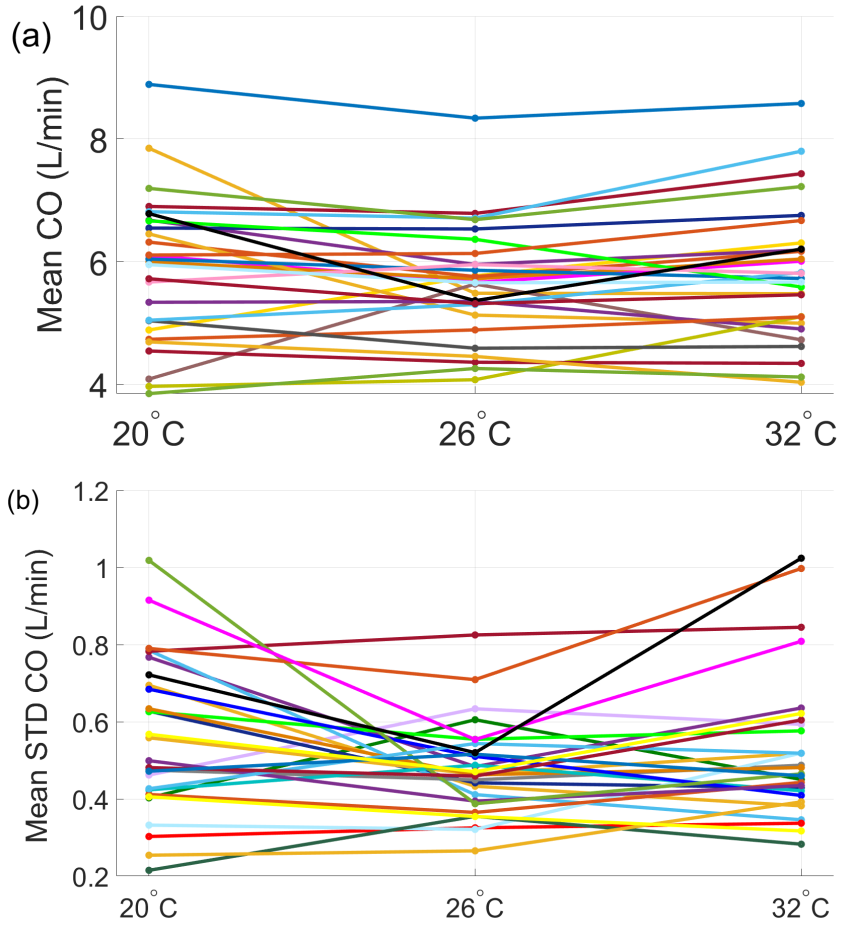

Figure 4.12: Mean values of (a) cardiac output and (b) STD of cardiac output at three ambient temperatures. The purpose of presenting the linear connections between points is simply to assist with visually identifying the changes that have occurred for specific subjects, with each subject being represented by a unique colour.

4.2.3.1 Spectral power of the cardiac output

Median values of time-averaged wavelet powers were determined for each individual across the three temperature conditions. The minimum frequency was left unspecified to allow the function to detect frequencies, as low as possible, and the maximum frequency was set to 2 Hz to allow the function detecting frequencies as low as possible. Here, the pre-processing is turned on and the central frequency is set to 1 Hz. Figure

4.13 reveals that the spectral components of the cardiac output signal extend a wide frequency range, beginning at 0.003 Hz and ending at the cardiac frequency.

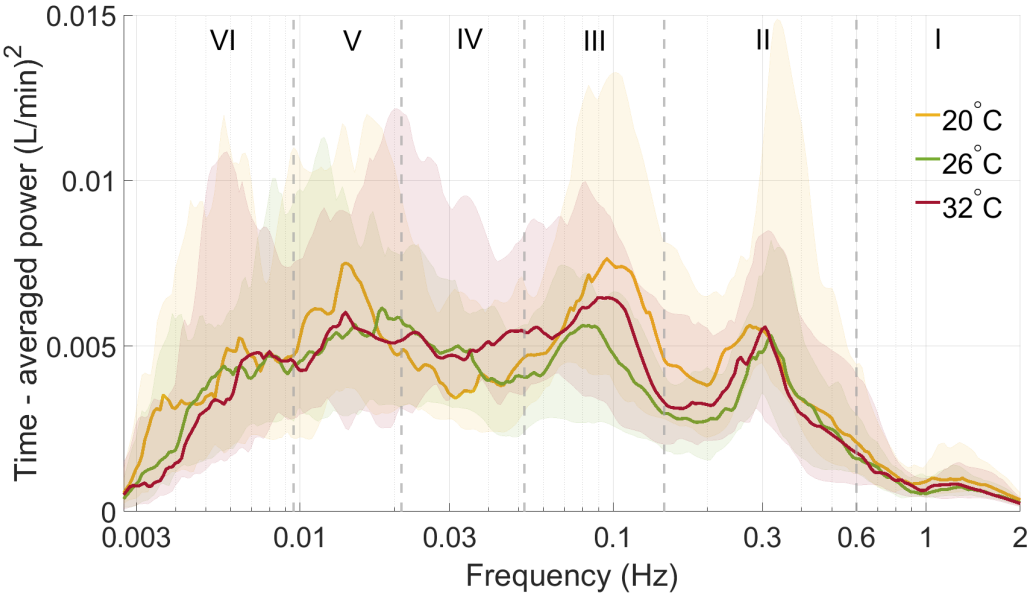

Figure 4.13: Time-averaged wavelet power of the cardiac output. Power is averaged over 32 min at three different ambient temperatures: 20°C, 26°C, and 32°C. Oscillations components in the cardiac output are separated by dashed lines. It was found that there was no statistically significant difference in the time-averaged wavelet power within any of the frequency intervals.

The time-averaged wavelet power of cardiac output was compared between all three ambient temperatures, and significant differences were not found by multi-comparison test in any of the frequency bands. However, significant differences obtained by the pair-wise test were found between 20°C-32°C in the neurogenic ($p = 0.006$) and myogenic bands ($p = 0.011$ and 0.027) between 20°C−32°C and 26°C−32°C, and finally in the respiration bands between 20°C−26°C and 20°C−32°C ($p = 0.013$ and 0.026, respectively) as shown in figure 4.14.

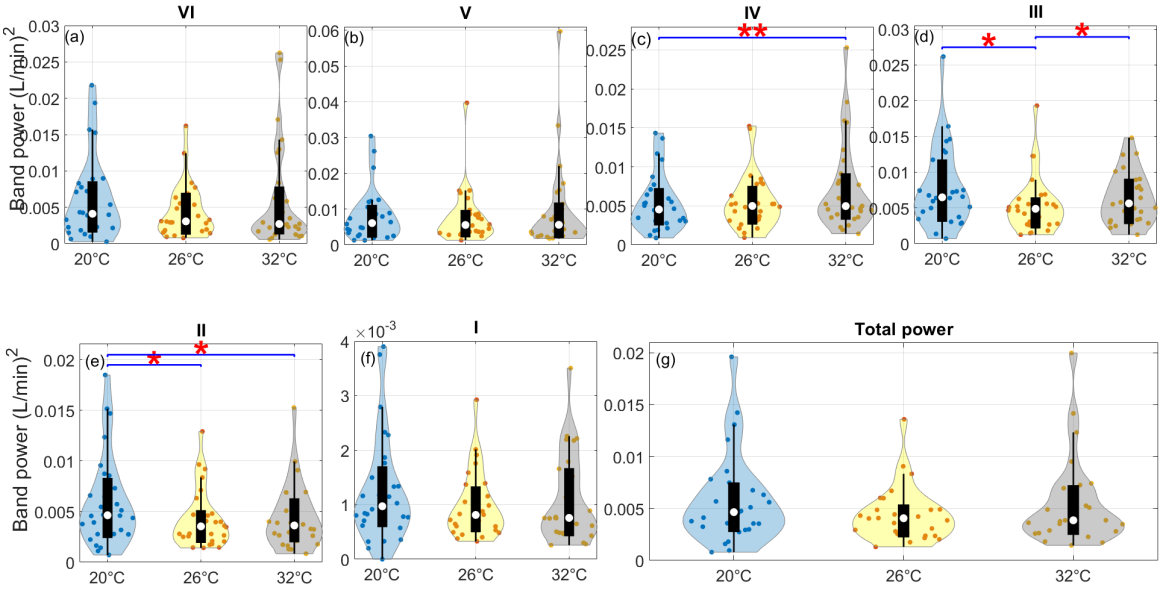

Figure 4.14: The median power of cardiac output within bands. The central circle indicates the median value. Wilcoxon signed rank test was applied for comparisons in each frequency band between the three ambient temperatures and statistical significance was set at $p < 0.05$. Significance is considered as $^{*}p < 0.05$, $^{**}p < 0.01$, $^{***}p < 0.001$.

4.2.4 Respiration and instantaneous respiration rate

The instantaneous respiration rate was extracted in a similar way to that performed in IHR, but in the frequency range of 0.145 - 0.6Hz. The mother wavelet used for ridge extraction is the lognormal wavelet, and the central frequency is 1Hz. Figure 4.15 shows the steps used in the extracting instantaneous respiration rate.

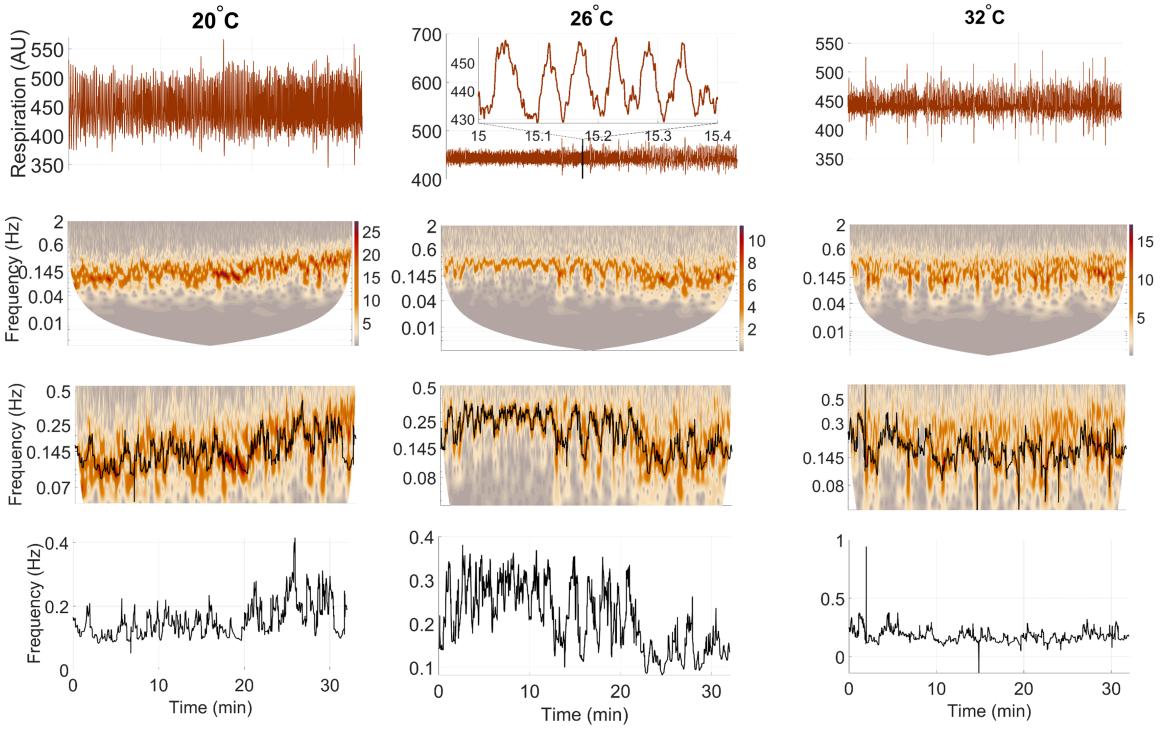

Figure 4.15: Example of extracting the instantaneous respiration rate from a respiration signal from one subject during heating. A typical respiration time series is shown in the first row at three different temperature. In the second row, the respiration signal undergoes a complete wavelet transformation. The third row shows a clear oscillating pattern around the expected respiration rate of 0.145 - 0.6 Hz. Time series of instantaneous respiration frequency produced from a wavelet transform via ridge extraction are shown in the fourth row.

Figure 4.16 (a) displays the respiration rate, while b) instantaneous respiration rate (standard deviation of respiration rate). No statistical differences were found in respiratory rate and respiration rate variability across the three ambient temperatures (b) as evaluated by a multi-comparison and pairwise test.

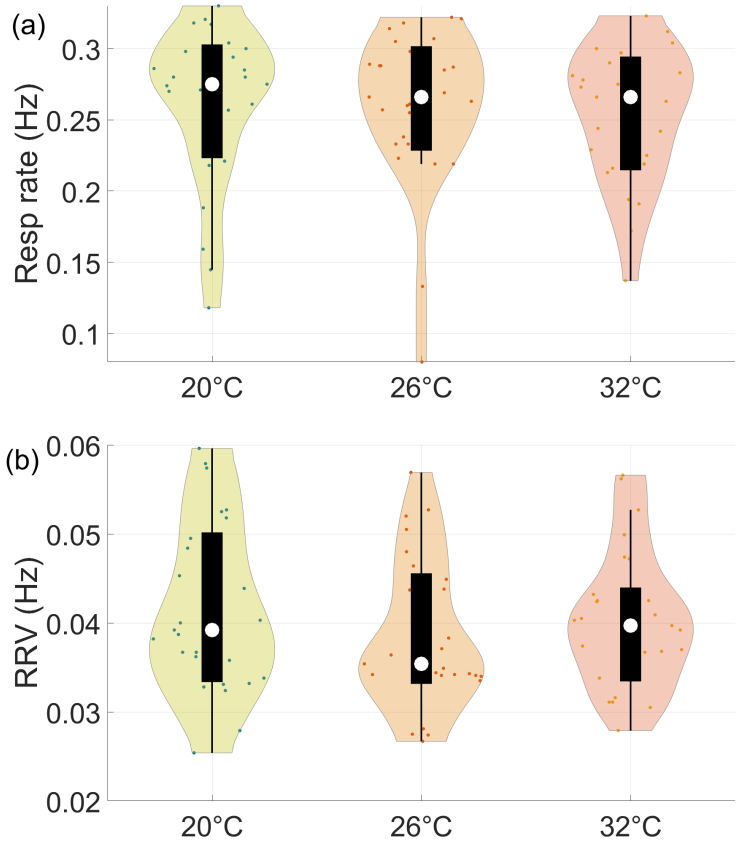

Figure 4.16: Violin plots of the (a) respiration rate and (b) respiration rates variability at three ambient temperatures. Tests for statistically significant differences were significance difference was performed for the respiration rate and RRV by Kruskal-Wallis (Group test) and Wilcoxon signed rank (pair test) for paired data. p -values for heart rate are recorded as follows: 20°C - 26°C (0.685), 20°C - 32°C (0.866), and 26°C - 32°C (0.224). While p -values for RRV, 20°C - 26°C (0.07), 20°C - 32°C (0.585), and 26°C - 32°C (0.264). In terms of group tests, significant differences were not observed in either the respiration rate (0.685), or the respiration rate variability (0.534).

A single respiration rate value for each individual was calculated by averaging the respiration rate signal across all ambient temperatures. These individual figures were then used to make comparisons between various ambient temperatures as shown in figure 4.17 (a). Similar steps were taken for the standard deviation of respiration rate

as shown in figure 4.17 (b).

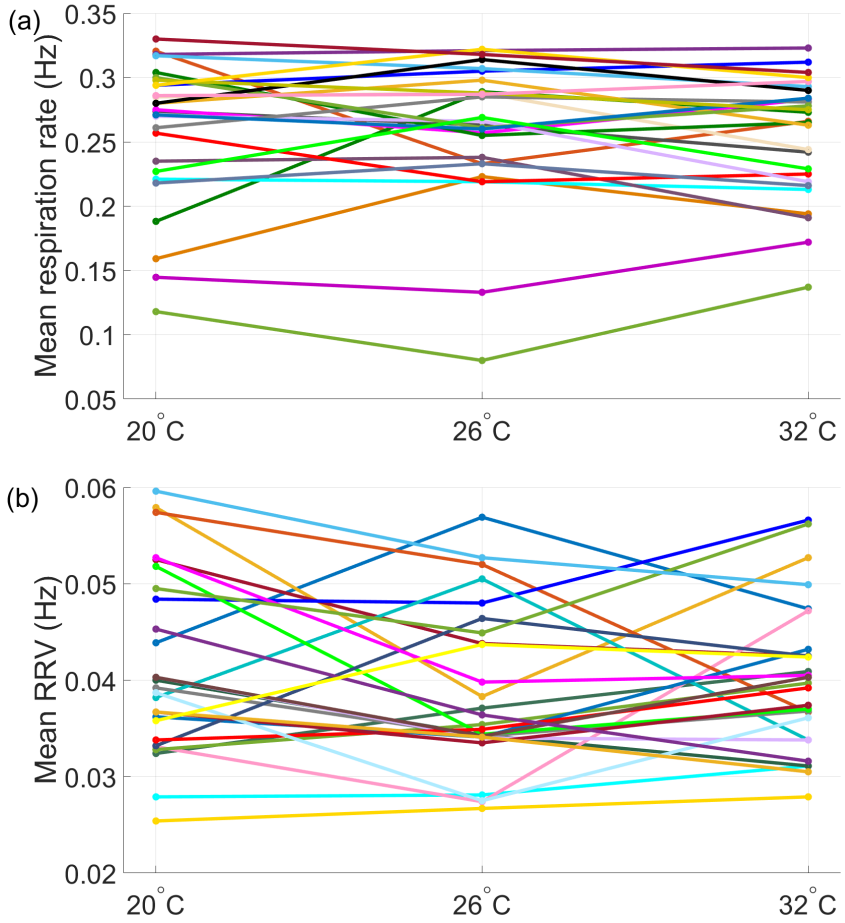

Figure 4.17: Mean values of (a) respiration rate (calculated by marked events) and (b) RRV (STD of wavelet ridge frequency) at three ambient temperatures. The purpose of presenting the linear connections between points is simply to assist with visually identifying the changes that have occurred for specific subjects, with each subject being represented by a unique colour.

4.2.5 Respiration (raw signals) and instantaneous respiration rate (IRR)

The influence that heat has on the wavelet power spectra of respiration time series is illustrated in figure 4.18. Time-averaged wavelet power was obtained for each subject

at three ambient temperatures, and then a median value was determined for each of those values. The minimum frequency was left unspecified, while the maximum frequency was set to 2 Hz in order to provide the function with the ability to calculate frequencies as low as is practically possible. In this instance, we have decided to turn preprocessing "on" and have set the central frequency to 1Hz.

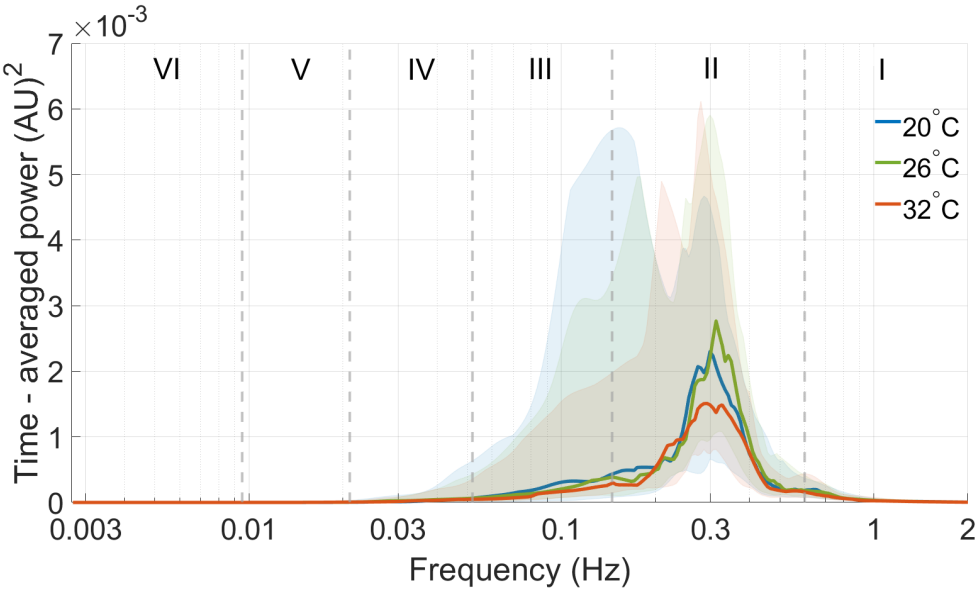

Figure 4.18: Time-averaged wavelet power of raw respiration time series. The dashed lines indicate the frequency bands of the respiration. No statistical significant difference in time averaged wavelet power was observed across the frequency intervals.

For each of the three ambient temperatures, the multi-comparison test indicated no statistically significant difference in median power with increasing power ($p > 0.05$). Using the paired Wilcoxon pairwise test, we find no statistically significant differences between any of the groups. Similarly, all of the respiration time series were entered into the ridge extraction function, and inside that function, we selected a frequency range of 0.145–0.6 Hz in which to extract the IRR using a lognormal wavelet with a centre frequency of 1 Hz. This resulted in the production of a time series of the variability of the respiration rate over time of the same length as the initial signal,

one for each participant in each temperature (i.e. 20°C, 26°C and 32°C). After that, each wavelet transform was computed by employing the Morlet wavelet function with a centre frequency of 1 Hz. The pre-processing was switched to the "on" setting. The IRR power spectral is shown in figure 4.19.

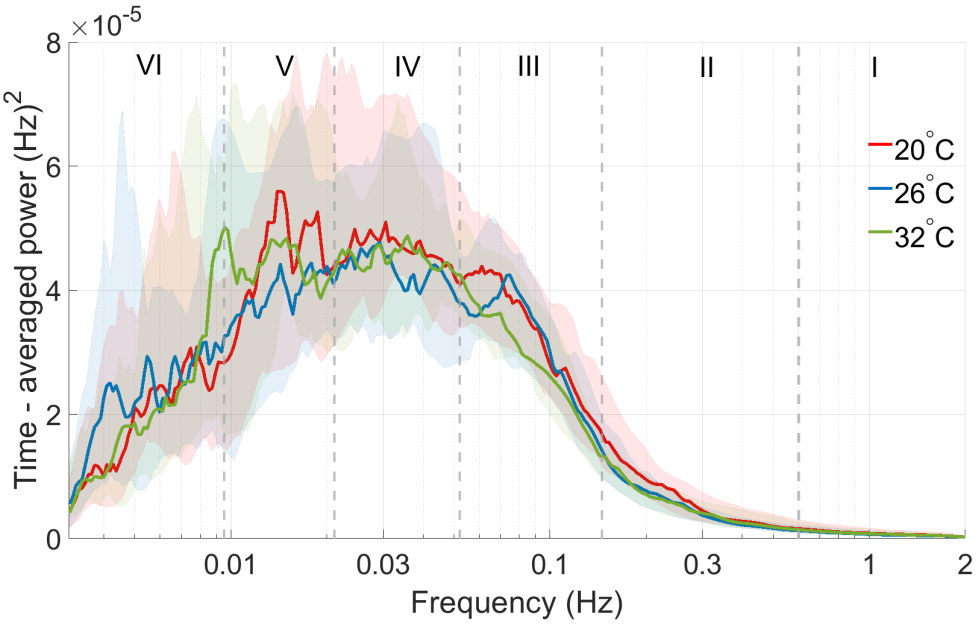

Figure 4.19: Time-averaged wavelet powers of instantaneous respiration rate as a function of frequency. The average spectral power over 32 minutes for a group at three different temperatures (20°C, 26°C, and 32°C) was estimated using wavelet transforms of the variability in respiratory rate. No statistically significant difference was determined by Kruskal-Wallis test in any of the frequency bands.

The Kruskal-Wallis tests showed no statistically significant differences across any of the examined frequency ranges ($p < 0.05$). In a similar pattern, the pair-wise test was applied for each power band and a statistically significant difference was revealed only in the respiration frequency band only ($p = 0.0095$) as shown in figure 4.20.

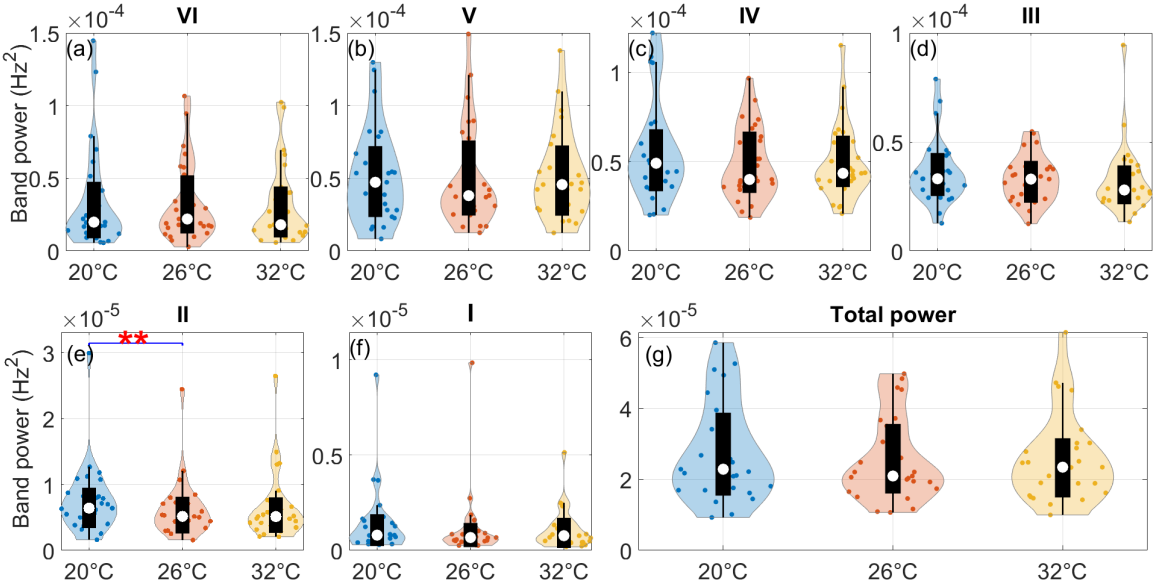

Figure 4.20: The median power of instantaneous respiration rate within bands. Wilcoxon signed rank test was applied for comparisons in each frequency band between the three ambient temperatures and statistical significance was set at $p < 0.05$. Significance is considered as $^{*}p < 0.05$, $^{**}p < 0.01$, $^{***}p < 0.001$.

4.2.6 Blood pressure analysis

4.2.6.1 Spectral power of blood pressure

The influence that heating has on the wavelet power spectra of blood pressure time series is illustrated in figure 4.21. At each of the three temperatures, the median of the time-averaged wavelet powers was determined for each individual. The frequency range of 0.0027 - 2Hz was determined and the central frequency was 1Hz. The pre-processing was set to 'on'.

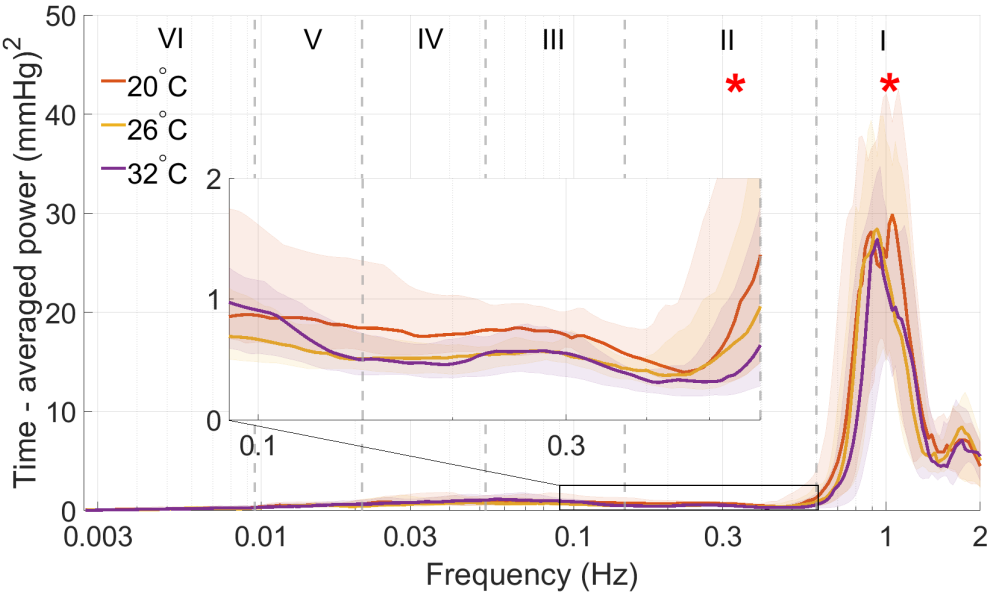

Figure 4.21: Time-averaged wavelet power for blood pressure. The spectral power calculated from the wavelet transforms of blood pressure for 32 minutes at each ambient temperature (20°C, 26°C, and 32°C). Statistically significant differences were observed in the power spectrum as shown by red stars in the specified frequency bands.

Significant differences were reveled at cardiac and respiration bands by both multi-comparison ($p = 0.026$, and 0.025, respectively) as well as pairwise test across all pairs of ambient temperature 20°C−26°C ($p = 0.006$) and 20°C−32°C ($p = 0.000$) and 26°C−32°C ($p = 0.000$). Significant differences were also observed by pair-wise test across all pairs of ambient temperature 20°C−26°C ($p = 0.012$) and 20°C−32°C ($p = 0.000$) and 26°C−32°C ($p = 0.005$) for the mentioned bands. Although the distribution of power was very low at other frequency bands, a significant difference was still observed in the myogenic band ($p = 0.045$). Significant differences were observed also in the total power between ambient temperatures as shown in figure 4.22.

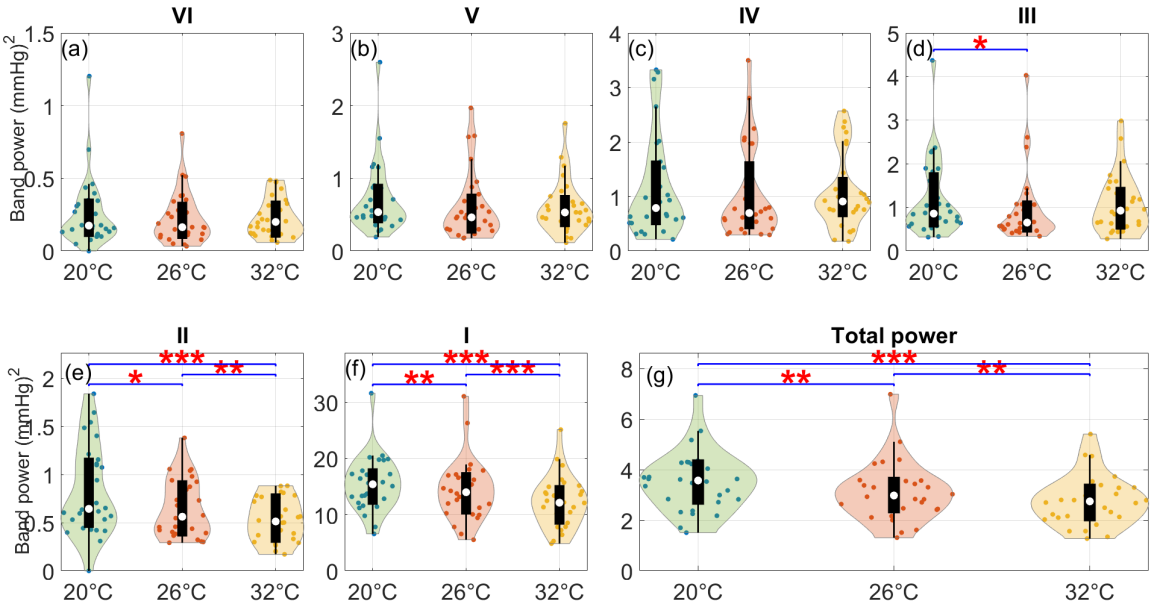

Figure 4.22: Violin plots show the median power content investigated for each frequency band including the total power in the blood pressure power spectrum. The central circle indicates the median value. The Wilcoxon signed rank test was applied for comparisons in each frequency band between the three ambient temperatures and statistical significance was set at $p < 0.05$. Significance is considered as $^*p < 0.05$,$^{**}p$ <0.01, $^{***}p$ <0.001 .

4.2.6.2 Systolic blood pressure analysis

Time domain analysis

Figure 4.23 is an illustration of violin plots that reflect the (a) median and (b) interquartile (25^{th} and 75^{th} percentiles) of systolic blood pressure signals at three different ambient temperatures. As can be seen, an increase in temperature is associated with a reduction in the median of the systolic blood pressure signals. On the other hand, the median of the interquartile range demonstrates an increase in accordance with the rising temperature. Both multi-comparison and pairwise tests were used to estimate the statistical difference between the three ambient temperatures whilst setting significance at ($p < 0.05$).

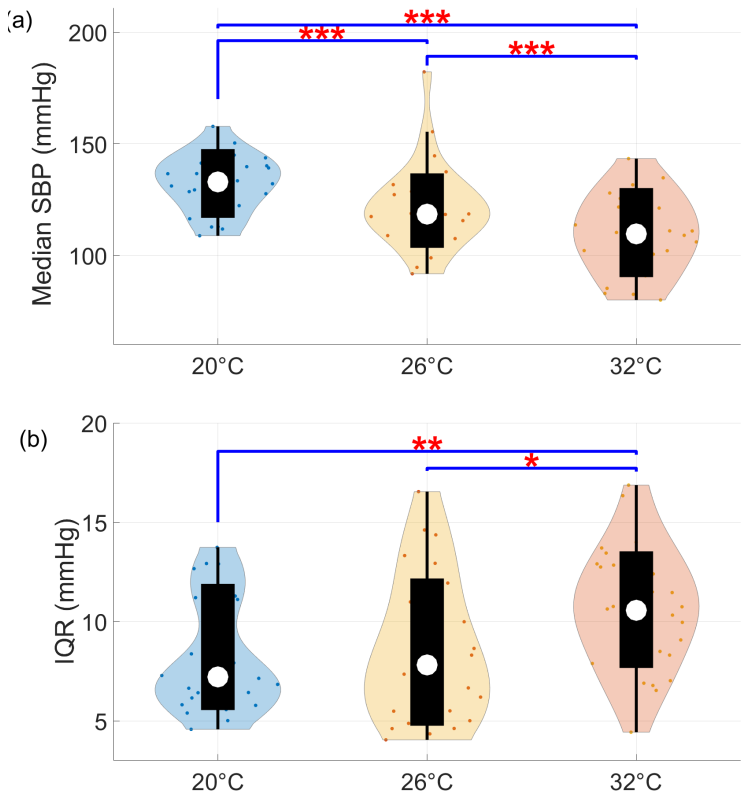

Figure 4.23: Violin plots of the (a) median systolic blood signals and (b) Interquartile range (IQR) for the same signals at three ambient temperatures. A statistically significant difference was observed in follows mean of sBP and interquartile of sBP by the Kruskal-Wallis (Group test) and Wilcoxon signed rank (pair test) for paired data. p -values for the medians are recorded as follows: 20°C - 26°C (0.000), 20°C - 32°C (0.000), and 26°C - 32°C (0.000). The p -values for the interquartile range were: 20°C - 26°C (0.982), 20°C - 32°C (0.001), and 26°C - 32°C (0.013). In terms of the group test, significant difference were observed in median values (0.000), and interquartile values (0.013).

4.2.6.3 Spectral power of the systolic blood pressure

Heat increases the wavelet power spectra of systolic blood pressure time series, as shown in figure 4.24 For each of the three ambient temperatures, the systolic blood pressure time series was analysed using the wavelet transforms for all subjects. With Morlet wavelet function, the default centre frequency of 1Hz was used. The frequency

range of the calculation were determined to be in between 0.0027Hz and 2Hz. An "on" setting for preprocessing was identified and each wavelet power signal was then averaged. After that, the median value was calculated for each frequency across all powers.

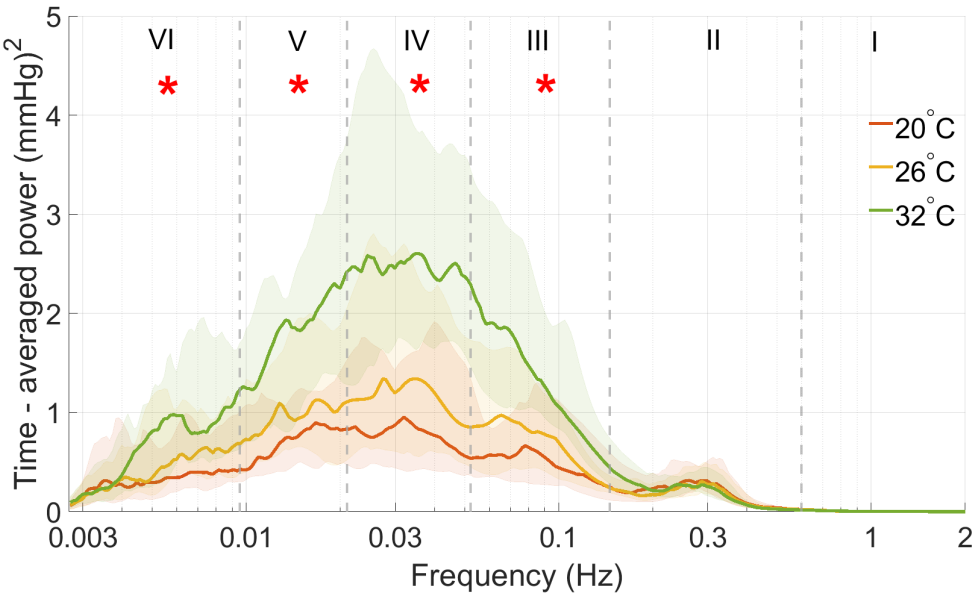

Figure 4.24: The time-averaged wavelet power for systolic blood pressure as functions of frequency. The spectral power was calculated from the wavelet transforms of systolic blood pressure for 32 minutes at each ambient temperature (20°C, 26°C, and 32°C). Statistically significant differences were observed in the power spectrum as shown by red stars in the specified frequency bands.

In terms of power, figure 4.24 shows that in the low frequency bands, the power of systolic blood pressure increased significantly with increasing ambient temperature. For all low frequency bands, the power is widely separated between high and low ambient temperatures.

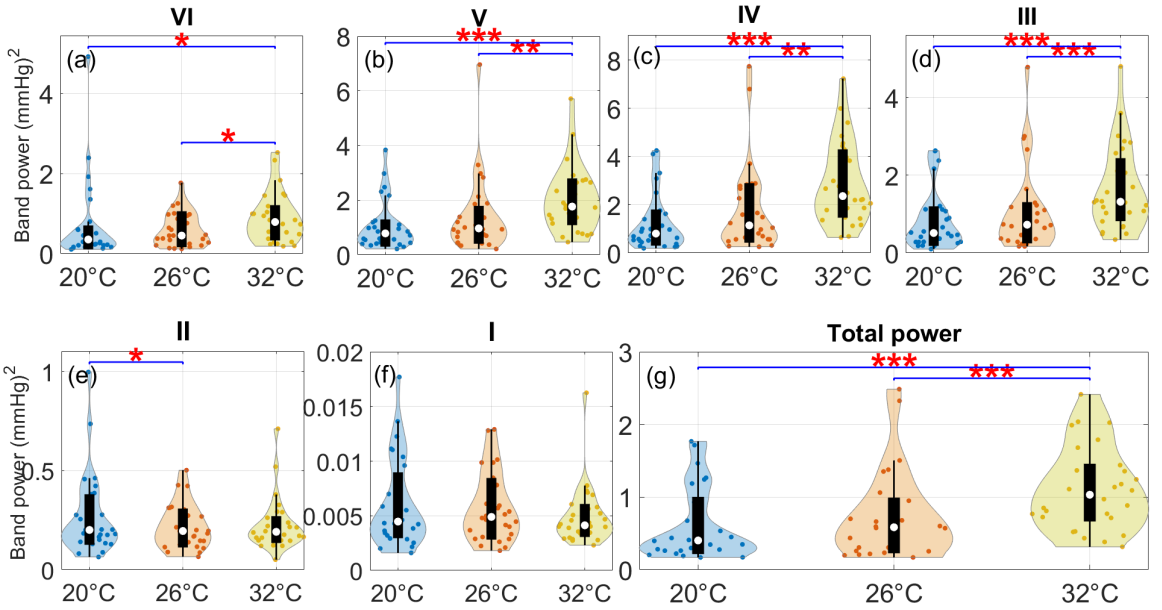

Figure 4.25: Violin plots show the median power content investigated for each frequency band including the total power in the systolic blood pressure power spectrum. The central circle indicates the median value. The Wilcoxon signed rank test was applied for comparisons in each frequency band between the three ambient temperatures and statistical significance was set at $p < 0.05$. Significance is considered as $^*p < 0.05$, $^{**}p$ <0.01, $^{***}p$ <0.001.

However, in the high frequency bands, gaps between curves reduced widely until dissipated. Nevertheless, significant difference observed through the Kruskal-Wallis test were found at all frequency bands except respiration and cardiac (p = 0.032, 0.000, 0.000, and 0.000). Similar significant differences were observed with the paired signed rank test for the pairs 20°C and 32°C and 26°C and 32°C, but in addition to the respiration band for the pair 20°C and 26°C, as shown in figure 4.25.

4.2.6.4 Diastolic blood pressure analysis in time domain

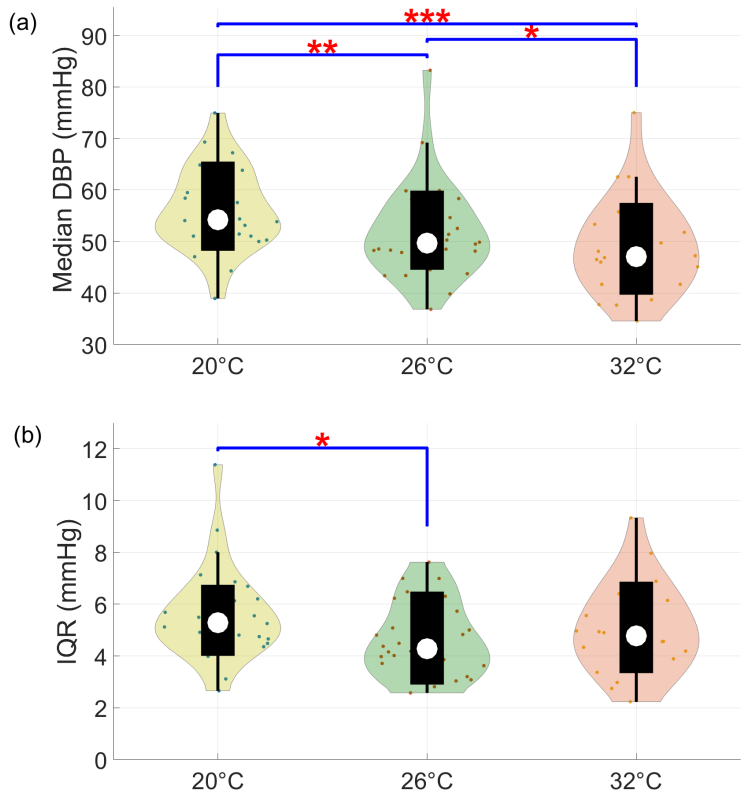

Figure 4.26: Violin plots of (a) the median diastolic blood signals and (b) Interquartile range (IQR) for the same signals at three ambient temperatures. A statistically significant difference was observed in the means of dBP and interquartile of dBP by the Kruskal-Wallis (Group test) and the Wilcoxon signed rank (pair test) for paired data. p -values for median are recorded as following: 20°C −26°C (0.003), 20°C - 32°C (0.000), and 26°C − 32°C (0.012). The p -values for the interquartile range, 20°C - 26°C (0.003), 20°C − 32°C (0.058), and 26°C − 32°C (0.116). In terms of the group test, significant difference were observed in median values (0.002), and interquartile values (0.085).

Figure 4.26 provides violin plots that depict (a) the median and (b) the interquartile range (25^{th} and 75^{th} percentiles) of diastolic blood pressure signals across three different ambient temperatures. As can be observed, the median diastolic blood pressure signals tends to drop as body temperature rises. However, as the temperature

increases, there is a consistent stability in the interquartile range's median, with a slight decrease in the range's median at 26°C.

4.2.6.5 Spectral power of the diastolic blood pressure

Similarly, a visual representation of the impact that heating has on the wavelet power spectra of the diastolic blood pressure time series can be seen in figure 4.27. Wavelet analysis was performed on each of the participant's diastolic blood pressure time series while they were exposed to each of the three different ambient temperatures.

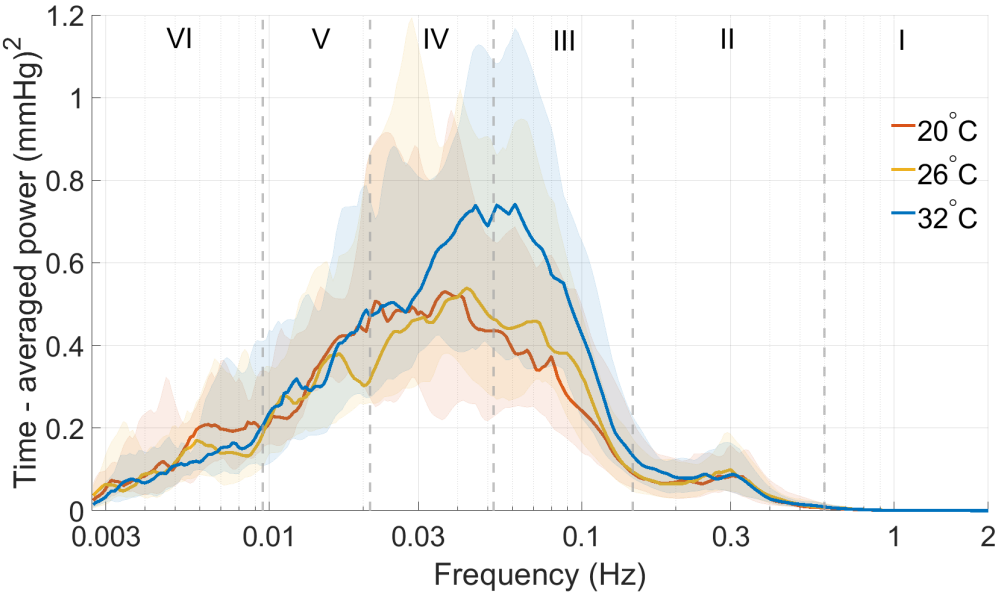

Figure 4.27: Time-averaged wavelet power for diastolic blood pressure. The spectral power was calculated from the wavelet transforms of diastolic blood pressure signals measured for 32 min at each ambient temperature (20°C, 26°C, and 32°C). No statistically significant differences were observed in the power spectrum in any of the frequency bands.

The Morlet mother wavelet was used, and its central frequency of the wavelet function was set to the default value of 1Hz. The frequency range was calculated to be from 0.0027 to 2Hz. The pre-processing was switched to the "on" position. Following that,

the time-averaged wavelet powers of every individual were calculated. Finally, the median value was determined for each frequency over all powers.

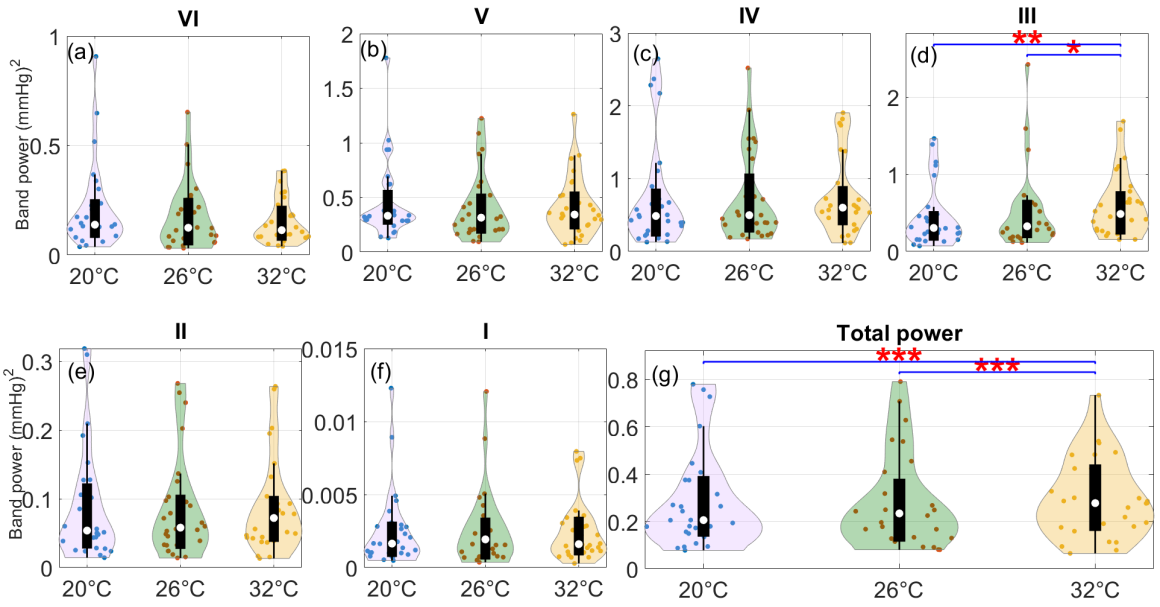

Figure 4.28: Violin plots show the median power content investigated for each frequency band investigated, including the total power in the diastolic blood pressure power spectrum. The central circle indicates the median value. The Wilcoxon signed rank test was applied for comparisons in each frequency band between the three ambient temperatures and the statistical significance was set at $p < 0.05$. Significance is considered as $^*p < 0.05$,$^{**}p$ <0.01, $^{***}p$ <0.001 .

Figure 4.27 shows the total median power of diastolic blood pressure spectrum increased with increasing temperature. Nevertheless, no significant differences were found by Kruskall-Wallis in any of the band. However, calculating Kruskal-wallis test across median showed a signficant (p =0.000). Similarly, significant differences calculated by signed rank test were only observed in the myogenic band between 20°C and 32°C as well as 26°C and 32°C (p = 0.006 and 0.031, respectively). Significant difference were observed within the pairs 20°C and 26°C as well as 20°C and 32°C (p = 0.000 and 0.000, respectively) as shown in figure 4.28.

4.2.7 Extracting instantaneous heart rate from blood pressure time series

For coherence analysis, instantaneous heart rate was extracted from blood pressure time series. Figure 4.29 shows an example of extracting IHR from blood pressure time series. The same parameters as used for ECG time series were also used for blood pressure signals. The entire blood pressure time series was entered into the ridge extraction function, and for the extraction of the IHR, a frequency range of 0.6–2Hz was used.

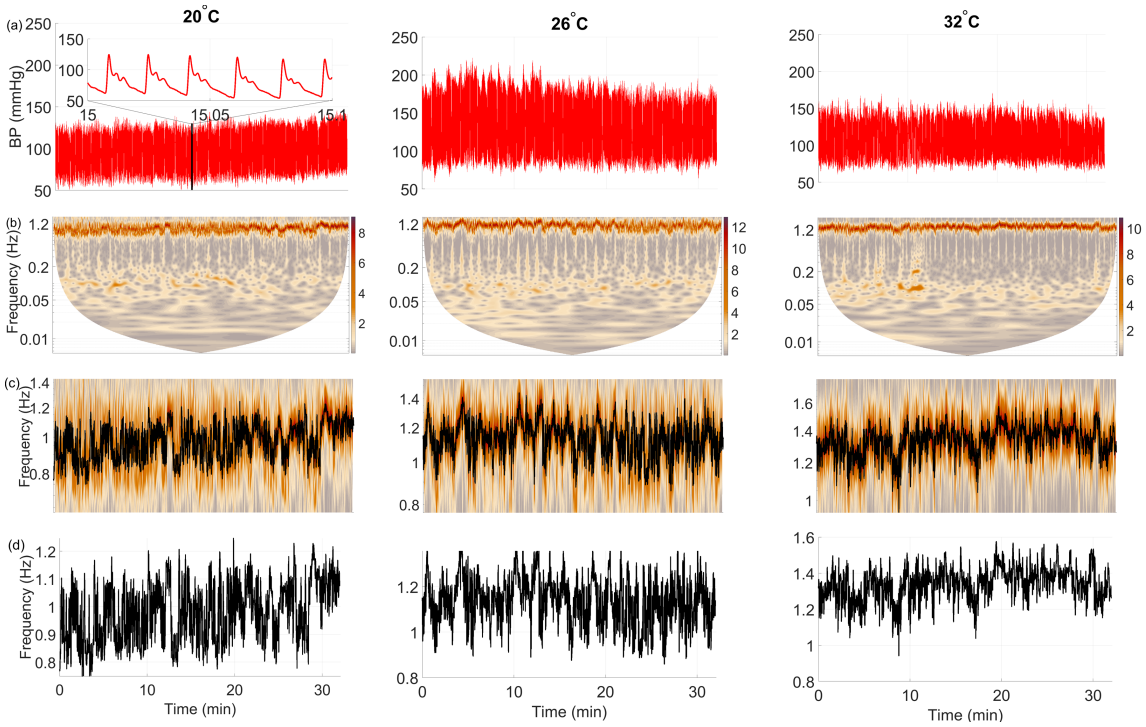

Figure 4.29: Examples of extracting instantaneous heart rate from a blood pressure signal for one subject at three different temperatures. Typical blood pressure time series are shown in the first row at three different temperatures. In the second row, the BP signals are wavelet transformed. The third row shows a clear oscillating pattern around the expected heart rate of 0.6 - 1.4Hz. Time series of instantaneous heart frequency after being extracted from wavelet transforms via ridge extraction, are shown in the fourth row.

This gave an output of time series of the variability of the heart rate over time of the same length as the original signal, one for each subject at each in each ambient temperature.

Mean values of instantaneous heart rate extracted from blood pressure were compared with instantaneous heart rate extracted from ECG signals at three ambient temperatures to see how they differed. Figure 4.30 shows that both means are almost identical.

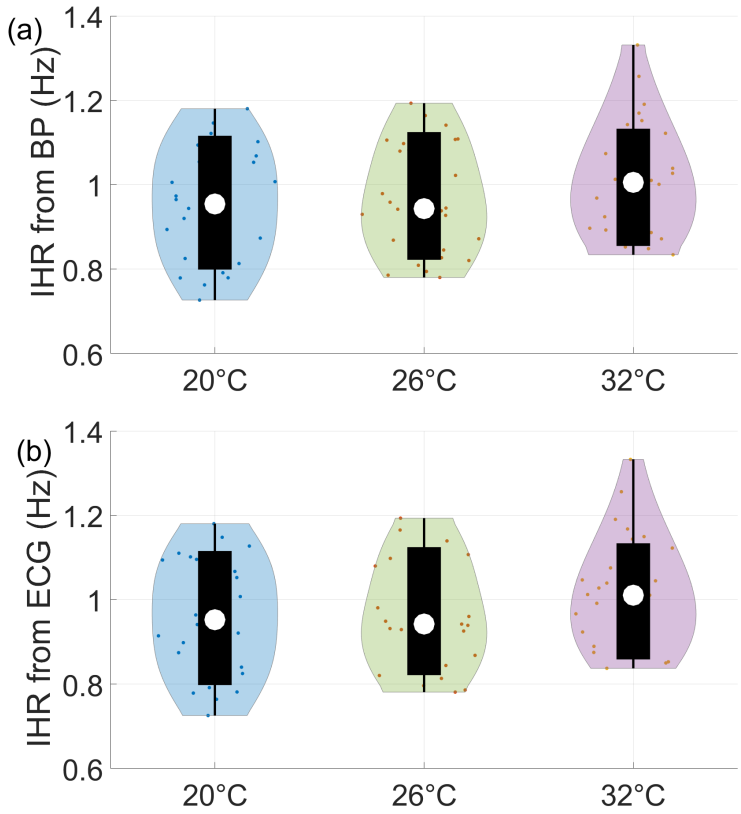

Figure 4.30: Violin plots of the mean for (a) instantaneous heart rate values extracted from blood pressure signals and (b) the instantaneous heart rate values extracted from ECG signals for the three ambient temperatures. The extracted values in both figures are almost the same.

4.3 Blood flow time series

Typical recordings of LDF blood flow time series, which were simultaneously obtained from the left, right index finger, and left forearm of the subjects at each of the three temperatures shown in figure 4.31, respectively.

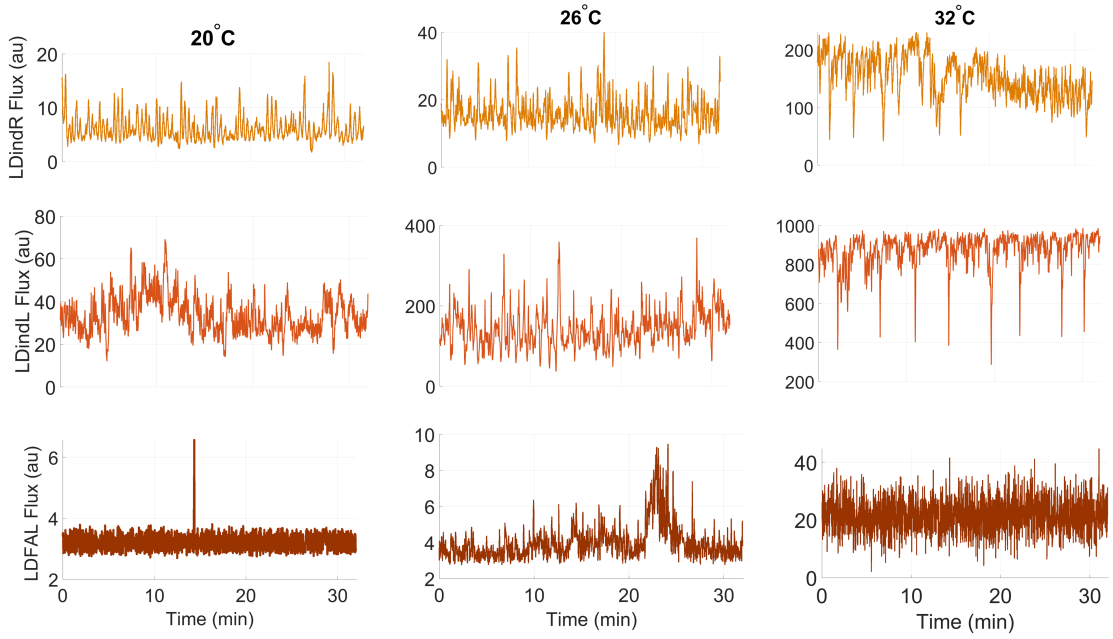

Figure 4.31: An example of three different blood flow time series measured from a subject under the effect of heating. The first row represents a typical blood flow measured on the right index finger. In the second row, blood flow measured from a left finger. The third row plots the blood flow signal measured on the left forearm.

4.3.1 Spectral power of the laser-Doppler flux right index finger (LDindR)

Figure 4.32 presents an illustration of the effect that heating has on the wavelet power spectra of the right index finger blood flow time series. All of the blood flow time series for each participant in each ambient temperature were wavelet processed for each of the three temperatures. The default central frequency of the wavelet function was

used, which is 1Hz, and a Morlet wavelet function was used. It was determined that the frequency range was between 0.002 and 1.6Hz. The pre-processing was setting to the "on" position. After that, time-averaged wavelet powers were calculated for each person. Lastly, at each frequency, the median value was taken across all powers.

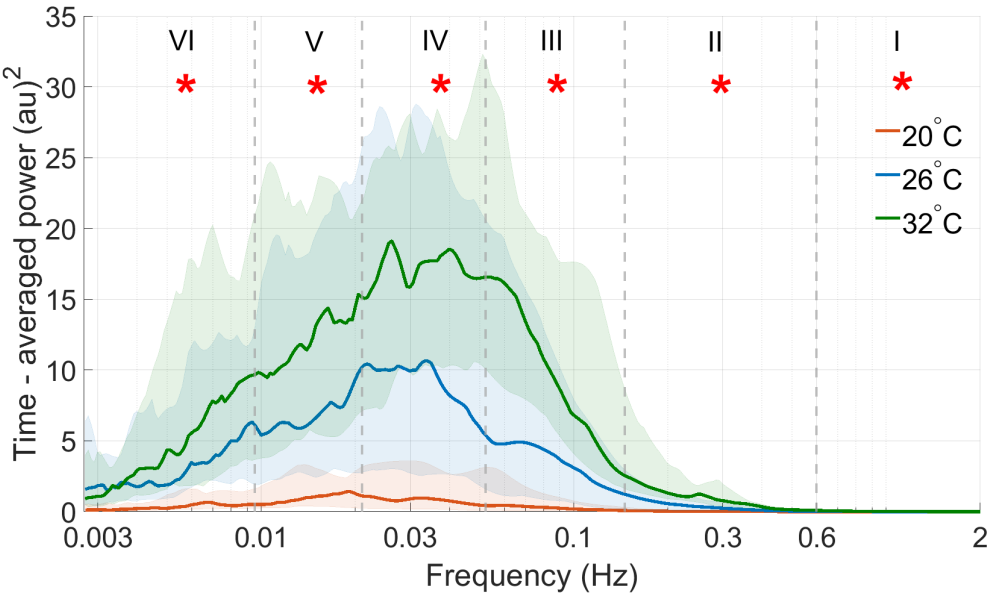

Figure 4.32: Time-averaged wavelet power of blood flow in the right index finger. Group median time-averaged spectral power calculated from the wavelet transforms of blood flow of right index finger for 32 minutes for each ambient temperature (20°C, 26°C, and 32°C). Significant differences were observed in power spectrum across all of the frequency intervals.

Statistical differences were observed in all frequency bands ($p < 0.05$) determined by multi-comparison is as shown with red asterisks in figure 4.32 and by the pair-wise test in figure 4.33. The distribution of power increases significantly at low frequency bands and decreased at high frequency bands. For all low frequencies, powers are widely separated. However, in the respiration band, the variation of the powers reduced markedly and disappearing at cardiac band. Stronger power is contained

in the neuroganic band.

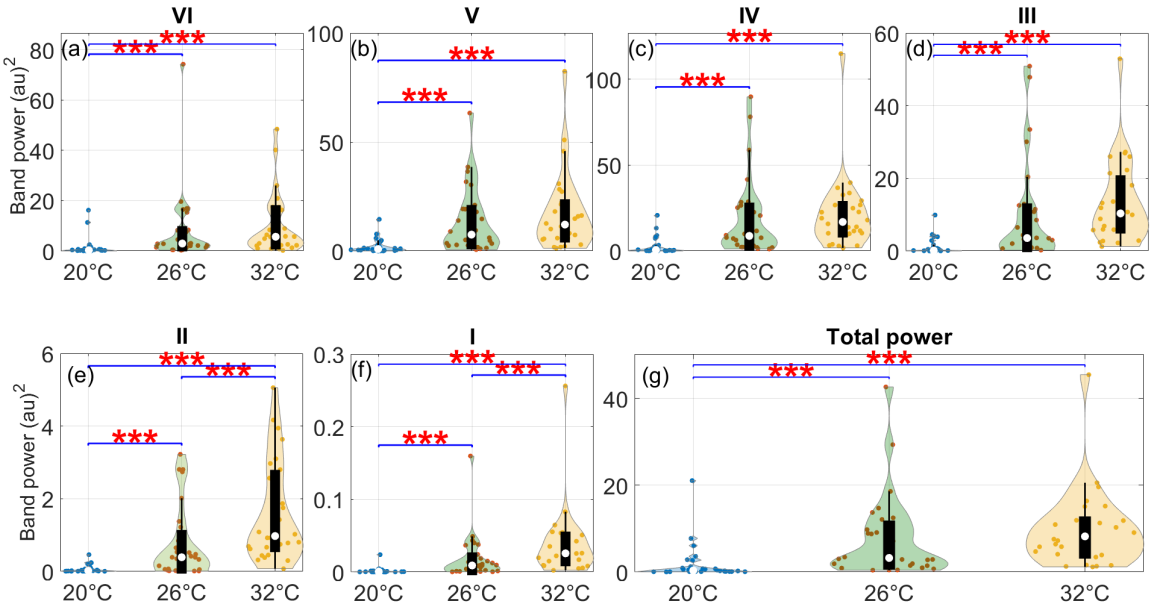

Figure 4.33: Violin plots show the median power content investigated for each frequency band including the total power in the blood flow of the right index finger power spectrum. The central circle indicates the median value. The Wilcoxon signed rank test was applied for comparisons in each frequency band between the three ambient temperatures and statistical significance was set at $p < 0.05$. Significance is considered as $*p < 0.05$,$**p$ <0.01, $***p$ <0.001 .

In a similar pattern, Wilcoxon signed-rank test was tested for each power band and revealed statistical significant differences ($p < 0.05$) in all frequency intervals including the total power as shown in figure 4.35.

4.3.1.1 Spectral power of the laser-Doppler flux left index finger (LDindL)

Figure 4.34 depicts the effect that heating has on the wavelet power spectra of the blood flow time series in the left index finger. All of the blood flow time series for each participant in each ambient temperature were wavelet transformed. The default central frequency was 1Hz, and a Morlet wavelet function was used. The frequency

range was between 0.002 and 2 Hz, and the central frequency was found to be 1Hz. The pre-processing was setting to the "on" position. After that, the time-averaged wavelet powers for each person were calculated. Finally, at each frequency, median value was taken across all powers.

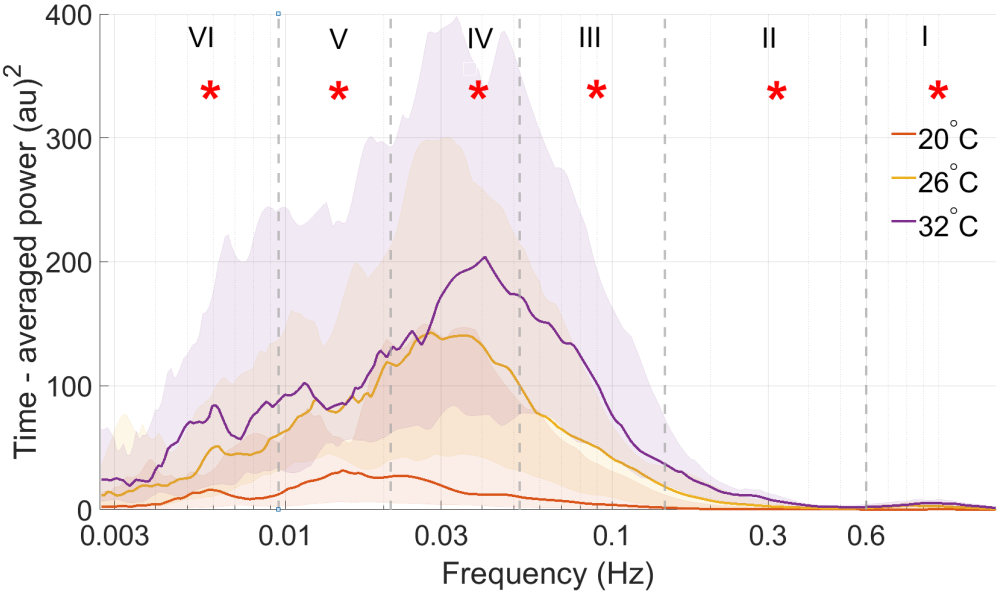

Figure 4.34: Time-averaged wavelet power of blood flow in the left index finger. The group median time-averaged spectral power was determined from the wavelet transforms of blood flow in the left index finger for a period of 32 minutes at each of three different ambient temperatures: 20°C, 26°C, and 32°C. Significant differences were observed in the power spectra across all of the frequency intervals.

Multi-comparison showed statistical differences at all frequency bands ($p < 0.05$) as illustrated with red asterisks in figure 4.34 and paired test in figure 4.35. The power distribution increases greatly at low frequencies and decreases at high frequencies. All low frequency bands have widely separated powers except respiration and cardiac bands.

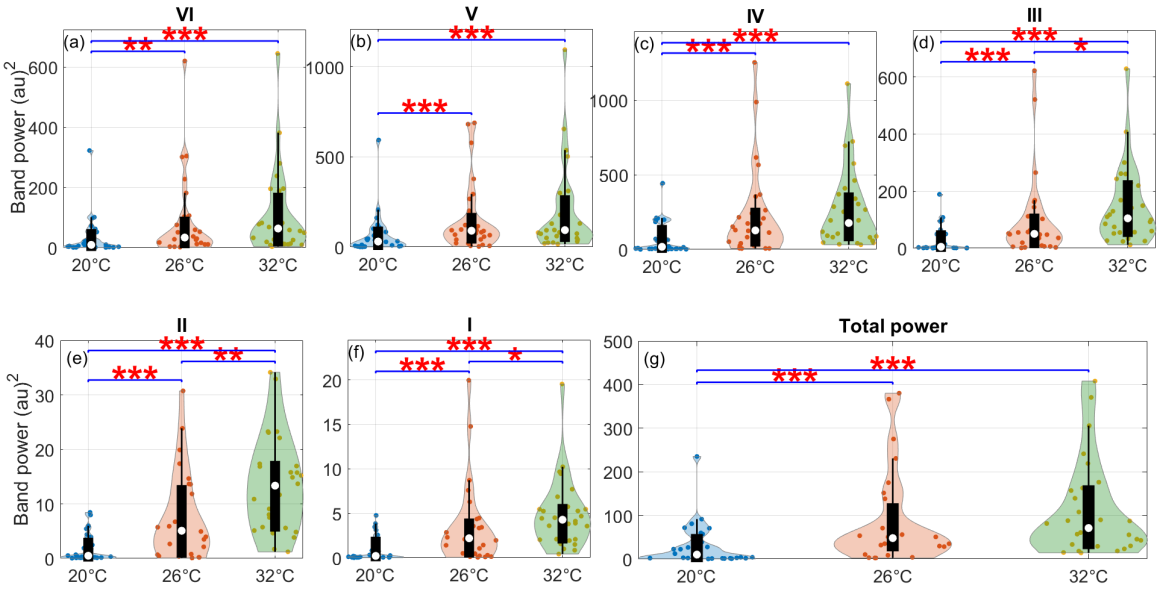

Figure 4.35: Median power of left index blood flow investigated for each frequency band including the total power in the blood flow of the left index finger power spectrum. The central circle indicates the median value. The Wilcoxon signed rank test was applied for comparisons in each frequency band between the three ambient temperatures and the statistical significance was set at $p < 0.05$. Significance is considered as $^*p < 0.05$,$^{**}p$ <0.01, $^{***}p$ <0.001.

4.3.2 Spectral power of the laser-Doppler flux in the left forearm

Figure 4.36 shows the effect of heat on the wavelet power spectra of the left forearm blood flow time series. All blood flow time series were wavelet converted at each of the three temperatures, with a Morlet wavelet function and a central frequency of 1Hz (the default). The minimum frequency was left undefined to allow the wavelet function to calculate the minimum possible value, while the maximum frequency was set to be 2 Hz. The time-averaged wavelet powers of each individual were then determined after that step was completed. In the end, the median value was determined over all the powers at each frequency.

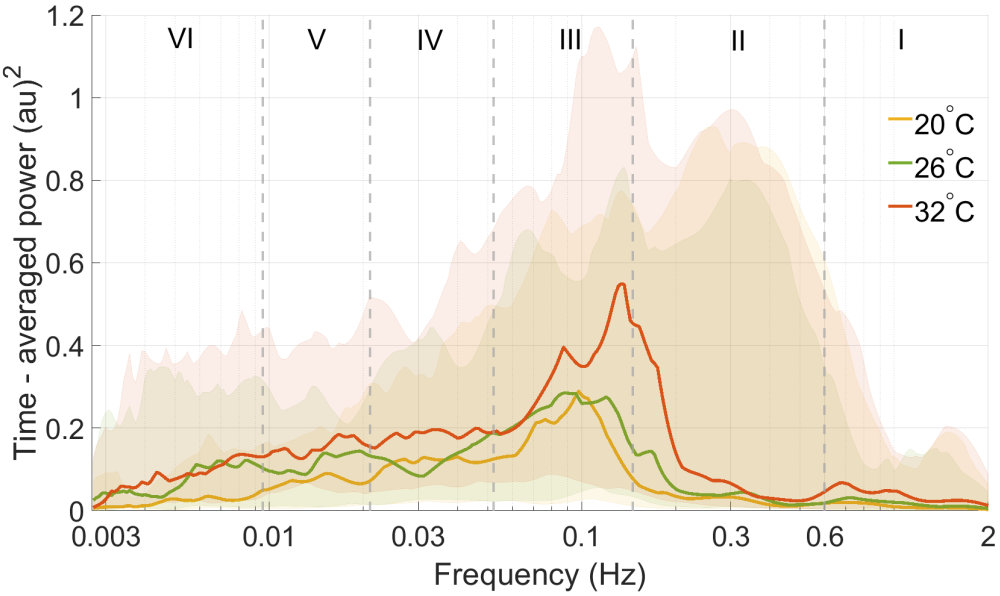

Figure 4.36: Time-averaged wavelet power of blood flow in the left forearm. The spectral power was determined from the wavelet transforms of blood flow in the left index finger for a period of 32 minutes at each of three different ambient temperatures: 20°C, 26°C, and 32°C. No statistical significant difference was found in the time-averaged wavelet power across all of the frequency intervals.

The distribution of power shows that myogenic band contains more power across the whole frequency range. In terms of significance, the multi-comparison test reveled no statistical significant difference ($p < 0.05$) in all frequency bands. However, significant differences determined by the pair-wise test revealed statistically significant between the lowest 20°C and highest 32°C ambient temperatures in all frequency bands ($p = 0.034$, 0.005, and 0.008, respectively) except the respiratory and cardiac bands (figure 4.37). Another significant difference was observed in neurogenic band ($p = 0.024$) between 26°C and 32°C.

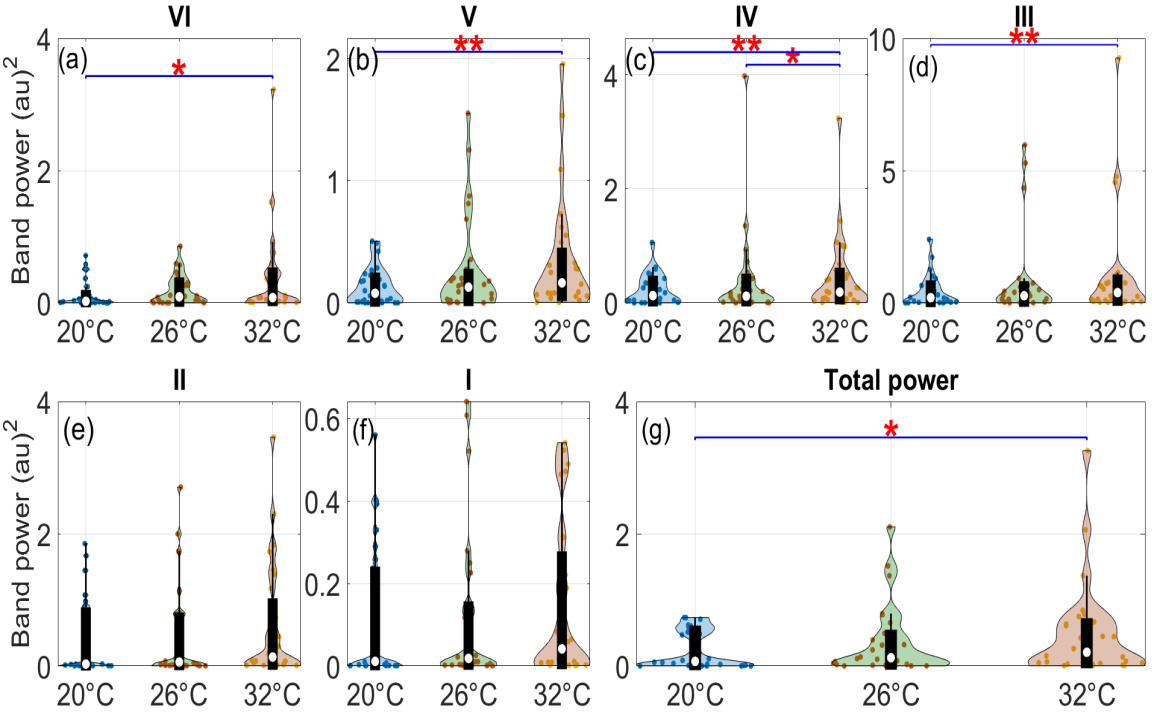

Figure 4.37: Violin plots show the median power content investigated for each frequency band including the total power in the blood flow of forearm blood flow power spectra. The pair-wise test was applied for comparisons in each frequency band between the three ambient temperatures and statistical significance was set at $p < 0.05$. Significant differences within the intervals are indicated by red asterisks. Significance is considered as $^*p < 0.05$,$^{**}p$ <0.01, $^{***}p$ <0.001 .

4.4 Wavelet phase coherence and phase shift analysis

4.4.1 Coherence between IHR and respiration

We employed wavelet phase coherence to identify the frequency bands where respiration and IHR interact with one another. Figure 4.38 (a) shows group median values of wavelet phase coherence between respiration and IHR (extracted from the

ECG) recordings at the three ambient temperatures. Although there was an increase in coherence at myogenic and respiration bands, however, this increase did not show any statistically significant differences as determined by the Kruskal Wallis test (multi-comparison test).

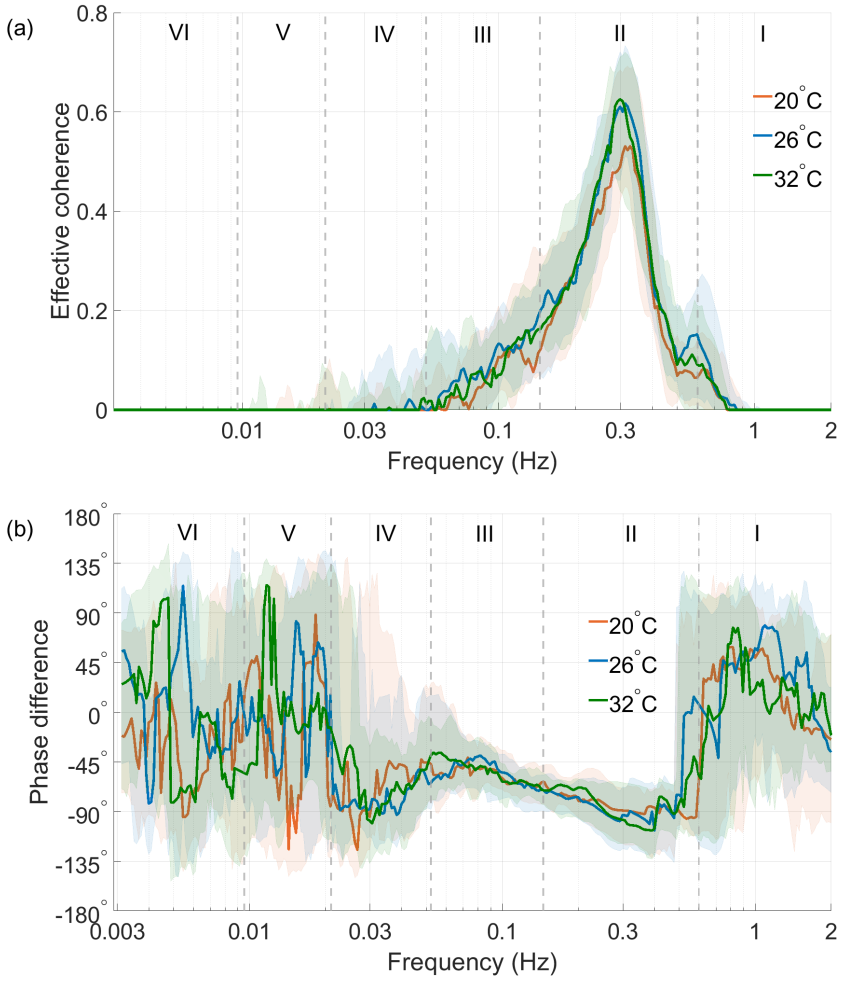

Figure 4.38: Group median values of a) Effective wavelet phase coherence between respiration and IHR for three ambient temperatures. b) Phase shift for the coherence shown in figure a). Shading indicates the range between the 25^{th} and 75^{th} percentiles in both figures. Dashed lines indicate the frequency intervals of oscillations observed in both figures. No significant difference was revealed ($p > 0.05$) by Kruskal-Wallis at the defined frequency intervals.

No significant difference was found in the phase shift in the IHR- respiration coherence across all frequency bands (Figure 4.38 (b)). The phase shift for of all ambient temperatures proved to be coherent within the myogenic and respiration frequency bands. The negative value of the shift indicates that the oscillations in the respiration are leading those in the IHR. However, significant differences determined by the pair-wise test ($p > 0.05$) were found in the cardiac ($p = 0.0025$) and respiration ($p = 0.0366$) bands and the total coherence ($p = 0.028$) as shown in figure 4.39.

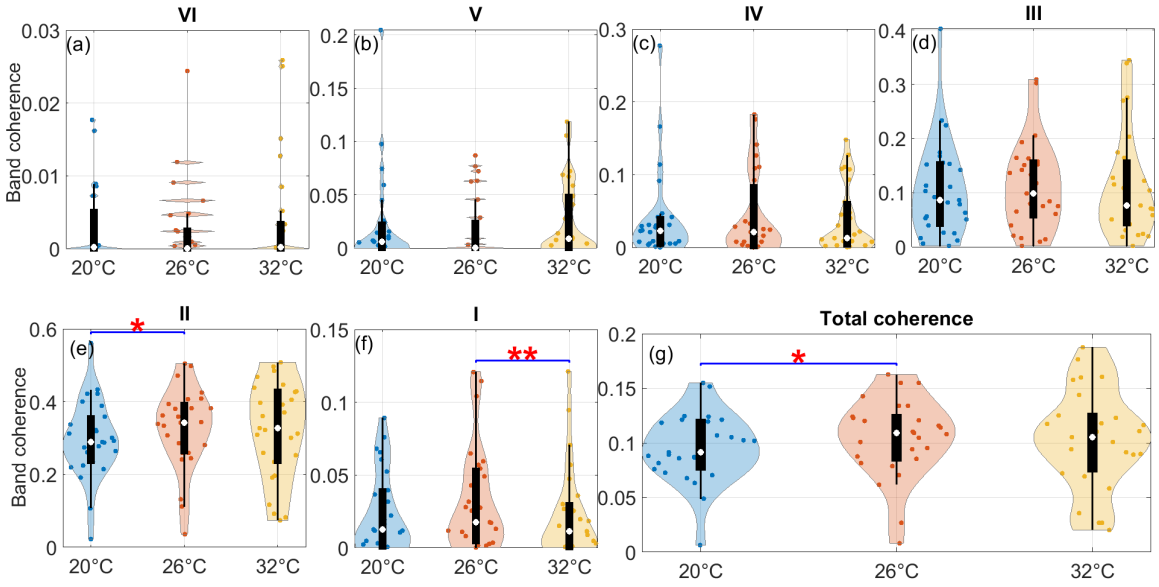

Figure 4.39: Spectral coherence of respiration-IHR within frequency bands. Violins compare the median coherence content within each frequency band including the total coherence in the respiration-IHR signal. The Wilcoxon signed rank test was applied for comparisons in each frequency band for the three ambient temperatures and statistical significance was set at $p < 0.05$. Significance is considered as $*p < 0.05$,$**p < 0.01$, $***p < 0.001$.

4.4.2 Coherence between respiration and blood pressure (Amplitude - Amplitude interaction)

The group median values of wavelet phase coherence was calculated between the respiration and blood pressure signals at three different ambient temperatures and the results are shown in figure 4.40 (a).

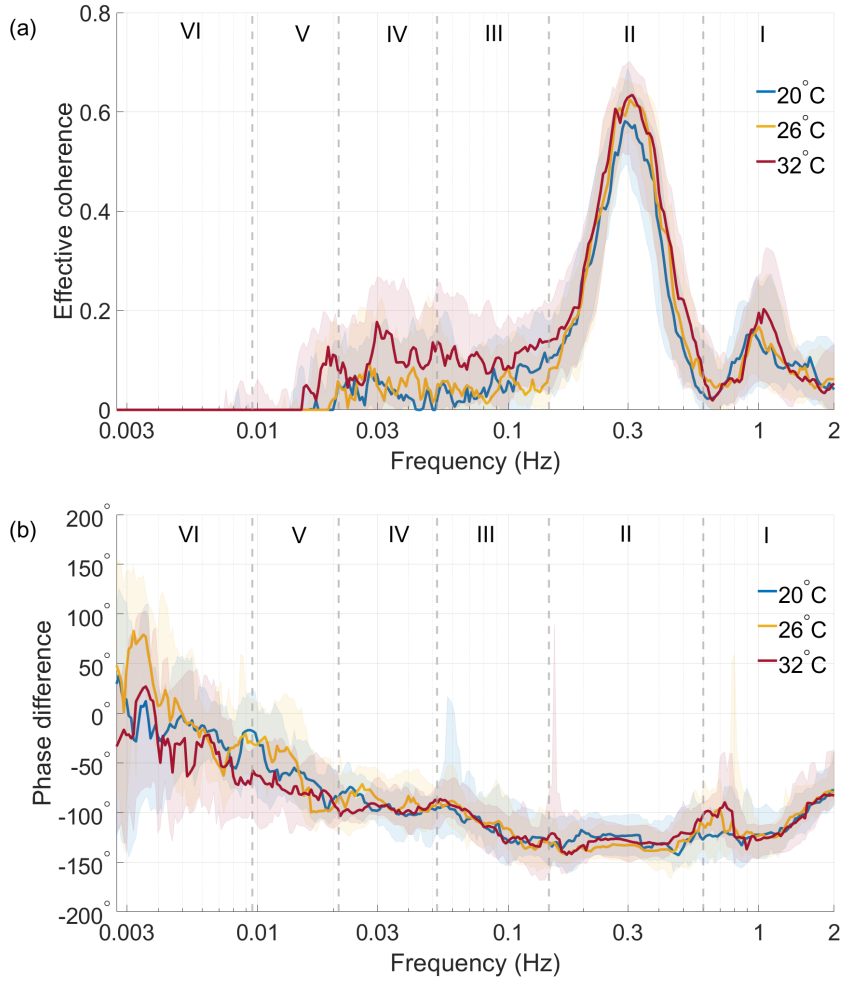

Figure 4.40: Group median values of a) Effective wavelet phase coherence between respiration and blood pressure for three ambient temperatures. b) Phase shift for the coherence shown in panel a). Shading indicates the range between the 25^{th} and 75^{th} percentiles in both figures. No significant difference was revealed ($p > 0.05$) by Kruskal-Wallis test in at the defined frequency intervals

All group temperatures showed clearly two broad peaks; a high peak in the respiration interval ($\sim$ 0.3Hz) and a low peak in the high frequency cardiac interval ($\sim$ 1Hz). The multi-comparison test showed that no significant differences were observed in respiration-blood pressure coherence and the phase difference (figure fig40 (b)). Significant differences determined by the pair-wise test were found in respiration-blood pressure coherence in the frequency intervals: V ($p = 0.0487$), III ($p = 0.0071$), II ($p = 0.0211$), ($p = 0.0325$) and in the total coherence ($p = 0.0239$) as shown in 4.41.

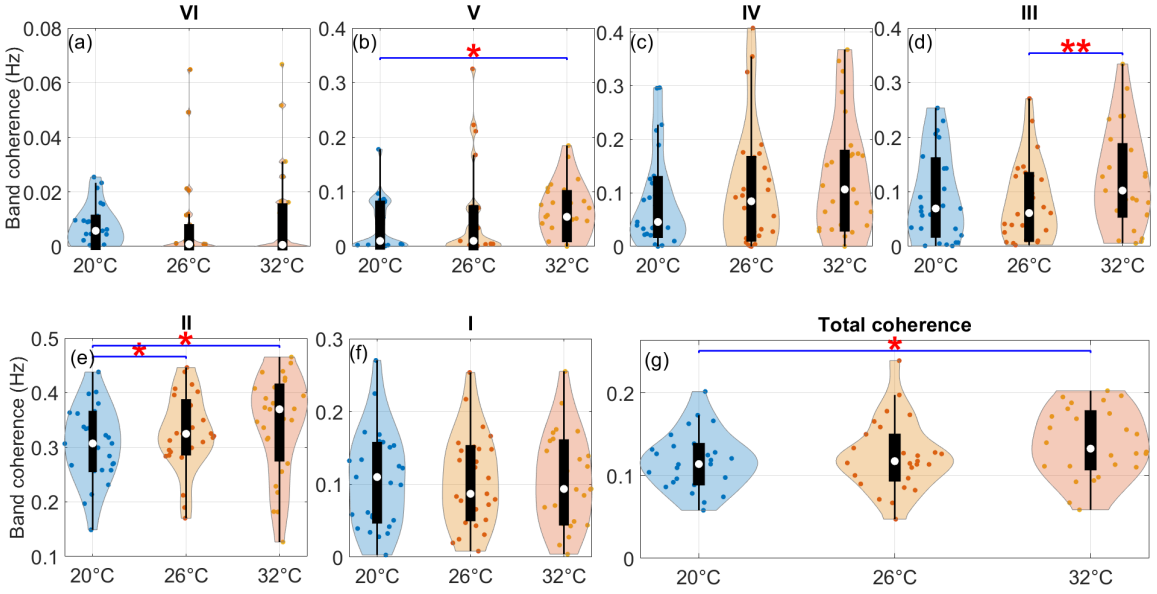

Figure 4.41: Spectral coherence of respiration and blood pressure within frequency bands. Violin plots compare the median coherence content within each frequency band including the total coherence in the respiration-BP signal. The Wilcoxon signed rank test was applied for comparisons in each frequency band for the three ambient temperatures and statistical significance was set at $p < 0.05$. Significance is considered as $^{*}p < 0.05$,$^{**}p$ <0.01, $^{***}p$ <0.001 .

Significant differences in the phase shift were found in the respiration-blood pressure coherence in the frequency intervals: VI ($p = 0.0325$), V ($p = 0.0016$), I ($p = 0.0345$), and in the total phase difference ($p = 0.0306$) as shown in figure 4.42.

The positive value of the shift indicates that the oscillations in the blood pressure lead those in the respiration.

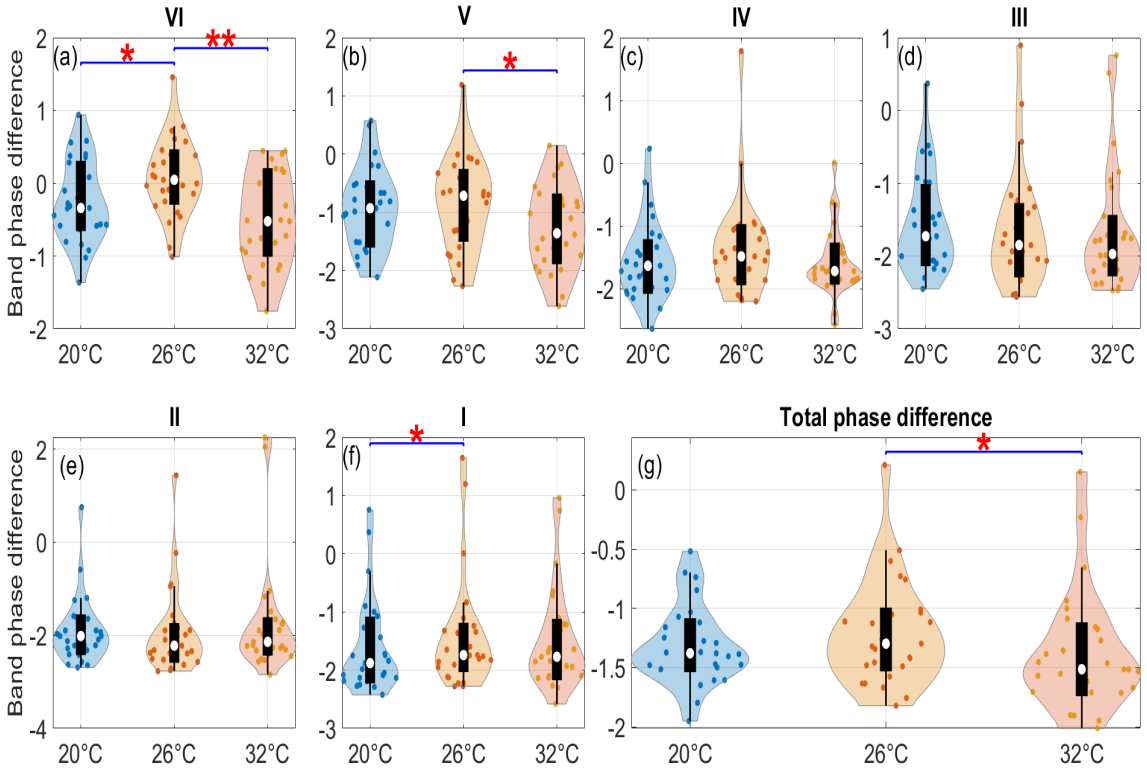

Figure 4.42: Spectral phase difference of respiration and blood pressure within frequency bands. Violin plots compare the median phase difference content within each frequency band including the total coherence in the respiration-BP signal. The unit of the phase is radian. The Wilcoxon signed rank test was applied for comparisons in each frequency band for the three ambient temperatures and statistical significance was set at $p < 0.05$. Significance is considered as $^{*}p < 0.05$,$^{**}p < 0.01$, $^{***}p < 0.001$.

4.4.3 Coherence of cardiac output with respiration

The group median values of wavelet phase coherence between cardiac output and respiration was calculated and the group median coherence is shown in figure 4.43 (a). High phase coherence was revealed at the frequency of respiration ($\sim$ 0.3 Hz)

for all subjects at each of the three ambient temperatures. Multi-comparison tests revelled low significant difference in the neurogenic band ($p = 0.0177$) only.

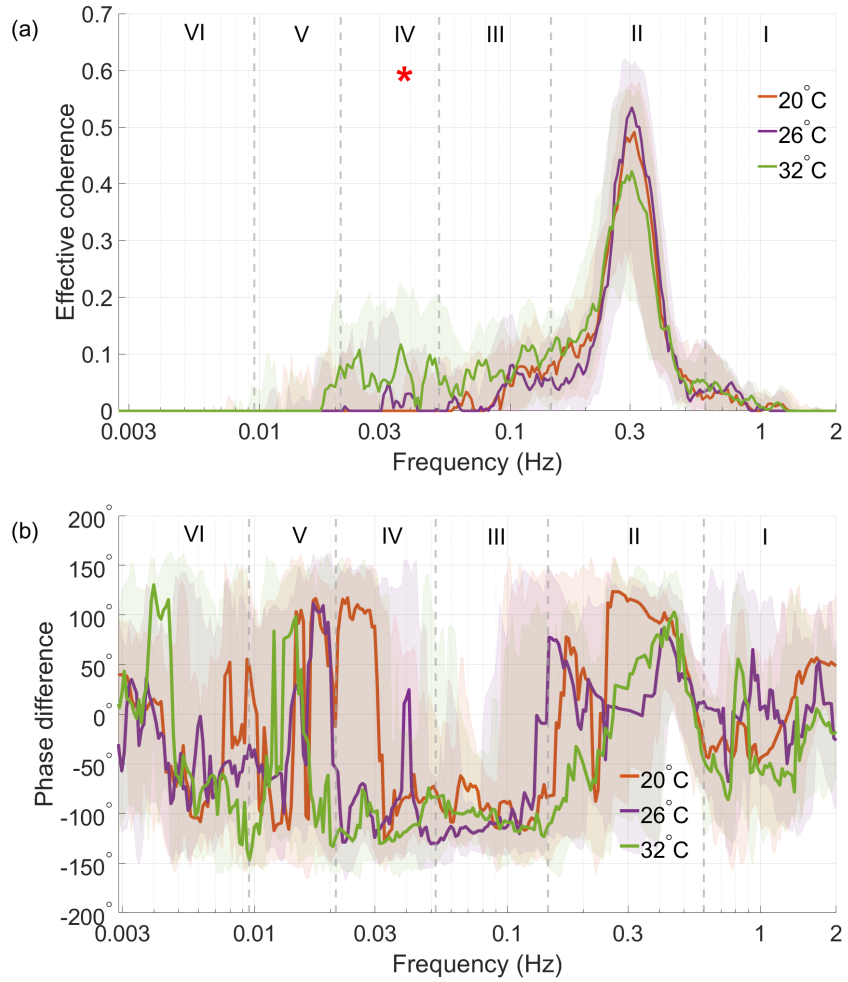

Figure 4.43: Group median values of a) Effective wavelet phase coherence between respiration and cardiac output for three ambient temperatures. b) Phase shift for the coherence shown in panel a). Shading indicates the range between the 25^{th} and 75^{th} percentiles in both figures. Significant difference were revealed ($p > 0.05$) by the Kruskal-Wallis test at the defined frequency intervals in panel (a) only as indicated by red asterisk.

While the pair-wise test showed significant differences in the neurogenic frequency intervals in the neurogenic between 20°C-32°C ($p = 0.0039$) and 26°C-32°C ($p =$

0.088), and myogenic between interval 26°C-32°C ($p = 0.0062$) as shown in figure 4.44. However, no significant difference in the phase shift was found in the cardiac output-respiration coherence across all frequency intervals (Figure 4.43 (b)).

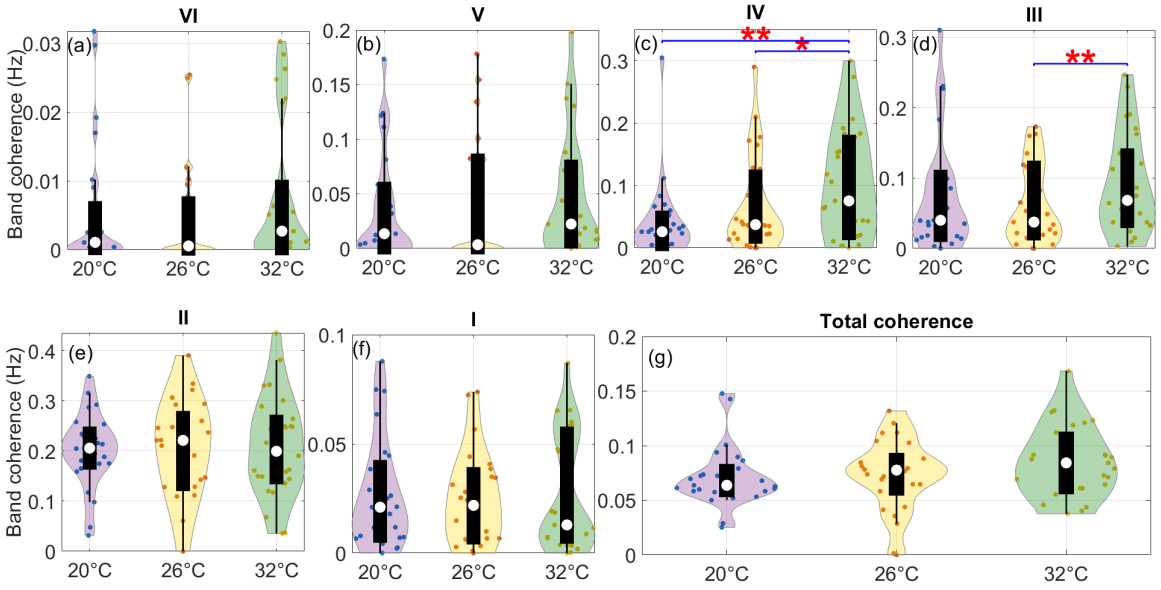

Figure 4.44: Spectral coherence of cardiac output and respiration within frequency bands. Violin plots compare the median coherence content within each frequency band including the total coherence in the cardiac output-respiration signal. The Wilcoxon signed rank test was applied for comparisons in each frequency band for the three ambient temperatures and the statistical significance was set at $p < 0.05$. Significance is considered as $^{*}p < 0.05$,$^{**}p < 0.01$, $^{***}p < 0.001$.

The phase shift is more pronounced at higher frequencies, indicating that there is, in fact, a common time-lag throughout all frequency ranges. The positive value of the shift in the respiration interval indicates that the oscillations in the cardiac output are leading those in the respiration. The pair-wise test showed a small but significant difference in the frequency interval of respiration between 20°C-32°C ($p = 0.0225$) as shown in figure 4.45.

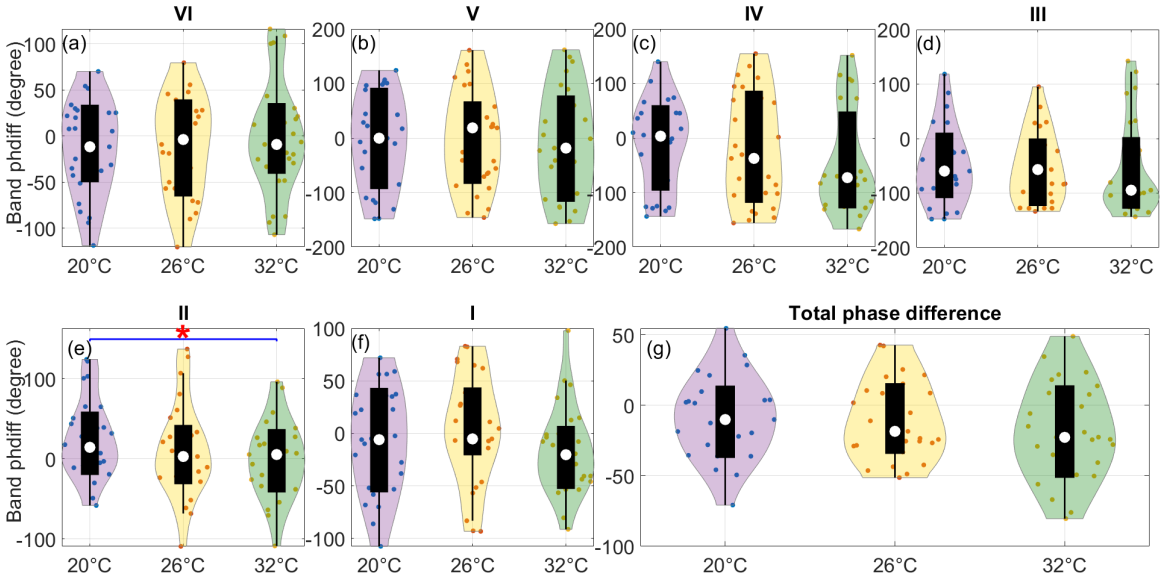

Figure 4.45: Spectral phase difference of cardiac output and respiration within frequency bands. Violin plots compare the median phase difference content within each frequency band including the total coherence in the cardiac output-respiration signal. The Wilcoxon signed rank test was applied for comparisons in each frequency band for the three ambient temperatures and the statistical significance was set at $p < 0.05$. Significance is considered as $^{*}p < 0.05$,$^{**}p < 0.01$, $^{***}p < 0.001$.

4.4.4 Coherence between IHR and IRR

The group median values of wavelet phase coherence between the IHR and IRR recordings at three different ambient room temperatures and the group median coherence is shown figure 4.46 (a).

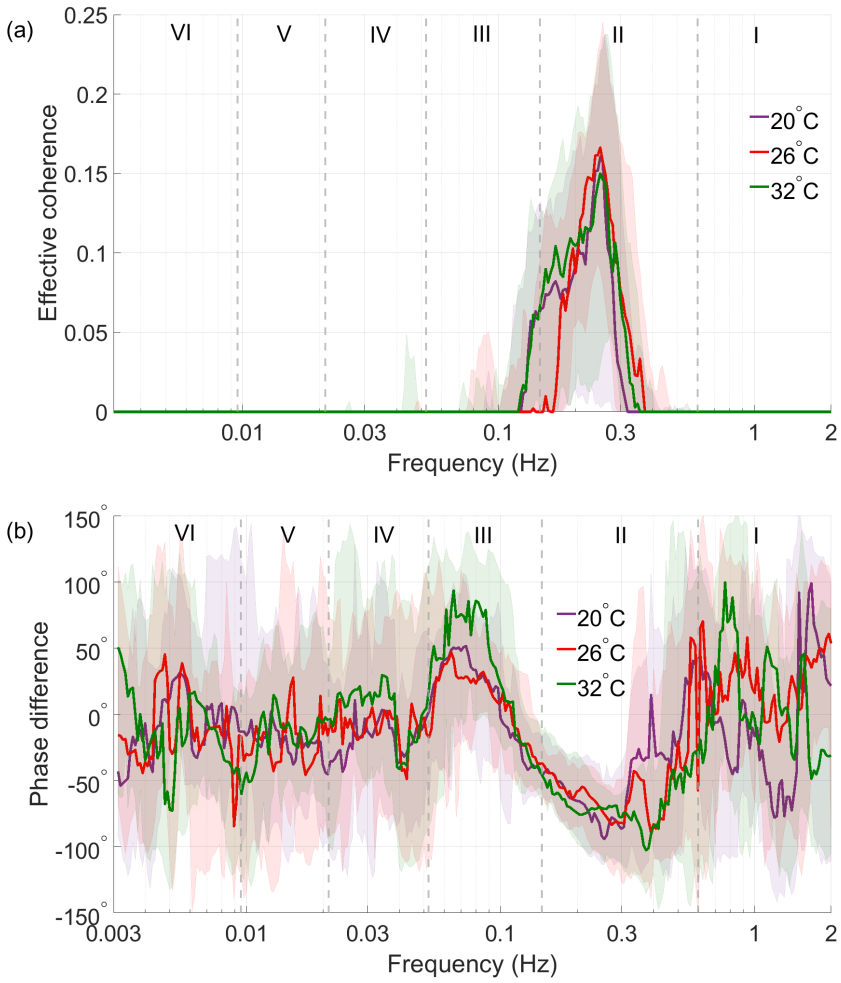

Figure 4.46: Group median values of a) Effective wavelet phase coherence between IRR and IHR for three ambient temperatures. b) Phase shift for the coherence shown in panel a). Shading indicates the range between the 25^{th} and 75^{th} percentiles in both figures. No significant difference was revealed ($p > 0.05$) by the Kruskal-Wallis test in the defined frequency intervals.

High phase coherence was revealed at the frequency of respiration ($\sim$ 0.3 Hz) for all subjects for each of the three ambient temperatures. No significant differences were found in the coherence of IHR and IRR either by multi-comparison or pairwise tests. However, no significant difference in the phase shift was found in the IHR-IRR coherence across all frequency intervals (Figure 4.46 (b)) by the multi-comparison

test.

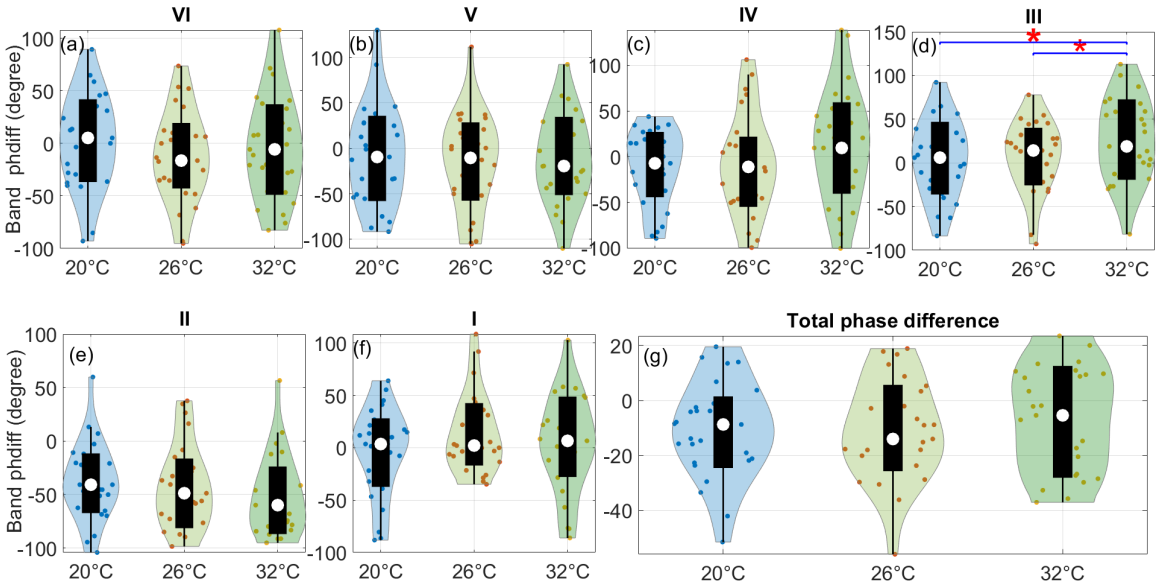

Figure 4.47: Spectral phase difference of IRR-IHR within frequency bands. Violin plots compare the median phase difference content within each frequency band including the total phase difference in the IRR-IHR signal. The Wilcoxon signed rank test was applied for comparisons in each frequency band for the three ambient temperatures and statistical significance was set at $p < 0.05$. Significance is considered as $^{*}p < 0.05$,$^{**}p$ <0.01, $^{***}p$ <0.001 .

The pair-wise test showed significant difference in the myogenic frequency interval of myogenic between 20°C-32°C ($p = 0.0461$) and 26°C-32°C ($p = 0.0211$) as shown in figure 4.47. The phase shift is more pronounced at higher frequencies. The negative value of the phase shift indicates that the oscillations in the IRR are leading those in the IHR.

4.4.5 Systolic and diastolic blood pressure coherence

The group median values of wavelet phase coherence between systolic and diastolic blood pressure signals was computed for the three different ambient temperatures as

shown in figure 4.48 (a).

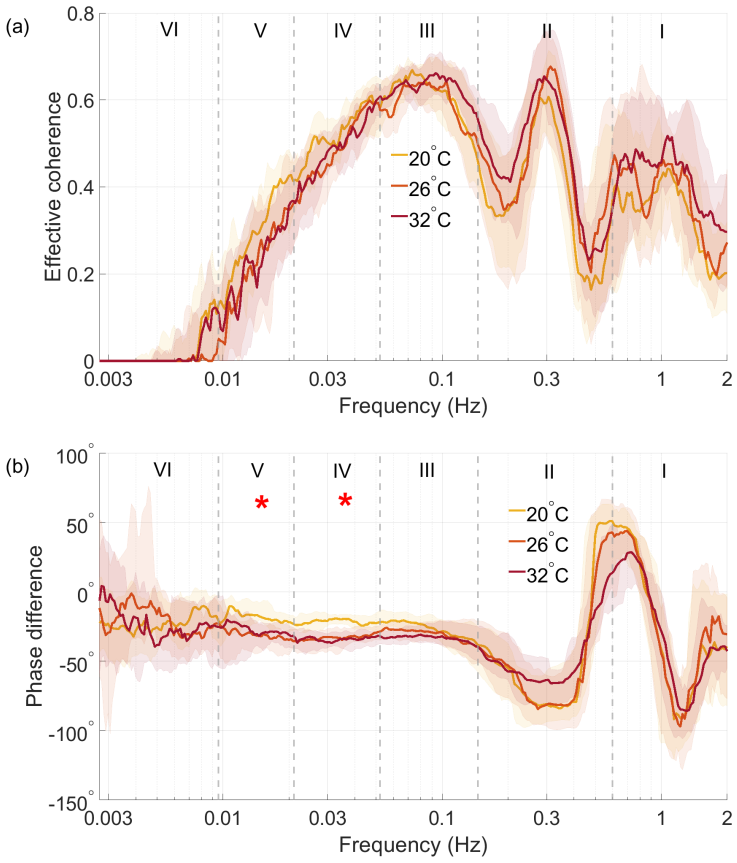

Figure 4.48: Group median values of a) Effective wavelet phase coherence between systolic blood pressure and diastolic blood pressure for three ambient temperatures. b) Phase shift for the coherence shown in figure a).

High phase coherence was revealed in the frequency intervals of myogenic ($\sim$ 0.1 Hz), respiratory ($\sim$ 0.3 Hz), and cardiac ($\sim$ 1 Hz) frequency intervals for all subjects at each of the three ambient temperatures. No significant differences was observed in systolic-diastolic blood pressure coherence.

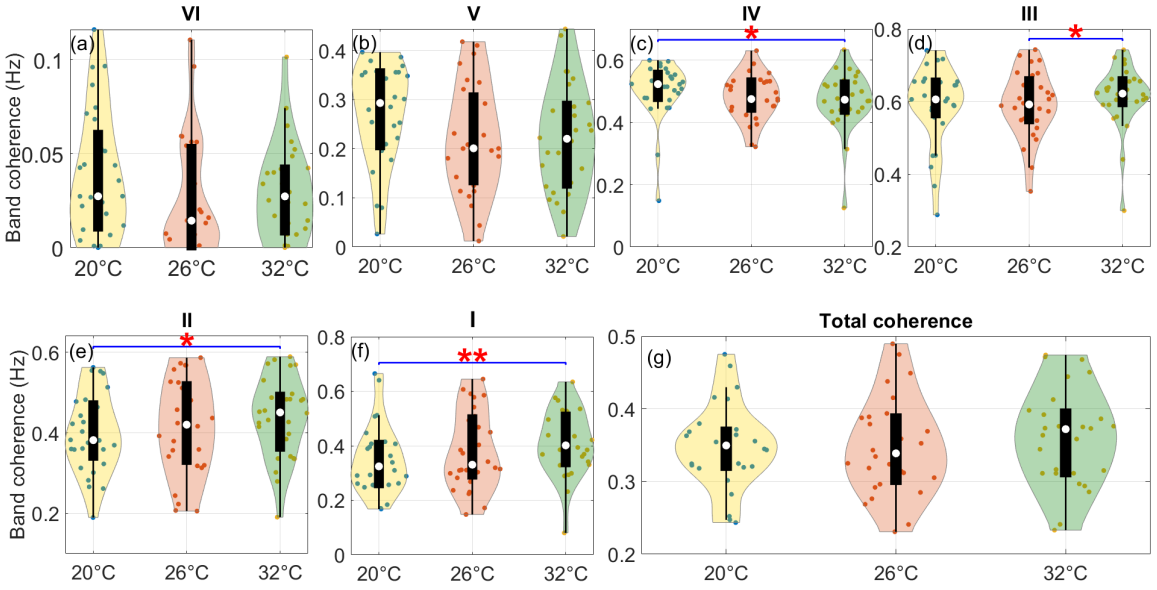

Figure 4.49: Spectral coherence of systolic blood pressure and diastolic blood pressure within frequency bands. Violin plots compare the median coherence content within each frequency band including the total coherence in the sBP-dBP signal. The Wilcoxon signed rank test was applied for comparisons in each frequency band for the three ambient temperatures and the statistical significance was set at $p < 0.05$. Significance is considered as $^{*}p < 0.05$,$^{**}p < 0.01$, $^{***}p < 0.001$.

However, significant differences in the phase shift were found in the systolic-diastolic pressure coherence in the frequency intervals: V ($p = 0.0035$) and IV ($p = 0.0000$). The pair-wise test showed significant difference in systolic-diastolic blood pressure coherence in the frequency intervals: IV ($p = 0.0404$), III ($p = 0.0404$), II ($p = 0.0215$), and I ($p = 0.0036$) as shown in figure 4.49. Significant differences in the phase shift were found in the cardiac output-respiration coherence across the following frequency intervals: V ($p = 0.0004$), ($p = 0.0228$), IV ($p = 0.0000$), ($p = 0.0002$), and III ($p = 0.0063$) as shown in figure 4.50. The positive value of the shift indicates that the oscillations in the systolic blood pressure are leading those in the diastolic.

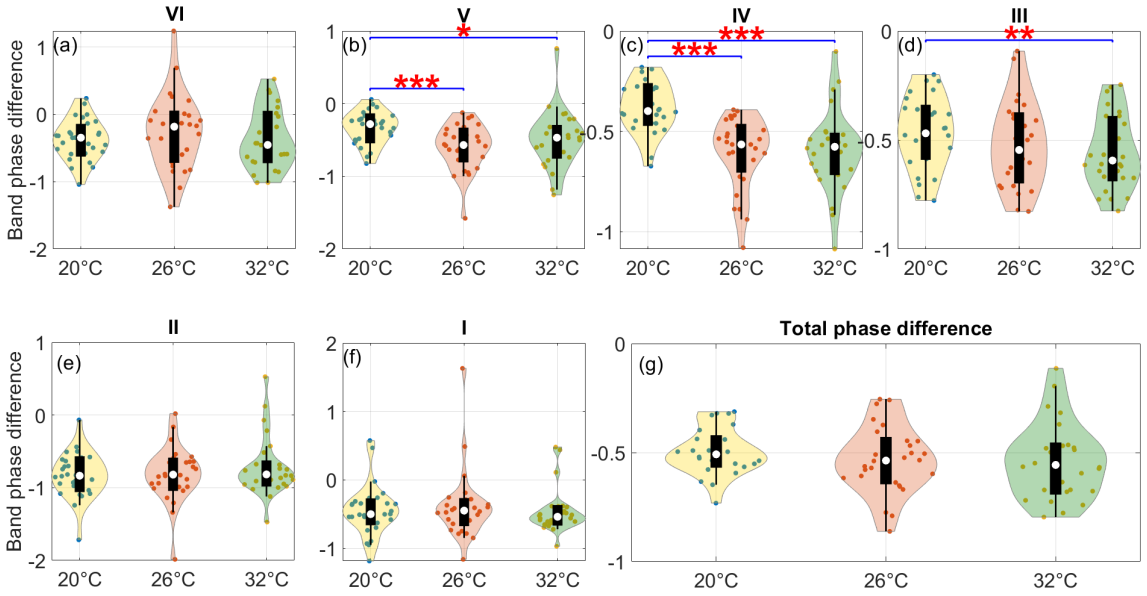

Figure 4.50: Spectral phase difference of systolic blood pressure and diastolic blood pressure within frequency bands. Violin plots compare the median phase difference content within each frequency band including the total phase shift in the sBP-dBP signal. The unit of the phase is radian. The Wilcoxon signed rank test was applied for comparisons in each frequency band for the three ambient temperatures and the statistical significance was set at $p < 0.05$. Significance is considered as $^{*}p < 0.05$,$^{**}p$ <0.01, $^{***}p$ <0.001.

4.4.6 Coherence between the IHR of ECG and blood pressure

Group median values of wavelet phase coherence between the IHR derived from ECG signals and from the blood pressure signals was computed as shown in figure 4.51 (a).

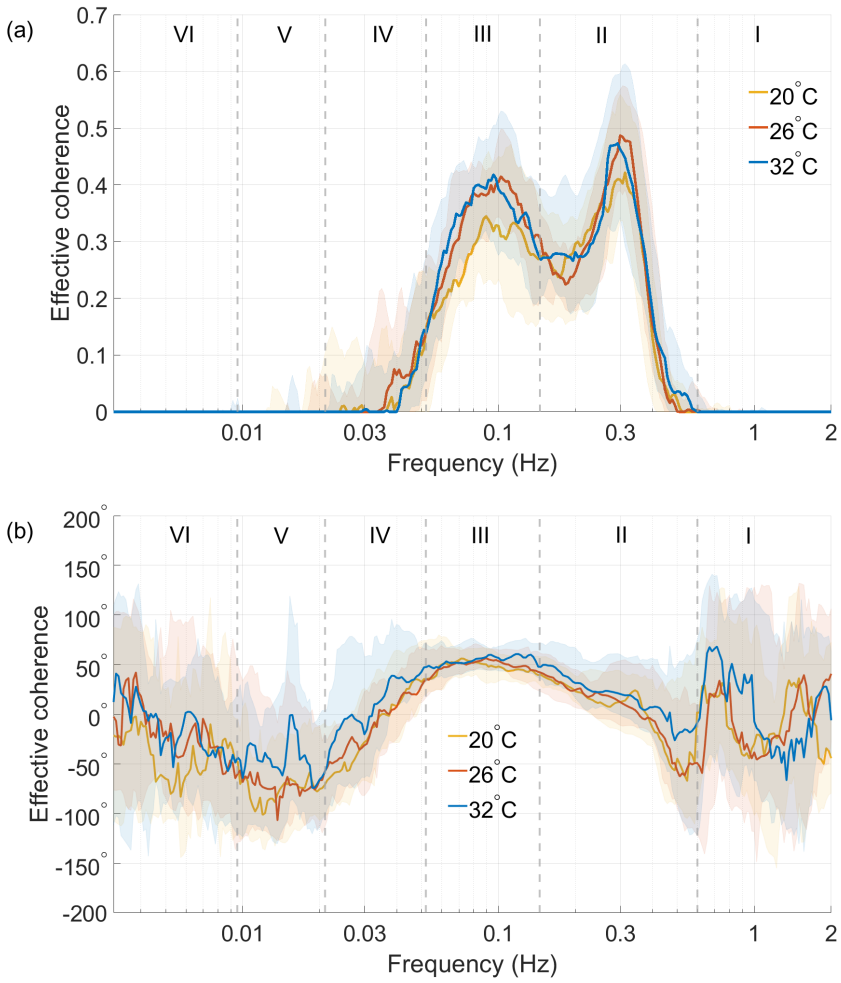

Figure 4.51: Group median values of a) Effective wavelet phase coherence between blood pressure and IHR (ECG) for three ambient temperature. b) Phase shift for the coherence shown in figure a). No significant difference was revealed ($p > 0.05$) by Kruskal-Wallis at the defined frequency intervals.

A broad peak is seen in the Myogenic of myogenic frequency ($\sim$ 0.1Hz), and respiratory ($\sim$ 0.3Hz) frequency intervals. No significant differences were revealed in IHR-blood pressure coherence as shown by a multi-comparison test. Similarly, no significant difference in the phase shift was found in the IHR-blood pressure coherence across all frequency intervals (Figure 4.51 (b)). The pair-wise test showed significant differences in the myogenic ($p = 0.0305$) and ($p = 0.0288$) frequency intervals as shown

in figure 4.52.

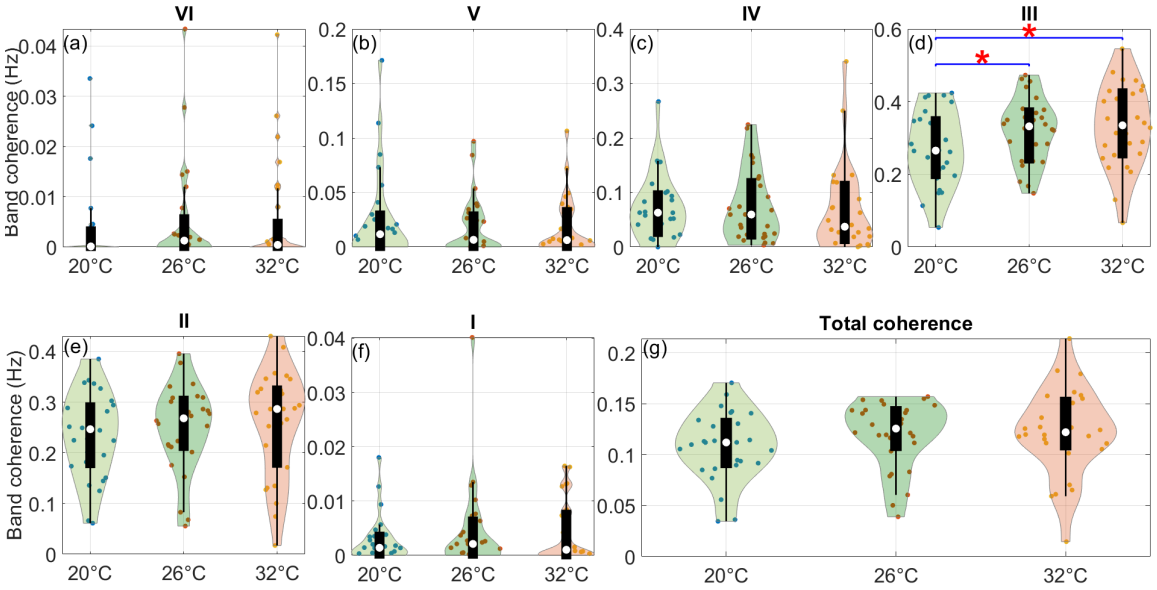

Figure 4.52: Spectral coherence of IHR (ECG) and blood pressure within frequency bands. Violin plots compare the median coherence content within each frequency band including the total coherence in the IHR-BP signal. The Wilcoxon signed rank test was applied for comparisons in each frequency band for the three ambient temperatures and statistical significance was set at $p < 0.05$. Significance is considered as $^{*}p < 0.05$,$^{**}p$ <0.01, $^{***}p$ <0.001 .

Significant differences in the phase shift were found in the IHR-IHR coherence in the frequency intervals: IV ($p = 0.0256$), ($p = 0.0215$), III ($p = 0.0101$), II ($p = 0.0051$), ($p = 0.0404$), and in the total coherence ($p = 0.0242$), ($p = 0.0202$) as shown in figure 4.53. The positive value of the shift were cardiac interval indicates that the oscillations in the IHR of ECG signals are leading those in the blood pressure.

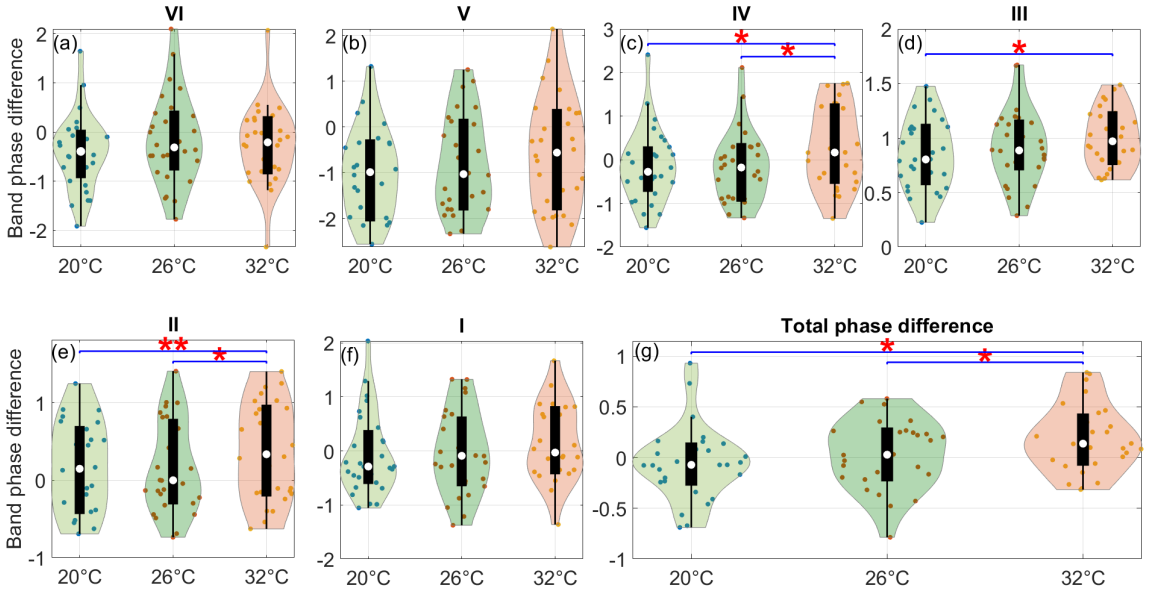

Figure 4.53: Spectral phase difference of IHR (ECG) and blood pressure within frequency bands. Violin plots compare the median phase difference content within each frequency band including the total coherence in the IHR-BP signal. The unit of the phase is radian. The Wilcoxon signed rank test was applied for comparisons in each frequency band for the three ambient temperatures and the statistical significance was set at $p < 0.05$. Significance is considered as $^{*}p < 0.05$,$^{**}p < 0.01$, $^{***}p < 0.001$.

4.4.7 Coherence between IHR and systolic or diastolic blood pressure

The group median values of wavelet phase coherence between oscillations in both systolic and diastolic with IHR were calculated as shown in figure 4.54 (a),(b). High phase coherence was revealed for both signal pairs at the frequency of myogenic (~ 0.1 Hz) and respiratory (~ 0.3 Hz) frequencies.

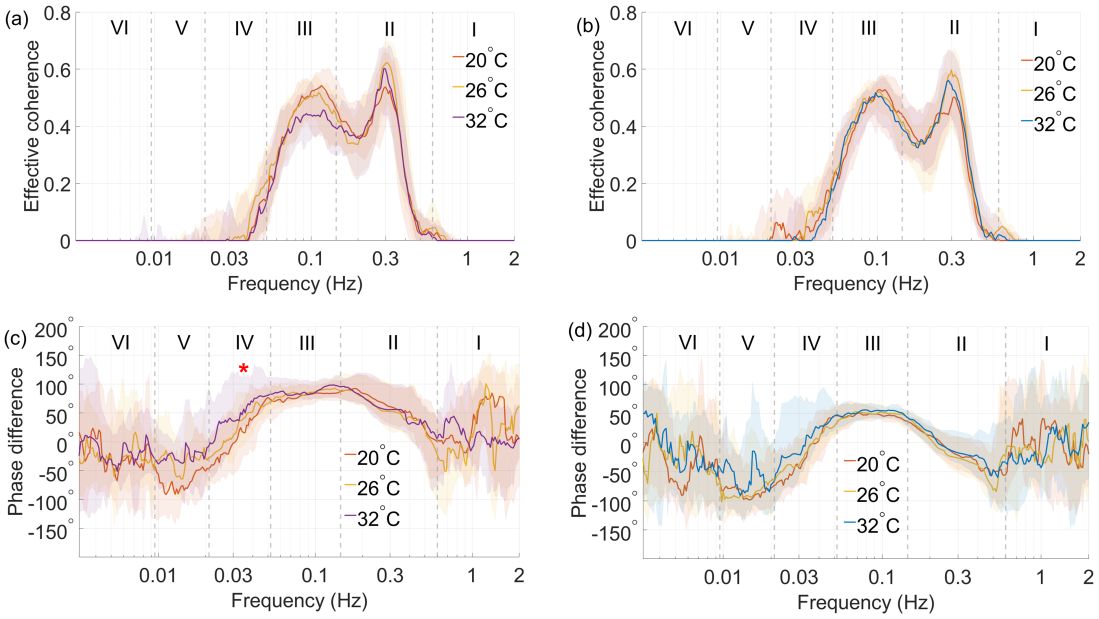

Figure 4.54: Group median values of the effective phase coherence between instantaneous heart rate and systolic and diastolic blood pressure. The phase coherence is computed between the instantaneous heart rate and (a) systolic blood pressure and (b) diastolic blood pressure, in the frequency interval between 0.003 Hz and 2 Hz. For each of the two cases, the group medians of the phase difference are shown underneath the coherence plots in (c) and (d). Where a statistically significant difference ($p < 0.05$) was revealed by the Kruskal Wallis test it is indicated by red asterisks at the defined frequency intervals.

No significant differences were exhibited in the coherence of systolic and diastolic BP with IHR by the multi-comparison test. However, a significant difference in the phase shift was found in the systolic pressure with IHR coherence in the neurogenic frequency interval ($p = 0.029$) as shown in figure 4.54 (c). The Pair-wise test revealed more significant differences in the phase-shifted coherenc sBP-IHR coherence at the frequency intervals: V ($p = 0.0404$), IV ($p = 0.0038$), ($p = 0.0272$), III ($p = 0.0305$), ($p = 0.0158$), as shown in figure 4.55. The positive value of the shift indicates that the oscillations in the IHR are leading those in the sBP.

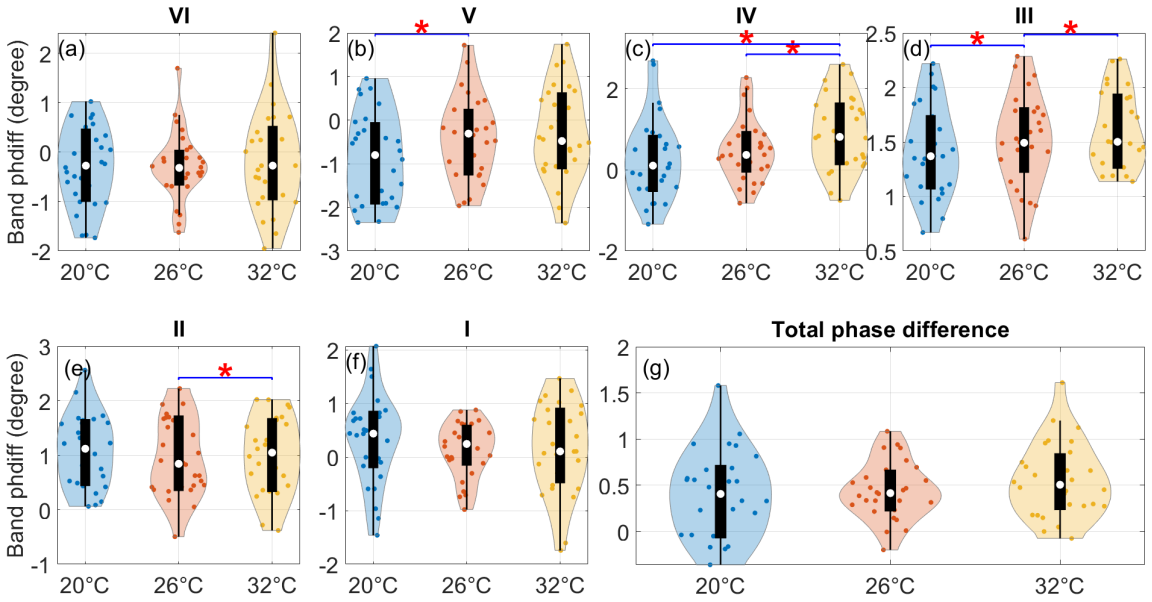

Figure 4.55: Spectral coherence of the systolic BP and IHR within frequency bands. Violin plots compare the median coherence content within each frequency band including the total coherence in the IHR-systolic signal. Wilcoxon signed rank test was applied for comparisons in each frequency band for the three ambient temperatures and statistical significance was set at $p < 0.05$. Significance is considered as $^{*}p < 0.05$,$^{**}p < 0.01$, $^{***}p < 0.001$.

The pair-wise test revealed more significant differences in the phase shift dBP-IHR coherence at the frequency intervals: IV ($p = 0.0202$), ($p = 0.0451$) as shown in figure 4.56. The positive value of the shift indicates that the oscillations in the IHR are leading those in the dBP.

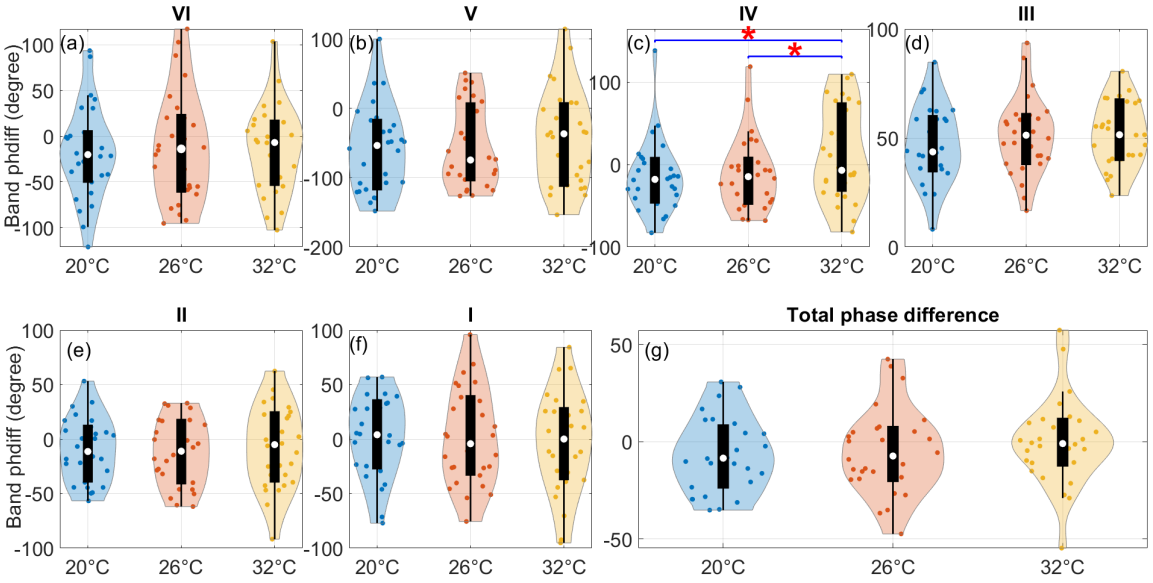

Figure 4.56: Spectral coherence of the diastolic BP and IHR within frequency bands. Violin plots compare the median coherence content within each frequency band including the total coherence in the IHR-diastolic BP signal. The Wilcoxon signed rank test was applied for comparisons in each frequency band for the three ambient temperatures and the statistical significance was set at $p < 0.05$. Significance is considered as $^{*}p < 0.05$,$^{**}p$ <0.01, $^{***}p$ <0.001.

4.5 Coherence of peripheral variables

4.5.1 Coherence between blood flows (left and right index finger)

The results of the calculation of wavelet phase coherence between two LDF blood flow recordings (left and right index fingers) made at three different ambient room temperatures are displayed in figure 4.57 (a).

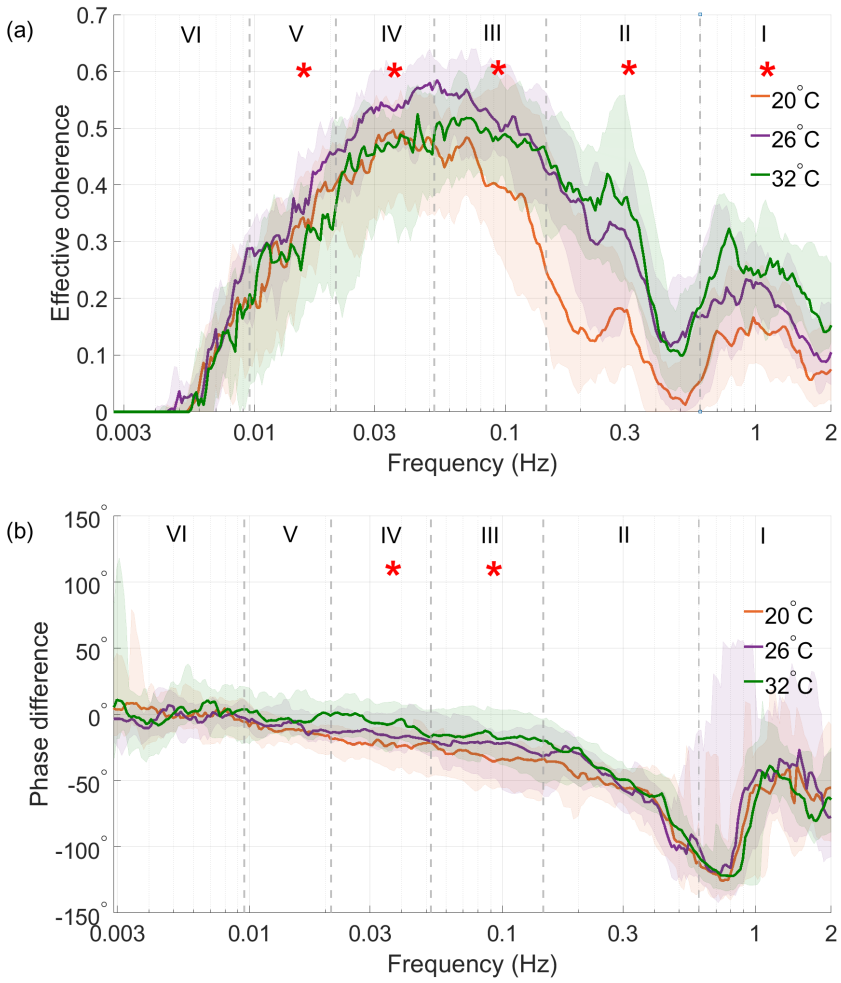

Figure 4.57: Group median values of a) Effective wavelet phase coherence between blood flow in the left and right index fingers blood flow for the three ambient temperature. b) Median phase shift for the coherence shown in figure a). The Kruskal Wallis test was used to reveal significant differences ($p < 0.05$) at the defined frequency intervals (indicated by asterisks).

High phase coherence was revealed in the frequency of neurogenic ($\sim$ 0.03 Hz) and myogenic ($\sim$ 0.06 Hz) frequency intervals, and low phase coherence in the cardiac ($\sim$ 1 Hz) interval for all subjects at the three ambient temperatures.

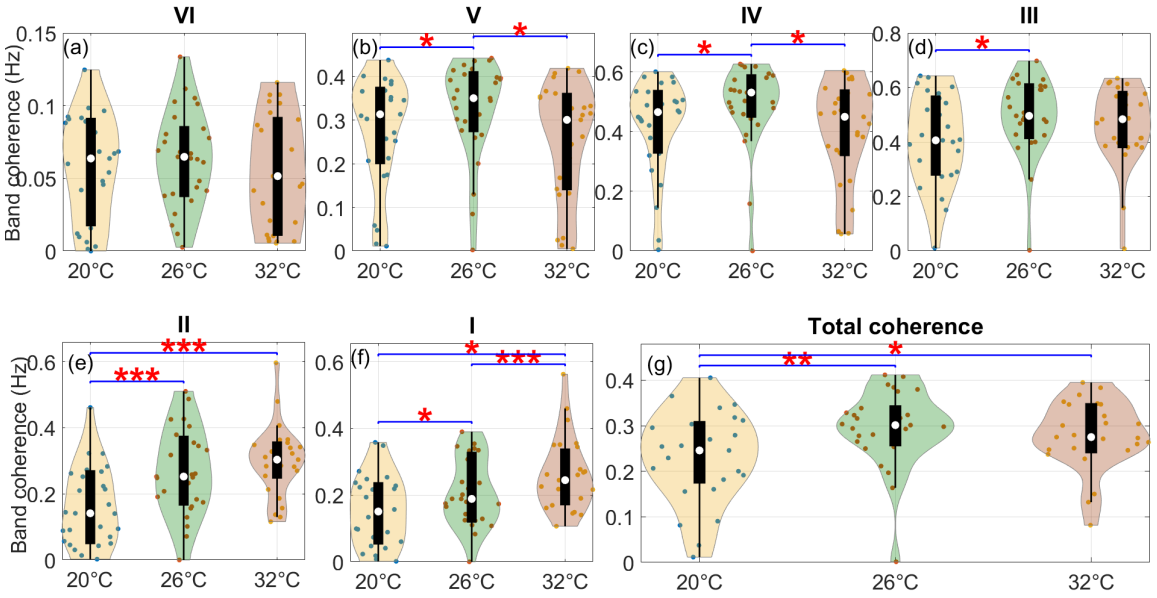

Figure 4.58: Spectral coherence of LDF at two index fingers within frequency bands. Violin plots compare the median coherence content within each frequency band including the total coherence in two index fingers signal. The Wilcoxon signed rank test was applied for comparisons in each frequency band for the three ambient temperatures and statistical significance was set at $p < 0.05$. Significance is considered as $^{*}p < 0.05$,$^{**}p$ <0.01, $^{***}p$ <0.001.

The multi-comparison test revealed significant differences in the frequency intervals V ($p = 0.0447$), IV ($p = 0.0357$), III ($p = 0.0474$), II ($p = 0.0000$), and I ($p = 0.0007$). Significant difference in the phase shift were found in right-left index coherence in the frequency intervals of V ($p = 0.0548$), IV ($p = 0.0185$), III ($p = 0.0348$) (Figure 4.57 (b)) as revelled by the multi-comparisons test. Similarly, the pair-wise test showed significant differences in the same frequency intervals of the right-left index finger coherence: V ($p = 0.019$), ($p = 0.019$), IV ($p = 0.0215$), ($p = 0.0148$), III ($p = 0.0158$), II ($p = 0.0006$), ($p = 0.00008$), I ($p = 0.0342$), ($p = 0.0002$), ($p = 0.011$) and in the total coherence ($p = 0.0041$), ($p = 0.0131$) as shown in figure 4.58.

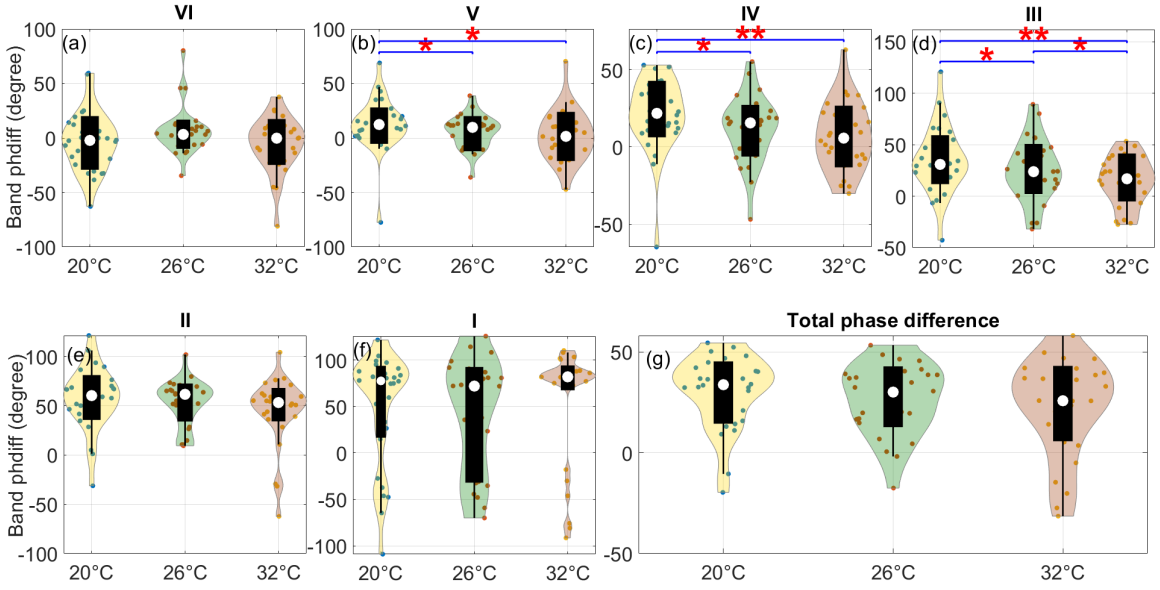

Figure 4.59: Spectral phase difference of LDF at two index fingers within frequency bands. Violin plots compare the median phase difference content within each frequency band including the total phase difference two index fingers signal. The Wilcoxon signed rank test was applied for comparisons in each frequency band for the three ambient temperatures and the statistical significance was set at $p < 0.05$. Significance is considered as $^{*}p < 0.05$,$^{**}p < 0.01$, $^{***}p < 0.001$.

A significant difference in the phase shift was found in the right-left index fingers, with coherence in the frequency intervals V ($p = 0.0451$), ($p = 0.0256$), IV ($p = 0.0088$), ($p = 0.0077$), III ($p = 0.0242$),($p = 0.0018$), and ($p = 0.0651$) (Figure 4.59). For all three ambient temperatures, oscillations at these frequencies are not perfectly coherent. The negative value of the phase shift demonstrates that the oscillations in the left finger blood flow are leading those in the right.

4.5.2 Coherence between the LDF blood flow in the left forearm and the LDF blood flow in the right or left index finger

The group median values of wavelet phase coherence between oscillations in finger blood flow (both right and left index fingers) with forearm blood flow were calculated , with the results shown in figure 4.60 (a), (b). Phase coherence was revealed for both signal pairs in the myogenic ($\sim$ 0.1 Hz) frequency intervals, respiration ($\sim$ 0.3 Hz) and cardiac ($\sim$ 1 Hz) frequency intervals.

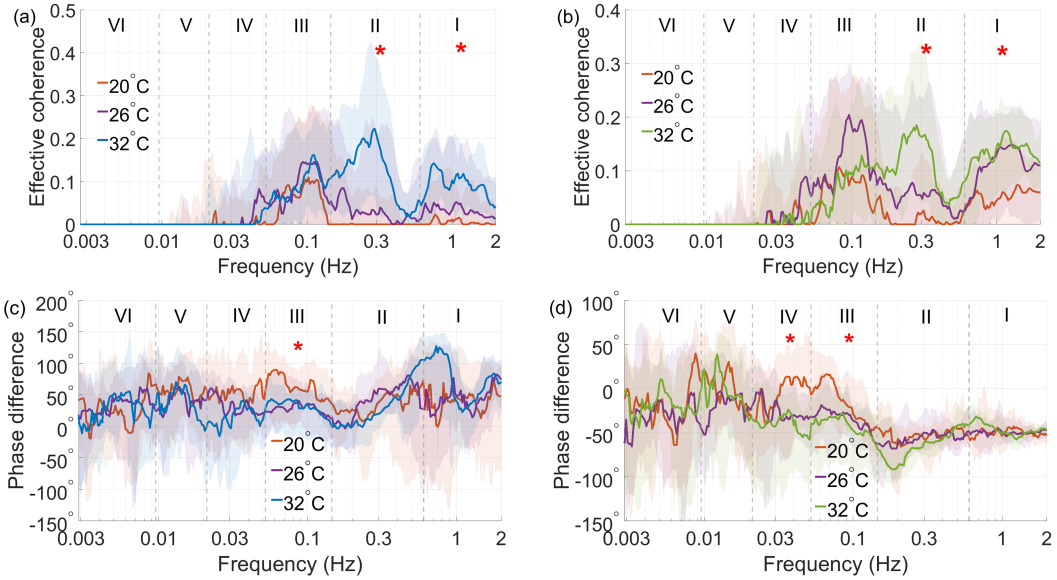

Figure 4.60: Group median values of the effective phase coherence between LDF on the two index fingers and the left forearm. The phase coherence between the left forearm and the blood flow signals recorded using LDF on the left arm and on (a) the right and (b) the left index fingers, in the frequency interval between 0.003 Hz and 2 Hz. For each of the two cases, the group medians of the phase difference are shown underneath the coherence plots in (c) and (d). Statistically significant differences ($p < 0.05$) were revealed by the Kruskal Wallis test and are indicated by red asterisks at the defined frequency intervals.

Significant differences were exhibited in the coherence of forearm with right II (p = 0.0003), I (p = 0.004) and left II (p = 0.013), I (p = 0.025) index as shown in the multi-comparison test.

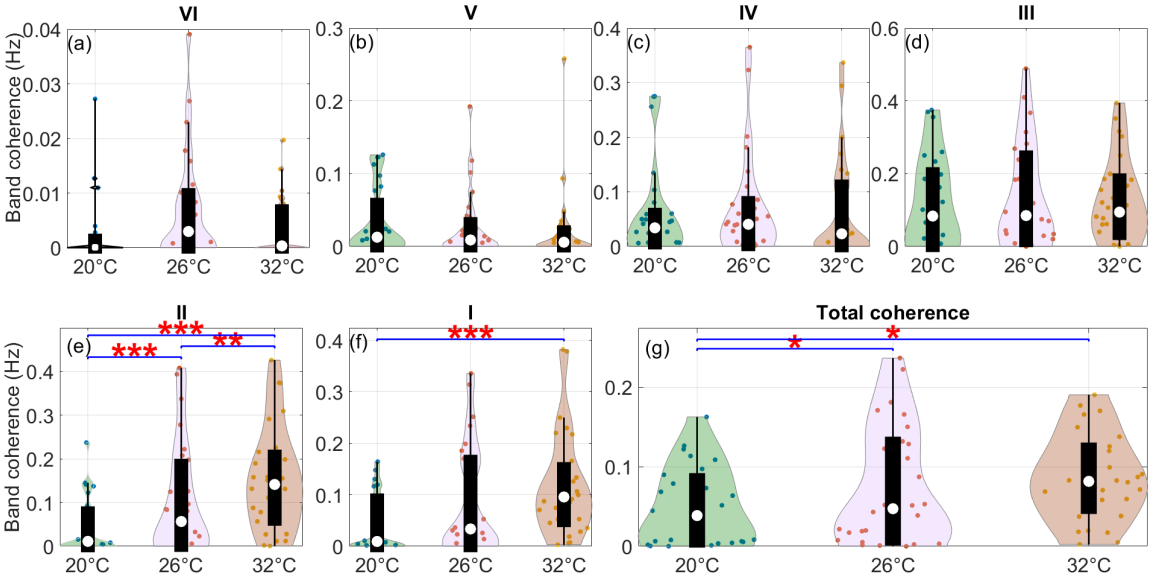

Figure 4.61: Spectral coherence of the right index finger and LDFAL within frequency bands. Violin plots compare the median coherence content within each frequency band including the total coherence in the between LDF blood flow oscillations in the left arm and right index finger. The Wilcoxon signed rank test was applied for comparisons in each frequency band for the three ambient temperatures and statistical significance was set at $p < 0.05$. Significance is considered as $^{*}p < 0.05$,$^{**}p$ <0.01, $^{***}p$ <0.001.

The coherence nearly disappears in the respiratory and cardiac frequency intervals in the group of ambient temperature 20°C at right-index finger blood flow. Moreover, both coherence signals showed significant differences in the phase shift of the right III (p = 0.0345) and left IV (p = 0.04), III (p = 0.009) index fingers with LDF coherence as shown in figure 4.60 (c), (d). A significant difference in the blood flow right-forearm coherence in the frequency intervals: IV (p = 0.0119), (p = 0.049), II (p = 0.0008), (p = 0.0000), (p = 0.0044), I (p = 0.0000) as shown in figure 4.61.

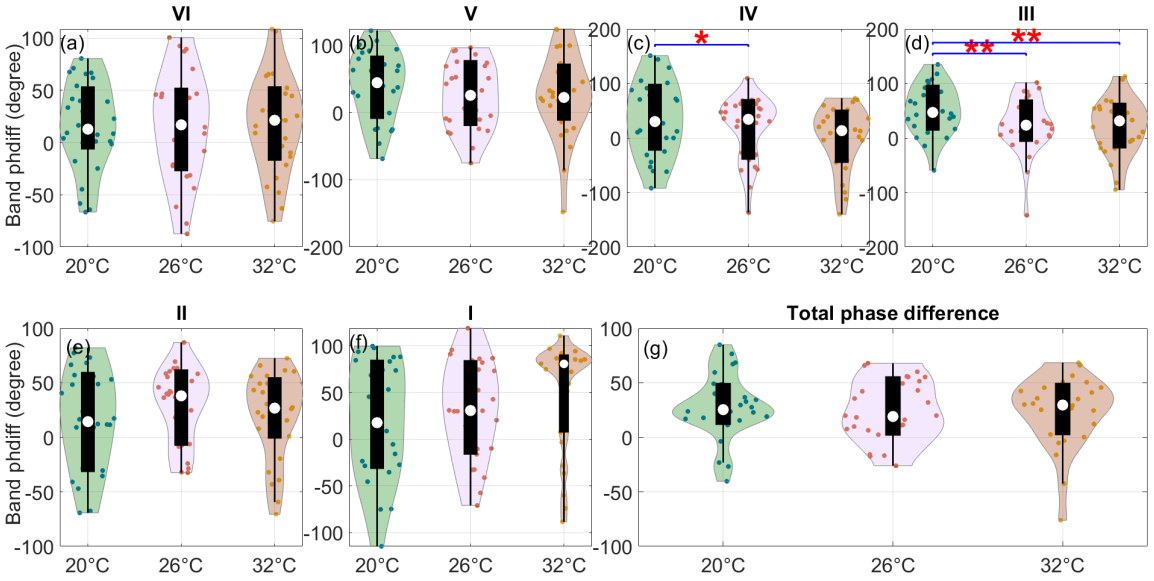

Figure 4.62: Spectral phase difference of between LDF blood flow oscillations in the left arm and right index finger within frequency bands. Violin plots compare the median phase difference content within each frequency band including the total phase difference in two index fingers signal. The Wilcoxon signed rank test was applied for comparisons in each frequency band for the three ambient temperatures and statistical significance was set at $p < 0.05$. Significance is considered as $^{*}p < 0.05$,$^{**}p < 0.01$, $^{***}p < 0.001$.

The pair-wise test revelled more significant differences in the phase shift right-forearm coherence in the frequency intervals: IV ($p = 0.0256$), III ($p = 0.0025$), ($p = 0.0055$) as shown in figure 4.62. The positive value of the shift indicates that the oscillations in the forearm are leading those in the right index finger. The pair-wise test revealed significant differences in forearm-left index finger coherence in the frequency intervals: V ($p = 0.0264$), II ($p = 0.0082$), ($p = 0.0001$), I ($p = 0.0124$), ($p = 0.0031$) as shown in figure 4.63.

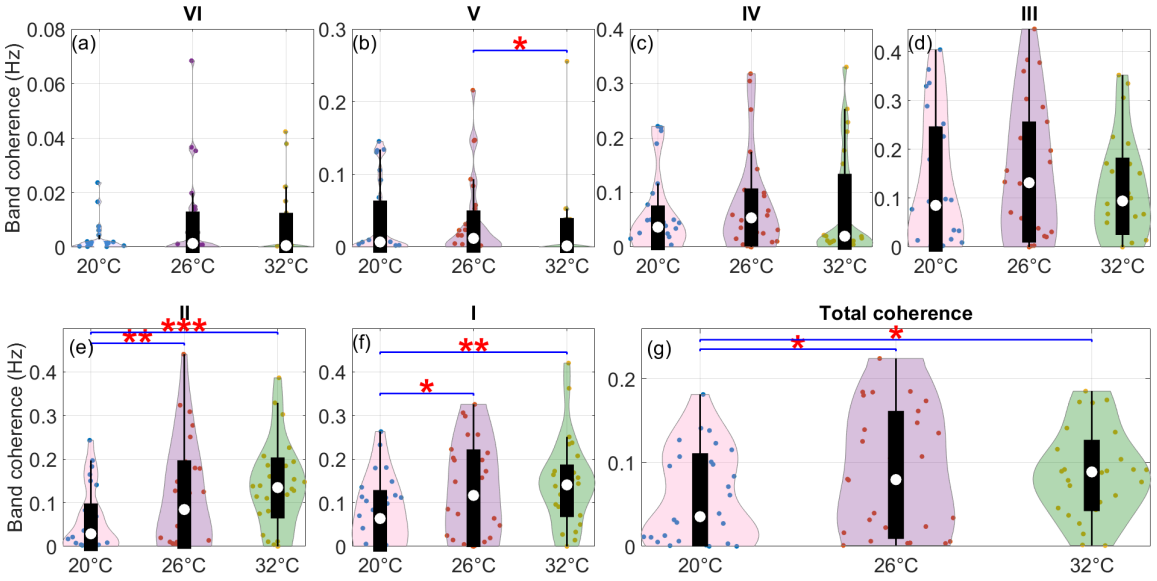

Figure 4.63: Spectral coherence of the left index finger and LDFAL within frequency bands. Violin plots compare the median coherence content within each frequency band including the total coherence in the between LDF blood flow oscillations in the left arm and left index finger. The Wilcoxon signed rank test was applied for comparisons in each frequency band for the three ambient temperatures and statistical significance was set at $p < 0.05$. Significance is considered as $^{*}p < 0.05$,$^{**}p$ <0.01, $^{***}p$ <0.001.

Significant differences in the blood flow right-sBP coherence in the frequency intervals: IV ($p = 0.0031$), ($p = 0.0158$), III ($p = 0.0067$), ($p = 0.0055$), II ($p = 0.0131$), I ($p = 0.0168$) and the total phase difference ($p = 0.0427$), ($p = 0.019$) are shown in figure 4.64.

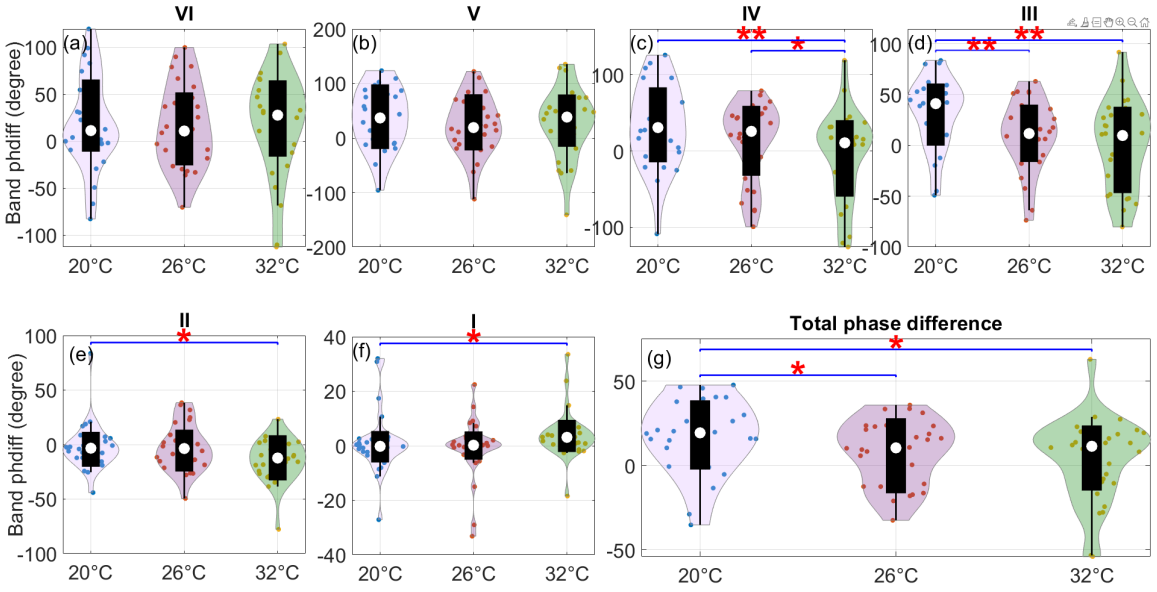

Figure 4.64: Spectral phase difference of the left index finger and LDFAL within frequency bands. Violin plots compare the median phase difference content within each frequency band including the total coherence between LDF blood flow oscillations in the left arm and left index finger. The Wilcoxon signed rank test was applied for comparisons in each frequency band for the three ambient temperatures and statistical significance was set at $p < 0.05$. Significance is considered as $^{*}p < 0.05$,$^{**}p < 0.01$, $^{***}p < 0.001$.

4.6 Systemic and peripheral interactions

4.6.1 Coherence between IHR and the LDF blood flow in the right or left index finger

The group median values of wavelet phase coherence between oscillations in both right and left index fingers with IHR was calculated as shown in figure 4.65 (a), (b). High phase coherence was revealed for both signal pairs at the frequency of myogenic (~ 0.1 Hz) and respiratory (~ 0.3 Hz) frequencies. Significant differences were exhibited in the coherence of right ($p = 0.0315$) and left ($p = 0.0259$) blood flow with IHR as

shown in the multi-comparison test.

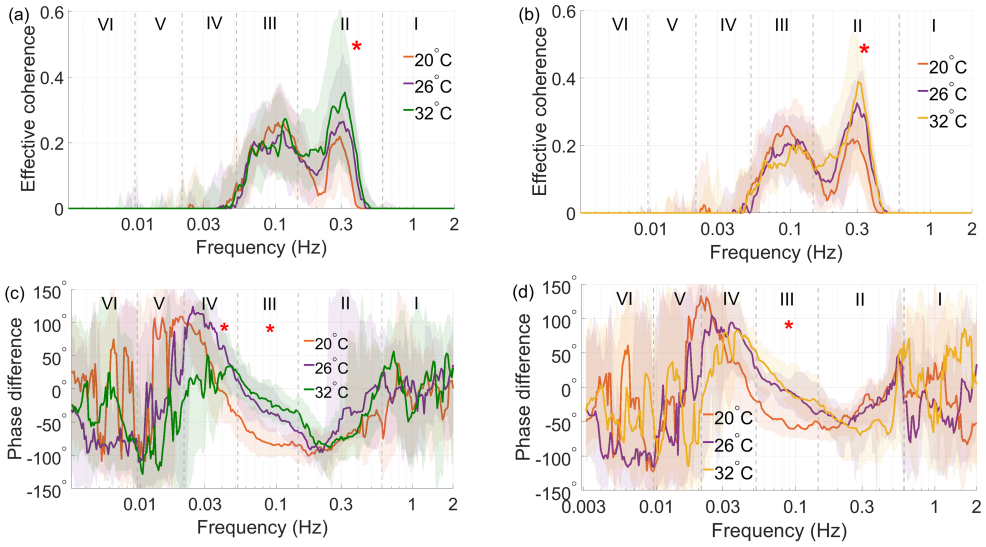

Figure 4.65: Group median values of the effective phase coherence between instantaneous heart rate and LDF at the two index fingers. Phase coherence between the instantaneous heart rate and the blood flow signal recorded using LDF in (a) the right and (b) the left index fingers, in the frequency interval between 0.003 Hz and 2 Hz. For each of the two cases, the group medians of the phase difference are shown underneath the coherence plots in (c) and (d). Statistically significant differences ($p < 0.05$) were revealed by the Kruskal Wallis test and indicated by red asterisks at the defined frequency intervals.

Significant differences in the phase shift were found in the right index finger with IHR coherence in the frequency intervals: of neurogenic ($p = 0.0174$) and myogenic ($p = 0.0000$) as shown in figure 4.65 (c). Phase shift in the left index finger was only exabitied significant in the myogenic interval ($p = 0.0000$) as shown in figure 4.65 (d).

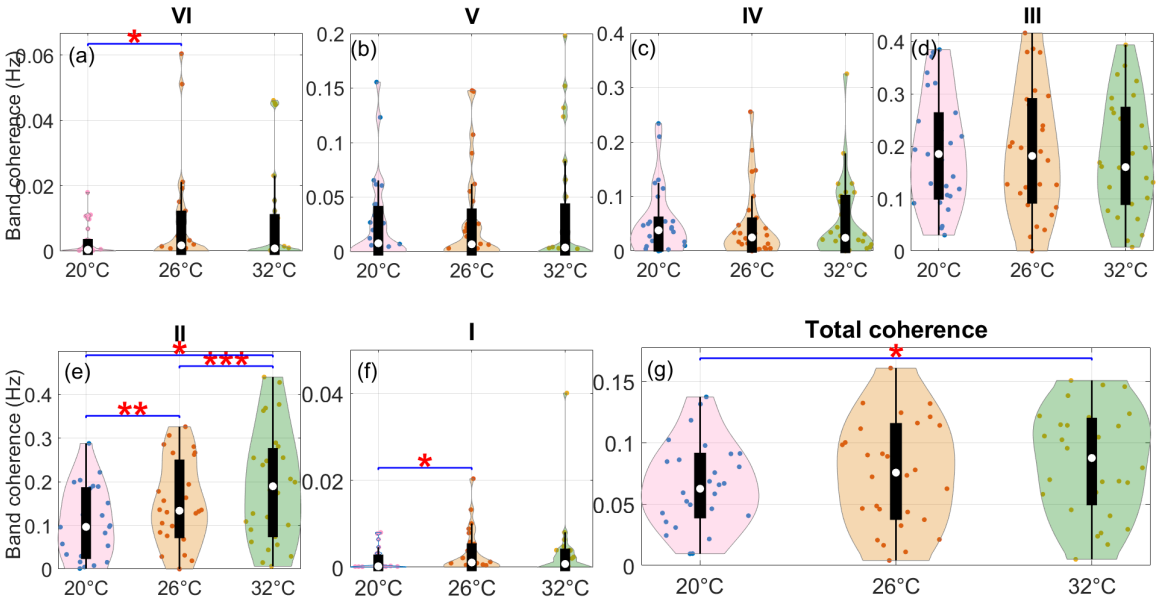

Figure 4.66: Spectral coherence between LDF at the right index finger and IHR within frequency bands. Violin plots compare the median coherence content within each frequency band including the total coherence between the right index finger and the IHR signal. Wilcoxon signed rank test was applied for comparisons in each frequency band for the three ambient temperatures and statistical significance was set at $p < 0.05$. Significance is considered as $^{*}p < 0.05$,$^{**}p < 0.01$, $^{***}p < 0.001$.

The pair-wise test revealed more significant differences in the right index finger-IHR coherence at the frequency intervals: VI ($p = 0.0211$), II ($p = 0.0033$), ($p = 0.0003$), ($p = 0.0288$), ($p = 0.0259$), I ($p = 0.0653$) and the total coherence ($p = 0.0323$) as shown in figure 4.66. The pairwise test revealed more significant differences in the phase shift right index-IHR coherence at the frequency intervals: V ($p = 0.0131$), IV ($p = 0.0148$), ($p = 0.0041$), III ($p = 0.0000$), ($p = 0.0002$), II ($p = 0.0047$) as shown in figure 4.67. The positive value of the shift indicates that the oscillations in the IHR are leading the ones in the right index.

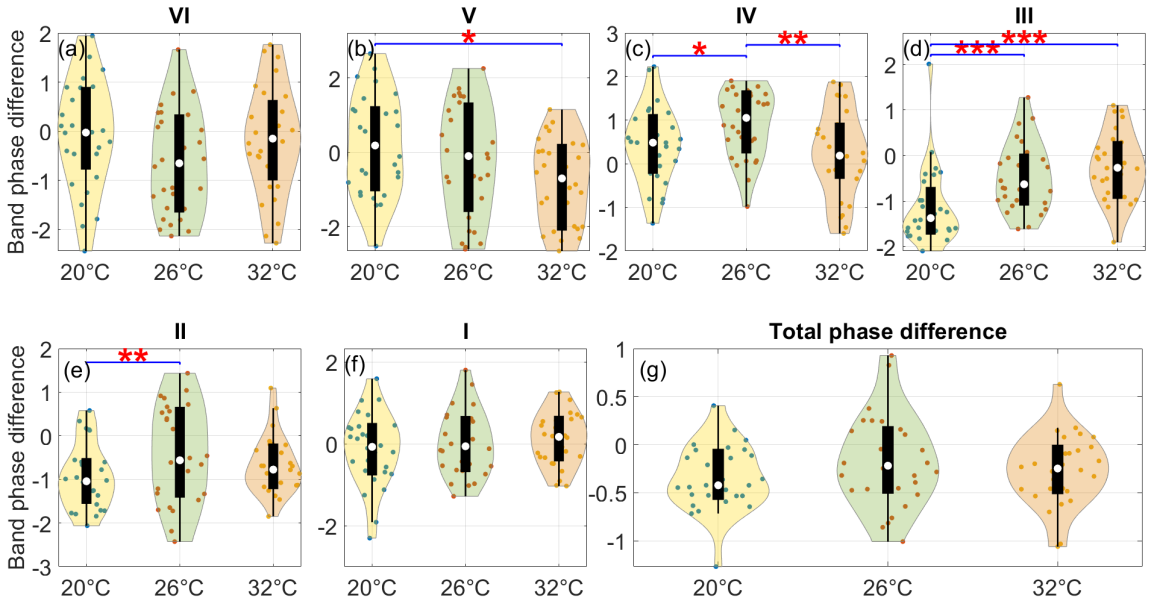

Figure 4.67: Spectral phase difference between LDF at the right index finger and IHR within frequency bands. Violin plots compare the median coherence content within each frequency band including the total phase difference between the right index finger and the IHR signal. The unit of the phase is radian. The Wilcoxon signed rank test was applied for comparisons in each frequency band for the three ambient temperatures and statistical significance was set at $p < 0.05$. Significance is considered as $^{*}p < 0.05$,$^{**}p$ <0.01, $^{***}p$ <0.001 .

The pairwise test revealed more significant differences in the left index finger-IHR coherence at the frequency intervals: VI ($p = 0.0476$), II ($p = 0.0009$), ($p = 0.002$) as shown in figure 4.68.

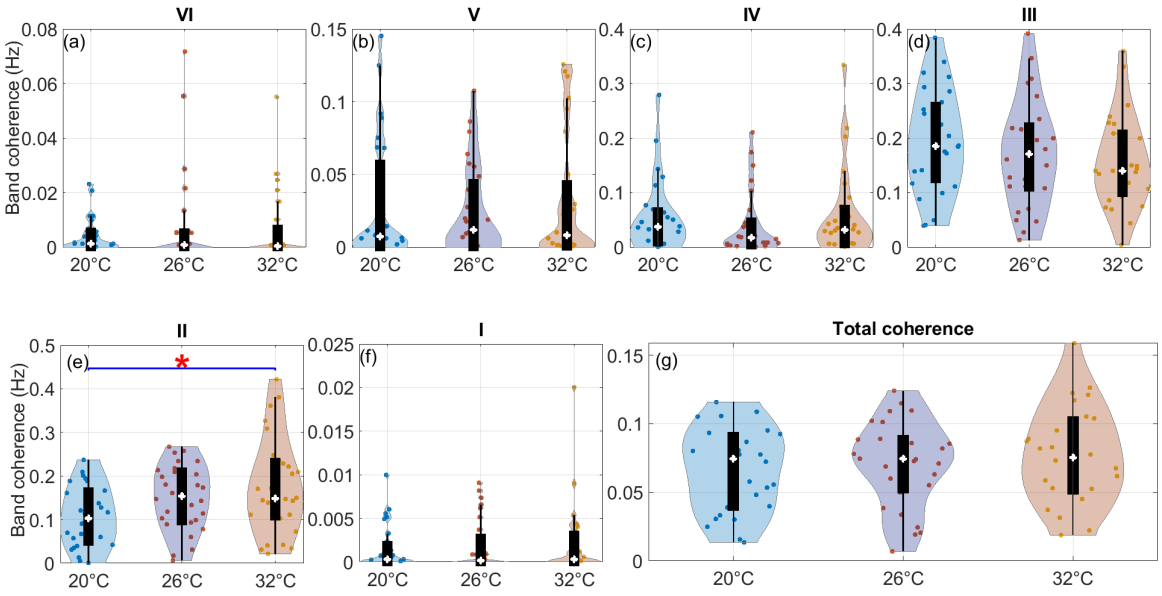

Figure 4.68: Spectral coherence between LDF at left index finger and IHR within frequency bands. Violin plots compare the median coherence content within each frequency band including the total coherence between the left index finger and IHR signals. The Wilcoxon signed rank test was applied for comparisons in each frequency band for the three ambient temperatures and statistical significance was set at $p < 0.05$. Significance is considered as $^{*}p < 0.05$,$^{**}p < 0.01$, $^{***}p < 0.001$.

Similarly, the pairwise test revealed more significant differences in the phase shift left index-IHR coherence in the frequency intervals: VI ($p = 0.0272$), III ($p = 0.0000$), ($p = 0.0008$) as shown in figure 4.69. The positive value of the shift indicates that the oscillations in the IHR are leading those in the left index finger.

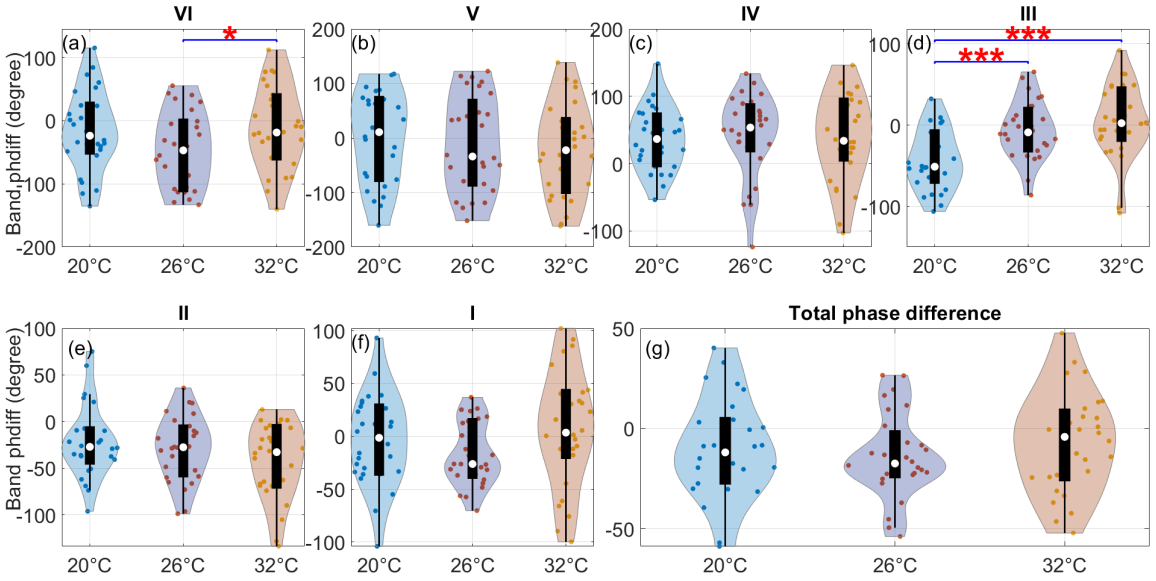

Figure 4.69: Spectral phase difference between LDF in the left index finger and IHR within frequency bands. Violin plots compare the median phase difference content within each frequency band including the total phase difference between the left index finger and IHR signal. Wilcoxon signed rank test was applied for comparisons in each frequency band for the three ambient temperatures and statistical significance was set at $p < 0.05$. Significance is considered as $^{*}p < 0.05$,$^{**}p < 0.01$, $^{***}p < 0.001$.

4.6.2 Coherence between the blood pressure and the LDF blood flow in the right and left index finger

The group median values of wavelet phase coherence between oscillations in both blood pressure and with blood flow (right and left index fingers) were calculated as shown in figure 4.70 (a),(b). High phase coherence was revealed for both signal pairs at the frequency intervals of neurogenic, myogenic (~ 0.1 Hz) and respiration (~ 0.3 Hz). Significant differences were exhibited in the coherence of BP-right index finger: II ($p = 0.0325$) as shown in multi-comparison test. Significant differences in the phase shift were found in the right index finger coherence in the frequency interval of neurogenic ($p = 0.0001$), myogenic ($p = 0.0000$) as shown in figure 4.70 (c). Similar

significant differences were observed in the phase shift of the left index finger coherence in the frequency intervals: neurogenic ($p = 0.0331$), myogenic ($p = 0.0000$) as shown in figure 4.70 (d).

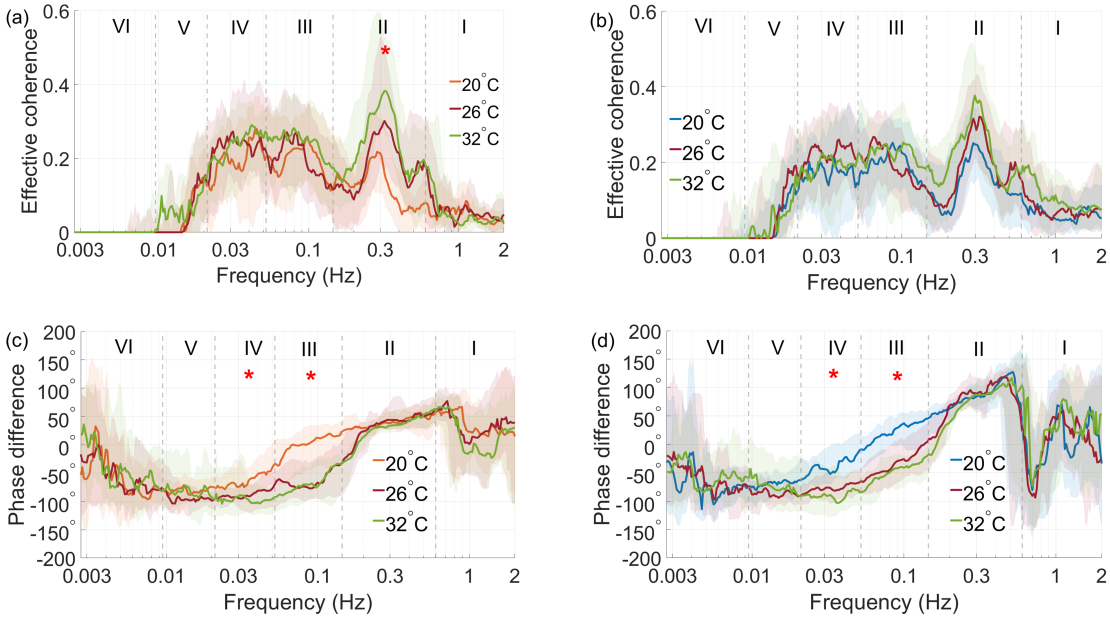

Figure 4.70: Group median values of the effective phase coherence between blood pressure and LDF at the two index fingers. Phase coherence between blood pressure and the blood flow signal recorded using LDF in (a) the right and (b) the left index fingers, in the frequency interval between 0.003 Hz and 2 Hz. For each of the two cases, the group medians of the phase difference are shown underneath the coherence plots in (c) and (d). A statistically significant difference ($p < 0.05$) was revealed by the Kruskal Wallis test and indicated by red asterisks at the defined frequency intervals.

A significant difference was observed in the blood flow right-BP coherence in the frequency intervals: II ($p = 0.0012$), ($p = 0.0002$), ($p = 0.0451$) and in the total coherence ($p = 0.0148$), ($p = 0.0044$) as shown in figure 4.71.

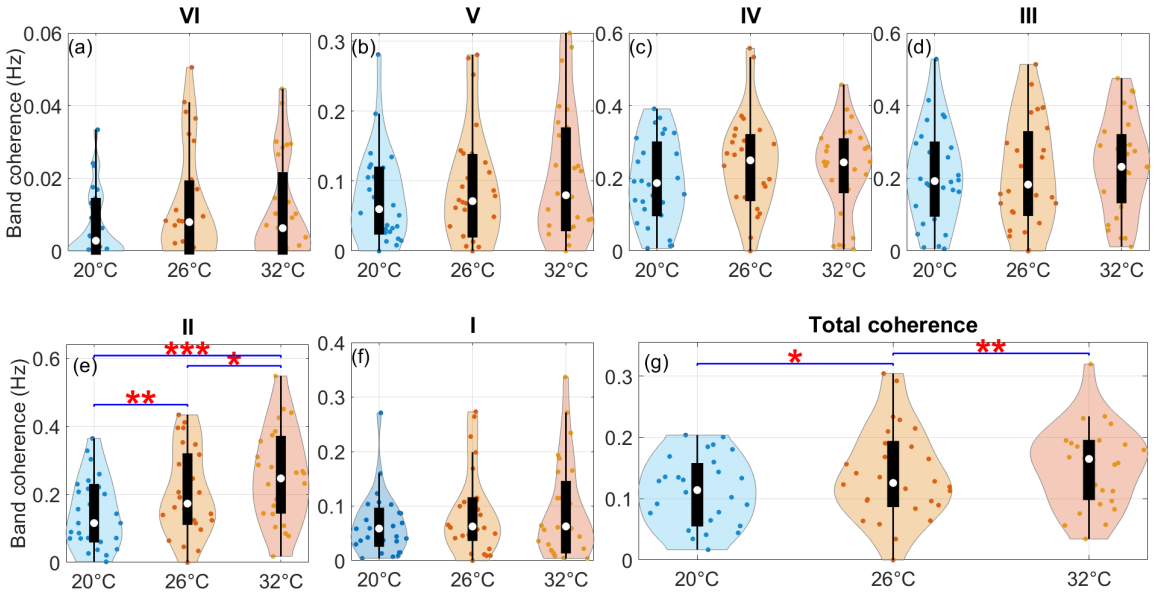

Figure 4.71: Spectral coherence between blood flow recorded on the right index finger and blood pressure within frequency bands. Violin plots compare the median coherence content within each frequency band including the total coherence in the right index finger-BP signal. The Wilcoxon signed rank test was applied for comparisons in each frequency band for the three ambient temperatures and statistical significance was set at $p < 0.05$. Significance is considered as $^{*}p < 0.05$,$^{**}p < 0.01$, $^{***}p < 0.001$.

The pairwise test revealed more significant differences in the phase shift BP-right index coherence in the frequency intervals: IV ($p = 0.0000$), ($p = 0.0059$), III ($p = 0.0000$), ($p = 0.0000$), ($p = 0.0242$) and the total phase shift ($p = 0.0108$) as shown in figure 4.72. The positive value of the shift indicates that the oscillations in the right index finger are leading those in the BP.

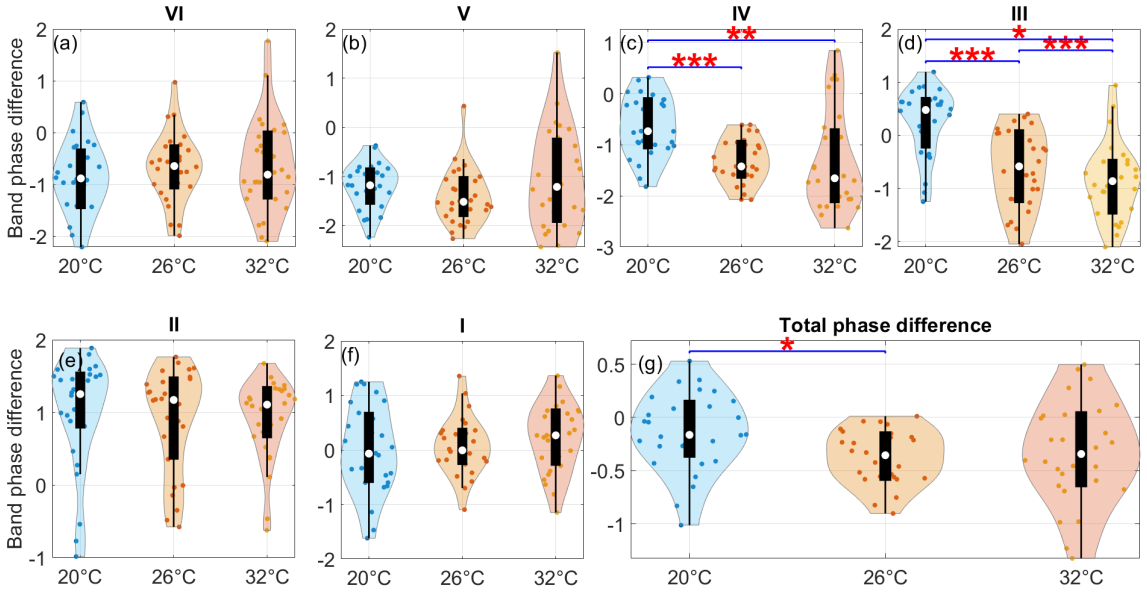

Figure 4.72: Spectral phase difference between blood flow recorded on the right index finger and blood pressure within frequency bands. Violin plots compare the median phase difference content within each frequency band including the total coherence in the right index finger-BP signal. The unit of the phase is radian. The Wilcoxon signed rank test was applied for comparisons in each frequency band for the three ambient temperatures and statistical significance was set at $p < 0.05$. Significance is considered as $^{*}p < 0.05$,$^{**}p < 0.01$, $^{***}p < 0.001$.

Significant differences were found in the blood flow left-BP coherence in the frequency intervals: II ($p = 0.0215$), ($p = 0.0063$), I ($p = 0.0083$), ($p = 0.0323$) as shown in figure 4.73.

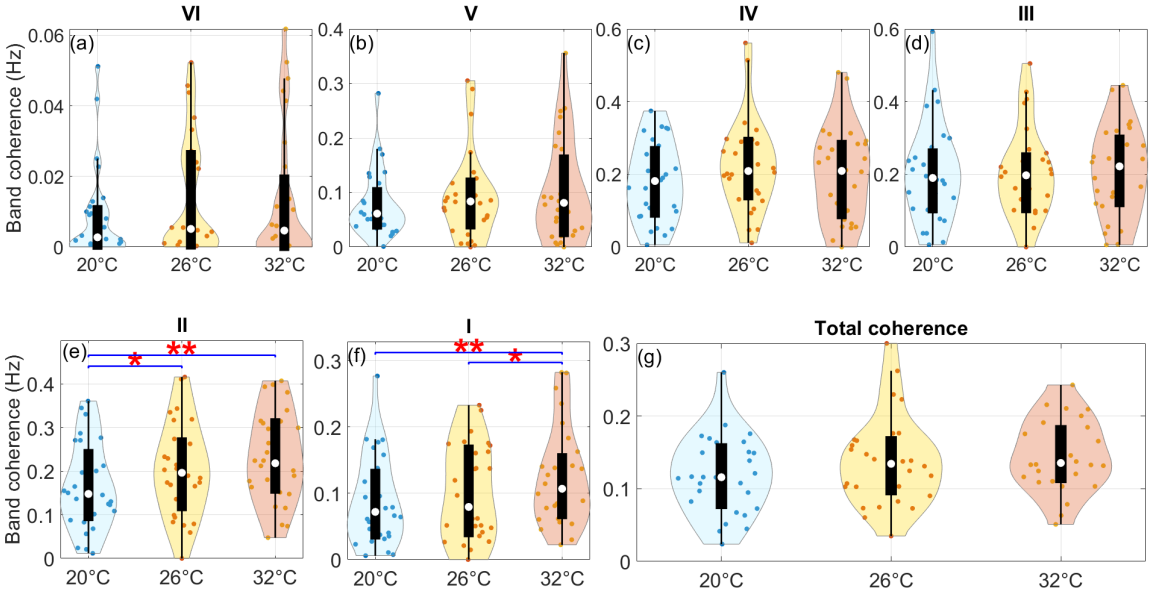

Figure 4.73: Spectral coherence between blood flow recorded on the left index finger and blood pressure within frequency bands. Violin plots compare the median coherence content within each frequency band including the total coherence in the left index finger-BP signal. The Wilcoxon signed rank test was applied for comparisons in each frequency band for the three ambient temperatures and statistical significance was set at $p < 0.05$. Significance is considered as $^{*}p < 0.05$,$^{**}p$ <0.01, $^{***}p$ <0.001.

The pairwise test revealed significant differences in the phase shift of BP-left index finger coherence at the frequency intervals: IV (p = 0.0041), III (p = 0.0000), (p = 0.0002), II (p = 0.0476) and the total phase difference (p = 0.0000) as and the total phase difference shown (p = 0.0067) in figure 4.74. The positive value of the shift indicates that the oscillations in the left index finger are leading those in the BP.

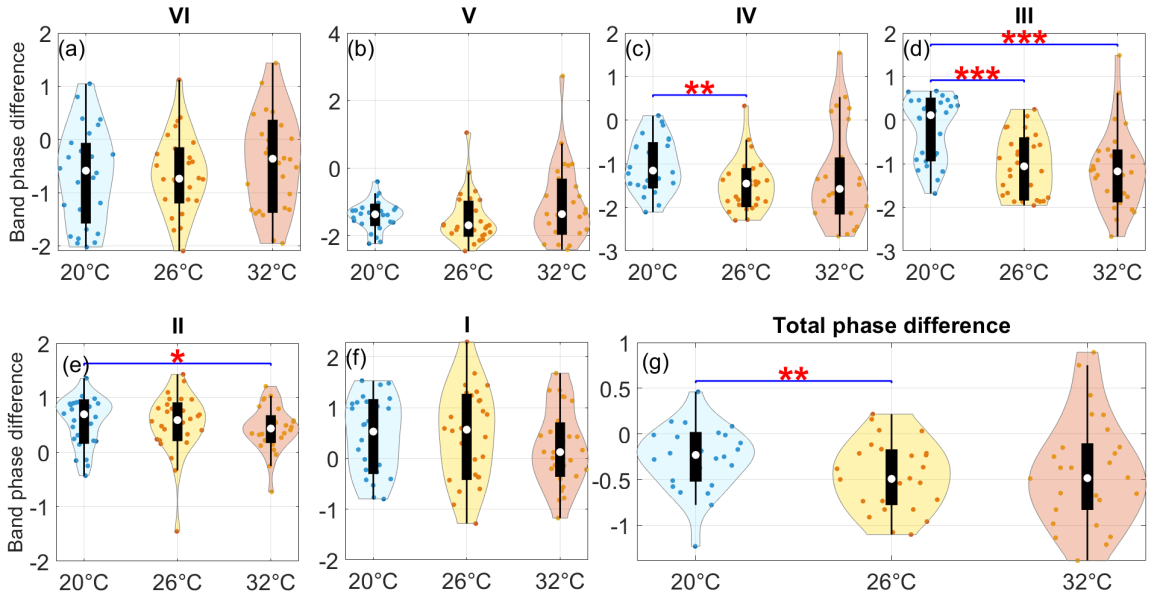

Figure 4.74: Spectral phase difference of recording blood flow at left index finger and blood pressure within frequency bands. Violin plots compare the median phase difference content within each frequency band including the total coherence in the left index finger-BP signal. The unit of the phase is radian. Wilcoxon signed rank test was applied for comparisons in each frequency band for the three ambient temperatures and statistical significance was set at $p < 0.05$. Significance is considered as $^{*}p < 0.05$,$^{**}p$ <0.01, $^{***}p$ <0.001.

4.6.3 Coherence between the systolic blood pressure and the LDF blood flow in the right and left index finger

Group median values of wavelet phase coherence between oscillations in both blood flow (right and left index fingers) and systolic blood pressure were calculated as shown in figure 4.75 (a),(b). High phase coherence was revealed for both signal pairs at the frequency intervals of neurogenic ($\sim$ 0.03 Hz), myogenic ($\sim$ 0.1 Hz), respiratory ($\sim$ 0.3 Hz) and cardiac ($\sim$ 1 Hz) oscillations. Significant differences were exhibited in the coherence of systolic with the right II ($p = 0.0315$) and left II ($p = 0.0174$) indices as shown in the multi-comparison test. Moreover, both coherence signals showed

significant differences in the phase shift between the right V ($p = 0.0466$), IV ($p = 0.0012$), III ($p = 0.0000$) and left IV ($p = 0.04$), III ($p = 0.0007$) index fingers and sBP coherence as shown in figure 4.75 (c),(d).

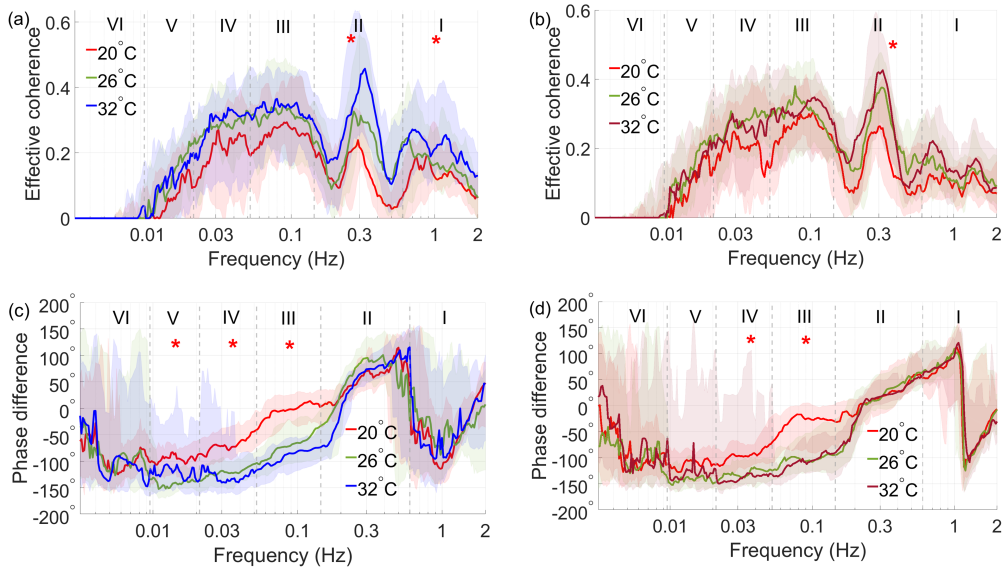

Figure 4.75: Group median values of the effective phase coherence between systolic blood pressure and LDF at the two index fingers. Phase coherence between systolic blood pressure and the blood flow signal recorded using LDF in (a) the right and (b) the left index fingers, in the frequency interval between 0.003 Hz and 2 Hz. For each of the two cases, the group medians of the phase difference are shown underneath the coherence plots in (c) and (d). A statistically significant difference ($p < 0.05$) was revealed by the Kruskal is Wallis test and indicated by red asterisks in the defined frequency intervals.

Significant differences in the blood flow right-sBP coherence were observed in the frequency intervals V ($p = 0.0272$), IV ($p = 0.0382$), II ($p = 0.0029$), ($p = 0.0003$), I ($p = 0.0228$),($p = 0.0003$), and the total coherence ($p = 0.0029$), ($p = 0.0002$) as shown in figure 4.76.

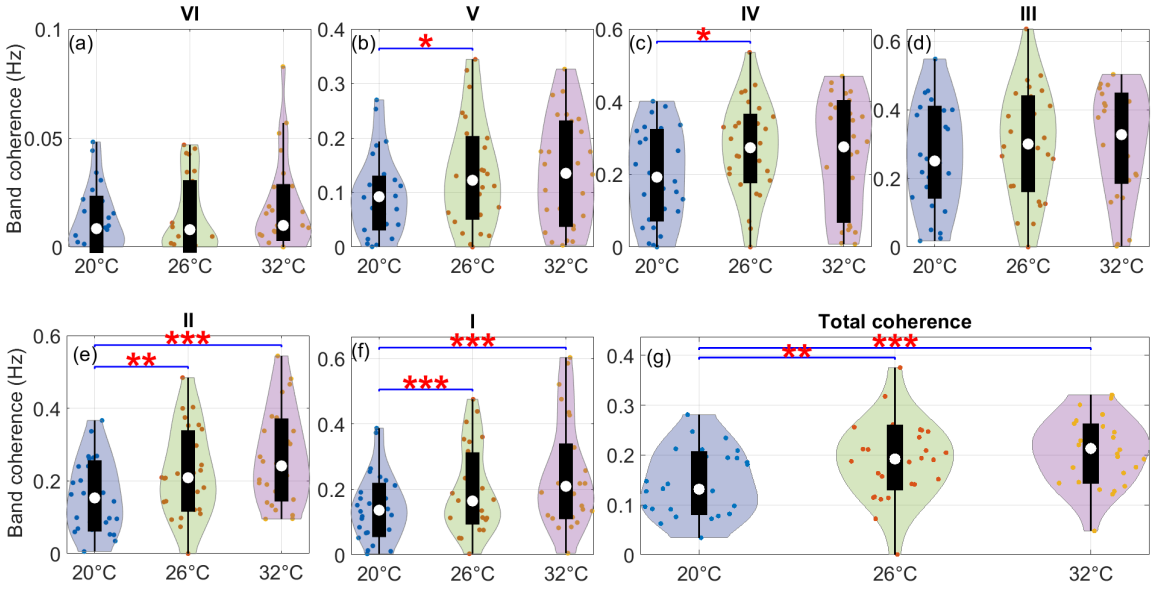

Figure 4.76: Spectral coherence between blood flow in the right index finger and sBP within frequency bands. Violin plots compare the median coherence content within each frequency band including the total coherence in the sBP-right index finger signal. The Wilcoxon signed rank test was applied for comparisons in each frequency band for the three ambient temperatures and statistical significance was set at $p < 0.05$. Significance is considered as $^{*}p < 0.05$,$^{**}p < 0.01$, $^{***}p < 0.001$.

The pairwise test revealed more significant differences in the phase shift sBP-right index coherence in the frequency intervals V ($p = 0.0427$), ($p = 0.0342$), IV ($p = 0.0002$), III ($p = 0.0000$), ($p = 0.0000$) as shown in figure 4.77. The positive value of the shift indicates that the oscillations in the right index finger are leading those in the sBP.

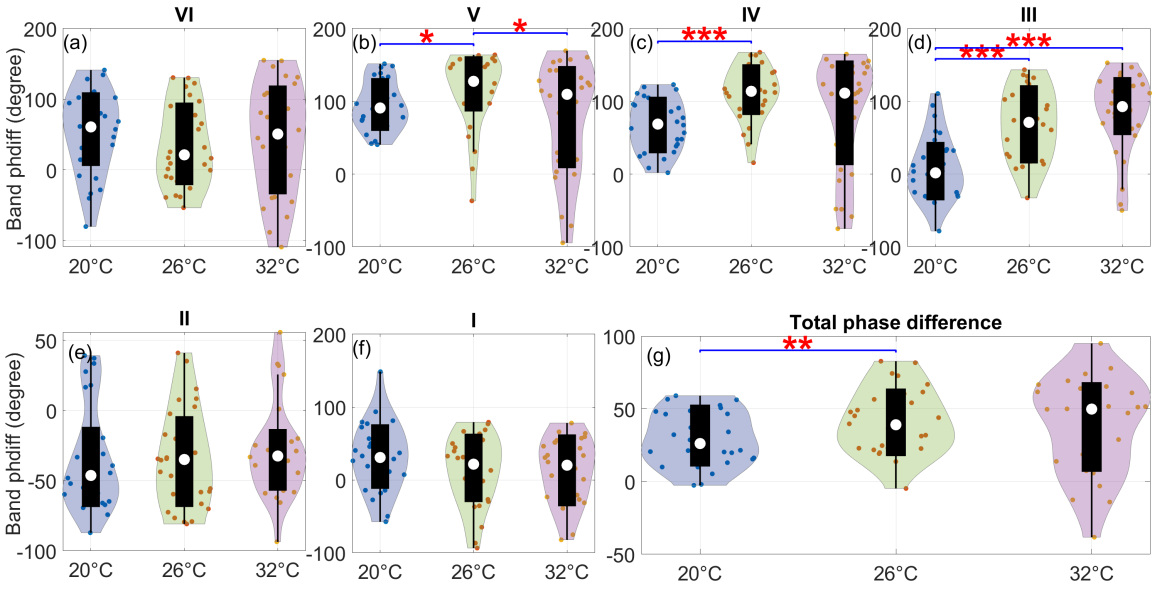

Figure 4.77: Spectral phase difference between blood flow recorded on the right index finger and sBP within frequency bands. Violin plots compare the median phase difference content within each frequency band including the total coherence in the left index finger-sBP signal. The Wilcoxon signed rank test was applied for comparisons in each frequency band for the three ambient temperatures and statistical significance was set at $p < 0.05$. Significance is considered as $^{*}p < 0.05$,$^{**}p$ <0.01, $^{***}p$ <0.001.

Significant differences were found between the blood flow left-sBP coherence in the frequency intervals: II ($p = 0.0044$), ($p = 0.0051$), I ($p = 0.0108$), ($p = 0.0067$), and the total coherence ($p = 0.019$), ($p = 0.0083$) as shown in figure 4.78.

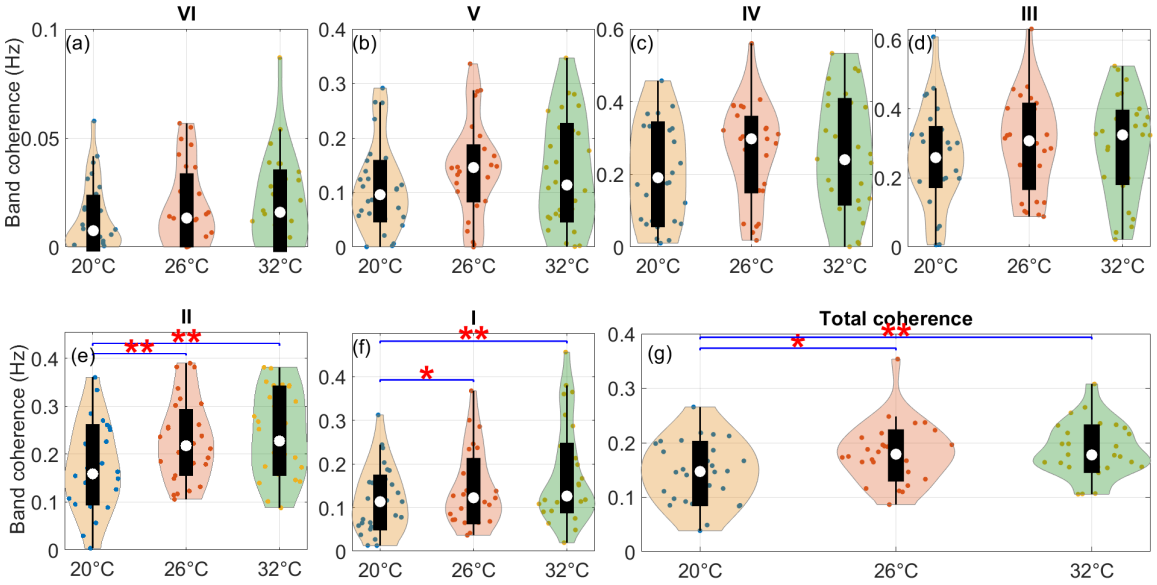

Figure 4.78: Spectral coherence between blood flow on the left index finger and sBP within frequency bands. Violin plots compare the median coherence content within each frequency band including the total coherence in the sBP-left index finger signal. The Wilcoxon signed rank test was applied for comparisons in each frequency band for the three ambient temperatures and statistical significance was set at $p < 0.05$. Significance is considered as $^{*}p < 0.05$,$^{**}p < 0.01$, $^{***}p < 0.001$.

The pairwise test revealed significant differences in the phase shift sBP-left index finger coherence at the frequency intervals: V ($p = 0.0115$), IV ($p = 0.0088$) and the total phase difference III ($p = 0.0000$), ($p = 0.0228$) as and the total phase difference shown ($p = 0.0018$) in figure 4.79. The positive value of the shift indicates that blood flow oscillations in the left index finger are leading those in the sBP.

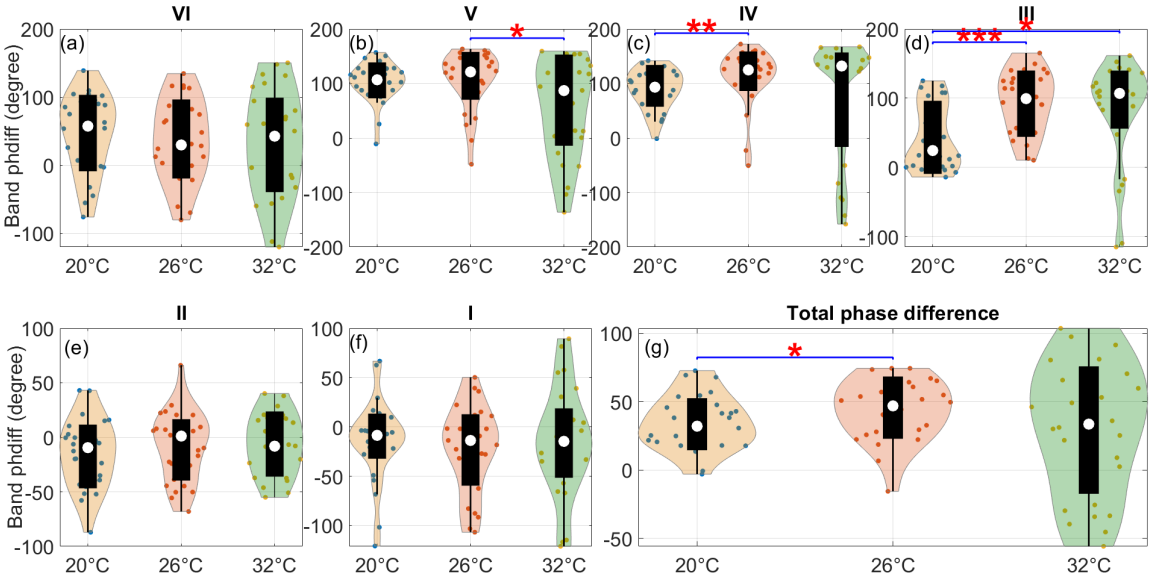

Figure 4.79: Spectral phase difference between blood flow recorded on the left index finger and sBP within frequency bands. Violin plots compare the median phase difference content within each frequency band including the total coherence in the left index finger-sBP signal. The Wilcoxon signed rank test was applied for comparisons in each frequency band for the three ambient temperatures and statistical significance was set at $p < 0.05$. Significance is considered as $^{*}p < 0.05$,$^{**}p < 0.01$, $^{***}p < 0.001$.

4.6.4 Coherence between the diastolic blood pressure and the LDF blood flow in the right and left index finger

Group median values of wavelet phase coherence between blood flow oscillations in the right and left index fingers and diastolic blood pressure were calculated as shown in figure 4.80 (a), (b). High phase coherence was revealed for both signal pairs in the frequency intervals of neurogenic (~ 0.03 Hz), myogenic (~ 0.1 Hz), and respiratory frequency intervals, (~ 0.3 Hz) and low coherence in the cardiac (~ 1 Hz) interval. Significant differences were exhibited in the coherence of diastolic with right II ($p = 0.0299$) and left I ($p = 0.0255$) index as shown in multi-comparison test. Moreover, there were significant differences in the phase shift s between blood flow oscillations in

the right IV ($p = 0.0006$), III ($p = 0.0000$) and left IV ($p = 0.0184$), III ($p = 0.0002$) index fingers and the dBP coherence as shown in figure 4.80 (c), (d).

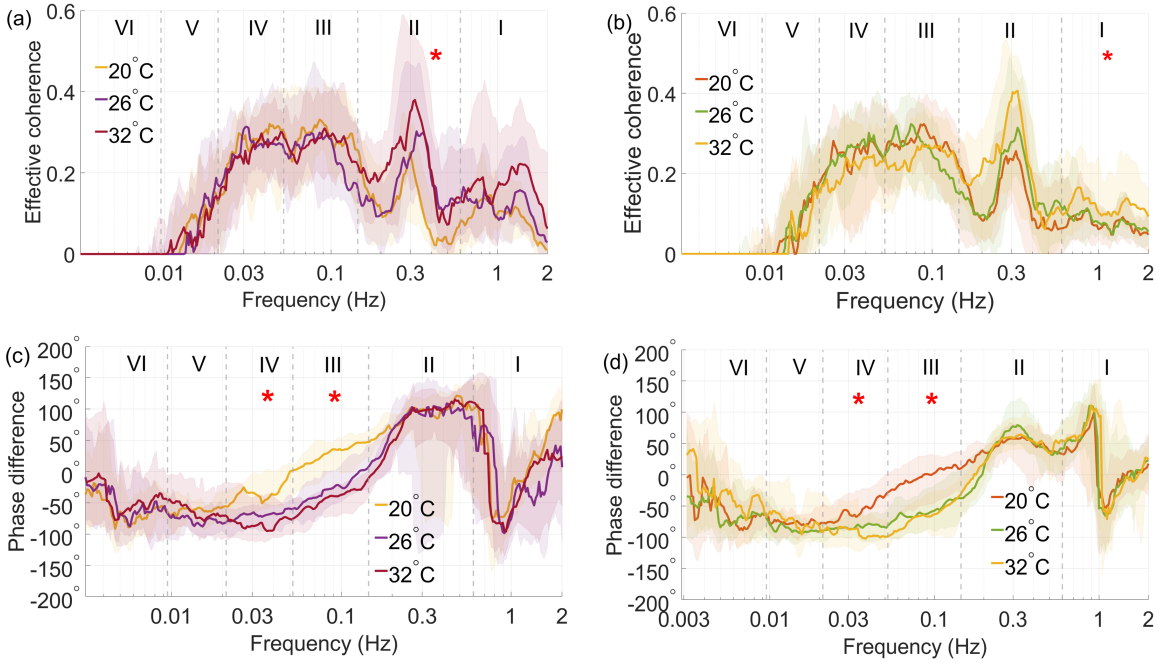

Figure 4.80: Group median values of the effective phase coherence between diastolic blood pressure and LDF at the two index fingers. Phase coherence between diastolic blood pressure and the blood flow signal recorded using LDF in (a) the right and (b) the left index fingers, in the frequency interval between 0.003 Hz and 2 Hz. For each of the two cases, the group medians of the phase difference are shown underneath the coherence plots in (c) and (d). Statistically significant differences ($p < 0.05$) were revealed by the Kruskal Wallis test and indicated by red asterisks at the defined frequency intervals.

Significant differences in the blood flow right-dBP coherence in the frequency intervals: II ($p = 0.0036$), II ($p = 0.0036$), ($p = 0.0008$), I ($p = 0.0256$), ($p = 0.002$), ($p = 0.0404$) are shown in figure 4.81.

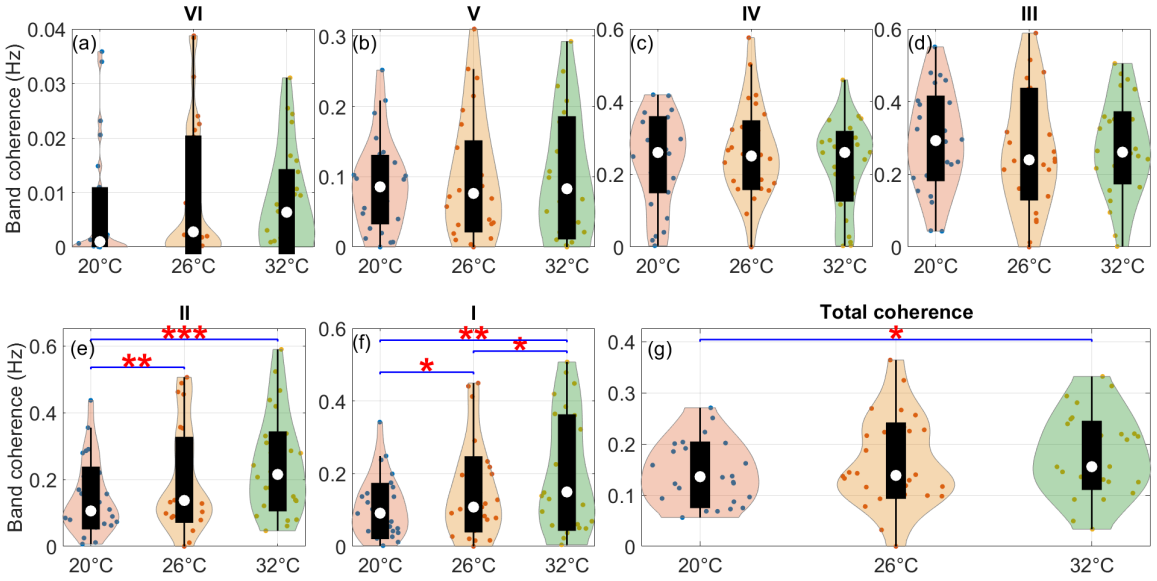

Figure 4.81: Spectral coherence of between blood flow oscillations on the right index finger and dBP within frequency bands. Violin plots compare the median coherence content within each frequency band including the total coherence in the dBP-right index finger signal. The Wilcoxon signed rank test was applied for comparisons in each frequency band for the three ambient temperatures and statistical significance was set at $p < 0.05$. Significance is considered as $^{*}p < 0.05$,$^{**}p$ <0.01, $^{***}p$ <0.001.

The pairwise test revealed more significant differences in the phase shift dBP-left index finger coherence at the frequency intervals: IV ($p = 0.0000$), ($p = 0.0000$), III ($p = 0.0000$), ($p = 0.0000$) as shown in figure 4.82. The positive value of the shift indicates that the oscillations in the right finger flow are leading those in the dBP.

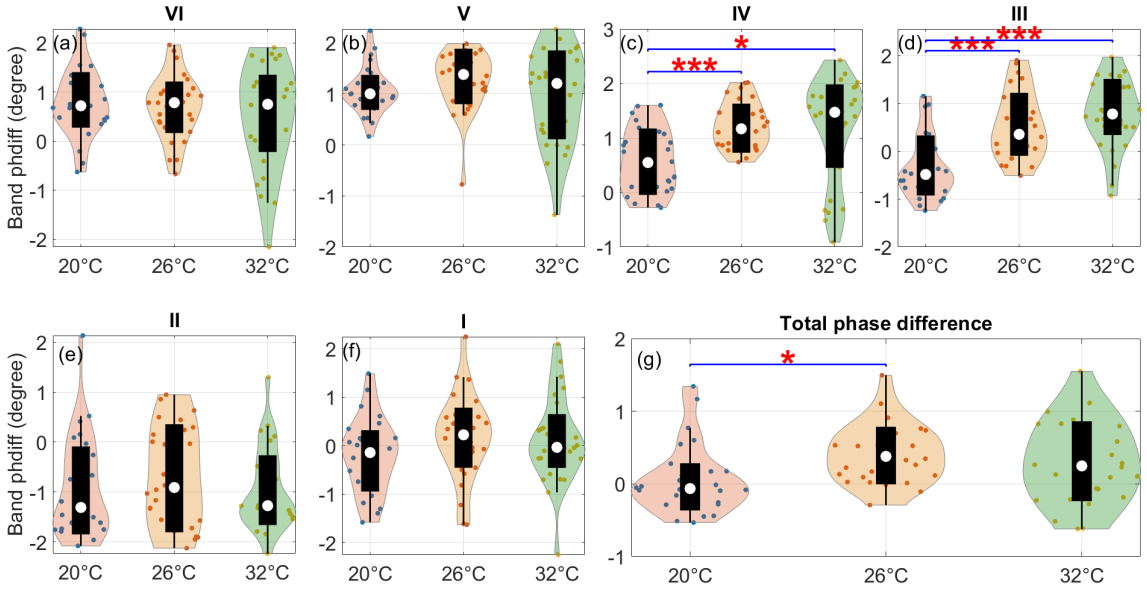

Figure 4.82: Spectral phase difference between blood flow recorded on the right index finger and dBP within frequency bands. Violin plots compare the median phase difference content within each frequency band including the total coherence in the right index finger-dBP signal. The unit of the phase is radian. The Wilcoxon signed rank test was applied for comparisons in each frequency band for the three ambient temperatures and statistical significance was set at $p < 0.05$. Significance is considered as $^{*}p < 0.05$,$^{**}p < 0.01$, $^{***}p < 0.001$.

A significant difference was observed in the blood flow right-sBP coherence in the frequency intervals: II ($p = 0.0202$), I ($p = 0.0038$),($p = 0.0072$) as shown in figure 4.83.

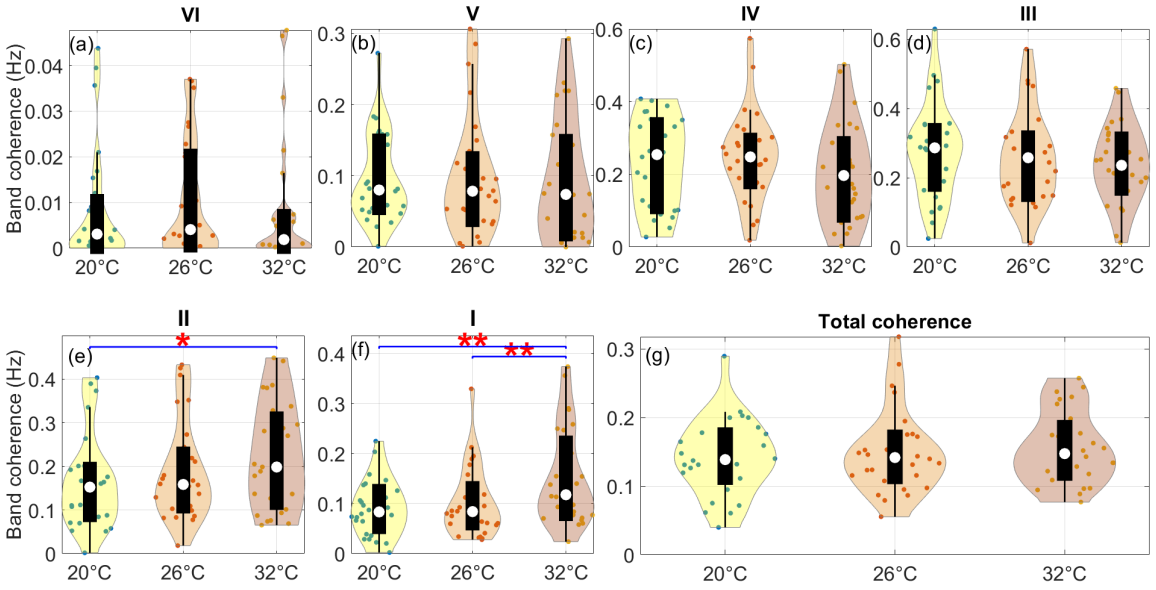

Figure 4.83: Spectral coherence between blood flow oscillations on the left index finger and dBP within frequency bands. Violin plots compare the median coherence content within each frequency band including the total coherence in the dBP-left index finger signal. The Wilcoxon signed rank test was applied for comparisons in each frequency band for the three ambient temperatures and statistical significance was set at $p < 0.05$. Significance is considered as $^{*}p < 0.05$,$^{**}p$ <0.01, $^{***}p$ <0.001.

The pairwise test revealed significant differences in the phase shift dBP-left index finger coherence at the frequency intervals: IV ($p = 0.0017$), III ($p = 0.0000$), ($p = 0.0004$) as shown in figure 4.84. The positive value of the shift indicates that the oscillations in the left index finger are leading those in the dBP.

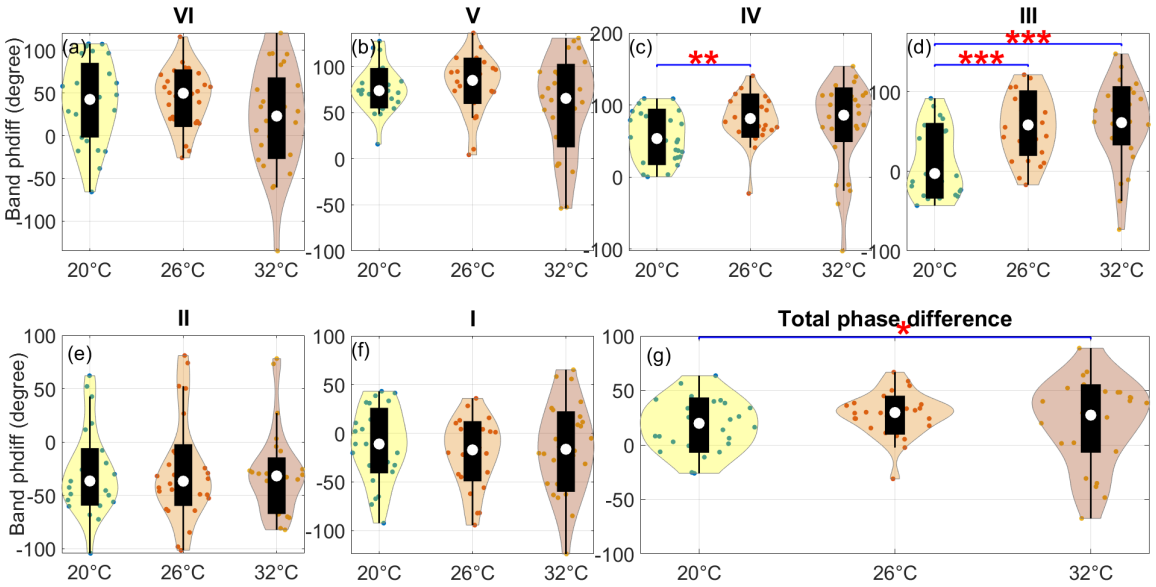

Figure 4.84: Spectral phase difference between blood flow oscillations recorded on the at left index finger and dBP within frequency bands. Violin plots compare the median phase difference content within each frequency band including the total coherence in the left index finger-dBP signal. The Wilcoxon signed rank test was applied for comparisons in each frequency band for the three ambient temperatures and statistical significance was set at $p < 0.05$. Significance is considered as $^{*}p < 0.05$,$^{**}p$ <0.01, $^{***}p$ <0.001.

4.6.5 Coherence between the cardiac output and the LDF blood flow in the right or the left index finger

Group median values of Wavelet phase coherence between oscillations in both index fingers and cardiac output were calculated and the group median coherences are shown in figure 4.85 (a), (b). High phase coherence was revealed for both signal pairs at the frequency of myogenic (~ 0.1 Hz) and respiration (~ 0.3 Hz) frequencies. The multi-comparison test showed that coherence between blood flow oscillations on both index fingers and cardiac output exhibited significant differences in the frequency intervals related to endothelial metabolic activity and neurogenic (right index: V ($p = 0.0023$),

IV ($p = 0.0015$) while left index: V ($p = 0.044$) and IV ($p = 0.0018$)).

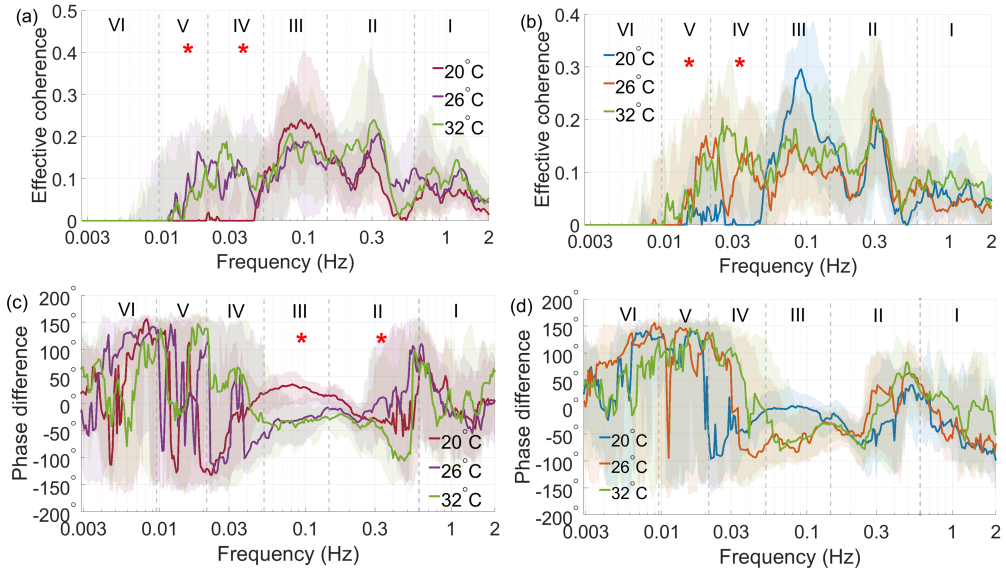

Figure 4.85: Group median values of the effective phase coherence between LDF blood flow oscillations on the two index fingers and cardiac output. Phase coherence between the cardiac output and the blood flow signal recorded using LDF in (a) the right and (b) the left index fingers, in the frequency interval between 0.003 Hz and 2 Hz. For each of the two cases, the group medians of the phase difference are shown underneath the coherence plots in (c) and (d). Statistically significant differences ($p < 0.05$) were revealed by the Kruskal Wallis test and are indicated by red asterisks in the defined frequency intervals.

The pairwise test revelled more significant differences in right index finger at the same frequency intervals in addition to respiration and cardiac for 20°C-26°C and 26°C-32°C (right index V ($p = 0.0009$), ($p = 0.016$), IV ($p = 0.001$), IV ($p = 0.008$), II ($p = 0.009$), ($p = 0.008$), and I ($p = 0.024$), ($p = 0.014$)) and the total coherence ($p = 0.0108$), ($p = 0.0115$) as shown in figure 4.86.

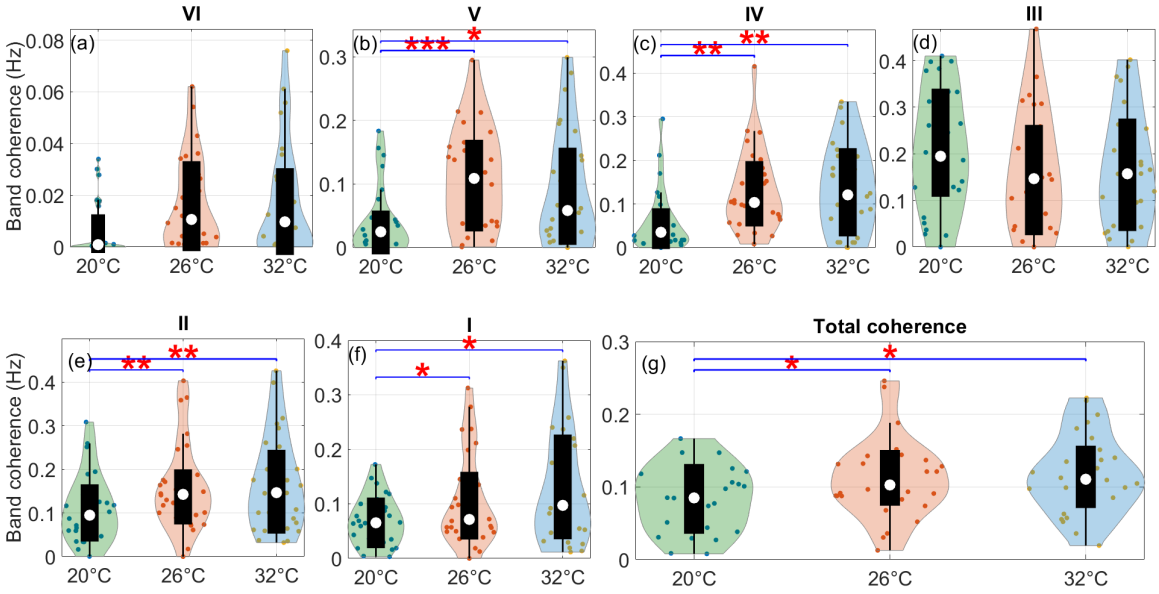

Figure 4.86: Spectral coherence between the right index finger blood flow and cardiac output within frequency bands. Violin plots compare the median coherence content within each frequency band including the total coherence in the cardiac output-right index finger signal. The Wilcoxon signed rank test was applied for comparisons in each frequency band for the three ambient temperatures and statistical significance was set at $p < 0.05$. Significance is considered as $^{*}p < 0.05$,$^{**}p < 0.01$, $^{***}p < 0.001$.

Significant differences in the phase shift were found in the cardiac output-blood flow of right index finger coherence across all frequency intervals (figure 4.85). The positive values of the shifts indicate that the oscillations in the cardiac output are leading the ones in the right index blood flow. The multi-comparison test between phase shifts at the three ambient temperatures revealed significance at the frequency intervals of respiration and myogenic III ($p = 0.0002$) and II ($p = 0.027$) frequency intervals. High significant differences were revealed in the same frequency intervals by the pairwise test (III ($p = 0.0003$), ($p = 0.0000$) and II ($p = 0.0067$) and ($p = 0.0007$) as shown in figure 4.87.

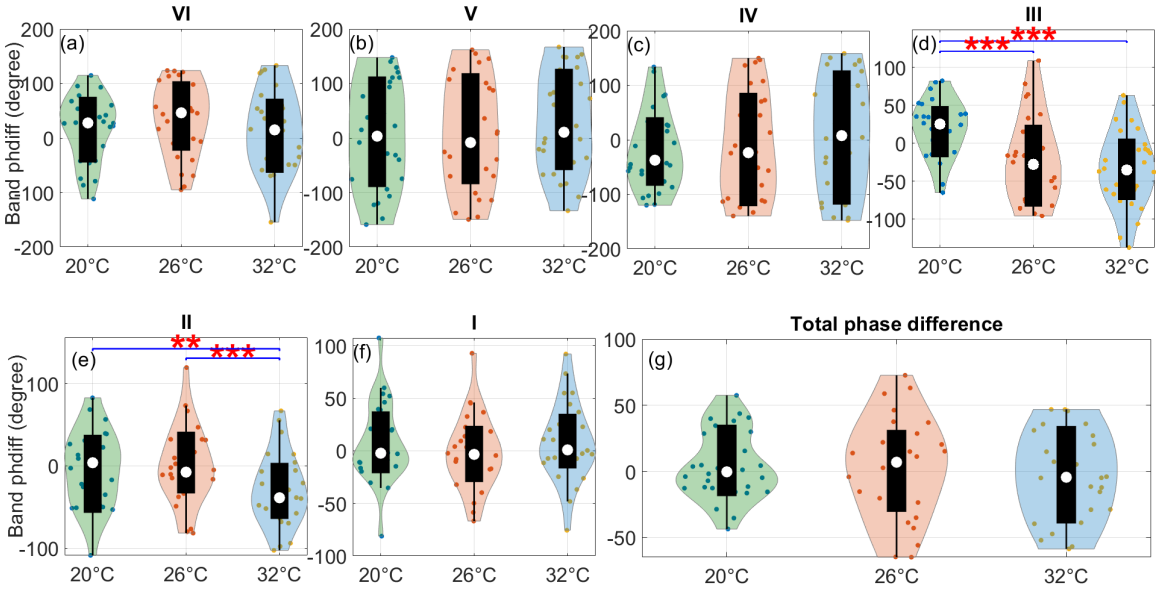

Figure 4.87: Spectral phase difference between blood flow oscillations on the right index finger and cardiac output within frequency bands. Violin plots compare the median phase difference content within each frequency band including the total coherence in the cardiac output-right index finger signal. The Wilcoxon signed rank test was applied for comparisons in each frequency band for the three ambient temperatures and statistical significance was set at $p < 0.05$. Significance is considered as $^{*}p < 0.05$,$^{**}p$ <0.01, $^{***}p$ <0.001.

The pairwise test exhibited significant differences in left index finger-cardiac output coherence for the frequency interval V ($p = 0.0225$), IV ($p = 0.007$), ($p = 0.001$), III ($p = 0.013$), and I ($p = 0.027$) as shown in figure 4.88.

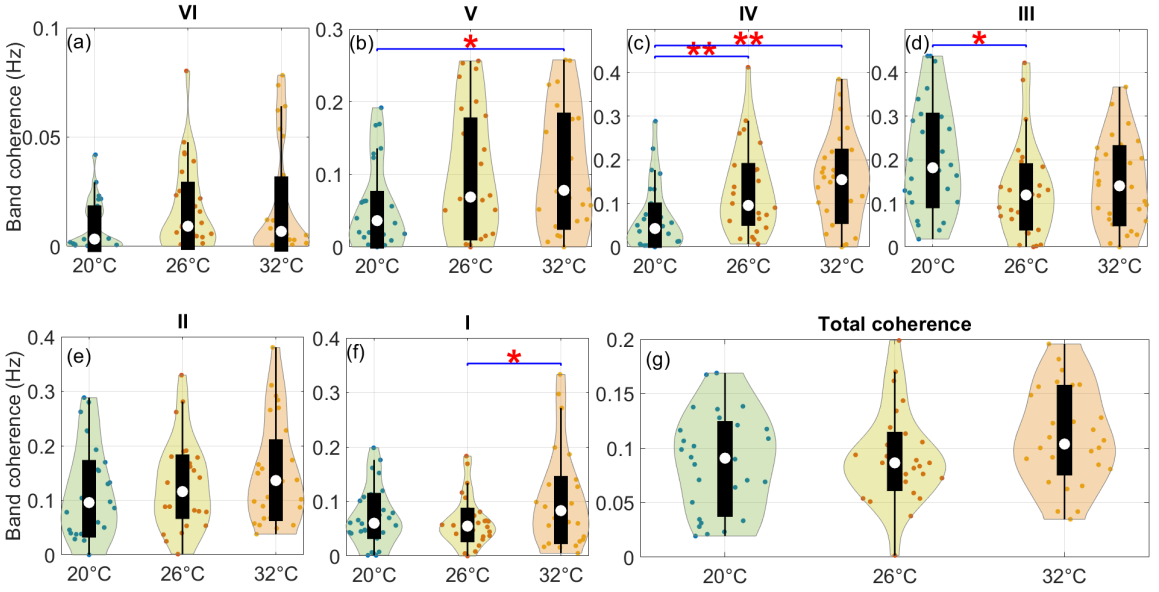

Figure 4.88: Spectral coherence between blood flow oscillations on the left index finger and cardiac output within frequency bands. Violin plots compare the median coherence content within each frequency band including the total coherence in the cardiac output-left index finger signal. The Wilcoxon signed rank test was applied for comparisons in each frequency band for the three ambient temperatures and statistical significance was set at $p < 0.05$. Significance is considered as $^{*}p < 0.05$,$^{**}p < 0.01$, $^{***}p < 0.001$.

No significant difference in the phase shift was found in the cardiac output-blood flow of left index finger coherence across all frequency intervals (figure 4.85 (d). The fact that the shift at the frequency intervals has positive values suggests that the oscillations in the cardiac output are occurring (leading) before those in the left index blood flow.

5. Discussion and summary

5.1 Introduction

In the present study, we evaluated the effects of whole body heating and cooling on the cardiovascular system relevant to thermoregulatory responses by means of a spectral analysis of the variables; HRV, systolic BP, diastolic BP, stroke volume, cardiac output, and finally blood flow (in two different vascular structures). The study focused on differences in the contributions of endothelial, sympathetic, myogenic, and cardiac activities in response to heating. Time-averaged power of the time-frequency representations analysed how the distribution of the power among the frequency bands studied changes.

The transformation of energy, or fuel, into the forms that living systems require is a necessary process. However, the elements that are required locally to generate this energy are continually transferred by the circulatory system through the blood circulation. On the other hand, this is carried out in an oscillating manner. Oscillating the flow of energy across the body is considerably more effective than a constant one. Blood flow is able to exchange nutrients and oxygen with tissues and remove waste products because the circulatory system works in an oscillating fashion, with blood flow being stepped-up to much larger arteries and then stepped-down to small microscopic blood vessels. From a physical perspective, life is quite similar to a thermodynamically open system, in which energy and matter are constantly flowing

from and into the environment. It follows that the underlying physiological oscillatory processes of living systems have their own inherent frequencies and amplitudes, which are continuously altered and modified by external disturbances (influences). In experiments, such characteristics can be examined visually by noninvasively tracking changes in skin microcirculation using LDF. The ability of LDF to detect oscillations in microvascular blood flow and analyse cardiovascular dynamics offers a valuable tool for evaluating human health. Because of this, LDF was used as the method of investigation for the research discussed here. In addition, oscillators of this kind are non-autonomous from a mathematical perspective, and as a result, they have to be dealt with in the same manner as other non-autonomous systems.

The methods for time-frequency analysis of biomedical signals have been systematically reviewed in this thesis. The continuous wavelet transform has been a mainstay for the analysis of such oscillatory signals because it employs a wavelet that can be shifted and stretched along the time series to ensure it tracks the time-varying characteristics of the oscillatory processes in, for example, blood flow [170], instantaneous heart rate frequency [171, 140]. The multiresolution wavelet transform was reportedly able to differentiate between healthy subjects and those with cardiac pathology [172]. The continuous wavelet transform, in conjunction with the Morlet mother wavelet, was able to extract characteristic frequencies in blood flow [40], and it was able to determine the physiological origin of these frequencies [173]. In addition to its use as a filter for de-noising individual events [174], the wavelet transform has been applied to the diagnosis of endothelial dysfunction in diabetes [175], post-acute myocardial infarction [176], congestive heart failure [77], and ageing [4]. The ability to resolve frequencies on a logarithmic scale is of great importance since it allows for the enclosing of a very wide frequency range, which is typically required for the study of physiological time series. The synchrosqueezed wavelet transform [177] has also been implemented, allowing for the detection of phase [160].

Time series that are generated from systems with time-varying frequencies and amplitudes present a number of separate, frequently conflicting obstacles that must be overcome: i) locating the essential oscillatory components, regardless of the time-variabilities of those components; ii) separating oscillatory components that are likely to have close characteristic frequencies, which can be very challenging in the presence of noise and time-variation; iii) in addition to the nearby frequencies, there may be a mixture of harmonics and fundamental components to be identified and distinguished from each other. When there are multiple oscillatory components, in particular in diverse physiological processes (of varied frequency), the question naturally arises as to whether or not the oscillations of those distinct components are related to one another. The question that needs to be answered is how to investigate the interactions that take place between the underlying physiological processes. This can be done by calculating measures of phase relationships (phase coherence), which are a form of synchronisation, between the oscillatory processes that take place at similar angular frequencies in different physiological parameters. This was the issue that needed to be addressed. These methods were discussed in detail in Chapter 3. Given the foregoing, it is clear that time-frequency approaches are required for any serious investigation of biomedical time series.

The goal of this study was to use cardiovascular variables to assess how a healthy young subject's cardiovascular system responded to exposure to three different ambient temperatures. During whole-body heating, we performed simultaneous recordings of blood flow (at two different skin structures), blood pressure, electrocardiogram, and respiration in young, healthy volunteers who were lying supine. We examined the results by calculating power and wavelet phase coherence. We analysed the regulation of the cardiovascular system at three different ambient temperatures (20°C, 26°C, and 32°C) using the variables that were described. These variables oscillate in a coordinated manner throughout a wide range of frequencies (0.0095-2Hz).

5.2 Median values of cardiovascular variables in time domain

When analysing a signal, an oscillatory component can be identified by its instantaneous frequency as well as its corresponding amplitude or power. In our analysis, we calculated the mean/median of each signal individually, and as a summary, we calculated the total median/mean of time series, power, and coherence. In the context of physiological analysis, what happens to the average value of a group of physiological measurements or parameters over time or in various conditions is referred to as the "dynamic of the total mean" in physiological analysis. Typically, numerous physiological parameters, such as heart rate, blood pressure, temperature, oxygen saturation are examined. A physiological parameter's total mean represents its average value across all observations in the data collection.

The total median values of all subjects in each of the the physiological parameters measured at the three ambient temperatures are shown in table 5.1. The overall result show that most of cardiovascular variables are relatively high at low temperature (20°C) with exception of IHR and IRR. IHR was only high at high temperature (32°C) while IRR was slightly higher at middle temperature (26°C) than at other ambient temperatures.

	20°C	26°C	32°C
IHR (Hz)	0.942	0.931	1.01
IRR (Hz)	0.284	0.289	0.286
SV (mL/min)	99.1	92.57	89.66
CO (L/min)	5.96	5.66	5.75
BP (mmHg)	68.93	63.97	60.59
sBP (mmHg)	132.9	118.5	109.6
dBP (mmHg)	54.27	49.58	46.74

Figure 5.1: Total median values of cardiovascular variables in the time domain. The median value of each individual signal was calculated across all ambient temperatures, and then the overall median value was obtained in each ambient temperature.

5.2.1 Heart rate variability (HRV) and instantaneous heart rate (IHR)

We found that heart rate increased significantly from low to high ambient temperature. It was approximately 57.6 beats/mins in low ambient temperature and 57 beats/mins at the middle temperature. At high ambient tempreture, heart rate increased by a median of 3 beats/min (60.6 beats/mins). Significant differences were found in heart rate between the low and high, and middle and high ambient temperatures (Figure 4.2 a)). Our result agree with those of Hideki et al.[178] who studied the effects of skin surface cooling and heating on the variability of heart rate (HRV), blood pressure (BPV), and baroreflex sensitivity (BRS) in 11 healthy individuals who were supine. In a styrene foam chamber, the studies were carried out at air temperatures of 18°C (mild), 24°C (moderate), 48°C (hot), and 60°C (very hot). The authors found

that heating induces an increase in the activity of the cardiac sympathetic nervous system, which might result in an increased heart rate. This is the result of the body's "fight or flight" reaction being triggered by the activation of the sympathetic nervous system. Jian et al. [179] investigated the effects of whole body heating and cooling on skin sympathetic nerve activity (SSNA), as well as the differences in SSNA that occur under heat stress as compared to normothermia or cooling. 17 healthy adults (10 men and 7 females) between the ages of 22 and 39 participated in the study. Both whole-body heating and cooling were applied to the subjects in a temperature-controlled (25°C) environment. The subjects' lower bodies were immersed in water at 42°C for 30 minutes during the heating protocol, and water at 18°C for 20 minutes during the cooling phase. The finding suggest that the response in to heating is mediated by the sympathetic nervous system.

Similarly, our results shows that instantaneous heart rate (extracted by ridge extraction method) is higher at high and middle temperatures than at low temperature. This variation demonstrated significant changes just like the case of heart rate (Figure 4.2 b). The influence that heat exposure has on HRV has only been detected in a limited number of studies. Twenty healthy people were tested by Sollerst et al. [180] at two different air temperatures: at 22°C, and 35°C, respectively. Both conditions were tested for 30 minutes. The individuals' heart rates were greater in the hot room condition compared to the baseline condition (the heart rate increased significantly by an average of roughly 4.5 beats/min in the hot room condition). According to the results, the parasympathetic system's withdrawal likely contributed to the elevated heart rate reported in the heated conditions.

5.2.2 Stroke volume

Our result demonstrate that, the mean of the stroke volume is high at low ambient temperature and decreased significantly from low to high temperatures (Figure 4.6

a). The median stroke volume decreased significantly from 98.26 mL/min under cool cooling conditions to 90 mL/min in a high ambient temperature. Median stroke volume at thermoneutral temperature (26°C) was slightly higher and significant than high ambient temperature (92.6 mL/min). Mean of stroke volume values showed to be high at cooling temperature (20°C) and low at high ambient temperature, as shown in figure 4.6 a).

Our result agree with those of Erik et al. [181] who used a rat model to evaluate the effects of reducing the temperature from 37°C to 15°C, experiencing hypothermia for 3 to 4 hours at 15°C, and then rewarming to 37°C. Stroke volume was observed to increase during cooling, decrease during stable hypothermia, and to fail to return to normal following rewarming. According to the findings of the study, an increase in stroke volume can be attributed to elevated preload during cooling, which was made possible by bradycardia through extended filling and the Frank-Starling relationship [182].

The decrease in stroke volume at high temperature is also observed by Joel et al. [183] who compared the effects of hyperthermia and heart rate on stroke volume during prolonged exercise in both hyperthermic and normothermic conditions. To induce hyperthermia, volunteers wore a vinyl rain jacket and nylon/spandex leg covers while being heated from both the front and rear by parabolic electric heaters. Under normothermic condition, a comfortable 23°C and 35% relative humidity were attained without the need of any cooling fans. According to the study, people who become hyperthermic during exercise show significant increases in heart rate and decreases in stroke volume. The increased heart rate due to hyperthermia may be responsible for the reduced ventricular filling time, which in turn reduces stroke volume. According to the study, heat decreased stroke volume during exercise, and this effect increased at higher heart rates.

5.2.3 Cardiac output

The mean of cardiac output values was high at low temperature (20°C) and low with high ambient temperature as shown in figure 4.11 a). Our finding shows that median cardiac output decreased significantly from 6.01L/min at cooling condition to 5.7L/min in high ambient temperature. Median cardiac output at the middle temperature (26°C) is similar to the value obtained in high ambient temperature (5.6L/min).

The reduction in cardiac output during hypothermia was observed by Joel et al. [183] who compared the effects of hyperthermia and heart rate on stroke volume during prolonged exercise in both hyperthermic and normothermic conditions. A decrease in stroke volume was noted in patients with stable hypothermia; this decrease in volume could be made greater by hypovolemia.

5.3 Respiration analysis

5.3.1 Respiration rate variability and instantaneous respiration rate

Our result demonstrate that respiration rate decreased slightly and insignificantly low from (0.275Hz) to high ambient temperature (Figure 4.16 a). Both middle and high temperature maintained the same median respiratory rates (0.266Hz). Similarly, the mean of respiration rate variability (standard deviations of respiratory rates) increased slightly and not significantly from low to high ambient temperatures. Interestingly, but insignificantly, the median of respiration rate variability at the middle temperature (26°C) is lower than at low and high ambient temperatures (Figure 4.16 b).

5.4 Blood pressure analysis

5.4.1 Systolic blood pressure

The distributions of median systolic blood pressure showed a decrease in median pressure as temperature increases. We find that, systolic blood pressure was roughly 132.9 mmHg at low ambient temperature, 118.45 mmHg in the middle, and 109.6 mmHg at high ambient temperature (Figure 4.23a). Kingma et al. [184] studied the effects of mild-cold (20.7±0.2°C) exposure on blood pressure and thermoregulation in young adults and older people. When exposed to mild cold, only young individuals demonstrated considerable non-shivering thermogenesis (NST). Vasoconstriction may be a contributor to the blood pressure response to mild cold exposure by raising peripheral resistance, which then leads to an increase in blood pressure. The decrease in systolic blood pressure between low and middle ambient temperature in our study was also observed by Parsons et al. [185] who examined the relationships between environmental temperature (17°C or 27°C) and posture on HRV during forced sinus arrhythmia (deep breathing), as well as the influences of environmental temperature and HRV and BP during standing and the cold pressor test. The study was performed on non-diabetic young adults (age 23±5 years) and elderly diabetic patients (age 54±15 years). The authors conclude that it is likely that cutaneous vasodilation, which results in a decrease in total peripheral resistance, is the reason for the reduction in systolic blood pressure that occurs in a warm room.

5.4.2 Diastolic blood pressure

Our result shows that, median diastolic blood pressure was 54.22 mmHg at low ambient temperature, 49.68 mmHg in the middle, and 47.05 mmHg at high ambient temperature (Figure 4.26 a)). Our result agree with those of Jody et al. [186] who examined the changes in sympathetic function that occur during whole-body cooling

in normotensive and hypertensive adults. The researchers in this study did not use a fixed temperature for the purpose of full body cooling. Instead, they used a water-perfused suit that covered the subject's complete body with the exception of the head, hands, feet, and lower left leg in order to control the mean temperature of the almost the whole of the subject's skin. The study found that systolic and diastolic blood pressure increased from baseline in both normotensive and hypertensive adults after whole-body cooling, but the pressor response to cooling became more pronounced in hypertension adults. Both normotensive and hypertension adults showed an increase in their muscle sympathetic nerve activity in response to cooling; however, the rise in those with hypertension was significantly greater. The study also found that the function of the sympathetic baroreflex was altered in hypertensive adults while they were being cooled down.

Fagius et al. [187] examined how a low ambient temperature affects the baroreflex, which controls sympathetic outflow to muscle arteries in humans. Thy found that muscular nerve sympathetic activity, despite the fact that it is not thought to play a role in the regulation of body temperature, is subject to the influence of ambient temperature and leads to an increase in blood pressure when the skin is exposed to low temperatures. It may therefore be concluded low is due to an increase in the activity of the sympathetic nerves in the muscles.

5.5 Oscillations and their power

The power spectra of signals with the same mean value can seem very different if they have different frequency contents or different distributions of power across frequencies. The power spectrum illustrates the power spectrum of each frequency component of a signal. The power spectra of two signals with the same mean value can be somewhat different if the signals have different frequency contents, amplitude changes, or noise

characteristics. Here are three signals that differ in their amplitude variations but we assume they have the same mean value (figure 5.2):

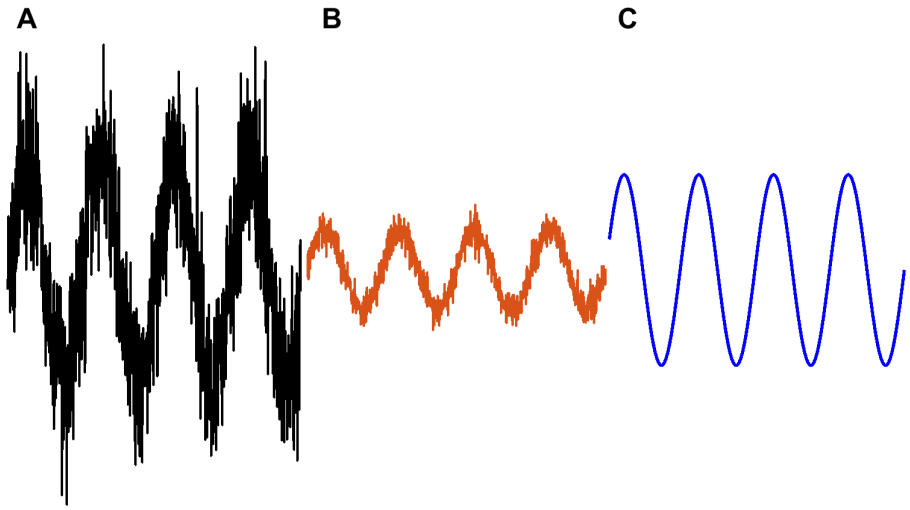

Figure 5.2: Signals with different amplitude but with the same mean value.

In signal B: the variations in this signal's amplitude around its mean value is small. As the values of the signal tend to remain near to the mean, the range of values that can be observed is narrower. Because of this, the amplitude variations have become smaller, which has led to a reduction in power. In signal A: this signal demonstrates greater amplitude variation around its mean value as compared to signal B. As the values of the signal deviate more considerably from the mean, the range of values that can be found in the signal is broadened. The amplitude of the fluctuations is higher, which results in an increase in the power. Both signals have the same mean value, but more power is associated with signal A due to its larger oscillations. Because power is calculated using squared amplitude values, larger variations will have a greater power.

In conclusion, two signals with the same mean values but different amplitudes

will have different powers. Even if two signals have the same mean values, the one with large amplitude variations will have more power. In context of physiological signals, the complex and dynamic human body's reactivity to varied stimuli explains physiological signal amplitude changes. Individual variances, regulatory systems, dynamic fluctuations, noise, measuring methodologies, and structural complexity of physiological interactions might cause observed variations.

	20°C	26°C	32°C
IHR $(Hz)^2$	0.00021	0.00016	0.00017
IRR $(Hz)^2$	6.54e-05	5.34e-05	6.37e-05
SV $(mL/min)^2$	0.616	0.575	0.767
CO $(L/min)^2$	0.0086	0.0071	0.0076
BP $(mmHg)^2$	0.891	0.718	0.801
sBP $(mmHg)^2$	0.83	1.34	2.23
dBP $(mmHg)^2$	0.426	0.435	0.506

Figure 5.3: Total median power values for power signals of the physiological oscillations. Following the calculation of the median power for each signal at each ambient temperature, the total median power was determined by taking the median power of all the median values into consideration.

5.5.1 Heart rate variability

Earlier analyses of the influence that heat exposure has on HRV are limited in number. Sollerst et al. [180] used two different air temperature conditions: one with a baseline temperature of 22°C, and another with a heated temperature of 35°C. Both conditions were tested for 30 minutes. The individuals' heart rates were greater in the hot room

condition compared to the baseline condition (the heart rate increased significantly by an average of roughly 4.5 beats/min in the hot room condition), and the FFT analysis showed that the high-frequency component fell while the low-frequency component increased. Based on these data, one can deduce that the withdrawal of parasympathetic activity was the primary cause of the increase in heart rate that was observed in the hot situation. Another study carried out by Carandall, et al. [188] elevated the skin temperature of fourteen healthy subjects by perfusing a tube-lined suit with warm water (46°C). The outcome of the study showed that high-frequency (0.2−0.3 Hz) fluctuations in heart rate were greatly reduced by whole-body heating, which was indicative of decreased vagal modulation of heart rate. Increased cardiac sympathetic regulation of heart rate was observed as well, with a greater ratio of spectral power between the low-frequency (0.03−0.15 Hz) and high-frequency ranges after heat stress. Finally, spectral power of heart rate in both low- and high-frequency areas was dramatically lowered due to whole-body heating.

Our time–frequency analyses, which have a frequency resolution that is logarithmic, have provided us with new insights into the range of heart rate variability spectra: fluctuations in the HRV power spectra in the frequency interval associated with myogenic activity (0.052 – 0.145 Hz), which corresponds to the LF interval, increased significantly in the whole body heating and decreased significantly in the frequency interval associated with respiration (0.145 – 0.6 Hz), which corresponds to HF interval (Figure 4.4). Vascular smooth muscle cells, found in blood vessels, can independently constrict and dilate (known as vasomotion) the arteries to regulate blood flow locally. The myogenic component of the HRV signal may also be indicative of the strength of cardiac smooth muscle contraction. In the study conducted by Raffaello et al. [189], it was proven that after a single bout of exercise, there was an enhanced amplitude of the periodic oscillations with a frequency of 0.1 Hz of the heart rate signal in humans.

5.5.2 Stroke volume

The spectral power of the stroke volume signal has a strong respiration component at all three ambient temperatures. Nevertheless, no significant difference is observed in this particular band. Our finding shows that stroke volume recorded at high ambient temperature has significantly more power within the low frequency intervals compared to other ambient temperatures (Figure 4.8). To the best of our knowledge, the wavelet power of stroke volume has not reported before.

5.5.3 Cardiac output

Wavelet analyses of cardiac output measured from all subjects show closely similar results. Our finding indicates that the cardiac output signal is made up of a variety of spectral components. The NO-dependent endothelium, myogenic and respiration activities are clearly observed for each ambient temperature. Evaluating significant thermal differences throughout the full $0.0027-2$ Hz frequency range revealed at the frequencies associated with the neurogenic, myogenic, and respiration intervals (Figure 4.13), suggesting that cardiac output is governed by a complex of mechanisms: NO-dependent mediated changes in vascular tone play a function in controlling systemic vascular resistance and cardiac output, resulting in vasodilation. Myogenic reactions: autoregulatory changes of blood vessel tone influences systemic vascular resistance, which in turn affects cardiac output. Changes in intrathoracic pressure caused by breathing have an effect on venous return, preload, and cardiac output. Neurogenic activity, especially sympathetic activity, affects cardiac output. For example, vasoconstriction and a change in heart rate and vascular resistance can have an effect on cardiac output when sympathetic activity is elevated.

To the best of my knowledge, the wavelet power of cardiac output has not been reported before.

5.5.4 Respiration, respiration rate and respiration rate variability

The following findings emerged from an examination of the amplitude-frequency spectra of oscillations produced by the respiratory system in response to local heating. After testing for statistical significance, it was found that the median values of the amplitudes of oscillations of respiration did not differ from one another in any of the frequency intervals (Figure 4.18). Whole-body heating led to a slight but insignificant increase in the peak frequency of respiration. It is worth mentioning that analysis of the amplitude-frequency spectra of oscillations of respiration at the three ambient temperatures showed that low frequency ranges were not anticipated to be significantly affected by breathing because they are below actual breathing frequencies. Breathing rate changes are unlikely to influence other parameters, such as thermoregulatory [190, 191, 4] or endothelial [73] mechanisms, that are known to contribute to very low frequency hemodynamic oscillations. In contrast, respiratory power for all ambient temperatures were shown to be high and matched at low frequency bands (Figure 4.19).

Studies on humans have shown that the waveform of respiration-triggered sympathetic [192, 193] and vagal [194] outflows is roughly sinusoidal and symmetrical (increases of outflows equal decreases) at typical breathing frequency. More information is provided in [195]. The significant difference between 20°C and 26°C was observed by a pair-wise test at the frequency interval associated with the respiration band. This significant difference could to the fact that respiration influences resting heart rate (HR). During inspiration, heart rate rises, and during exhalation, it falls. This phenomenon is known as respiratory sinus arrhythmia (RSA) [196]. The parasympathetic nervous system is responsible for rapid changes in HR and facilitates the efferent control of RSA via the vagus nerve [197].

5.5.5 Microvascular blood flow

The following findings were found by an examination of the time averaged power spectra of oscillations in the blood flow of the right and left index fingers when the whole body was responding to heating. When carrying out the statistical significance tests, highly significant differences were detected between the median power in all frequency intervals for both right and left index fingers (Figure 4.32 and 4.34). Whole-body heating increased power significantly in the frequency bands corresponding to endothelial nitric oxide-independent and neurogenic processes.

When compared to blood flow recorded from the right index finger, left index finger blood flow had much greater power across the whole frequency range (Figure 4.34). Comparison of the time-averaged power spectra reveals that the distribution of power is quite similar in both instances. Note that a Kruskal–Wallis test was used to obtain the significant difference across all frequency bands represented by the asterisk. In contrast, the blood spectra of the index fingers and the left forearm are strikingly dissimilar. Spectra of the index finger show most of the power is at the neurogenic frequency, while on the other hand, the local heating of the skin on the left forearm generated an increase in the amplitudes of oscillations of the blood flow in the skin within the range of myogenic activity frequencies of $0.052-0.145$ Hz (Figure 4.36). The increase in power in neurogenic band in both fingers is due to the sympathetic nervous system respond with increased activity in the muscles, which likely results in increased blood flow to the the skin [198].

The microvasculature of the skin varies greatly according to geographical region. Narrow, low-flow capillaries supply most of the skin's nutrients. High shunt blood flow is only possible in the extremities, particularly the face and the tips of the fingers and toes, due to the greater density of arteriovenous anastomoses in these areas. This suggests that LDF recordings might exhibit spatial variations due to differences in skin structure between study areas and the little area of skin in contact with the

optical fibre [199]. It is important to note that the vascular architecture of the fingers and those of the forearm skin are distinct. The finger is a common site for AVAs (arteriovenous anastoinoses) while AVAs do not exist in the skin of the forearm. We believe that AVAs are responsible for this heat-induced vasoconstriction of the finger, which may explain the differential in response in the skin blood flow to local heating between these two skin locations [200]. When comparing ambient temperatures of 20°C and 32°C, the difference in the temperatures of fingers is significant. When the temperature in the environment falls below the lower range of the thermoneutral zone, all AVAs are shut down. They are most likely accessible above the upper limit of the thermoneutral zone, where the temperature is relatively stable. Hence, the frequency and amplitude of the flow peaks increase from the lower end to the middle of the thermoneutral zone, but they begin to diminish again as the ambient temperature rises further towards the upper end of the thermoneutral zone, which is the temperature at which all AVAs are open. This pattern repeats itself from the lower end to the middle of the thermoneutral zone [3].

5.5.6 Blood flow in the forearm

Unlike index fingers (glabrous skin), time averaged power spectra indicates that the distribution of power is greatest at myogenic frequency across all three ambient temperatures. Vascular smooth muscle cells, found in blood vessels, can independently constrict and dilate the arteries to regulate blood flow locally. The range of frequencies between 0.052 and 0.145 Hz is associated with this myogenic activity. Therefore, the increase in power or amplitude in this band could be due to an increased volume of blood entering the arterioles as a result of smooth muscle relaxation (vasodilatation) in response to whole-body heating of the body. This would also increase the activity of pre-capillary sphincters, which control the amount of blood entering the capillary bed [201]. Our findings 4.36 are in agreement with what was discovered by other

researchers. For instance, a number of researchers have demonstrated that local heating leads to an increase in the spectral power of oscillations in skin blood flow throughout the whole frequency range [202, 203, 38, 204].

5.5.7 Blood pressure

Clear cardiac oscillation at 1Hz are present across all signals 4.21, and very low oscillations can be seen at respiration frequency (0.3Hz). The cardiac cycle has a significant impact on blood pressure, which explains why the cardiac band contains most of the power in blood pressure signals. The waveform of blood pressure is influenced by pulsatile pressure pulses generated by the heart's cyclic contraction and relaxation during the cardiac cycle. These pulsating pressure waves They create the cardiac band and have a dominant frequency that is proportional to the heart rate. Therefore, the cardiac band predominates the power spectrum of blood pressure data, which reflects the impact of the cardiac cycle on blood pressure variation. Similar wavelet amplitude spectral of blood pressure with a broad peak are observed in [205, 206] at the cardiac frequency.

5.5.7.1 Systolic blood pressure

The earliest frequency-domain analysis of the influence that heat exposure has on systolic blood pressure was that by Carandall et al. [188]. Their study concluded that the spectral power of systolic blood pressure was dramatically decreased in both the low- and high-frequency bands by whole-body heating. The changes in the cutaneous vasculature may effectively buffer the size of the variations in systolic blood pressure, allowing for a reduction in low-frequency fluctuations in systolic blood pressure under heat stress despite increased sympathetic activity.

Our time-frequency analysis showed a similar decrease in the low and high

frequency bands (associated with myogenic and respiration frequency bands, respectively) in the power spectra of systolic pressure. Assessing their statistical significance showed that whole body heating increases the power of systolic blood pressure significantly in all frequency intervals except those associated with respiration and heart beat (Figure 4.24). Our result agrees with that of with Stankovski Tomislav et al. [195] who obtained significant differences in the neurogenic and myogenic bands.

5.5.7.2 Diastolic blood pressure

In comparison to systolic blood pressure, diastolic blood pressure has receive much less attention from researchers and limited study discussed diastolic blood pressure under the effect of heating. We find that the power diastolic blood pressure spectra increased with increasing ambient temperature. A significant difference was observed only in the myogenic band (Figure 4.27). Other researchers [195] obtained significant difference in both neurogenic and myogenic bands.

The possible explanation for the significant observed in myogenic band is the ability of blood vessels to adapt to pressure changes which is reflected in myogenic activity, therefore an increase in power could be indicative of more active myogenic responses. As the body tries to maintain thermal homeostasis, the increased blood flow caused by vasodilation may result in greater diastolic blood pressure variability during heating. To the best of my knowledge, examination of heating on diastolic blood pressure has not reported before.

5.6 Phase coherence and phase difference analysis

The human body is an interconnected network, consisting of multicomponent organ systems that constantly communicate with one another through a variety of feedback mechanisms and at a variety of spatial and temporal scales. This

interaction is intended to optimise and coordinate the function of these organ systems [207, 208, 209, 210]. The cardiovascular system can be thought of as a network of connected oscillators that involve the cardiac, respiratory, and vascular systems [211]. Phase coherence was hypothesised to be a useful tool for identifying the presence of functional relationships between various physiological processes and revealing how they affect peripheral blood flow regulation [211, 212, 213, 214, 215, 216, 217, 218]. We conducted a comprehensive study of IHR, respiration, IRR, skin blood flow (with different sites) and tissue blood volume oscillations in healthy volunteers at rest to analyze phase interactions between these physiological processes.

5.6.1 Median phase coherence of peripheral variables

Table 5.4 displays the total effective phase coherence between index finger and forearm skin blood flows. The total phase coherence is obtained as an integral of the effective phase coherence (showed in chapter 4) by taking the logarithmic scale into account. It is clear that total phase coherence values are high at high ambient temperature. The evaluation of each pair will now be discussed.

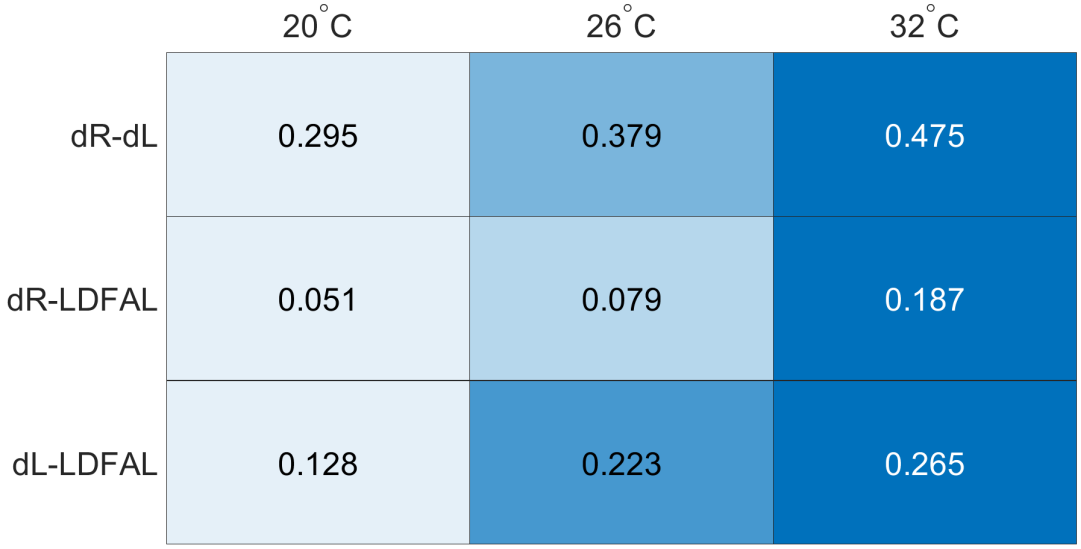

Figure 5.4: Total median effective phase coherence values for peripheral variables. First row represents total median phase coherence values between right and left index fingers at each ambient temperature. Second row represents total median phase coherence values between right index finger and left forearm at each ambient temperature. Third row represents total median phase coherence values between left index finger and left forearm at each ambient temperature.

We obtained high significant phase coherence for right−left index fingers across all frequency intervals for most subjects at the three ambient temperatures (Figure 4.57). These findings make sense considering that low-frequency oscillations in skin blood flow are initiated by a number of physiological processes, including the activity of smooth muscle cells in the artery walls, neurogenic regulation, and vasomotor activity of the endothelium [38]. The arteriovenular anastomoses in the acral regions are highly innervated by the sympathetic nervous system; hence sympathetic activity is necessary for normal peripheral blood flow [219]. Numerous arterio-venous anastomoses connect the palmar finger skin to the underlying blood vessels, and their tone is controlled only by sympathetic innervation baroreceptors have no effect on this system [220, 221]. Myogenic response, the response of the muscle layer of the vascular

wall to a change in pressure, is another potential mechanism for synchronisation of blood flow oscillations. As a result of the reaction from the vascular muscle layer, or the so-called Bayliss effect [222], lowering arterial blood pressure causes a temporary dilatation of the arteries, while raising it causes a constriction. Given that myogenic activity is characterised as a response to a pressure wave, it is possible that the pressure wave is effective in propagating to the periphery. In addition to perhaps being involved in the synchronisation of cardiovascular oscillations, the myogenic response may also be involved in the process of respiratory sinus arrhythmia (RSA). RSA refers to the variability of one's heart rate in synchronisation with one's respiration. This variability is connected with an increase in one's heart rate during inspiration and a reduction in one's heart rate during expiration [223, 224, 225]. Similar phase coherence between left and right fingers was obtained by Arina et al. [225] who looked at how deep, regulated breathing affects the degree of correlation between the phases of respiratory-related cutaneous blood flow oscillations of the left and right fingers in healthy young females. The study showed that as breathing depth was increased, phase coherence increased across all the frequencies examined.

It is obvious that oscillations within the frequency intervals associated with myogenic, respiratory and cardiac activities are common for skin blood flow oscillations of index fingers and left forearm. We found that phase interactions between signals from the right index finger and forearm showed a similar pattern with phase interactions between skin blood flow signals of left index finger and left forearm (Figures 4.60 (a), (b)). Our finding showed that phase coherence increases significantly with heating at respiration and cardiac frequency intervals for blood flow in both cases. Although the peripheral blood flow is regulated by local mechanisms generating oscillations at the frequency associated with the myogenic band, the significant phase coherence obtained in both the respiration and cardiac intervals reveals the role played by the central mechanism that synchronizes myogenic oscillations of myogenci throughout

the cardiovascular system [226, 35, 227, 228]. The result obtained is in agreement with those of Irina et al.[218] who investigated the phase interaction between resting heart rate, respiration, and micro-hemodynamic oscillations of the upper and lower limbs in healthy subjects. The study was carried out at room temperature of 20–24°C after a 20-minute adaptation period. They found that oscillations in tissue blood volume (TBV) and skin blood flow (SBF) shared frequency intervals associated with respiratory and cardiac activity. They also discovered that phase interactions between TBV signals at the finger and toe were analogous to those between SBF signals at the forearm and the foot. Skin blood perfusion and tissue blood volume regulation may both be causes. It is believed that the intrinsic myogenic activity of smooth muscle cells in resistance arteries is the local origin of these oscillations.

The results obtained were compared with those we had previously obtained as well as with the findings of other authors. Highly significant phase coherence was found between SBF on the left and right forearms in the cardiac and myogenic instances in young healthy persons while they were at rest [212] with a constant room temperature of 23 ± 1°C. Other researchers found a significant level of coherence between the oscillations of cardiac SBF and SBF in the ankles [217] with a controlled ambient temperature of 20°C–21°C and constant low illumination.

Differences in coherence between the forearm and index finger may have to do with the anatomy of the vascular bed in the fingers and toes, as well as the skin on the forearm and foot. Arteriovenous anastomoses abound in finger and toe tissue. In contrast, the dorsal forearm/foot surface skin has fewer anastomoses and is primarily defined by nutrient-rich blood flow [229].

5.6.2 Median phase coherence of systemic variables

Table 5.5 displays the systemic coherence values. The total phase coherence is obtained as an integral of the effective phase coherence (showed in chapter 4) by taking the logarithmic scale into account. Total median of effective phase coherence values for systemic variables were found to be high at middle and high ambient temperatures but not the at low temperature. Evaluation of each pair will be discussed.

	20°C	26°C	32°C
IHR-BP	0.117	0.141	0.153
IHR-sBP	0.176	0.185	0.181
IHR-dBP	0.162	0.172	0.183
Resp-IHR	0.142	0.184	0.158
Resp-BP	0.285	0.277	0.3
sBP-dBP	0.672	0.673	0.811
Resp-CO	0.127	0.131	0.125

Figure 5.5: Total median of effective phase coherence values for systemic variables at the three ambient temperatures. Phase coherence for each pair was computed in chapter 4, and each row in this table represents the total median value of that phase coherence at each ambient temperature.

5.6.2.1 Phase coherence between IHR and respiration

Although the curves of IHR-respiration match perfectly between middle and high temperatures, coherence at low temperature is showed to be lower at both the fundamental and harmonic peaks (figure 4.38 a)). These observations revealed significant differences in the frequencies associated with respiration and heart rate.

Modulation of heart rate by respiratory frequency is affected by variations in ambient temperature, and coherence gives further insight into these changes. Given that the high frequency component in IHR reflects the influence of breathing on the heart rate [230, 231, 115], the significant reduction in cardiac interval coherence between IHR (derived from the ECG) and breathing for all ambient temperatures implies an impairment in RSA. It is well known that, the interaction of the sympathetic and parasympathetic branches of the autonomic nervous system is what causes respiratory sinus arrhythmia (RSA). Within the context of this interaction, the vagus nerve, which is an essential component of the parasympathetic nervous system, plays a crucial function. Its activity slows down during inspiration, which enables an increase in the rate at which the heart beats. On the other hand, vagal activity will rise during expiration, which will result in a slower heart rate. However, our findings show a breakdown of the sympathetic and parasympathetic regulation that controls heart rate variability.

5.6.2.2 Phase coherence between respiration and blood pressure

Heating significantly increased the phase coherence between blood pressure and respiration at the myogenic and respiratory frequencies (Figure 4.40). To my knowledge, phase coherence between respiration and blood pressure has not previously been reported.

It is mentioned that although there have been relatively few research on the affect that respiration has on blood pressure, it has been generally accepted that increasing the depth and rate of respiration increases the 'aspiratory' action of the thorax and, as a result, the flow of blood to the right heart. This is something that is discussed in the article. Because of the rapid regulation of the R-R interval by the systolic pressure (baroreflex) and the Windkessel approximation of the systemic arterial system, the respiratory variations in diastolic blood pressure are typically small when compared

to variations in systolic blood pressure. The amplitude of blood pressure respiratory oscillations is dependent on the respiratory pattern [196].

The study by Vera et al. [232] investigateddiscussed the effect of respiration on the blood pressure by analysing the effects of slow breathing on fluctuations in the heart rate and blood pressure of healthy subjects. The authors found that respiration has the ability to counteract changes in both the time and frequency domains of hemodynamic activity. The peaks at nonrespiratory frequencies ($0.01-0.05$Hz) during synchronised respiration were identical to those observed during rest; however, the diastolic blood pressure was significantly lower during synchronised respiration. This lends credence to the idea that respiration can play a role in the oscillations of blood pressure, particularly during the diastolic phase. However, the long-term effects of respiration on blood pressure were not investigated in this study; hence, additional research is required to achieve a comprehensive understanding of the link between respiration and blood pressure.

5.6.2.3 Phase coherence between cardiac output and respiration

We obtained highly significant phase coherence between cardiac output and respiration oscillations at the frequency associated with neurogenic and myogenic processes, for most subjects (Figure 4.34). To the best of my knowledge, coherence between respiration and cardiac output has not been reported before. A possible explanation for the significance in myogenic frequency is that vasodilation occurs in the skin and other peripheral tissues as a result of heat. By relaxing blood vessels, the body's internal temperature is lowered and more blood is pumped to the surface, where the heat it carries can be dispersed through perspiration. Vascular dilation causes a greater outflow of blood, which may reduce blood's return to the heart (venous return). With less blood coming back from the veins, preload drops and that has an effect on stroke volume and consequently cardiac output.

5.6.2.4 Phase coherence between IHR (derived from ECG) and IRR (derived from respiration)

Although not significant, median phase coherence for IRR-IHR appears to be high in the respiration band for all ambient temperatures (Figure 4.46). Significant changes in phase coherence were obtained in myogenic band between high and other ambient temperatures (Figure 4.47).

5.6.2.5 Phase coherence between systolic and diastolic blood pressure

Our finding shows that heating increased phase coherence significantly between systolic and diastolic blood pressure at the frequency intervals associated with neurogenic, myogenic, respiration, and cardiac (Figure 4.48). Coherence between systolic and diastolic blood pressure in the microcirculation has not previously reported.

5.6.2.6 Phase coherence between the IHR of ECG and blood pressure

We observed significant phase coherence between IHR and blood pressure oscillations in the myogenic frequency band but no significant changes s the result of altering the ambient temperatures (Figure 4.51).

5.6.2.7 Phase coherence between IHR (derived from ECG) and systolic or diastolic blood pressure

The pattern of spectral phase coherence between blood pressure and IHR was shown to be the same when systolic and diastolic signals were analysed figure 4.54 a) and b). In both comparisons, there was no significant difference as a result of increasing ambient temperature. To the best of my knowledge, coherence between systolic and diastolic blood pressure has not been reported before.

5.6.3 Median phase coherence of systematic−peripheral variables

Table 5.6 displays the total coherence between index finger and forearm skin blood flow. The total phase coherence is obtained as an integral of the effective phase coherence (showed in chapter 4) by taking the logarithmic scale into account. It is clear that total median coherence showed to be high at high ambient temperature for all pairs except IHR−dL. Evaluation of each pair will be discussed.

	20°C	26°C	32°C
IHR-dR	0.054	0.074	0.095
IHR-dL	0.062	0.086	0.082
BP-dR	0.126	0.182	0.208
BP-dL	0.192	0.226	0.266
CO-dR	0.145	0.172	0.202
CO-dL	0.151	0.146	0.173
sBP-dR	0.25	0.323	0.415
sBP-dL	0.244	0.282	0.314
dBP-dR	0.183	0.234	0.338
dBP-dL	0.189	0.203	0.269

Figure 5.6: Total median of effective phase coherence values for systemic−peripheral variables at three ambient temperatures. Each row represents a pair of phase coherence computed in chapter 4 between two variables and each row in this table represents the total median value of that phase coherence at each ambient temperature

5.6.3.1 Phase coherence between IHR (derived from ECG) and the LDF blood flow in the right or left index finger

We obtained highly significant median values for the wavelet phase coherence of LDF blood flow (left and right index fingers) with IHR oscillations in most participants

at the frequency of 0.3 Hz associated with the respiratory band (Figure 4.65 a) and b)). During heating, the phase coherence was found to increase significantly in the respiratory band.

Our results agree with those of Sheppard et al.[191] who examined the oscillatory dynamics of vasoconstriction and vasodilation in connection to blood flow, skin temperature, and instantaneous heart rate (IHR). In the latter investigation, the temperature of the plate was gradually increased in two stages: first to 24°C, then to 42°C. The temperature at which the basal recordings were made was around 32 degrees Celsius. It was found that there is a considerable rise in phase coherence between blood flow and IHR in all intervals, and that distinct peaks in phase coherence occur at the respiratory and myogenic frequencies.It was concluded that the mechanisms of vasodilation and vasoconstriction, which occur in response to changes in temperature, play an important part in the process of altering the relationship between blood flow and IHR.

5.6.3.2 Phase coherence between blood pressure and the LDF blood flow in the right or left index finger

We observed a significant increase in phase coherence between skin blood flow oscillations in the right index finger and blood pressure with increasing ambient temperature at the respiratory frequency (Figure 4.70). To the best of my knowledge, coherence between skin blood flow and blood pressure has not reported before. A possible explanation for our observation is that during RSA, the autonomic nervous system and the cardiovascular system work together to regulate the relationship between cutaneous blood flow and blood pressure oscillations at the respiratory frequency. Under the effect of heating, vasodilation causes changes in cutaneous blood flow, which can affect the resistance in peripheral blood arteries and cause blood pressure fluctuations. In other word, heating elevates the cyclic fluctuations

in skin blood flow due to RSA, contributing to blood pressure oscillations at the respiratory frequency.

5.6.3.3 Phase coherence between systolic blood pressure and the LDF blood flow in the right or left index finger

Wavelet phase coherence increased significantly with increasing ambient temperature at respiratory and cardiac frequencies between blood flow of right index finger and systolic blood pressure (Figure 4.75a)). However, a significant increase in phase coherence was observed only in the cardiac frequency band between blood flow left index finger and systolic blood pressure (Figure 4.75b)). To the best of our knowledge, coherence between skin blood flow and systolic blood pressure has not previously been reported.

We infer that the significant increase in cardiac frequency occurs on account of increased cutaneous blood flow when the blood vessels of the skin widen as a result of autonomic influences (such as the withdrawal of sympathetic activity). This vasodilation can occur at the same time as the systolic maxima in the cardiac cycle, which can result in increased synchronisation between the oscillations of skin blood flow and sBP at the frequency of the cardiac cycle.

5.6.3.4 Phase coherence between diastolic blood pressure and the LDF blood flow in the right or left index finger

Heating increased the wavelet phase coherence significantly at the respiratory frequency between blood flow of the right index finger and diastolic blood pressure (Figure 4.80 a)). However, a significant increase in phase coherence was observed only in the cardiac frequency band between blood flow in the left index finger and diastolic blood pressure (Figure 4.80 b)). To the best of my knowledge, coherence between diastolic blood pressure and blood flow in the index fingers has not been reported

before.

5.6.3.5 Phase coherence between the cardiac output and the LDF blood flow in the right or left index finger) with cardiac output

Significant phase coherence was obtained between cardiac output and blood flow of left and right index fingers in the endothelial metabolic and neurogenic bands (Figure 4.85 a) and b)). To best of my knowledge, phase coherence between cardiac output and skin blood flow in the index fingers has not previously been reported.

A possible explanation for the differences observed in these two specific bands is that multiple regulatory mechanisms interact in a dynamic process to keep skin blood flow oscillations synchronised with cardiac output oscillations at endothelial and neurogenic frequencies. Under the effect of any external influence such as temperature, skin blood vessels are able to dilate or constrict to control blood flow. Both local and systemic factors control the rate at which the diameters of these vessels change. In terms of local effect, the endothelium is crucial for controlling blood flow and vascular tone, involving the release of vasodilators like nitric oxide (NO). Such a substance affects the vessel diameter and consequently skin blood flow.

6. Concluding remarks

6.1 Summary

To summarise, the following constitute the primary components of this thesis:

- The physiological and thermoregulation background of cardiovascular dynamics and its associated oscillations in the healthy state is reviewed.
- The methods by which the physiological variables under consideration can be evaluated are discussed.
- An introduction to non-linear dynamical systems and the tools for investigating them using time series data is provided.
- At each of the three ambient temperatures for which data were available, the applicability of laser Doppler flowmetry for analysing the dynamics of microvascular blood flow in healthy subjects was investigated. The electrocardiogram (ECG), blood pressure, stroke volume, and heart rate were all measured.

The primary purpose of this thesis has been to examine the dynamics of the cardiovascular system as it relates to rising environmental temperatures. Blood flow, cardiac output, electrocardiogram, blood pressure, and respiratory rate had all been measured and the aim was to analyse the data and understand them.

Time series analysis techniques were applied to the corresponding signals in order

to better understand their origins and characteristics as time series from oscillatory, thermodynamically open, nonstationary, nonlinear, and nonautonomous systems. These findings provided a new knowledge of the vasculature under the influence of heating, which was characterised by changes in cardiovascular oscillations as measured in cold, mild, and high ambient temperature conditions. The myogenic, neurogenic, and endothelial frequency intervals all exhibit different oscillations, and these oscillations provide a means of correlating the observed variances in spectrum and coherence with the oscillations associated with vasomotion.

We used the wavelet transform and wavelet phase coherence techniques to analyse cardiovascular signals acquired from young volunteers who were being exposed to the three different ambient temperatures.

6.2 Original contributions

The following original contributions of this work can be summarised as:

- Time-averaged power was calculating for most of the cardiovascular variables and some of them were for the first time, such as cardiac output and stroke volume.

- The instantaneous heart rate frequencies (derived from ECG signals) for three different ambient temperature were compared in the frequency interval $0.0027-2.0$ Hz. The time-averaged power mostly differed significantly between between the three ambient temperatures in intervals II and III.

- Both systolic and diastolic blood pressure signals were derived by a linear interpolation method for the three ambient temperatures and their medians were compared. The time-averaged power was calculated for each variable and it was found that systolic blood pressure differs significantly with increasing ambient

temperature in the intervals III, IV, V, and VI while the time-averaged power for the three ambient temperatures differs significantly in frequency interval III.

- Time-averaged power was calculated for two different skin sites (index finger and forearm). Power increased significantly with increasing temperature across all frequency intervals: I, II, III, IV, V, and VI for index fingers. Time-averaged power in the forearm increased significantly at frequency intervals associated with III, IV, V, and VI.

- Differences in wavelet phase coherence was obtained between blood flow in the left and right index fingers in the frequency intervals associated with I, II, III, IV, and V, at the three ambient temperatures, and wavelet phase coherence between blood flow in the forearm and both index fingers in the cardiac and respiration frequency intervals at the three ambient temperatures.

- The findings for peripheral blood flow are sensitive to the particulars of sympathetic innervations of the skin zones. Forearm skin blood flow relies heavily on respiratory wave transmission passive mechanisms because of its comparatively poor sympathetic innervations. Apart from passive mechanisms, a neurogenic component clearly dependent on breathing rate will play a significant role in the blood flow of finger skin.

- Differences in wavelet phase coherence was found between instantaneous heart frequency and blood flow in the right index finger at the three temperatures. Similarly, differences in wavelet phase coherence between instantaneous heart frequency and blood flow in the left index finger at the three ambient temperatures.

- Differences in wavelet phase coherence was found between respiration and blood pressure at temperatures 32°C and other ambient temperatures, and wavelet

phase coherence between respiration and cardiac output across all ambient temperatures at neurogenic band.

- Differences in wavelet phase coherence was found between systolic and diastolic blood pressure at temperatures 32°C and low temperatures (20°C).

- Differences in wavelet phase coherence was found between instantaneous heart frequency and blood pressure at temperatures 32°C and 20°C, and middle (26°C) with low (20°C). No differences in wavelet phase coherence between instantaneous heart frequency and systolic blood pressure. Similarly, no differences in wavelet phase coherence between instantaneous heart frequency and diastolic blood pressure.

- Differences in wavelet phase coherence was found between instantaneous heart frequency and blood flow in the left index finger at all temperatures, and wavelet phase coherence between instantaneous heart frequency and blood flow in the left index finger at all temperatures.

- Differences in wavelet phase coherence was found between blood pressure and blood flow in the right index finger at all ambient temperatures, and wavelet phase coherence between blood pressure and blood flow in the left index finger at temperature 32°C and other ambient temperatures. In addition, middle temperature and low temperature.

- Differences in wavelet phase coherence was obtained between systolic blood pressure and blood flow in the right index finger at all ambient temperatures. Similarly, differences wavelet phase coherence was obtained between systolic blood pressure and blood flow in the left index finger at all ambient temperatures.

- Differences in wavelet phase coherence was found between diastolic blood pressure and blood flow in the right index finger at all ambient temperatures. Similarly, differences wavelet phase coherence was found between diastolic blood pressure and blood flow in the left index finger at all ambient temperatures.

- Differences in wavelet phase coherence between cardiac output and blood flow in the right index finger at all temperatures, and wavelet phase coherence between cardiac output and blood flow in the left index finger at all temperatures.

6.3 Future work

The following projects would follow on naturally from the research reported in this thesis, and would offer promising opportunities for the future:

- Investigating the cardiovascular response on males and females separately. The current study was performed on both male and female, but the number of subjects was too small for analyses of data from the two sub-groups to be useful. It will obviously be important to understand the ways in which males and females circulatory systems react differently to being exposed to heat by using the same analysis methods as in this study.

- Investigating how age influences responses to whole-body heating using the same analysis methods as used in the present study, which was restricted to young people.

- Investigating how non-healthy (e.g. diabetic) people respond to whole-body heating using the same analysis methods used here. The current study was performed on healthy people.

Appendices

Appendices

The following sections provide additional result that are not included in the main text. In section A.1, the coherence between IRR and the LDF blood flow in the right and the left index finger is shown. In section B2, we present the coherence between IHR extracted from blood pressure and IHR of ECG. In section C, additional coherence analysis between IRR and blood pressure is presented. In section D, we show the coherence between IRR and systolic or diastolic blood pressure. In section E, a single calculation of maximum coherence and its corresponding frequency peak for the coherence of IHR and respiration. Tables of physiological parameters are listed in F.6 G.7, H.8 and J.10 summarize the average values. while the summary of all values across all parameters is provided in section I.9. Finally, section K.11 provides data arrangements and approvals for the study protocol.

A.1 Coherence between IRR and the LDF blood flow in the right and left index finger

Group median values of wavelet phase coherence was calculated between blood flow (right and left index fingers) and IRR signals for all subjects at three ambient temperatures are shown in figure 6.1 (a) and (b). Median phase coherence reveals a single, broad peaks at the respiratory frequency range. The coherence disappears in

the respiratory frequency interval in the group of 20°C for the right index finger, while coherence in the left index finger is low for all ambient temperatures. No significant difference were observed in all coherence and phase shift figures by multi-comparison and pair-wise tests.

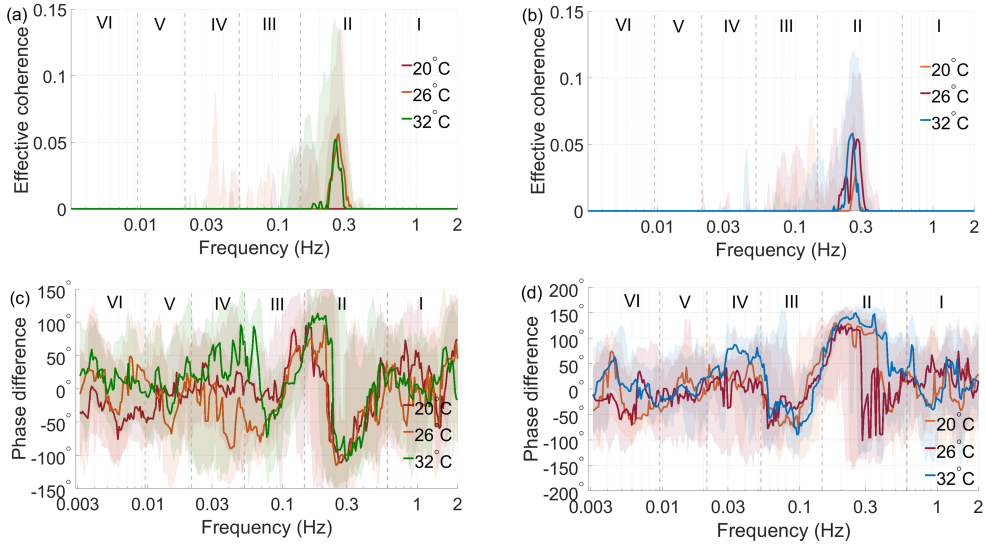

Figure 6.1: Group medians of the effective phase coherence between instantaneous respiration rate and LDF at the two index fingers. Phase coherence between the instantaneous respiration rate and the blood flow signal recorded using LDF in (a) the right and (b) the left index fingers, in the frequency interval between 0.003 Hz and 2 Hz. For each of the two cases, the group medians of the phase difference are shown underneath the coherence plots in (c) and (d). Statistical significant difference ($p < 0.05$) was reveled by Kruskal Wallis test and indicated by red asterisks at the defined frequency intervals in figure (c).

B.2 Blood pressure coherence analysis

B.2.1 Coherence between IHR of BP and IHR of ECG

Group median values of Wavelet phase coherence between IHR of ECG signals with IHR of blood pressure was calculated and the group median coherence is shown in

figure 6.2 (a). High phase coherence was revealed at the frequency of myogenic (~ 0.1 Hz) for all subjects at the three ambient temperatures. No significant difference was revelled by multi-comparison test for IHR-IHR coherence.

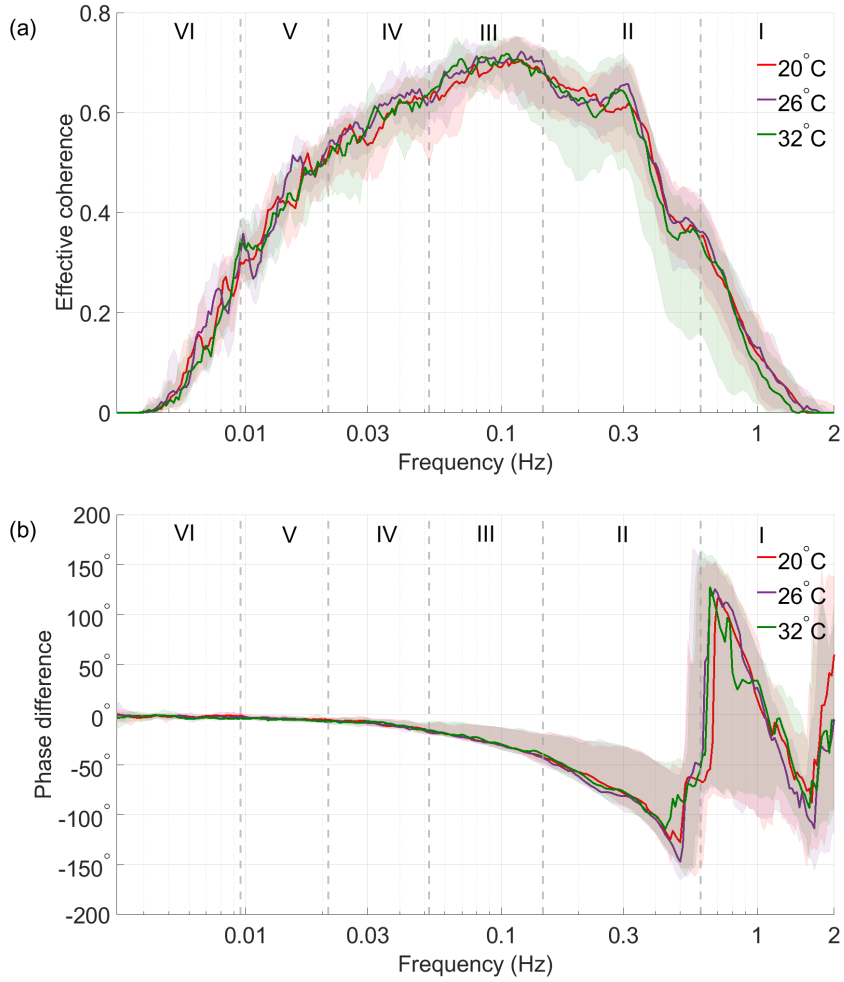

Figure 6.2: Median a) Effect wavelet phase coherence between IHR (ECG) and IHR (BP) for three ambient temperature. b) Phase shift for the coherence shown in figure a). No significant difference was reveled ($p > 0.05$) by Kruskal-Wallis at the defined frequency intervals.

While pairwise test showed significant difference in the frequency intervals neurogenic ($p = 0.0083$) as shown in figure 6.3.

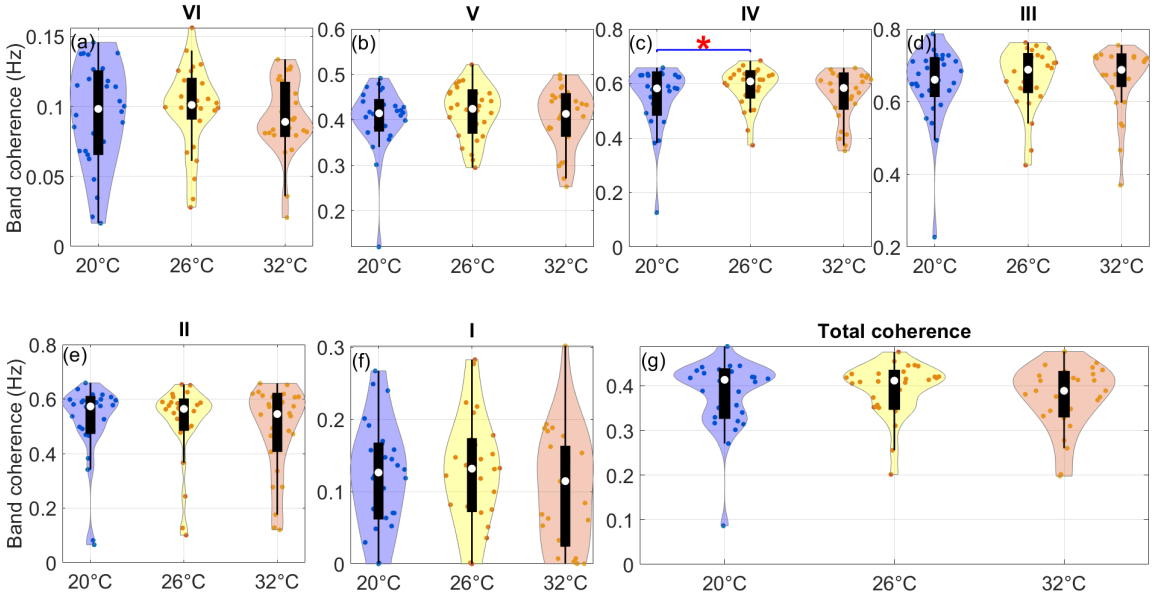

Figure 6.3: Spectral coherence of IHR signals extracted from BP and ECG within frequency bands. Violin plots compare the median coherence content within each frequency band including the total coherence in IHR-IHR signal. Wilcoxon signed rank test was applied for comparisons in each frequency band for the three ambient temperatures and statistical significance was set at $p < 0.05$. Significance is considered as $^{*}p < 0.05$,$^{**}p$ <0.01, $^{***}p$ <0.001 .

No significant difference in the phase shift was found in the IHR-IHR coherence across all frequency intervals (Figure 6.2 (b)) either by multiple-comparison and pairwise tests. The phase shift is showed to be coherent at all frequency intervals. The positive value of the shift at cardiac interval indicates that the oscillations in the IHR of ECG signals are leading the ones in the IHR of blood pressure.

C.3 Coherence between IRR and blood pressure (Amplitude - Frequency interaction)

Group median values of wavelet phase coherence between the IRR extracted from respiration signals and blood pressure signals was computed for all subjects at three ambient temperature and shown in figure 6.4 (a).

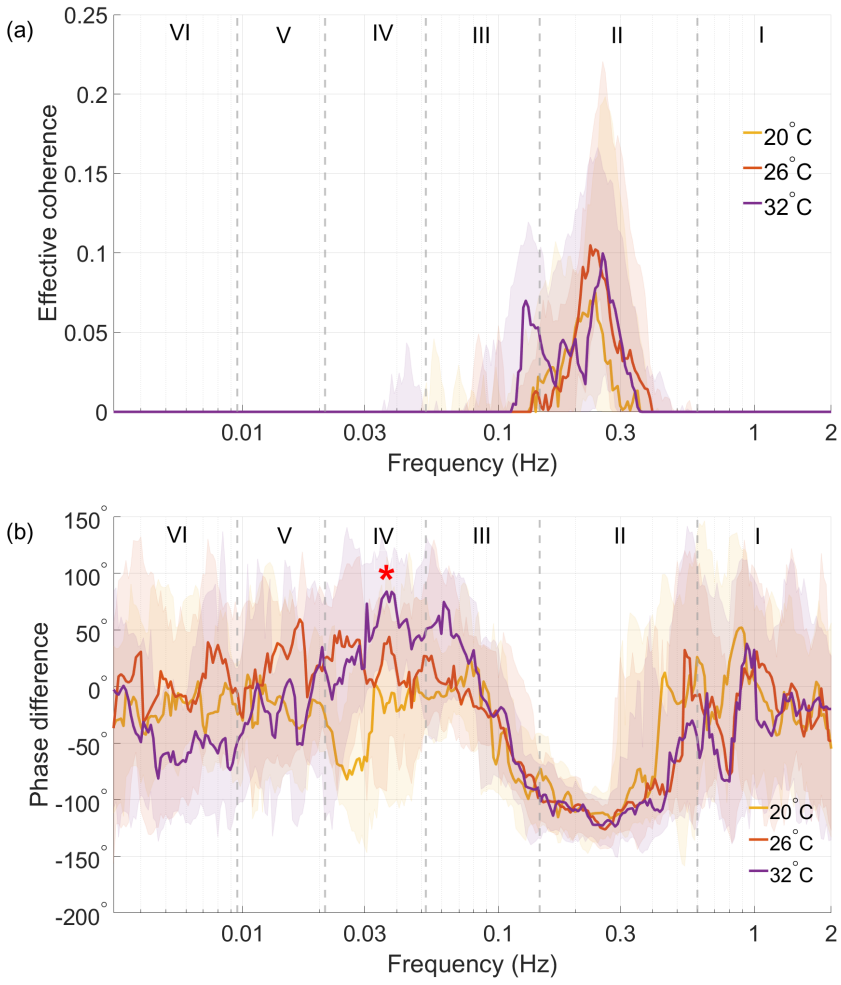

Figure 6.4: Median a) Effect wavelet phase coherence between Respiration and IHR for three ambient temperature. b) Phase shift for the coherence shown in figure a). Significant difference was reveled ($p > 0.05$) by Kruskal-Wallis at the defined frequency intervals in phase shift only (indicated by asterisk).

All group temperatures had a single, broad peak in median phase coherence at respiration band. No significant difference were observed in IRR-blood pressure coherence between all ambient temperatures by multi-comparison and pairwise. A significant difference in the phase shift was found in the IRR-blood pressure coherence in the frequency interval of myogenic ($p = 0.0032$) as shown in figure 6.4 (b). Pairwise test showed significant difference in the frequency interval neurogenic between ($p = 0.0366$) and ($p = 0.0009$) as shown in figure 6.5. The positive value of the shift indicates that the oscillations in the blood pressure are leading the ones in the IRR.

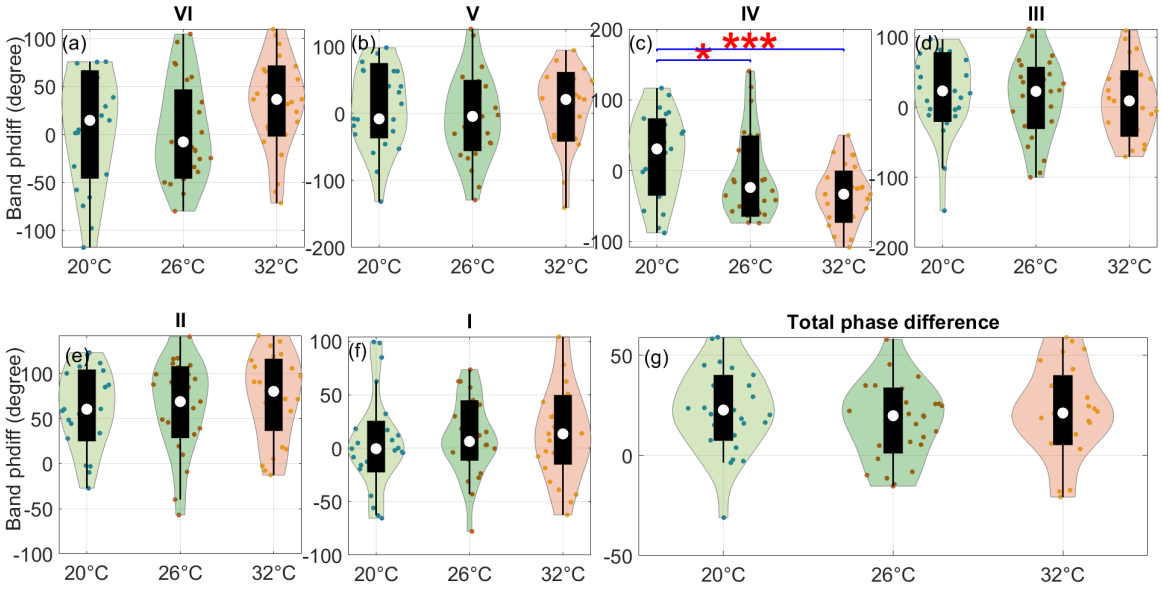

Figure 6.5: Spectral phase difference of IRR and blood pressure within frequency bands. Violin plots compare the median phase difference content within each frequency band including the total coherence in the IRR-BP signal. Wilcoxon signed rank test was applied for comparisons in each frequency band for the three ambient temperatures and statistical significance was set at $p < 0.05$. Significance is considered as $^{*}p < 0.05$,$^{**}p$ <0.01, $^{***}p$ <0.001 .

D.4 Coherence between IRR and systolic or diastolic blood pressure

Group median values of wavelet phase coherence between oscillations in both systolic and diastolic with IRR at three ambient temperatures were calculated as shown in figure 6.6 (a),(b). High phase coherence was revealed for both signal pairs at the frequency of respiration ($\sim$ 0.3 Hz). No significant differences exhibited in the coherence of systolic and diastolic BP with IRR as shown in multi-comparison test. However, significant difference in the phase shift were found in both systolic (p = 0.0032) and diastolic (p = 0.0128) pressure with IRR coherence in the frequency interval of neurogenic as shown in figure 6.6 (c),(d).

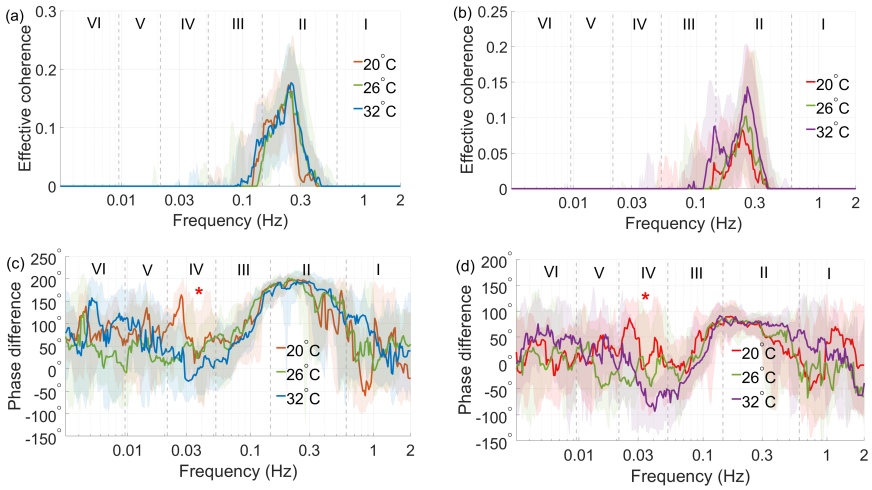

Figure 6.6: Group medians of the effective phase coherence between instantaneous heart rate with systolic and diastolic blood pressure. Phase coherence between the instantaneous heart rate and (a) systolic blood pressure and (b) diastolic blood pressure, in the frequency interval between 0.003 Hz and 2 Hz. For each of the two cases, the group medians of the phase difference are shown underneath the coherence plots in (c) and (d). Statistical significant difference ($p < 0.05$) was reveled by Kruskal Wallis test and indicated by red asterisks at the defined frequency intervals in figure (c).

Pairwise test revelled more significant differences in the phase shift sBP-IRR coherence at the frequency intervals IV ($p = 0.0009$) as shown in figure 6.7. The positive value of the shift indicates that the oscillations in the IRR are leading the ones in the sBP.

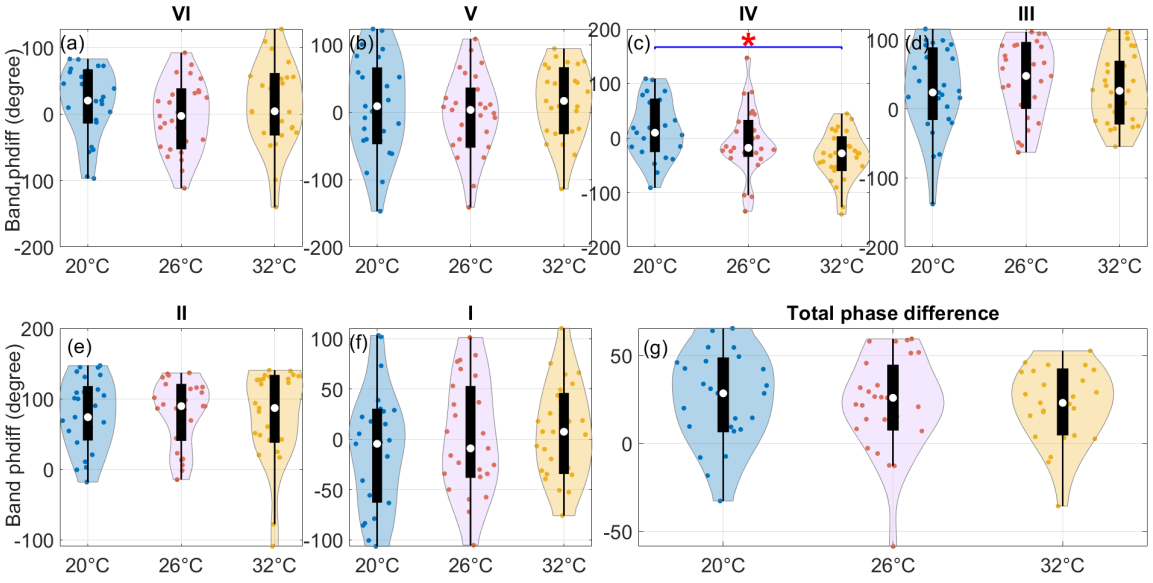

Figure 6.7: Spectral coherence of the left index finger and cardiac output within frequency bands. Violins compare the median coherence content within each frequency band including the total coherence in the cardiac output-left index finger signal. Wilcoxon signed rank test was applied for comparisons in each frequency band for the three ambient temperatures and statistical significance was set at $p < 0.05$. Significance is considered as $^{*}p < 0.05$,$^{**}p < 0.01$, $^{***}p < 0.001$.

Similarly, pairwise test revelled more significant differences in the phase shift dBP-IRR coherence at the frequency intervals IV ($p = 0.0116$) as shown in figure 6.8. The positive value of the shift indicates that the oscillations in the IRR are leading the ones in the dBP.

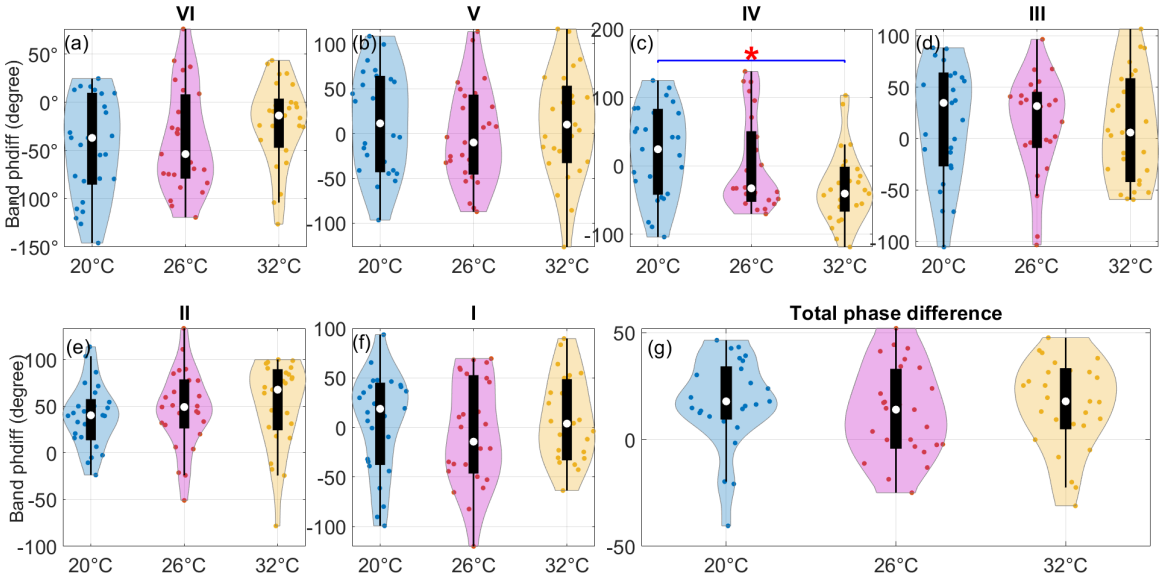

Figure 6.8: Spectral coherence of the left index finger and cardiac output within frequency bands. Violins compare the median coherence content within each frequency band including the total coherence in the cardiac output-left index finger signal. Wilcoxon signed rank test was applied for comparisons in each frequency band for the three ambient temperatures and statistical significance was set at $p < 0.05$. Significance is considered as $^{*}p < 0.05$,$^{**}p < 0.01$, $^{***}p < 0.001$.

E.5 Maximum coherence and corresponding frequency peaks

Maximum coherence was calculated for each subject across all the ambient temperatures and demonstrated in violin plot (Figure 6.9 (a)). The median values of the maximum values varies slightly at the coherence value of 0.6, and the highest median was observed at 26°C (0.633). However, the figure shows clearly that, the lowest value was for temperature 20°C (0.58). The corresponding frequency peak was also calculated and represented in figure 6.9 (b). The median value for each temperature is nearly the same (0.3Hz), median frequency peaks at temperature 26°C

had a slight decrease compared to other (0.29Hz). While, frequency peaks at ambient temperatures 20°C and 32°C had exactly the same value (0.30Hz).

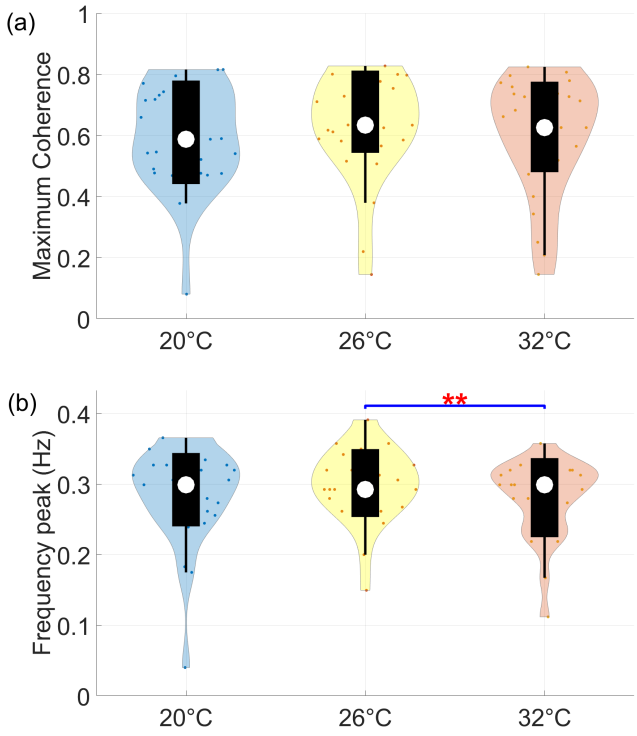

Figure 6.9: Violin plot represents the distribution of the values of the maximum coherence and corresponding peak frequency. Statistical significance difference was observed in mean of maximum coherence and responding frequency peak of IHR-Respiration coherence by Kruskal-Wallis (Group test) and Wilcoxon signed rank (pair test) for paired data. p -values for median are recorded as following: 20°C - 26°C (0.061), 20°C - 32°C (0.414), and 26°C - 32°C& (0.118). While p -values for frequency peak, 20°C - 26°C (0.518), 20°C- 32°C (0.081), and 26°C - 32°C (0.004). In terms of group test, no significant difference were observed in mean values (0.535), and frequency peaks values (0.485).

F.6 Average values of stroke volume and cardiac output

No	Stroke volume			Cardiac output		
	20°C	**26°C**	**32°C**	**20°C**	**26°C**	**32°C**
1	79.79± 6.06	82.78± 6.17	77.38± 3.76	4.88 ± 0.40	5.77± 0.61	6.30± 0.45
2	94.10 ± 4.54	95.08± 7.57	90.74± 9.07	6.10± 0.46	5.66 ± 0.63	6.01± 0.59
3	112.71± 7.34	80.72± 5.71	78.49±5.93	7.85± 0.69	5.48 ± 0.43	5.48± 0.38
4	92.98± 9.35	81.75± 5.47	79.76±5.74	6.68± 0.77	5.95± 0.48	6.19± 0.64
5	105.74± 5.99	108.36± 5.52	108.58± 5.27	6.55± 0.63	6.53± 0.44	6.75± 0.43
6	62.81± 12.15	84.13± 5.05	65.05± 5.88	4.09 ± 0.78	5.63 ± 0.41	4.73 ± 0.35
7	142.71 ± 9.55	136.91± 9.19	136.07± 9.28	6.90± 0.78	6.79 ± 0.83	7.43± 0.84
8	127.49± 10.56	116.51± 7.08	117.51± 6.69	6.00± 0.47	5.72± 0.45	6.04± 0.49
9	106.20±5.46	98.20± 5.02	102.91± 5.29	6.32± 0.63	5.76± 0.55	6.17± 0.58
10	94.56± 5.62	84.47± 5.93	80.80± 7.15	6.45± 0.56	5.13± 0.46	5.00± 0.52
11	75.90±3.52	75.13± 3.32	73.76± 3.71	5.34±0.30	5.35± 0.33	4.90± 0.34
12	82.32± 5.48	80.50±5.47	92.11± 6.89	3.97±0.33	4.07± 0.32	5.10± 0.52
13	120.42± 5.78	115.87 ± 4.45	121.11± 3.92	6.81± 0.63	6.71 ± 0.46	7.80± 0.48
14	88.19± 7.14	79.72± 6.61	73.33±5.74	4.54± 0.42	4.36± 0.49	4.34± 0.42
15	108.97± 4.21	109.14± 5.05	105.83± 5.46	6.04± 0.21	5.86± 0.35	5.72± 0.28
16	96.07± 9.08	93.32± 7.26	92.71± 6.04	4.73± 0.41	4.89± 0.36	5.10± 0.44
17	81.60± 6.48	76.56± 5.09	74.19± 6.86	4.69± 0.68	4.45± 0.51	4.03±0.41
18	86.02± 6.15	79.32± 5.05	73.71± 5.66	5.04±0.50	4.59±0.39	4.62±0.43
19	70.96± 7.52	87.14± 6.56	77.19± 6.20	3.85± 1.02	4.26 ± 0.39	4.12± 0.46
20	111.89± 7.33	108.48± 6.21	109.97±7.24	5.04± 0.43	5.30± 0.54	5.82± 0.52
21	103.33± 6.79	96.48± 7.13	88.26± 11.41	6.66± 0.48	6.36 ±0.46	5.59± 0.60
22	143.92± 7.52	141.50± 9.62	135.98±5.81	8.89± 0.47	8.34 ± 0.52	8.58± 0.46
23	118.03± 7.06	118.15± 7.44	119.15± 8.17	6.11± 0.79	6.13 ± 0.71	6.67± 1.00
24	84.78± 4.26	88.03± 4.33	82.64± 5.90	5.67±0.25	5.95±0.27	5.81± 0.39
25	89.11± 5.47	85.59± 5.53	79.47±5.32	5.95± 0.41	5.66 ± 0.35	5.67± 0.32
26	127.02± 10.57	106.33± 6.57	117.94±9.28	7.19± 0.92	6.68 ± 0.55	7.22± 0.81
27	100.45± 5.94	92.23± 5.27	90.11±8.34	6.78± 0.72	5.36± 0.52	6.20± 1.02
28	105.13± 5.78	92.94± 5.12	95.16±5.65	5.72± 0.57	5.31± 0.47	5.46± 0.62

Table 6.1: Mean and standard deviation values of stroke volume and cardiac output for each subject at the three ambient temperatures.

G.7 Average values of systolic and diastolic blood pressure

No	Diastolic BP			Systolic BP		
	20°C	**26°C**	**32°C**	**20°C**	**26°C**	**32°C**
1	64.69± 4.65	83.64± 6.26	75.35±4.70	127.72± 5.16	183.34±11.91	143.19± 7.72
2	63.30± 4.46	44.13± 6.03	47.31± 5.11	130.05± 6.21	97.25± 10.70	94.02± 10.28
3	62.08± 4.08	51.78± 4.38	47.05± 3.31	133.42± 9.81	92.97 ± 9.28	81.58± 6.90
4	59.16±6.08	58.44±4.43	56.13± 4.88	143.02± 7.75	155.50± 4.93	131.92± 10.22
5	53.72± 3.17	42.92± 3.04	56.46±4.34	123.05± 4.70	115.58 ± 3.40	120.37±7.31
6	65.20± 3.36	49.38± 2.42	37.73±2.27	138.79±14.46	117.97 ± 7.07	84.73± 9.23
7	53.59± 4.91	49.74±5.46	47.98± 4.50	140.82± 10.11	118.19 ± 11.32	111.16± 9.60
8	51.11± 7.81	58.10± 5.76	49.48±5.17	145.54 ± 11.40	144.75± 7.50	129.14± 8.47
9	63.08± 4.57	48.47± 4.11	42.06± 3.95	143.17±5.69	122.98 ±3.64	109.32± 7.06
10	52.96± 3.12	52.42± 2.94	40.36± 3.47	108.68± 4.79	108.04 ± 4.76	83.09± 5.29
11	74.75±3.28	68.92± 3.46	63.21±5.22	150.23± 4.27	131.06 ± 5.85	111.20± 9.06
12	58.90±3.41	54.63± 2.33	53.59±2.45	111.90± 4.73	108.55 ± 4.06	111.20± 5.16
13	57.68±3.30	56.06± 2.09	51.70±2.25	139.04± 4.07	128.47 ±4.03	125.21± 5.63
14	50.77± 3.51	49.08± 4.59	46.41±3.69	136.68± 4.24	110.76 ± 5.93	94.10± 5.40
15	69.74± 3.10	59.97± 2.68	62.79±3.08	157.06±6.14	132.75 ± 7.47	128.13± 6.91
16	44.55± 3.77	44.33± 2.68	41.72±3.68	116.17± 4.36	118.12 ± 3.71	113.63± 4.83
17	39.00± 5.84	37.44±3.89	39.45±3.98	112.86± 8.23	105.97 ± 7.03	107.32±8.77
18	50.37± 4.49	43.40±2.95	35.52±3.92	122.60± 5.21	107.48 ± 5.05	93.53± 8.08
19	67.27± 3.65	58.33± 3.60	43.40±3.77	130.15± 5.76	131.60±5.76	100.71± 6.28
20	51.19± 3.30	48.17± 2.77	53.44± 2.93	128.17± 4.28	121.76 ± 7.52	122.52± 8.93
21	57.36± 3.89	47.77± 3.73	44.82±3.48	137.20± 4.94	117.97 ± 4.70	105.97± 11.36
22	57.81±4.29	55.98± 4.75	53.35±3.68	142.72± 8.89	128.00± 9.07	122.17± 7.88
23	47.19± 6.13	50.59± 5.37	56.03±6.31	139.63± 9.32	127.62 ± 8.19	134.92± 11.01
24	50.42± 2.01	48.14± 2.28	44.31±2.45	122.88± 4.60	117.48 ± 3.49	102.08± 6.59
25	50.16±2.22	39.64± 2.70	38.11±1.78	112.72±3.18	98.89 ± 4.19	85.80± 4.00
26	53.19± 6.27	59.75± 3.63	55.83±5.40	140.49± 7.18	137.49 ± 3.19	127.59±6.40
27	54.46± 4.65	48.66± 3.55	47.97±5.89	131.54± 5.82	114.87 ± 5.82	103.55± 9.07
28	53.66± 3.98	46.73±3.11	46.69±3.40	132.13±5.69	117.54± 6.13	107.21± 8.05

Table 6.2: Mean and standard deviation values of systolic and diastolic blood pressure for each subject at the three ambient temperatures.

H.8 Average values of heart and respiration rates

No	Heart rate			Respiration rate		
	20°C	**26°C**	**32°C**	**20°C**	**26°C**	**32°C**
1	0.99±0.12	1.14± 0.12	1.34± 0.11	0.24± 0.06	0.26 ±0.05	0.26±0.06
2	1.05± 0.08	0.93±0.09	1.05±0.11	0.32±0.04	0.27±0.04	0.29±0.04
3	1.13± 0.11	1.11± 0.09	1.14±0.08	0.25±0.06	0.30±0.04	0.29±0.05
4	1.17± 0.09	1.19±0.10	1.27±0.15	0.28±0.04	0.28 ±0.04	0.27±0.04
5	1.00±0.10	0.98±0.08	1.01±0.08	0.25±0.04	0.25 ±0.03	0.24±0.03
6	1.07± 0.08	1.10±0.07	1.19±0.07	××	××	××
7	0.78±0.09	0.81 ±0.10	0.89±0.10	0.24±0.07	0.24 ±0.07	0.24±0.06
8	0.76±0.06	0.79±0.07	0.83±0.07	0.25±0.04	0.26±0.04	0.24±0.05
9	0.96± 0.09	0.95±0.09	0.97 ±0.07	0.29±0.06	0.28 ±0.05	0.28±0.04
10	1.11±0.11	1.11±0.10	1.01±0.08	0.24±0.05	0.24±0.05	0.27±0.06
11	1.15±0.06	1.16±0.07	1.08±0.07	0.27±0.05	0.26 ±0.05	0.25±0.04
12	0.78±0.06	0.82±0.06	0.90±0.07	0.29±0.04	0.29±0.04	0.26±0.05
13	0.92±0.08	0.94±0.06	1.05±0.07	0.29± 0.04	0.31 ±0.04	0.31±0.04
14	0.83±0.07	0.87±0.09	0.95±0.08	0.31±0.05	0.28 ±0.05	0.29±0.04
15	0.90±0.05	0.87±0.05	0.88±0.05	0.28±0.04	0.27 ±0.04	0.25±0.05
16	0.79±0.06	0.84±0.06	0.88±0.07	0.27±0.04	0.31 ± 0.05	0.31±0.05
17	0.93±0.14	0.94±0.10	0.88±0.09	0.30±0.05	0.32 ±0.04	0.27±0.04
18	0.94±0.08	0.93±0.07	1.01±0.10	0.31 ±0.04	0.34±0.04	0.32±0.04
19	0.84±0.07	0.79±0.07	0.85±0.08	0.31±0.05	0.28 ±0.05	0.30±0.06
20	0.72±0.05	0.78±0.07	0.85±0.07	0.31±0.04	0.30 ±0.04	0.29±0.04
21	1.05±0.07	1.08± 0.09	1.04± 0.09	0.33±0.04	0.32 ±0.04	0.29±0.04
22	1.01±0.06	0.96±0.06	1.03±0.06	0.29±0.04	0.27 ±0.04	0.29±0.04
23	0.82±0.10	0.83±0.09	0.90±0.13	0.29±0.04	0.29 ±0.04	0.29±0.04
24	1.09±0.05	1.11±0.05	1.15±0.05	0.28±0.04	0.29 ±0.04	0.30±0.03
25	1.09±0.07	1.08±0.06	1.17±0.05	0.30±0.05	0.33 ±0.04	0.30±0.03
26	0.90± 0.12	1.02±0.10	0.99±0.13	0.26±0.05	0.26 ±0.04	0.25±0.05
27	1.10±0.14	0.94±0.09	1.12±0.16	0.27± 0.05	0.28 ±0.05	0.27±0.05
28	0.87±0.08	0.92 ±0.08	0.93±0.09	0.33±0.04	0.31±0.04	0.31 ±0.04

Table 6.3: Mean and standard deviation values of heart rate and respiration rate variability for each subject at the three ambient temperatures.

I.9 Total average values of physiological time series

After obtaining mean and standard deviation values for each subject at three ambient temperatures, we calculated the total mean values across all subjects at three ambient temperatures to check how close the values are with median values obtained in summary and discussion chapter. We found that the difference between mean and median values are minor and is in the account of the data are normally distributed.

	20°C	26°C	32°C
IHR (Hz)	0.956	0.965	1.012
IRR (Hz)	0.282	0.286	0.275
SV (mL/min)	100.5	96.26	94.28
CO (L/min)	5.887	5.645	5.816
BP (mmHg)	75.08	69.92	66.26
sBP (mmHg)	132.1	121.9	110.2
dBP (mmHg)	56.33	52.02	49.22

Figure 6.10: Total average values of cardiovascular variables in the time domain. The mean value of each individual signal was calculated across all ambient temperatures to see how close the values will be compared to the median values, and then the overall mean value was obtained in each ambient temperature.

J.10 Average values of blood flow signals

No	Left index finger			Right index finger			Left forearm		
	20°C	**26°C**	**32°C**	**20°C**	**26°C**	**32°C**	**20°C**	**26°C**	**32°C**
1	33.4±8.7	142.4±45.6	875.2±86.1	9.9±3.2	11.6± 5.7	96.8±24.3	16.3± 6.1	26.1± 8.9	212.4± 39.7
2	125.2±116.7	379.4±137.1	480.5±102.9	15.2± 11.6	93.1± 30.3	103.3±28	36.4± 7.4	66.7± 13.1	76.4± 9.6
3	71.5± 38.6	287.3± 71.5	355.8±54.3	15.7± 7.5	92.9± 25.9	86.7± 15.6	30.2± 7.6	86.9± 23.6	126.8± 20.1
4	22.3± 13.5	56.6± 28.8	268.4± 49.3	7.7 ± 3.7	19.6± 14.0	83.5±28.3	27.1± 10.9	28.4± 7.1	38.5± 10.9
5	13.0± 7.1	29.0± 10.4	520.6± 54.7	6.1± 2.3	15.8± 4.6	153.1±35.9	3.2±0.3	4.0± 0.9	21.5± 5.8
6	12.1± 3.4	91.0±61.0	394.3± 49.2	6.3± 2.1	78.5± 43.8	144.0±21.5	20.0±6.0	26.6± 6.5	41.8± 10.6
7	323.8± 47.4	269.0±65.9	194.4±33.8	48.4± 18.2	117.7± 19.5	124.1±18.0	3.8±0.7	4.1± 1.0	4.3± 0.9
8	84.1± 88.9	66.5± 54.8	278.0±107.3	18.5±12.6	21.3± 10.1	76.4±31.4	8.6± 2.9	9.4± 3.1	25.7± 7.5
9	16.6± 11.7	84.6± 49.3	117.2±41.0	7.0±4.0	21.7± 12.0	50.4±15.0	21.0± 5.8	6.9±1.0	10.4± 1.6
10	43.0± 13.4	42.7±13.4	225.9±44.7	21.3± 5.9	75.8± 15.8	105.5±16.9	5.9±1.2	6.2± 1.3	19.3± 4.3
11	96.3± 26.4	232.6± 39.2	98.9±27.8	16.0± 5.8	55.5±9.5	38.0±7.3	7.3±1.2	28.5±7.8	35.9± 7.0
12	84.1± 81.2	198.0± 111.7	341.0± 125.1	7.0± 3.4	18.3 ±9.8	61.4±24.7	3.6± 0.6	5.0±3.4	8.6±1.9
13	23.8± 15.7	47.1± 21.4	76.8±28.2	8.7±3.0	14.7± 4.7	27.5 ±8.2	3.3±0.3	3.3±0.3	4.7± 0.5
14	63.2± 27.2	316.9± 92.2	463.2±63.6	8.2± 2.9	42.6 ± 11.9	65.5±9.9	4.2±0.9	8.3± 2.3	8.0± 2.1
15	106.5±89.0	222.2 ± 100.0	230.3± 88.3	27.4±23.3	55.7± 24.9	63.9± 23.5	20.0± 5.3	15.4± 8.0	14.0±1.9
16	11.7± 6.0	21.2± 10.7	63.0±38.2	5.5± 1.2	10.7± 4.6	31.3±13.5	3.3± 0.2	10.9± 8.7	3.4±0.6
17	228.9± 73.9	406.9± 41.4	326.0± 38.1	56.8± 28.9	184.6± 36.7	115.5±22.0	12.4±9.4	18.3± 8.6	19.6±8.0
18	96.8± 50.6	220.9± 50.7	233.0±58.9	15.3± 12.9	50.4±21.1	56.3±21.0	7.3± 1.8	15.0± 6.5	25.3±7.3
19	18.5±9.2	68.0± 39.7	230.3±68.2	6.8±2.5	25.1±12.5	55.5±13.8	3.3± 0.3	3.2± 0.2	9.4±7.9
20	82.1± 58.1	526.9± 146.6	537.2±142.6	9.6±4.5	99.4 ± 32.3	84.7±22.4	10.0 ±3.5	23.9± 9.4	19.2±7.7
21	20.9± 12.8	87.5±52.5	251.1±89.4	8.4± 2.2	20.3 ±8.7	35.9±10.6	15.9 ±10.6	15.7±3.0	37.5±9.0
22	230.8± 148.0	309.7±129.4	431.4± 127.4	36.1± 23.4	57.1± 27.6	82.6±26.0	10.6± 8.9	3.3± 0.3	5.6±1.7
23	201.3±65.0	281.8± 80.1	349.8 ± 90.3	101.5±38.7	141.3±44.0	179.5±45.6	3.3±0.3	3.2 ±0.2	3.9±0.7
24	57.6± 63.3	54.5± 46.5	256.3±87.1	12.0±13.5	13.7 ±7.8	118.3±27.7	12.9±9.9	9.8±8.9	5.1±1.3
25	31.1±12.3	172.7±41.4	269.2± 45.1	9.8±2.7	78.2 ± 15.0	100.7±17.8	4.1± 4.0	4.1±0.7	10.0±2.0
26	22.0± 10.8	40.2±14.1	242.2± 74.4	16.4±8.9	26.8 ±7.6	161.4±30.3	5.5±2.1	6.9±1.8	12.0±3.4
27	43.9±32.9	154.9±50.7	208.7±70.5	18.0±14.3	74.4±20.2	84.0±23.9	7.4±1.7	9.0±1.4	18.6±6.9
28	16.1±8.1	142.0±58.3	195.0±42.2	10.2±3.8	56.3±25.1	104.1±21.9	7.8±2.2	19.5 ± 2.9	20.3±3.4

Table 6.4: Mean and standard deviation values of left forearm, left index finger and right index finger for each subject at the three ambient temperatures.

K.11 Data arrangements and approvals

In the following agreement to use the data as well as ethics approval is provided as background of this work.

UNIVERSITETET I OSLO
DET MEDISINSKE FAKULTET

Maja Elstad
Institutt for medisinske basalfag, UiO
PO Box 1130 Blindern
0317 Oslo

Regional komité for medisinsk og helsefaglig forskningsetikk Sør-Øst C (REK Sør-Øst C)
Postboks 1130 Blindern
NO-0318 Oslo

Telefon:+47 22 84 55 21

E-post: post@helseforskning.etikkom.no
Nettadresse: http://helseforskning.etikkom.no

Date: 15.01.2013
Deres ref.:
Our ref.: IRB 0000 1870

To whom it may concern

Exemption from ethics approval regarding the study:
"The temperature regulation role of skin with and without arteriovenous anastomoses".

We hereby confirm that the Regional Committee for Medical and Health Research Ethics, section South-East C, Norway has received the project "The temperature regulation role of skin with and without arteriovenous anastomoses" for review.
The project was discussed on the 29th of November 2012.

The ethics committee system consists of seven independent regional committees, with authority to either approve or disapprove medical research studies conducted within Norway, or by Norwegian institutions, in accordance with ACT 2008-06-20 no. 44: Act on medical and health research (the Health Research Act).

The abovementioned study is exempt from review in Norway, cf. §§ 2 and 9 of The Act. The project can be implemented without the approval by the Regional Committee for Medical Research Ethics.

Please do not hesitate to contact the Regional Committee for Medical and Health Research Ethics, section South-East C (REK Sør-Øst C) if further information is required.

Yours sincerely,

Arvid Heiberg MD, PhD (sign.)
Professor of Medicine,
University of Oslo

Chair Regional Committee
for Medical and Health Research Ethics,
section South-East C

Tor Even Svanes
Senior Advisor

Regional Committee for
Medical and Health
Research Ethics, section
South-East C

Figure 6.11: Exemption ethics approval.

UiO : Institute of Basic Medical Sciences
Faculty of Medicine, University of Oslo

Oslo, December 2023

Collaboration agreement

In accordance with our prior correspondence via email, I hereby confirm my consent for the sharing of collected data (anonymous form without any identification) with Sultan Alatawi, under Professor Aneta Stefanovska's supervision. It is understood that the outcomes derived from this collaboration were presented in Sultan Alatawi's PhD Thesis, submitted to Lancaster University in September 2023. It is already agreed that joint journal publications by the Oslo and Lancaster teams will follow.

Yours sincerely,

Maja Elstad

(MD, PhD)

Associate Professor

Group Leader CIRCON

Human Integrative Cardiovascular Control

Institute of Basic Medical Sciences

University of Oslo

Oslo, Norway

Institute of Basic Medical Sciences
PO Box 1113 Blindern
0317 Oslo, Norway

Maja Elstad
Associate Professor
maja.elstad@medisin.uio.no

Figure 6.12: Collaboration agreement.

Bibliography

[1] K. Premkumar, *The massage connection: anatomy and physiology*. Lippincott Williams & Wilkins, 2004.

[2] M. Zhang, *Computational modeling and simulation of hand-specific heat transfer and thermoregulation during cold stress*. PhD thesis, Iowa State University, 2021.

[3] L. Walløe, "Arterio-venous anastomoses in the human skin and their role in temperature control," *Temperature*, vol. 3, no. 1, pp. 92–103, 2016.

[4] Y. Shiogai, A. Stefanovska, and P. V. E. McClintock, "Nonlinear dynamics of cardiovascular ageing," *Physics reports*, vol. 488, no. 2-3, pp. 51–110, 2010.

[5] W. B. Liedtke, "Deconstructing mammalian thermoregulation," *Proceedings of the National Academy of Sciences*, vol. 114, pp. 1765–1767, feb 8 2017.

[6] C. Fernández-Peña, A. Reimúndez, F. Viana, V. M. Arce, and R. Señarís, "Sex differences in thermoregulation in mammals: Implications for energy homeostasis," *Frontiers in Endocrinology*, vol. 14, mar 8 2023.

[7] D. L. Kellogg, "Thermoregulatory and thermal control in the human cutaneous circulation," *Frontiers in Bioscience*, vol. S2, no. 3, pp. 825–853, 2010.

[8] W. P. Cheshire, "Thermoregulatory disorders and illness related to heat and cold stress," *Autonomic Neuroscience*, vol. 196, pp. 91–104, 4 2016.

[9] A. Stevenson, *Oxford dictionary of English*. Oxford University Press, USA, 2010.

[10] S. D. Shpilfoygel, R. A. Close, D. J. Valentino, and G. R. Duckwiler, "X-ray videodensitometric methods for blood flow and velocity measurement: A critical review of literature," *Medical Physics*, vol. 27, pp. 2008–2023, 9 2000.

[11] M. I. Bogachev, O. A. Markelov, N. S. Pyko, and S. A. Pyko, "Blood pressure x2014; Heart rate syncronization coefficient as a complementary indicator of baroreflex mechanism efficiency," *2015 XVIII International Conference on Soft Computing and Measurements (SCM)*, 5 2015.

[12] N. B. Suvorov, A. V. Belov, K. G. Kuliabin, A. A. Anisimov, T. V. Sergeev, and O. A. Markelov, "High Precision Human Skin Temperature Fluctuations Measuring Instrument," *Sensors*, vol. 21, p. 4101, jun 15 2021.

[13] A. Stefanovska, M. Bracic Lotric, S. Strle, and H. Haken, "The cardiovascular system as coupled oscillators?," *Physiological Measurement*, vol. 22, pp. 535–550, aug 1 2001.

[14] J. S. Petrofsky, "Resting Blood Flow in the Skin: Does it Exist, and What is the Influence of Temperature, Aging, and Diabetes?," *Journal of Diabetes Science and Technology*, vol. 6, pp. 674–685, 5 2012.

[15] G. Lancaster, *Oscillations in Microvascular Flow: Their Relationship to Tissue Oxygenation, Cellular Metabolic Function and Their Diagnostic Potential for Detecting Skin Melanoma-Clinical, Experimental and Theoretical Investigations*. Lancaster University (United Kingdom), 2016.

[16] J. R. Levick, *An introduction to cardiovascular physiology*. Butterworth-Heinemann, 2013.

[17] C. M. McEniery, I. B. Wilkinson, and A. P. Avolio, "Age, hypertension and arterial function," *Clinical and Experimental Pharmacology and Physiology*, vol. 34, no. 7, pp. 665–671, 2007.

[18] M. Pugsley and R. Tabrizchi, "The vascular system: An overview of structure and function," *Journal of pharmacological and toxicological methods*, vol. 44, no. 2, pp. 333–340, 2000.

[19] J. R. Pappenheimer, *Handbook of Physiology: The cardiovascular system*, vol. 2. American Physiological Society, 1980.

[20] P. F. Davies, "Flow-mediated endothelial mechanotransduction," *Physiological reviews*, vol. 75, no. 3, pp. 519–560, 1995.

[21] W. C. Aird, "Phenotypic heterogeneity of the endothelium: Ii. representative vascular beds," *Circulation research*, vol. 100, no. 2, pp. 174–190, 2007.

[22] W. F. Ganong, "Review of medical physiology," *Dynamics of blood and lymph flow*, vol. 30, pp. 525–541, 1995.

[23] K. Hirata, M. Yutani, and T. Nagasaka, "Increased hand blood flow limits other skin vasodilation," *Journal of Thermal Biology*, vol. 18, no. 5-6, pp. 325–327, 1993.

[24] K. Gorgas, P. Böck, F. Tischendorf, and S. B. Currî, "The fine structure of human digital arterio-venous anastomoses (hoyer-grosser's organs)," *Anatomy and embryology*, vol. 150, pp. 269–289, 1977.

[25] T. Bergersen, J. Hisdal, and L. Walløe, "Perfusion of the human finger during cold-induced vasodilatation," *American Journal of Physiology-Regulatory, Integrative and Comparative Physiology*, vol. 276, no. 3, pp. R731–R737, 1999.

[26] C. M. Black, "Anatomy and physiology of the lower-extremity deep and superficial veins," *Techniques in Vascular and Interventional Radiology*, vol. 17, no. 2, pp. 68–73, 2014.

[27] C. B. Wenger, M. F. Roberts, E. R. Nadel, and J. Stolwijk, "Thermoregulatory control of finger blood flow," *Journal of applied physiology*, vol. 38, no. 6, pp. 1078–1082, 1975.

[28] T. H. Maiman *et al.*, "Stimulated optical radiation in ruby," 1960.

[29] H. Cummins, N. Knable, and Y. Yeh, "Observation of diffusion broadening of rayleigh scattered light," *Physical Review Letters*, vol. 12, no. 6, p. 150, 1964.

[30] C. Riva, B. Ross, and G. B. Benedek, "Laser doppler measurements of blood flow in capillary tubes and retinal arteries," *Investigative Ophthalmology & Visual Science*, vol. 11, no. 11, pp. 936–944, 1972.

[31] M. Stern, "In vivo evaluation of microcirculation by coherent light scattering," *Nature*, vol. 254, no. 5495, pp. 56–58, 1975.

[32] D. Watkins and G. A. Holloway, "An instrument to measure cutaneous blood flow using the doppler shift of laser light," *IEEE Transactions on Biomedical Engineering*, no. 1, pp. 28–33, 1978.

[33] G. E. Nilsson, T. Tenland, and P. A. Oberg, "Evaluation of a laser doppler flowmeter for measurement of tissue blood flow," *IEEE Transactions on Biomedical Engineering*, no. 10, pp. 597–604, 1980.

[34] J. C. Fischer, P. M. Parker, and W. W. Shaw, "Comparison of two laser doppler flowmeters for the monitoring of dermal blood flow," *Microsurgery*, vol. 4, no. 3, pp. 164–170, 1983.

[35] U. Hoffmann, A. Yanar, U. K. Franzeck, J. M. Edwards, and A. Bollinger, "The frequency histogram—a new method for the evaluation of laser doppler flux motion," *Microvascular research*, vol. 40, no. 3, pp. 293–301, 1990.

[36] E. Salerud, T. Tenland, G. Nilsson, and P. Oberg, "Rhythmical variations in human skin blood flow.," *International journal of microcirculation, clinical and experimental*, vol. 2, no. 2, pp. 91–102, 1983.

[37] J. K. Wilkin, "Periodic cutaneous blood flow during postocclusive reactive hyperemia," *American Journal of Physiology-Heart and Circulatory Physiology*, vol. 250, no. 5, pp. H765–H768, 1986.

[38] A. Stefanovska, M. Bracic, and H. Kvernmo, "Wavelet analysis of oscillations in the peripheral blood circulation measured by laser Doppler technique," *IEEE Transactions on Biomedical Engineering*, vol. 46, no. 10, pp. 1230–1239, 1999.

[39] G. Hildebrandt, "The autonomous time structure and its reactive modifications in the human organism," in *Temporal disorder in human oscillatory systems*, pp. 160–175, Springer, 1987.

[40] A. Stefanovska, "Physics of the human cardiovascular system," *Contemporary Physics*, vol. 40, no. 1, pp. 31–55, 1999.

[41] M. Di Rienzo, G. Mancia, and G. Parati, *Computer analysis of cardiovascular signals*, vol. 13. Ios press, 1995.

[42] J. P. Saul, R. D. Berger, P. Albrecht, S. Stein, M. H. Chen, and R. Cohen, "Transfer function analysis of the circulation: unique insights into cardiovascular regulation," *American Journal of Physiology-Heart and Circulatory Physiology*, vol. 261, no. 4, pp. H1231–H1245, 1991.

[43] V. Ticcinelli, T. Stankovski, P. V. McClintock, and A. Stefanovska, "Ageing of the couplings between cardiac, respiratory and myogenic activity in humans," in *2015 37th Annual International Conference of the IEEE Engineering in Medicine and Biology Society (EMBC)*, pp. 7366–7369, IEEE, 2015.

[44] M. Bračič and A. Stefanovska, "Wavelet analysis in studying the dynamics of blood circulation," *Nonlinear Phenomena in Complex Systems*, vol. 2, no. 1, pp. 68–77, 1999.

[45] A. Stefanovska and P. Krošelj, "Correlation integral and frequency analysis of cardiovascular functions," *Open systems & information dynamics*, vol. 4, pp. 457–478, 1997.

[46] D. L. Eckberg, "Topical review: The human respiratory gate," *The Journal of physiology*, vol. 548, no. 2, pp. 339–352, 2003.

[47] M. Clynes, "Respiratory sinus arrhythmia: laws derived from computer simulation," *Journal of Applied Physiology*, vol. 15, no. 5, pp. 863–874, 1960.

[48] A. Bollinger, A. Yanar, U. Hoffmann, and U. Franzeck, "Is high-frequency flux motion due to respiration or to vasomotion activity? 1," in *Vasomotion and flow motion*, vol. 20, pp. 52–58, Karger Publishers, 1993.

[49] M. Mück-Weymann, H. Albrecht, D. Hiller, O. Hornstein, and R. Bauer, "Respiration-dependence of cutaneous laser doppler flow motion," *VASA. Zeitschrift fur Gefasskrankheiten*, vol. 23, no. 4, pp. 299–304, 1994.

[50] L. A. Martinez-Lemus, X. Wu, E. Wilson, M. A. Hill, G. E. Davis, M. J. Davis, and G. A. Meininger, "Integrins as unique receptors for vascular control," *Journal of vascular research*, vol. 40, no. 3, pp. 211–233, 2003.

[51] B. Folkow, "Description of the myogenic hypothesis," *Circ Res*, vol. 15, no. 1, pp. 279–287, 1964.

[52] P. C. Johnson, "The myogenic response," *The resistance vasculature*, pp. 159–168, 1980.

[53] H. D. Kvernmo, A. Stefanovska, M. Bracic, K. A. Kirkebøen, and K. Kvernebo, "Spectral analysis of the laser doppler perfusion signal in human skin before and after exercise," *Microvascular research*, vol. 56, no. 3, pp. 173–182, 1998.

[54] M. Hubscher, A. Bernjak, and A. Stefanovska, "Assessment of exercise-induced changes of the microcirculation by wavelet transformation," *Deutsche Zeitschrift für Sportmedizen*, vol. 57, no. 1, pp. 14–18, 2006.

[55] A. Bandrivskyy, A. Bernjak, P. McClintock, and A. Stefanovska, "Wavelet phase coherence analysis: application to skin temperature and blood flow," *Cardiovascular engineering: an international journal*, vol. 4, pp. 89–93, 2004.

[56] G. D. Thomas, "Neural control of the circulation," *Advances in physiology education*, vol. 35, no. 1, pp. 28–32, 2011.

[57] E. Kirkman and M. Sawdon, "Neurological and humoral control of blood pressure," *Anaesthesia & Intensive Care Medicine*, vol. 11, no. 5, pp. 159–164, 2010.

[58] R. Kitney, T. Fulton, A. McDonald, and D. Linkenst, "Transient interactions between blood pressure, respiration and heart rate in man," *Journal of biomedical engineering*, vol. 7, no. 3, pp. 217–224, 1985.

[59] A. Stefanovska, S. Strle, and P. Krošelj, "On the overestimation of the correlation dimension," *Physics Letters A*, vol. 235, no. 1, pp. 24–30, 1997.

[60] C. Crandall and J. Gonzalez-Alonso, "Cardiovascular function in the heat-stressed human," *Acta physiologica*, vol. 199, no. 4, pp. 407–423, 2010.

[61] G. J. Hodges and J. M. Johnson, "Adrenergic control of the human cutaneous circulation," *Applied Physiology, Nutrition, and Metabolism*, vol. 34, no. 5, pp. 829–839, 2009.

[62] N. Charkoudian, "Skin blood flow in adult human thermoregulation: how it works, when it does not, and why," in *Mayo clinic proceedings*, vol. 78, pp. 603–612, Elsevier, 2003.

[63] M. Hashim and A. Tadepalli, "Cutaneous vasomotor effects of neuropeptide y," *Neuropeptides*, vol. 29, no. 5, pp. 263–271, 1995.

[64] L. B. Rowell, "Cardiovascular adjustments to thermal stress," *Comprehensive physiology*, pp. 967–1023, 2011.

[65] D. Kellogg Jr, J. Johnson, and W. Kosiba, "Selective abolition of adrenergic vasoconstrictor responses in skin by local iontophoresis of bretylium," *American Journal of Physiology-Heart and Circulatory Physiology*, vol. 257, no. 5, pp. H1599–H1606, 1989.

[66] P. E. Pergola, J. M. Johnson, D. Kellogg Jr, and W. Kosiba, "Control of skin blood flow by whole body and local skin cooling in exercising humans," *American Journal of Physiology-Heart and Circulatory Physiology*, vol. 270, no. 1, pp. H208–H215, 1996.

[67] H. Koepchen, "History of studies and concepts of blood pressure waves," *Mechanism on blood pressure waves*, pp. 3–23, 1984.

[68] M. Sinski, J. Lewandowski, P. Abramczyk, K. Narkiewicz, and Z. Gaciong,

"Why study sympathetic nervous system," *J Physiol Pharmacol*, vol. 57, no. Suppl 11, pp. 79–92, 2006.

[69] G. Valenza, L. Citi, J. P. Saul, and R. Barbieri, "Measures of sympathetic and parasympathetic autonomic outflow from heartbeat dynamics," *Journal of applied physiology*, vol. 125, no. 1, pp. 19–39, 2018.

[70] M. Di Rienzo, G. Parati, A. Radaelli, and P. Castiglioni, "Baroreflex contribution to blood pressure and heart rate oscillations: time scales, time-variant characteristics and nonlinearities," *Philosophical Transactions of the Royal Society A: Mathematical, Physical and Engineering Sciences*, vol. 367, no. 1892, pp. 1301–1318, 2009.

[71] R. Gordan, J. K. Gwathmey, and L.-H. Xie, "Autonomic and endocrine control of cardiovascular function," *World journal of cardiology*, vol. 7, no. 4, p. 204, 2015.

[72] C. Zhang, P. A. Rogers, D. Merkus, J. M. Muller-Delp, C. P. Tiefenbacher, B. Potter, J. D. Knudson, P. Rocic, and W. M. Chilian, "Regulation of coronary microvascular resistance in health and disease," in *Microcirculation*, pp. 521–549, Elsevier, 2008.

[73] P. Kvandal, A. Stefanovska, M. Veber, H. D. Kvermmo, and K. A. Kirkebøen, "Regulation of human cutaneous circulation evaluated by laser doppler flowmetry, iontophoresis, and spectral analysis: importance of nitric oxide and prostaglandines," *Microvascular research*, vol. 65, no. 3, pp. 160–171, 2003.

[74] J. M. Stewart, I. Taneja, M. S. Goligorsky, and M. S. Medow, "Noninvasive measure of microvascular nitric oxide function in humans using very low-frequency cutaneous laser doppler flow spectra," *Microcirculation*, vol. 14, no. 3, pp. 169–180, 2007.

[75] H. D. Kvernmo, A. Stefanovska, K. A. Kirkebøen, and K. Kvernebo, "Oscillations in the human cutaneous blood perfusion signal modified by endothelium-dependent and endothelium-independent vasodilators," *Microvascular research*, vol. 57, no. 3, pp. 298–309, 1999.

[76] S. A. Landsverk, P. Kvandal, A. Bernjak, A. Stefanovska, and K. A. Kirkeboen, "The effects of general anesthesia on human skin microcirculation evaluated by wavelet transform," *Anesthesia & Analgesia*, vol. 105, no. 4, pp. 1012–1019, 2007.

[77] A. Bernjak, P. Clarkson, P. V. McClintock, and A. Stefanovska, "Low-frequency blood flow oscillations in congestive heart failure and after β1-blockade treatment," *Microvascular research*, vol. 76, no. 3, pp. 224–232, 2008.

[78] P. Kvandal, S. A. Landsverk, A. Bernjak, A. Stefanovska, H. D. Kvernmo, and K. A. Kirkebøen, "Low-frequency oscillations of the laser doppler perfusion signal in human skin," *Microvascular research*, vol. 72, no. 3, pp. 120–127, 2006.

[79] P. Scholander, R. Hock, V. Walters, F. Johnson, and L. Irving, "Heat regulation in some arctic and tropical mammals and birds," *The Biological Bulletin*, vol. 99, no. 2, pp. 237–258, 1950.

[80] G. of Terms for Thermal Physiology, "Revised by the commission for thermal physiology of the international union of physiological sciences (iups thermal commission)," *Pflugers Arch*, vol. 410, no. 4–5, pp. 567–587, 1987.

[81] T. L. Bergman, A. S. Lavine, F. P. Incropera, and D. P. DeWitt, *Introduction to heat transfer*. John Wiley & Sons, 2011.

[82] I. B. Mekjavic and O. Eiken, "Contribution of thermal and nonthermal factors to

the regulation of body temperature in humans," *Journal of applied physiology*, vol. 100, no. 6, pp. 2065–2072, 2006.

[83] M. V. Savage and G. L. Brengelmann, "Control of skin blood flow in the neutral zone of human body temperature regulation," *Journal of applied physiology*, vol. 80, no. 4, pp. 1249–1257, 1996.

[84] G. L. Brengelmann and M. V. Savage, "Temperature regulation in the neutral zone," *Annals of the New York Academy of Sciences*, vol. 813, no. 1, pp. 39–50, 1997.

[85] B. Kingma, A. Frijns, and W. van Marken Lichtenbelt, "The thermoneutral zone: implications for metabolic studies," *Frontiers in Bioscience-Elite*, vol. 4, no. 5, pp. 1975–1985, 2012.

[86] D. L. Kellogg Jr, "In vivo mechanisms of cutaneous vasodilation and vasoconstriction in humans during thermoregulatory challenges," *Journal of applied physiology*, vol. 100, no. 5, pp. 1709–1718, 2006.

[87] C. F. Consolazio, L. R. O. Matoush, R. A. Nelson, J. B. Torres, and G. J. Isaac, "Environmental temperature and energy expenditures," *Journal of Applied Physiology*, vol. 18, no. 1, pp. 65–68, 1963.

[88] P. O. Fanger, "Assessment of man's thermal comfort in practice," *Occupational and Environmental Medicine*, vol. 30, no. 4, pp. 313–324, 1973.

[89] L. Schellen, W. D. van Marken Lichtenbelt, M. G. Loomans, J. Toftum, and M. H. De Wit, "Differences between young adults and elderly in thermal comfort, productivity, and thermal physiology in response to a moderate temperature drift and a steady-state condition," *Indoor air*, vol. 20, no. 4, pp. 273–283, 2010.

[90] I. O. for Standardization, *Ergonomics of the thermal environment: analytical determination and interpretation of thermal comfort using calculation of the PMV and PPD indices and local thermal comfort criteria.* International Organization for Standardization, 2005.

[91] F. H. Fenton, A. Gizzi, C. Cherubini, N. Pomella, and S. Filippi, "Role of temperature on nonlinear cardiac dynamics," *Physical Review E*, vol. 87, no. 4, p. 042717, 2013.

[92] C. J. Gordon, "The mouse thermoregulatory system: Its impact on translating biomedical data to humans," *Physiology & behavior*, vol. 179, pp. 55–66, 2017.

[93] D. Mitchell, E. P. Snelling, R. S. Hetem, S. K. Maloney, W. M. Strauss, and A. Fuller, "Revisiting concepts of thermal physiology: predicting responses of mammals to climate change," *Journal of Animal Ecology*, vol. 87, no. 4, pp. 956–973, 2018.

[94] T. Ogawa, N. Ohnishi, K. Imai, and J. Sugenoya, "Thermoregulatory responses of old men to gradual changes in ambient temperature," *Journal of Thermal Biology*, vol. 18, no. 5-6, pp. 345–348, 1993.

[95] K. Natsume, T. Ogawa, J. Sugenoya, N. Ohnishi, and K. Imai, "Preferred ambient temperature for old and young men in summer and winter," *International journal of biometeorology*, vol. 36, no. 1, pp. 1–4, 1992.

[96] J. M. Collaco, L. J. Appel, J. McGready, and G. R. Cutting, "The relationship of lung function with ambient temperature," *PloS one*, vol. 13, no. 1, p. e0191409, 2018.

[97] M. M. Jensen and M. Brabrand, "The relationship between body temperature, heart rate and respiratory rate in acute patients at admission to a medical

care unit," in *Scandinavian Journal of Trauma, Resuscitation and Emergency Medicine*, vol. 23, pp. 1–1, Springer, 2015.

[98] Y. Cho, S. J. Julier, N. Marquardt, and N. Bianchi-Berthouze, "Robust tracking of respiratory rate in high-dynamic range scenes using mobile thermal imaging," *Biomedical optics express*, vol. 8, no. 10, pp. 4480–4503, 2017.

[99] P. N. Giang, D. V. Dung, K. B. Giang, H. V. Vinhc, and J. Rocklöv, "The effect of temperature on cardiovascular disease hospital admissions among elderly people in thai nguyen province, vietnam," *Global health action*, vol. 7, no. 1, p. 23649, 2014.

[100] Y. Inoue, M. Nakao, T. Araki, and H. Ueda, "Thermoregulatory responses of young and older men to cold exposure," *European journal of applied physiology and occupational physiology*, vol. 65, no. 6, pp. 492–498, 1992.

[101] K. Lossius, M. Eriksen, and L. Walløe, "Thermoregulatory fluctuations in heart rate and blood pressure in humans: effect of cooling and parasympathetic blockade," *Journal of the autonomic nervous system*, vol. 47, no. 3, pp. 245–254, 1994.

[102] P. Jansen, M. Leineweber, and T. Thien, "The effect of a change in ambient temperature on blood pressure in normotensives," *Journal of human hypertension*, vol. 15, no. 2, pp. 113–117, 2001.

[103] H. Shin, "Ambient temperature effect on pulse rate variability as an alternative to heart rate variability in young adult," *Journal of clinical monitoring and computing*, vol. 30, no. 6, pp. 939–948, 2016.

[104] L. Madaniyazi, Y. Zhou, S. Li, G. Williams, J. J. Jaakkola, X. Liang, Y. Liu, S. Wu, and Y. Guo, "Outdoor temperature, heart rate and blood pressure

in chinese adults: effect modification by individual characteristics," *Scientific reports*, vol. 6, no. 1, pp. 1–9, 2016.

[105] T. E. Wilson and C. G. Crandall, "Effect of thermal stress on cardiac function," *Exercise and sport sciences reviews*, vol. 39, no. 1, p. 12, 2011.

[106] A. J. Lafrenz, J. E. Wingo, M. S. Ganio, and K. J. Cureton, "Effect of ambient temperature on cardiovascular drift and maximal oxygen uptake.," *Medicine and science in sports and exercise*, vol. 40, no. 6, pp. 1065–1071, 2008.

[107] H. Lian, Y. Ruan, R. Liang, X. Liu, and Z. Fan, "Short-term effect of ambient temperature and the risk of stroke: a systematic review and meta-analysis," *International journal of environmental research and public health*, vol. 12, no. 8, pp. 9068–9088, 2015.

[108] M. Di Rienzo and A. Porta, "Cardiovascular variability [introduction to the special issue]," *IEEE engineering in medicine and biology magazine*, vol. 28, no. 6, pp. 16–17, 2009.

[109] A. Porta, M. Di Rienzo, N. Wessel, and J. Kurths, "Addressing the complexity of cardiovascular regulation," 2009.

[110] S. Saxena, V. Kumar, and S. Hamde, "Feature extraction from ecg signals using wavelet transforms for disease diagnostics," *International Journal of Systems Science*, vol. 33, no. 13, pp. 1073–1085, 2002.

[111] R. Rodríguez, A. Mexicano, J. Bila, S. Cervantes, and R. Ponce, "Feature extraction of electrocardiogram signals by applying adaptive threshold and principal component analysis," *Journal of applied research and technology*, vol. 13, no. 2, pp. 261–269, 2015.

[112] R. Ruangsuwana, G. Velikic, and M. Bocko, "Methods to extract respiration information from ecg signals," in *2010 IEEE International Conference on Acoustics, Speech and Signal Processing*, pp. 570–573, IEEE, 2010.

[113] S. Meek and F. Morris, "Introduction. ii—basic terminology," *Bmj*, vol. 324, no. 7335, pp. 470–473, 2002.

[114] D. Iatsenko, P. V. McClintock, and A. Stefanovska, "Nonlinear mode decomposition: a noise-robust, adaptive decomposition method," *Physical Review E*, vol. 92, no. 3, p. 032916, 2015.

[115] P. G. Katona and F. Jih, "Respiratory sinus arrhythmia: noninvasive measure of parasympathetic cardiac control," *Journal of Applied Physiology*, vol. 39, pp. 801–805, nov 1 1975.

[116] M. B. Lotrič and A. Stefanovska, "Synchronization and modulation in the human cardiorespiratory system," *Physica A: Statistical Mechanics and its Applications*, vol. 283, no. 3-4, pp. 451–461, 2000.

[117] W. F. Boron and E. Boulpaep, "Medical physiology: A cellular and molecular approach, updated 2nd ed," 2005.

[118] V. Rajan, B. Varghese, T. G. van Leeuwen, and W. Steenbergen, "Review of methodological developments in laser doppler flowmetry," *Lasers in medical science*, vol. 24, no. 2, pp. 269–283, 2009.

[119] J. Zhong, A. M. Seifalian, G. E. Salerud, and G. E. Nilsson, "A mathematical analysis on the biological zero problem in laser doppler flowmetry," *IEEE transactions on biomedical engineering*, vol. 45, no. 3, pp. 354–364, 1998.

[120] D. Lathrop, "Nonlinear dynamics and chaos: With applications to physics, biology, chemistry, and engineering," *Physics Today*, vol. 68, no. 4, p. 54, 2015.

[121] A. Goldbeter *et al.*, "Biochemical oscillations and cellular rhythms," *Biochemical Oscillations and Cellular Rhythms*, 1997.

[122] P. Clemson, G. Lancaster, and A. Stefanovska, "Reconstructing time-dependent dynamics," *Proceedings of the IEEE*, vol. 104, no. 2, pp. 223–241, 2016.

[123] S. H. Strogatz, "Exploring complex networks," *nature*, vol. 410, no. 6825, pp. 268–276, 2001.

[124] P. T. Clemson and A. Stefanovska, "Discerning non-autonomous dynamics," *Physics Reports*, vol. 542, no. 4, pp. 297–368, 2014.

[125] P. E. Kloeden and C. Pötzsche, "Nonautonomous dynamical systems in the life sciences," in *Nonautonomous dynamical systems in the life sciences*, pp. 3–39, Springer, 2013.

[126] F. M. Pouzols and A. Lendasse, "Effect of different detrending approaches on computational intelligence models of time series," in *The 2010 International Joint Conference on Neural Networks (IJCNN)*, pp. 1–8, IEEE, 2010.

[127] A. R. Kiselev, A. S. Karavaev, V. I. Gridnev, M. D. Prokhorov, V. I. Ponomarenko, E. I. Borovkova, V. A. Shvartz, Y. M. Ishbulatov, O. M. Posnenkova, and B. P. Bezruchko, "Method of estimation of synchronization strength between low-frequency oscillations in heart rate variability and photoplethysmographic waveform variability," *Russian Open Medical Journal*, vol. 5, no. 1, pp. 0101–0101, 2016.

[128] N. E. Huang, "Computing instantaneous frequency by normalizing hilbert transform," 2005.

[129] B. Boashash, "Estimating and interpreting the instantaneous frequency of a

signal. i. fundamentals," *Proceedings of the IEEE*, vol. 80, no. 4, pp. 520–538, 1992.

[130] D. Iatsenko, P. V. McClintock, and A. Stefanovska, "Extraction of instantaneous frequencies from ridges in time–frequency representations of signals," *Signal Processing*, vol. 125, pp. 290–303, 2016.

[131] N. E. Huang, Z. Wu, S. R. Long, K. C. Arnold, X. Chen, and K. Blank, "On instantaneous frequency," *Advances in adaptive data analysis*, vol. 1, no. 02, pp. 177–229, 2009.

[132] S. Sahoo, P. Biswal, T. Das, and S. Sabut, "De-noising of ecg signal and qrs detection using hilbert transform and adaptive thresholding," *Procedia Technology*, vol. 25, pp. 68–75, 2016.

[133] N. Mitrou, A. Laurin, T. Dick, and J. Inskip, "A peak detection method for identifying phase in physiological signals," *Biomedical Signal Processing and Control*, vol. 31, pp. 452–462, 2017.

[134] R. M. Stern, W. J. Ray, and K. S. Quigley, *Psychophysiological recording*. Oxford University Press, USA, 2001.

[135] M. Bračič and A. Stefanovska, "Wavelet-based analysis of human blood-flow dynamics," *Bulletin of mathematical biology*, vol. 60, no. 5, pp. 919–935, 1998.

[136] X. Yu, Z. Mei, C. Chen, and W. Chen, "Ranking power spectra: A proof of concept," *Entropy*, vol. 21, no. 11, p. 1057, 2019.

[137] D. Iatsenko, P. V. McClintock, and A. Stefanovska, "Linear and synchrosqueezed time–frequency representations revisited: Overview, standards of use, resolution, reconstruction, concentration, and algorithms," *Digital Signal Processing*, vol. 42, pp. 1–26, 2015.

[138] A. Guillet, A. Arneodo, and F. Argoul, "Tracking rhythms coherence from polysomnographic records: A time-frequency approach," *Frontiers in Applied Mathematics and Statistics*, vol. 7, 2021.

[139] B. Cazelles, M. Chavez, D. Berteaux, F. Ménard, J. O. Vik, S. Jenouvrier, and N. C. Stenseth, "Wavelet analysis of ecological time series," *Oecologia*, vol. 156, no. 2, pp. 287–304, 2008.

[140] M. B. Lotric, A. Stefanovska, D. Stajer, and V. Urbancic-Rovan, "Spectral components of heart rate variability determined by wavelet analysis," *Physiological measurement*, vol. 21, no. 4, p. 441, 2000.

[141] F. T. Yu and G. Lu, "Short-time fourier transform and wavelet transform with fourier-domain processing," *Applied optics*, vol. 33, no. 23, pp. 5262–5270, 1994.

[142] G. Jamous, L.-G. Durand, Y.-E. Langlois, T. Lanthier, P. Pibarot, and S. Carioto, "Optimal time-window duration for computing time/frequency representations of normal phonocardiograms in dogs," *Medical and Biological Engineering and Computing*, vol. 30, no. 5, pp. 503–508, 1992.

[143] A. Agaskar and Y. M. Lu, "Uncertainty principles for signals defined on graphs: Bounds and characterizations," in *2012 IEEE International Conference on Acoustics, Speech and Signal Processing (ICASSP)*, pp. 3493–3496, IEEE, 2012.

[144] B.-L. Li and H.-i. Wu, "Wavelet transformation of chaotic biological signals," in *Proceedings of the 1995 Fourteenth Southern Biomedical Engineering Conference*, pp. 185–188, IEEE, 1995.

[145] C. Torrence and G. P. Compo, "A practical guide to wavelet analysis," *Bulletin of the American Meteorological society*, vol. 79, no. 1, pp. 61–78, 1998.

[146] P. S. Addison, *The illustrated wavelet transform handbook: introductory theory and applications in science, engineering, medicine and finance*. CRC press, 2017.

[147] P. S. Addison, J. Walker, and R. C. Guido, "Time–frequency analysis of biosignals," *IEEE engineering in medicine and biology magazine*, vol. 28, no. 5, pp. 14–29, 2009.

[148] A. Biswas, H. Cresswell, R. Viscarra Rossel, and B. Si, "Characterizing scale- and location-specific variation in non-linear soil systems using the wavelet transform," *European journal of soil science*, vol. 64, no. 5, pp. 706–715, 2013.

[149] R. Carmona, W.-L. Hwang, and B. Torresani, *Practical Time-Frequency Analysis: Gabor and wavelet transforms, with an implementation in S*. Academic Press, 1998.

[150] D. P. Allen and C. D. MacKinnon, "Time–frequency analysis of movement-related spectral power in eeg during repetitive movements: A comparison of methods," *Journal of neuroscience methods*, vol. 186, no. 1, pp. 107–115, 2010.

[151] M. Priestley, "Wavelets and time-dependent spectral analysis," *Journal of Time Series Analysis*, vol. 17, no. 1, pp. 85–103, 1996.

[152] T. L. Leise and M. E. Harrington, "Wavelet-based time series analysis of circadian rhythms," *Journal of biological rhythms*, vol. 26, no. 5, pp. 454–463, 2011.

[153] A. Macedo, "Signal analysis and coherence using the continuous wavelet transform," 2013.

[154] J. M. Hurtado, L. L. Rubchinsky, and K. A. Sigvardt, "Statistical method

for detection of phase-locking episodes in neural oscillations," *Journal of neurophysiology*, vol. 91, no. 4, pp. 1883–1898, 2004.

[155] T. Schreiber, "Interdisciplinary application of nonlinear time series methods," *Physics reports*, vol. 308, no. 1, pp. 1–64, 1999.

[156] A. Bernjak, A. Stefanovska, P. V. McCLINTOCK, P. J. Owen-Lynch, and P. B. Clarkson, "Coherence between fluctuations in blood flow and oxygen saturation," in *The Random and Fluctuating World: Celebrating Two Decades of Fluctuation and Noise Letters*, pp. 345–356, World Scientific, 2022.

[157] A. Bernjak, J. Cui, S. Iwase, T. Mano, A. Stefanovska, and D. L. Eckberg, "Human sympathetic outflows to skin and muscle target organs fluctuate concordantly over a wide range of time-varying frequencies," *The Journal of Physiology*, vol. 590, no. 2, pp. 363–375, 2012.

[158] G. Lancaster, D. Iatsenko, A. Pidde, V. Ticcinelli, and A. Stefanovska, "Surrogate data for hypothesis testing of physical systems," *Physics Reports*, vol. 748, pp. 1–60, 2018.

[159] T. Schreiber and A. Schmitz, "Surrogate time series," *Physica D: Nonlinear Phenomena*, vol. 142, no. 3-4, pp. 346–382, 2000.

[160] D. Iatsenko, A. Bernjak, T. Stankovski, Y. Shiogai, P. J. Owen-Lynch, P. Clarkson, P. V. McClintock, and A. Stefanovska, "Evolution of cardiorespiratory interactions with age," *Philosophical Transactions of the Royal Society A: Mathematical, Physical and Engineering Sciences*, vol. 371, no. 1997, p. 20110622, 2013.

[161] R. Turner, A. Samaranayaka, and C. Cameron, "Parametric vs nonparametric

statistical methods: which is better, and why?," *New Zealand Medical Student Journal*, vol. 0, Apr 2020.

[162] C. M. Kitchen, "Nonparametric vs parametric tests of location in biomedical research," *American Journal of Ophthalmology*, vol. 147, p. 571–572, Apr 2009.

[163] P. Mishra, C. Pandey, U. Singh, A. Keshri, and M. Sabaretnam, "Selection of appropriate statistical methods for data analysis," *Annals of Cardiac Anaesthesia*, vol. 22, no. 3, p. 297, 2019.

[164] R. Hoermann, J. E. M. Midgley, R. Larisch, and J. W. Dietrich, "Who is afraid of non-normal data? choosing between parametric and non-parametric tests: a response," *European Journal of Endocrinology*, vol. 183, p. L1–L3, Aug 2020.

[165] N. Crichton, "Information point: Wilcoxon signed rank test.," *Journal of clinical nursing*, vol. 9, no. 4, pp. 584–584, 2000.

[166] A. Ghasemi and S. Zahediasl, "Normality tests for statistical analysis: A guide for non-statisticians," *International Journal of Endocrinology and Metabolism*, vol. 10, p. 486–489, Dec 2012.

[167] A. Field, *Discovering Statistics Using IBM SPSS Statistics*. SAGE, Jan 2013.

[168] B. Barton and J. Peat, *Medical Statistics*. John Wiley Sons, Oct 2014.

[169] J. L. Hintze and R. D. Nelson, "Violin plots: A box plot-density trace synergism," *The American Statistician*, vol. 52, p. 181–184, May 1998.

[170] M. Bracic, "Wavelet-based Analysis of Human Blood-flow Dynamics," *Bulletin of Mathematical Biology*, vol. 60, pp. 919–935, 9 1998.

[171] Fusheng Yang and Wangcai Liao, "Modeling and decomposition of HRV signals with wavelet transforms," *IEEE Engineering in Medicine and Biology Magazine*, vol. 16, no. 4, pp. 17–22, 1997.

[172] S. Thurner, M. C. Feurstein, and M. C. Teich, "Multiresolution Wavelet Analysis of Heartbeat Intervals Discriminates Healthy Patients from Those with Cardiac Pathology," *Physical Review Letters*, vol. 80, pp. 1544–1547, feb 16 1998.

[173] A. Stefanovska, "Coupled Oscillatros: Complex But Not Complicated Cardiovascular and Brain Interactions," *IEEE Engineering in Medicine and Biology Magazine*, vol. 26, pp. 25–29, 11 2007.

[174] A. Effern, K. Lehnertz, T. Grunwald, G. Fernandez, P. David, and C. E. Elger, "Time adaptive denoising of single trial event- related potentials in the wavelet domain," *Psychophysiology*, vol. 37, pp. 859–865, 11 2000.

[175] V. Urbančič-Rovan, A. Bernjak, A. Stefanovska, K. Ažman-Juvan, and A. Kocijančič, "Macro- and microcirculation in the lower extremities—Possible relationship," *Diabetes Research and Clinical Practice*, vol. 73, pp. 166–173, 8 2006.

[176] K. Ažman-Juvan, A. Bernjak, V. Urbančič-Rovan, A. Stefanovska, and D. Štajer, "Skin Blood Flow and Its Oscillatory Components in Patients with Acute Myocardial Infarction," *Journal of Vascular Research*, vol. 45, pp. 164–172, oct 26 2007.

[177] I. Daubechies, J. Lu, and H.-T. Wu, "Synchrosqueezed wavelet transforms: An empirical mode decomposition-like tool," *Applied and Computational Harmonic Analysis*, vol. 30, pp. 243–261, 3 2011.

[178] H. Kinugasa and K. Hirayanagi, "Effects of Skin Surface Cooling and Heating on Autonomic Nervous Activity and Baroreflex Sensitivity in Humans," *Experimental Physiology*, vol. 84, pp. 369–377, 3 1999.

[179] J. Cui, M. Sathishkumar, T. E. Wilson, M. Shibasaki, S. L. Davis, and C. G. Crandall, "Spectral characteristics of skin sympathetic nerve activity in heat-stressed humans," *American Journal of Physiology-Heart and Circulatory Physiology*, vol. 290, pp. H1601–H1609, 4 2006.

[180] J. J. Sollers, T. A. Sanford, R. Nabors-Oberg, C. A. Anderson, and J. F. Thayer, "Examining changes in hrv in response to varying ambient temperature," *IEEE engineering in medicine and biology magazine*, vol. 21, no. 4, pp. 30–34, 2002.

[181] E. S. Dietrichs, B. Håheim, T. Kondratiev, E. Traasdahl, and T. Tveita, "Effects of hypothermia and rewarming on cardiovascular autonomic control in vivo," *Journal of Applied Physiology*, vol. 124, pp. 850–859, apr 1 2018.

[182] S. J. SARNOFF and E. BERGLUND, "Ventricular Function," *Circulation*, vol. 9, pp. 706–718, 5 1954.

[183] J. D. Trinity, M. D. Pahnke, J. F. Lee, and E. F. Coyle, "Interaction of hyperthermia and heart rate on stroke volume during prolonged exercise," *Journal of Applied Physiology*, vol. 109, pp. 745–751, 9 2010.

[184] B. R. M. Kingma, A. J. H. Frijns, W. H. M. Saris, A. A. van Steenhoven, and W. D. van Marken Lichtenbelt, "Increased systolic blood pressure after mild cold and rewarming: relation to cold-induced thermogenesis and age," *Acta Physiologica*, vol. 203, pp. 419–427, aug 12 2011.

[185] S. Parsons, A. R. Scott, and I. A. Macdonald, "The effect of posture and

environmental temperature on cardiovascular reflexes in normal subjects and diabetes mellitus," *Clinical Autonomic Research*, vol. 2, pp. 147–151, 6 1992.

[186] J. L. Greaney, W. L. Kenney, and L. M. Alexander, "Sympathetic function during whole body cooling is altered in hypertensive adults," *Journal of Applied Physiology*, vol. 123, pp. 1617–1624, dec 1 2017.

[187] J. FAGIUS and R. KAY, "Low ambient temperature increases baroreflex-governed sympathetic outflow to muscle vessels in humans," *Acta Physiologica Scandinavica*, vol. 142, pp. 201–209, 6 1991.

[188] C. G. Crandall, R. Zhang, and B. D. Levine, "Effects of whole body heating on dynamic baroreflex regulation of heart rate in humans," *American Journal of Physiology-Heart and Circulatory Physiology*, vol. 279, pp. H2486–H2492, nov 1 2000.

[189] R. Furlan, S. Piazza, S. Dell'Orto, E. Gentile, S. Cerutti, M. Pagani, and A. Malliani, "Early and late effects of exercise and athletic training on neural mechanisms controlling heart rate," *Cardiovascular Research*, vol. 27, pp. 482–488, mar 1 1993.

[190] A. Bernjak, J. Cui, S. Iwase, T. Mano, A. Stefanovska, and D. L. Eckberg, "Human sympathetic outflows to skin and muscle target organs fluctuate concordantly over a wide range of time-varying frequencies," *The Journal of Physiology*, vol. 590, pp. 363–375, dec 6 2011.

[191] L. W. Sheppard, V. Vuksanović, P. V. E. McClintock, and A. Stefanovska, "Oscillatory dynamics of vasoconstriction and vasodilation identified by time-localized phase coherence," *Physics in Medicine and Biology*, vol. 56, pp. 3583–3601, may 23 2011.

[192] D. L. Eckberg, C. Nerhed, and B. G. Wallin, "Respiratory modulation of muscle sympathetic and vagal cardiac outflow in man.," *The Journal of Physiology*, vol. 365, pp. 181–196, aug 1 1985.

[193] D. L. ECKBERG, R. F. REA, O. K. ANDERSSON, T. HEDNER, J. PERNOW, J. M. LUNDBERG, and B. G. WALLIN, "Baroreflex modulation of sympathetic activity and sympathetic neurotransmitters in humans," *Acta Physiologica Scandinavica*, vol. 133, pp. 221–231, 6 1988.

[194] D. L. Eckberg, Y. T. Kifle, and V. L. Roberts, "Phase relationship between normal human respiration and baroreflex responsiveness.," *The Journal of Physiology*, vol. 304, pp. 489–502, jul 1 1980.

[195] T. Stankovski, W. H. Cooke, L. Rudas, A. Stefanovska, and D. L. Eckberg, "Time-frequency methods and voluntary ramped-frequency breathing: a powerful combination for exploration of human neurophysiological mechanisms," *Journal of Applied Physiology*, vol. 115, pp. 1806–1821, dec 15 2013.

[196] J.-L. Elghozi, D. Laude, and A. Girard, "Effects of respiration on blood pressure and heart rate variability in humans," *Clinical and experimental pharmacology and physiology*, vol. 18, no. 11, pp. 735–742, 1991.

[197] N. Japundzic, M.-L. Grichois, P. Zitoun, D. Laude, and J.-L. Elghozi, "Spectral analysis of blood pressure and heart rate in conscious rats: effects of autonomic blockers," *Journal of the autonomic nervous system*, vol. 30, no. 2, pp. 91–100, 1990.

[198] D. A. Low, D. M. Keller, J. E. Wingo, R. M. Brothers, and C. G. Crandall, "Sympathetic nerve activity and whole body heat stress in humans," *Journal of applied physiology*, vol. 111, no. 5, pp. 1329–1334, 2011.

[199] S. Kubli, B. Waeber, A. Dalle-Ave, and F. Feihl, "Reproducibility of laser doppler imaging of skin blood flow as a tool to assess endothelial function," *Journal of cardiovascular pharmacology*, vol. 36, no. 5, pp. 640–648, 2000.

[200] T. Nagasaka, K. Hirata, T. Nunomura, and M. Cabanac, "The effect of local heating on blood flow in the finger and the forearm skin," *Canadian journal of physiology and pharmacology*, vol. 65, no. 6, pp. 1329–1332, 1987.

[201] M. M. Mallette, G. J. Hodges, G. W. McGarr, D. A. Gabriel, and S. S. Cheung, "Spectral analysis of reflex cutaneous vasodilatation during passive heat stress," *Microvascular Research*, vol. 111, pp. 42–48, 2017.

[202] M. J. Geyer, Y.-K. Jan, D. M. Brienza, and M. L. Boninger, "Using wavelet analysis to characterize the thermoregulatory mechanisms of sacral skin blood flow," *The Journal of Rehabilitation Research and Development*, vol. 41, no. 6, p. 797, 2004.

[203] Y.-K. Jan, B. D. Struck, R. D. Foreman, and C. Robinson, "Wavelet analysis of sacral skin blood flow oscillations to assess soft tissue viability in older adults," *Microvascular Research*, vol. 78, pp. 162–168, 9 2009.

[204] Yih-Kuen Jan and Fuyuan Liao, "Synchronization of sacral skin blood flow oscillations in response to local heating," *2011 Annual International Conference of the IEEE Engineering in Medicine and Biology Society*, 8 2011.

[205] M. Gruszecki, G. Lancaster, A. Stefanovska, J. P. Neary, R. T. Dech, W. Guminski, A. F. Frydrychowski, J. Kot, and P. J. Winklewski, "Human subarachnoid space width oscillations in the resting state," *Scientific Reports*, vol. 8, feb 15 2018.

[206] A. Gruszecka, M. Waskow, M. A. Malkiewicz, J. P. Neary, J. Singh, T. Teckchandani, G. P. Kratzig, M. Wszedybyl-Winklewska, A. F. Frydrychowski, J. Rumiński, N. Głowacka, P. Lass, P. J. Winklewski, and M. Gruszecki, "Mild poikilocapnic hypoxia increases very low frequency haemoglobin oxygenation oscillations in prefrontal cortex," *Biological Research*, vol. 54, 12 2021.

[207] R. Fossion, A. L. Rivera, and B. Estañol, "A physicist's view of homeostasis: how time series of continuous monitoring reflect the function of physiological variables in regulatory mechanisms," *Physiological Measurement*, vol. 39, p. 084007, aug 31 2018.

[208] R. P. Bartsch, K. K. L. Liu, A. Bashan, and P. C. Ivanov, "Network Physiology: How Organ Systems Dynamically Interact," *PLOS ONE*, vol. 10, p. e0142143, nov 10 2015.

[209] P. C. Ivanov and R. P. Bartsch, "Network Physiology: Mapping Interactions Between Networks of Physiologic Networks," *Understanding Complex Systems*, pp. 203–222, 2014.

[210] R. Rizzo, X. Zhang, J. W. J. L. Wang, F. Lombardi, and P. C. Ivanov, "Network Physiology of Cortico–Muscular Interactions," *Frontiers in Physiology*, vol. 11, nov 26 2020.

[211] V. Ticcinelli, T. Stankovski, D. Iatsenko, A. Bernjak, A. E. Bradbury, A. R. Gallagher, P. B. M. Clarkson, P. V. E. McClintock, and A. Stefanovska, "Coherence and Coupling Functions Reveal Microvascular Impairment in Treated Hypertension," *Frontiers in Physiology*, vol. 8, oct 13 2017.

[212] A. V. Tankanag, A. A. Grinevich, T. V. Kirilina, G. V. Krasnikov, G. M. Piskunova, and N. K. Chemeris, "Wavelet phase coherence analysis of the skin

blood flow oscillations in human," *Microvascular Research*, vol. 95, pp. 53–59, 9 2014.

[213] A. Perrella, M. Sorelli, F. Giardini, L. Frassineti, P. Francia, and L. Bocchi, "Wavelet Phase Coherence Between the Microvascular Pulse Contour and the Respiratory Activity," *IFMBE Proceedings*, pp. 311–314, may 30 2018.

[214] A. Tankanag, G. Krasnikov, and I. Mizeva, "A pilot study: Wavelet cross-correlation of cardiovascular oscillations under controlled respiration in humans," *Microvascular Research*, vol. 130, p. 103993, 7 2020.

[215] L. Xie, B. Liu, X. Wang, M. Mei, M. Li, X. Yu, and J. Zhang, "Effects of different stresses on cardiac autonomic control and cardiovascular coupling," *Journal of Applied Physiology*, vol. 122, pp. 435–445, mar 1 2017.

[216] A. V. Tankanag, A. A. Grinevich, I. V. Tikhonova, A. V. Chaplygina, and N. K. Chemeris, "Phase synchronization of skin blood flow oscillations in humans under asymmetric local heating," *Biophysics*, vol. 62, pp. 629–635, 7 2017.

[217] Y. A. Abdulhameed, G. Lancaster, P. V. E. McClintock, and A. Stefanovska, "On the suitability of laser-Doppler flowmetry for capturing microvascular blood flow dynamics from darkly pigmented skin," *Physiological Measurement*, vol. 40, p. 074005, aug 2 2019.

[218] I. V. Tikhonova, A. A. Grinevich, and A. V. Tankanag, "Analysis of phase interactions between heart rate variability, respiration and peripheral microhemodynamics oscillations of upper and lower extremities in human," *Biomedical Signal Processing and Control*, vol. 71, p. 103091, 1 2022.

[219] M. Nitzan, I. Faib, and H. Friedman, "Respiration-induced changes in tissue

blood volume distal to occluded artery, measured by photoplethysmography," *Journal of Biomedical Optics*, vol. 11, no. 4, p. 040506, 2006.

[220] A. I. Krupatkin, "Blood flow oscillations at a frequency of about 0.1 Hz in skin microvessels do not reflect the sympathetic regulation of their tone," *Human Physiology*, vol. 35, pp. 183–191, 3 2009.

[221] H. N. Mayrovitz and E. E. Groseclose, "Inspiration-Induced Vascular Responses in Finger Dorsum Skin," *Microvascular Research*, vol. 63, pp. 227–232, 3 2002.

[222] W. M. Bayliss, "On the local reactions of the arterial wall to changes of internal pressure," *The Journal of Physiology*, vol. 28, pp. 220–231, may 28 1902.

[223] A. Angelone and N. A. Coulter, "Respiratory sinus arrhythmia: a frequency dependent phenomenon," *Journal of Applied Physiology*, vol. 19, pp. 479–482, may 1 1964.

[224] J. A. Taylor, C. W. Myers, J. R. Halliwill, H. Seidel, and D. L. Eckberg, "Sympathetic restraint of respiratory sinus arrhythmia: implications for vagal-cardiac tone assessment in humans," *American Journal of Physiology-Heart and Circulatory Physiology*, vol. 280, pp. H2804–H2814, jun 1 2001.

[225] A. V. Tankanag, G. V. Krasnikov, and N. K. Chemeris, "Phase Coherence of Finger Skin Blood Flow Oscillations Induced by Controlled Breathing in Humans," *Understanding Complex Systems*, pp. 281–289, 2021.

[226] A. Bollinger, U. Hoffmann, and U. Franzeck, "Evaluation of flux motion in man by the laser doppler technique," *Journal of Vascular Research*, vol. 28, no. Suppl. 1, pp. 21–26, 1991.

[227] M. Intaglietta, *Vasomotion and Flow Modulation in the Microcirculation:*

Satellite Symposium to the Annual Meeting of the Microcirculatory Society, Las Vegas, Nev., April 28-29, 1988, vol. 15. S Karger Ag, 1989.

[228] J.-U. Meyer, P. Borgström, L. Lindbom, and M. Intaglietta, "Vasomotion patterns in skeletal muscle arterioles during changes in arterial pressure," *Microvascular Research*, vol. 35, pp. 193–203, 3 1988.

[229] M. Mück-Weymann, H.-P. Albrecht, D. Hager, D. Hiller, O. Hornstein, and R. Bauer, "Respiratory-Dependent Laser–Doppler Flux Motion in Different Skin Areas and Its Meaning to Autonomic Nervous Control of the Vessels of the Skin," *Microvascular Research*, vol. 52, pp. 69–78, 7 1996.

[230] F. Yasuma and J.-i. Hayano, "Respiratory Sinus Arrhythmia," *Chest*, vol. 125, pp. 683–690, 2 2004.

[231] J. B. Hinnant, L. Elmore-Staton, and M. El-Sheikh, "Developmental trajectories of respiratory sinus arrhythmia and preejection period in middle childhood," *Developmental Psychobiology*, vol. 53, pp. 59–68, sep 29 2010.

[232] V. Novak, P. Novak, J. de Champlain, A. R. Le Blanc, R. Martin, and R. Nadeau, "Influence of respiration on heart rate and blood pressure fluctuations," *Journal of Applied Physiology*, vol. 74, pp. 617–626, feb 1 1993.